Geometallurgical Evaluation of the Nkout (Cameroon) and Putu (Liberia) Iron Ore Deposits

Submitted by
Kelvin Frederick Esebewa Anderson
to the University of Exeter as a thesis for the degree of
Doctor of Philosophy in Earth Resources
In April 2014

I certify that all material in this thesis which is not my own work has been identified and that no material has previously been submitted and approved for the award of a degree by this or any other University.

Signature: ……..

Dedicated to the late Dr Richard Latiff

1956 - 2012

Abstract

The Nkout (Cameroon) and Putu (Liberia) oxide facies iron ore deposits comprise fresh magnetite banded iron formation (BIF) at depth, which weathers towards the surface, forming high grade martite–goethite ores. This study aimed to improve the mineralogical understanding of these deposits in order to predict their metallurgical responses. It concentrated on developing the QEMSCAN® technique and testing its application to these ore types, but also used a variety of other analysis methods. The QEMSCAN® species identification protocol was developed to include three goethite entries: goethite/limonite, phosphorus-bearing and aluminium-bearing goethite. QEMSCAN® was also used to distinguish between the iron oxides using their backscattered electron signals. To test the correlation between the mineralogy and metallurgical characteristics, magnetic separations were carried out.

The samples were divided into 4 main groups based on their whole rock Fe content, determined by XRF analysis, and their degree of weathering: enriched material, weathered magnetite itabirite, transitional magnetite itabirite and magnetite itabirite. Quartz and Al oxide and hydroxide minerals such as gibbsite are the major gangue minerals in the magnetite BIF and martite–goethite ores respectively. From the QEMSCAN® analysis it was concluded that the iron oxides are closely associated and liberation of them individually is poor. Liberation increases when they are grouped together as iron oxide. Chamosite concentrations > 6 wt. % significantly lower liberation of the iron oxides. From the metallurgical testing, it was concluded that iron oxide modal mineralogy gives an indication of iron recovery but other QEMSCAN® data such as mineral association and liberation could be important especially if the iron oxide minerals are not liberated. Grain size and instrument characteristics also affect recovery of iron minerals.

There is no evidence to show that there is any structural control on the BIF mineralisation at Nkout because metamorphism has significantly affected the lithological characteristics. The BIF mineralised zones occur as stacks with no particular stratigraphic relationship. Alteration and stratigraphy are the main controls on the martite–goethite ores. These results are applicable to most other BIFs so that as direct shipping ores are exhausted, the approach used here can help to develop the lower grade portions of the deposits.

Acknowledgements

To God be the glory for all things are possible through him. I am indebted to Professor Frances Wall who guided and scrutinised my work from conception till the end. Special thanks go to Dr. Charlie Moon and Dr. Gavyn Rollinson who co-supervised this work. I thank several staff members at Camborne School of Mines especially Dr. Jens Andersen, Dr. Ben Williamson, Dr. Richard Pascoe, Dr. Rob Fitzpatrick, Mr Stephen Pendray and the rest of the CSM lab staff for their various scientific advice and assistance. I am grateful for the support of the Commonwealth Scholarship Commision in the UK for sponsoring this research. I acknowledge Afferro Mining Inc and the Putu Iron Ore Mining (PIOM) for their support during field work exercises and the provision of samples. I am particularly grateful to Peter Taylor, former Chief Operating Officer of Afferro Mining Inc, for providing logistic support for the field work to be conducted in their company's license area in Cameroon. I would not have received samples from PIOM if it was not authorised by their then Chief Executive Officer, Dr Nigel Keiser. Special thanks also go to the then Chief Geologist at PIOM, Mr Hector Galam, who carefully selected samples representative of the variability within the Putu deposit. I thank my colleagues in the CSM PhD room especially Abdurrahman Abdulqadir, Amos Ambo, Shekwonyadu Iyakwari, Daniel Parvaz, Ben Snook and Klaas-Peter van der Wielen. These guys were my first point of contact for academic, social and counselling issues. I also received great support from members of Penryn Methodist Church especially Mrs Rose Webber and Mrs Gillian Jackson. They accepted my family into their homes and made Penryn a home away from home for us. Solomon Rodgers, a friend from my undergraduate days in Sierra Leone who is now a British citizen residing in London, welcomed and hosted my family to his home with open hands throughout our stay here in the UK. This acknowledgement won't be complete if I don't recognise the immense contribution of my wife Mrs Emmanuella Anderson. She is my strong pillar of support, the mother of my sons (Emmrick and Kelvin Jr) and my best friend. I could not have done this without her being there to take care of my home. Thanks also go to my sister, Mrs Winifred Bangura and brothers, Olu, Syl and Desmond for their support and encouragement. If only my late parents, Mr Samuel Anderson and Mrs Ayodele Anderson were here to see this day; they made lots of sacrifices to get me where I am today and for that I am thankful. May their souls rest in peace.

List of Contents

List of Figures

List of Tables

List of Accompanying Material

One CD-Rom containing appendices 1 – 3.

Chapter 1

Introduction

1.1 Context

Africa is a growing region for the development and production of iron ore deposits and it is becoming important as a supplier to China, Europe and North America, being strategically located closer to these markets than Australia and Brazil; the major exporters of iron ore. Africa is closer to China than Brazil, closer to the USA than Australia and closer to Europe than both Brazil and Australia and as such there are shipping cost implications and advantages. Africa's biggest exporter is South Africa with about 5% of the world's market (Figure 1.1). By 2015, at least 20 mines are expected to open in West and Central Africa including in Cameroon, Gabon, Guinea, Ivory Coast, Liberia and Sierra Leone. These countries contain vast unexploited iron ore deposits and the new mines have the potential of producing up to 600 million tonnes a year (Bell, 2011). This is equivalent to 62 % of the global production in 2012 and 38 % of the expected production in 2015 (Bell, 2011). This amount of production would give the region a say in global iron ore pricing, breaking the unofficial Australia-Brazil cartel.

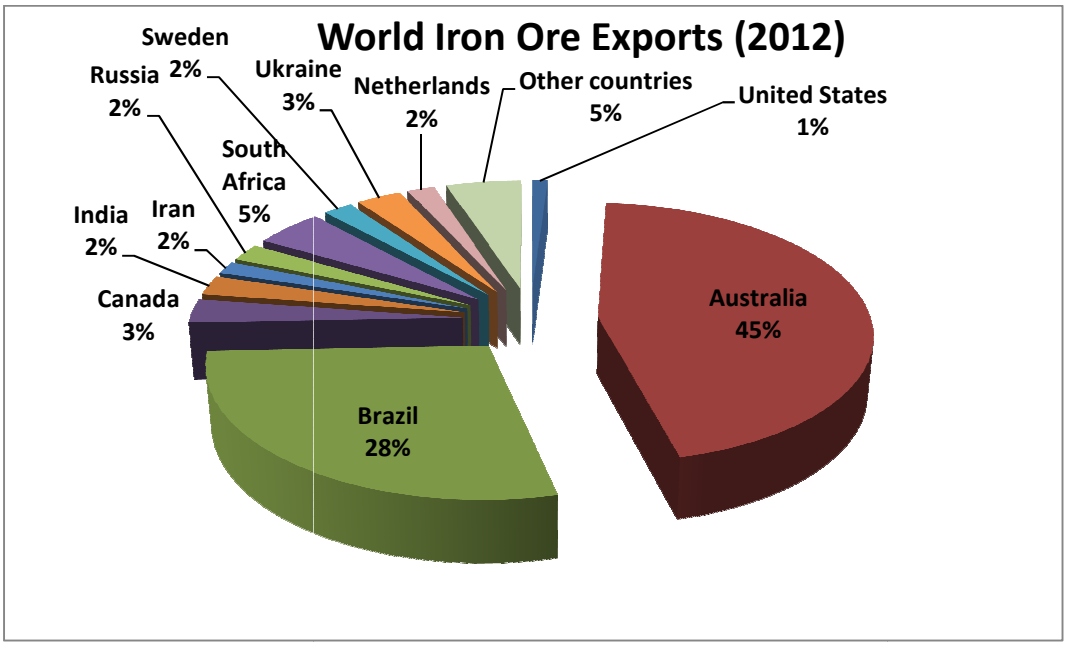

Figure 1.1 Estimated world iron ore exports for 2012 (USGS, 2013 and International Steel Statistics Bureau, 2013).

Mining giants such as BHP Billiton, Rio Tinto, Vale and ArcelorMittal are investing heavily in the region but the Chinese have the potential to be the combined largest investors. China, the world's largest producer of magnetite ore in particular and iron ore in general (Figure 1.2), hopes to import half of its iron ore from Chinese-owned mines elsewhere in the world so is keen to acquire a presence in the emerging iron ore province of West and Central Africa (Bell, 2011).

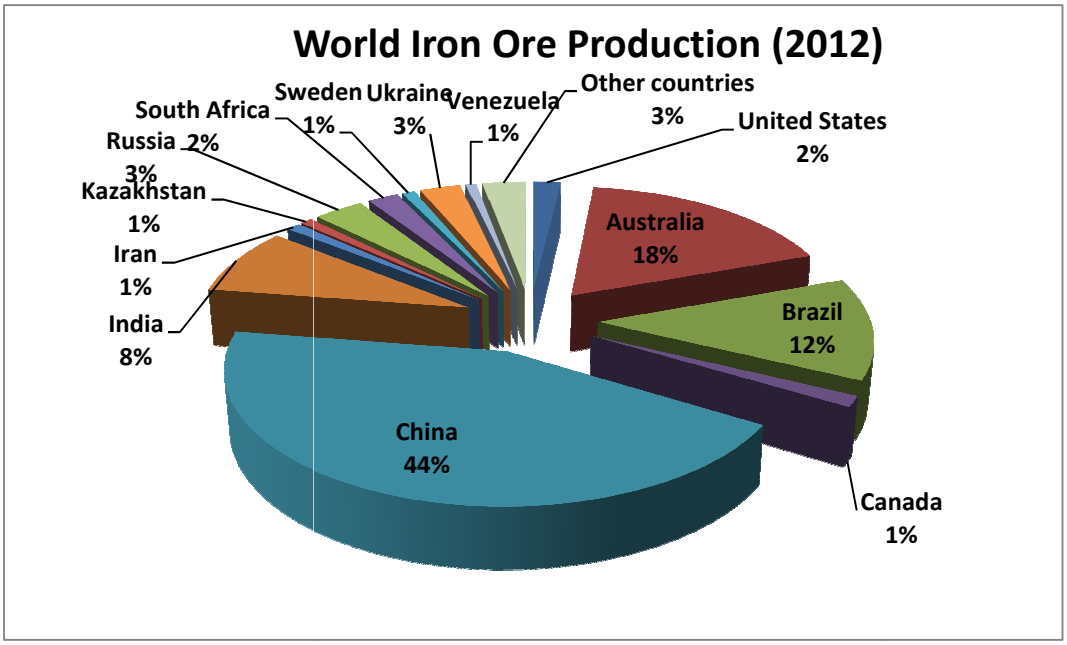

Figure 1.2 Estimated world mine production of Iron Ore in 2012 (Data from USGS, 2013).

China and India, who together constitute about 37% of the world's population, have seen a momentous growth in their demand and consumption of steel. China's forecasted steel production and iron ore requirements are illustrated in Figure 1.3 (Els, 2012) whilst according to the Steel Ministry of India, "Between 2008-09 and 2012-13, the demand for iron ore has gone up from 87.4 million tonnes (Mt) to 124.8 Mt," (Hindu newspaper, 2013). The manufacture of iron and steel constitutes an estimated 98 % of the iron ore shipped in the world and the rest is used in the manufacture of, for example, ballast, cement and agricultural products. Falling shipping prices and the evolution of markets towards magnetite concentrates for pelletisation are making projects in West and Central Africa more competitive. Furthermore, these regions have been stable for the past decade after years of rebel insurrections making them

attractive for investment. Their governments are also making it easier for mining and exploration companies to register and invest in their mining sectors.

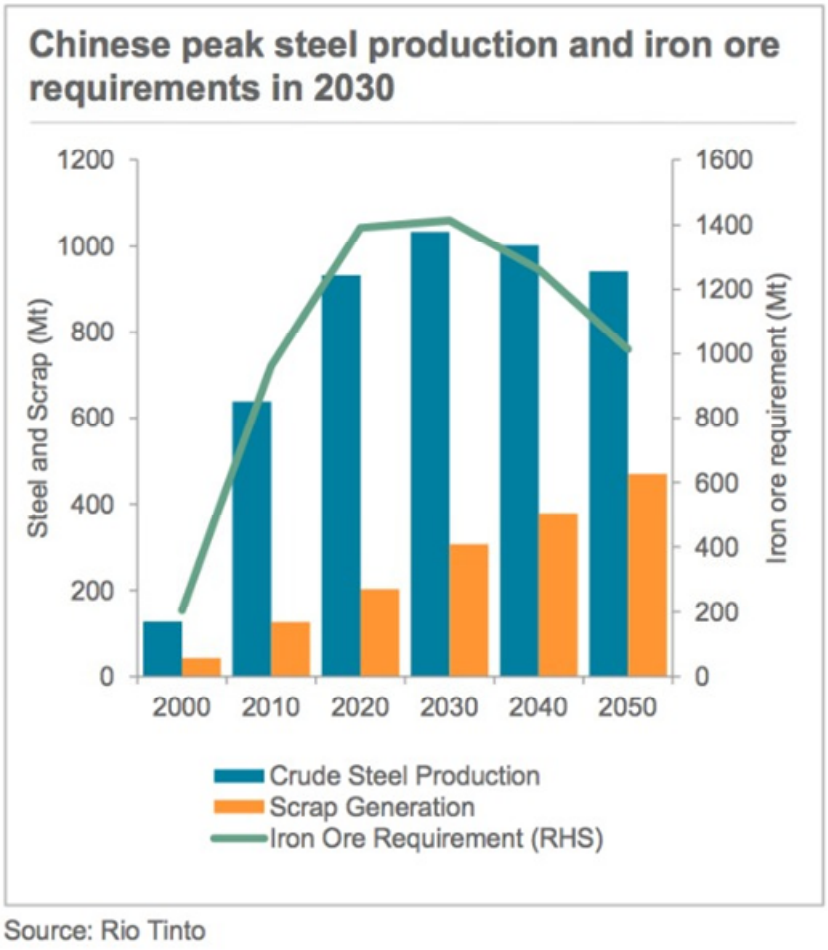

Figure 1.3 China's forecasted steel production and iron ore requirements up till 2050 (Els, 2012).

The bulk of the iron ore deposits in this region are from magnetite deposits even though there are also world class hematite deposits present, such as the Simandou deposit in Guinea which is being developed by mining giants Rio Tinto and Vale (Cope, 2008). The mining industry in general has seen a renewed interest in magnetite deposits even though hematite is usually higher grade, easier to mine, process and considered a direct shipping ore (DSO). The production costs for magnetite are higher as more energy is needed to crush and grind magnetite ore compared to hematite ore. Not all magnetite deposits will meet the customer specifications because the nature and amount of gangue minerals that are deleterious to the iron making processes can be as important as the amount of iron. It can be expensive to get rid of gangue minerals but the quality of the products from magnetite deposits could be excellent, clean and a

viable alternative to hematite. A good magnetite deposit can be beneficiated to between 4 to 6% higher iron content than a hematite DSO. Furthermore magnetite can be used in the production of pellets that are ideal for blast furnaces because they are not only a very clean high grade feed but also give high production rates and usually do not have problems with phosphorus, which is one of the major deleterious elements for steel makers. Phosphorus > 0.08 % limits the range of steels that can be produced from a particular ore (Clout and Simonson, 2005). There are also potential energy benefits to magnetite ores because less energy is needed to create steel from clean magnetite than from hematite thereby reducing green house gas emissions such as CO_2.

This study focuses on fresh magnetite deposits in Cameroon (Central Africa) and Liberia (West Africa), which weather and oxidise towards the surface forming hematite caps. These deposits are the Nkout Iron Ore Deposit in Cameroon and the Putu Iron Ore Deposit in Liberia. They are primarily itabirites (see Chapter 2) similar to those in Brazil. Figure 1.4 shows the study areas, as well as the property locations of companies actively mining or developing iron ore deposits in these emerging iron ore provinces. An understanding of how the geology of the deposits correlates with the metallurgical characteristics (geometallurgy) is crucial to their successful development. A particular feature of these deposits is the progressive weathering and alteration of the magnetite banded iron formations to goethite and hematite assemblages and also strong stratigraphic controls on the mineralization. It is also important to understand the elemental compositions and mineralogical relationships of the iron rich minerals in relation to deleterious elements such as phosphorus, aluminium, and silicon. The ease of beneficiation plays an important role in the evaluation of magnetite iron ore deposits. Other factors essential in evaluating magnetite iron ore deposits include; high iron recoveries, maximum concentrate yield and large reserves amenable to open-cast mining at reasonable stripping ratios (Plessis et al., 1997).

1.2 Description of the problem

The oxidised caps of the Nkout and Putu deposits contain significant quantities of goethite and clay minerals in addition to hematite. They are therefore mainly

hematite (martite) - goethite rather than a DSO hematite ore and need to be beneficiated before export. Martite is the name given to hematite that is a pseudomorph of magnetite. Goethite can incorporate elements such phosphorus, aluminium and silicon into its lattice (Ramanaidou et al., 2008) making it difficult to separate. These lattice-bound elements are much more difficult to remove than discrete mineral phases such as apatite. Goethite is also renowned for its relatively high loss on ignition (LOI) due to the presence of OH (Ramanaidou et al., 2008). Loss on ignition is a penalty property of iron ores as it devalues the cost of iron ore exports.

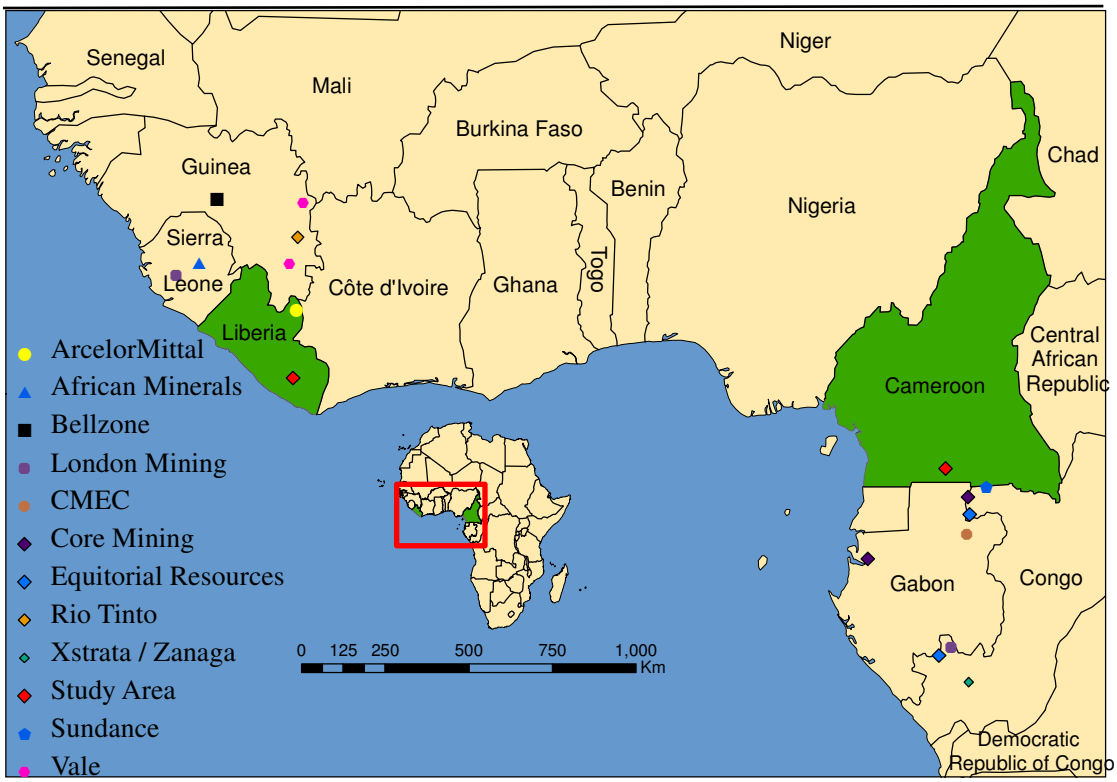

Figure 1.4 Selected companies and the locations of their iron ore projects in West and Central Africa (Modified from Afferro Mining, 2012).

The Nkout deposit is owned by International Mining and Infrastructure Corporation Plc (IMIC) and the Putu deposit is owned by Putu Iron Ore Mining (PIOM), a subsidiary of Severstal International. These companies aim to initially develop the potential martite-goethite deposit so that they can fund the mining of the magnetite ores. Hard hematite/goethite rocks are scarce in the areas and most of the martite-goethite ore occurs as laterites/saprolites. These, just as the magnetite ores, will have to be processed to increase their Fe content and at

the same time reduce their Al, P and Si contents. The magnetite to hematite/goethite ratio in a deposit determines routes of processing and hence operational costs. For example, since magnetite is ferromagnetic and hematite paramagnetic, magnetite can be removed using less expensive low intensity magnetic separation whilst hematite requires high intensity magnetic separation, which is relatively more expensive. This study aimed to improve the mineralogical and geochemical knowledge of these deposits and test their metallurgical performance during beneficiation, and as such can be described as a geometallurgical evaluation. The geometallurgical characterisation of these iron ore deposits, which marrying the geological, mineralogical and metallurgical properties of the iron ore, will not only aid the processing but also help to produce a flow sheet for mining of the ore.

Research on the geometallurgy of banded iron formations (BIFs) in Liberia and Cameroon is at an early stage. Work has been done in house by mining companies working in these areas especially using Quantitative Evaluation of Minerals using a Scanning Electron Microscope (QEMSCAN®) as a tool for the characterisation of these deposits but not much information is available to the academic world. A tool that can accurately differentiate been the various iron oxides can have greater positive effects on the economy of the projects than techniques that just use the chemistry. As more metallurgically complex deposits are developed and mining of large-scale, magnetite deposits becomes more commonplace, the significance of characterising their metallurgical response will increase.

1.3 Location of the study areas and previous work

1.3.1 Nkout Iron Ore Project

The Republic of Cameroon is located on the western edge of Central Africa. It is bounded to the south-west by the Gulf of Guinea, to the west by the Federal Republic of Nigeria, to the north by Lake Chad, to the north east by the Republic of Chad, to the east by the Central Africa Republic and to the south by the Republics of Congo, Gabon and Equatorial Guinea (Figure 1.5). The main cities in Cameroon are Yaoundé, the capital of Cameroon, Duoala, the commercial capital and largest city and Garoua the capital of the north region.

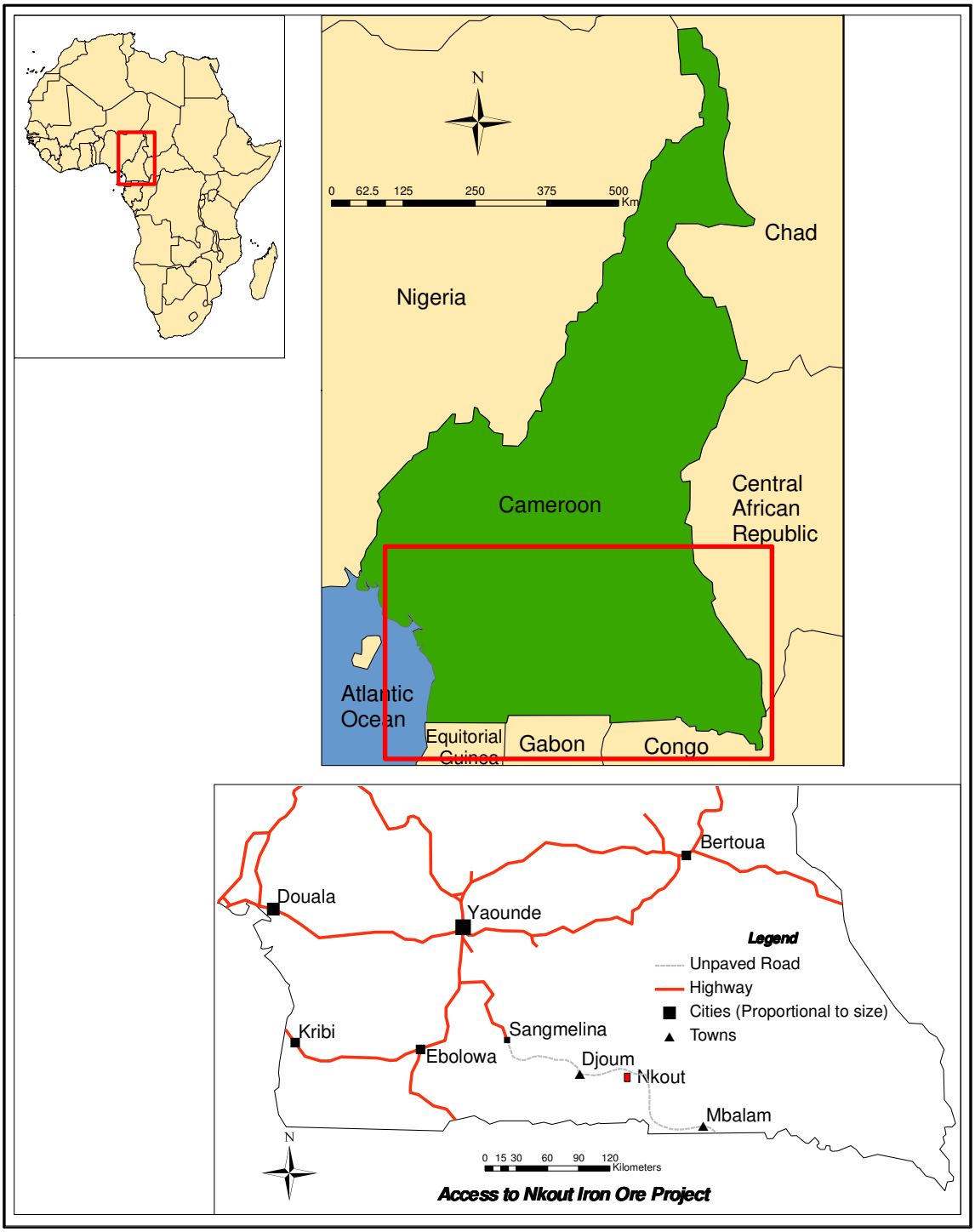

Figure 1.5 Location of and access to the Nkout Iron ore project with respect to Cameroon and Africa (modified from Afferro Mining Inc., internal reports).

The Nkout license is located approximately 284 km south east of the capital Yaoundé in the southern part of Cameroon. There is good tar road from Yaoundé to Sangmelima (approximately 150 km) and dirt road from there to the license (Figure 1.5). The major town closest to the license is Djoum which is approximately 120 km south east of Sangmelima and about 14 km north west of the license. Most of the casual workers working at Nkout live in Djoum and

other smaller villages in the vicinity whilst most of the professional and skilled members of staff are based on the camp site.

The Nkout deposit along with the nearby Ngoa deposit was discovered during reconnaissance geological mapping of the Abong Mbang West Map in the 1950s by the Bureau de Recherches Géologiques et Minières (BRGM) (Maurizot and Abessolo, 1985). Due to the remoteness of the area and the perceived small size of the deposit, no further work was done at the time. The BRGM studied the itabirites of the Nkout hills again in the 1980s after commissioning an airborne magnetic survey. The ground work was limited to ground control of a radiometric anomaly within nearby granitic formations even though the airborne magnetic data revealed a 10 km long dipole identified as a large, basic - ultra basic intrusive with associated BIF's which included the Nkout hills. A sample from Ngoa was found to contain 65 % iron and the strike extent of the Nkout deposit was estimated to be 8 km. The remoteness of the location and the small size of the deposit made the target of low interest at the time.

In 2008, African Aura Resources conducted a regional soil sampling campaign exploring for gold mineralization over central Nkout in its Djoum licence in southern Cameroon. The original license was to explore the surface and subsurface for gold, silver, copper, lead, zinc, uranium, platinum group elements and diamonds. The regional soil sampling survey was conducted over central Nkout with a line spacing of 100m and samples collected every 50m. The field geologists noticed strong magnetic deflections on their compasses and grab samples were collected for lab analysis. Iron mineralization was identified but as the regional survey was for gold, the mapping detail was insufficient to determine its full extent. A reconnaissance mapping program was then conducted at the end of 2008 focussing on iron mineralisation, and assays of some grab samples gave hematite+magnetite content greater than 90 % (~ 63% Fe) (Norton, 2009). Airborne magnetic and remote sensing data along with multi element analysis of the soil grids completed across the Nkout hill led to the investigation of its iron potential and subsequently the license was amended to include iron.

In 2009, a detailed preliminary mapping and reconnaissance sampling program was proposed to prepare for a future reconnaissance drilling program which tested the true iron mineralization potential of the deposit and the strike extent to the east and west in areas that had not been visited previously. Also in 2009, Suh et al., presented a paper entitled “Geology and ore fabrics of the Nkout high-grade haematite deposit, southern Cameroon” during the 10th Biennial SGA Meeting of The Society for Geology Applied to Mineral Deposits in Townsville Australia. Before this research, this was the only paper published specifically on the Nkout deposit though papers have been written on the nearby Mbalam (Figure 1.5) itabirite hosted iron ore district (Nforba et al., 2011) and several on the Congo craton (Shang et al., 2004; Lerouge et al., 2006). To date 54,500m has been drilled at Nkout.

1.3.2 Putu Iron Ore Project

The Republic of Liberia is located on the west coast of West Africa (Figure 1.5). It is bounded on the West by the Republic of Sierra Leone, to the north by the Republic of Guinea, to the east by the Republic of Ivory Coast and to the south west by the Atlantic Ocean. The Putu Iron Ore Project is located in the south-east of Liberia in Grand Gedeh County, approximately 320 km to the south-east of the capital city of Monrovia (Figure 1.6). The deposit is divided into two mountain ranges namely Jideh and Montroh which have different trends. Jideh has a NNE – SSW trend whilst Montroh has an E – W trend. There is a good tar road from Monrovia to Ganta (approximately 150 km) which is the border town with the Republic of Guinea. The major town closest to the deposit is called Zwedru (Figure 1.6) which is about 21 km south of the Putu Mountains and the road from Ganta to Zwedru is a laterite one. The deposit is in the outskirts of a small mining town called Tiamans.

Historical information on the Putu range goes back to 1953. The Putu iron ore deposit was discovered by the Liberian American-Swedish Mineral Company (LAMCO) in 1953 but operations were suspended due to the discovery of iron ore with DSO potential in Mount Nimba (Swindell, 1967). The Liberian government had 50 % shares in this company. In the late 60’s the license for the Putu range was secured by a joint venture between the Bong Mining

Company (BMC) and the German Liberian Mining Company (DELIMCO). Just like what happened with LAMCO, work on Putu was suspended when BMC and DELMCO merged to develop a much higher grade iron ore i.e. the Bong Mine.

Figure 1.6 Location and access to the Putu Iron Ore Mining Inc. (PIOM) project (modified from European Country of Origin Information Network, 2013).

The current ongoing exploration started in 2005 when the then Mano River Resources, secured the licenses for the Putu range. Mano River Resources went into a joint venture with Severstal of Russia in 2008 in which the shares

were divided into 38.5 % and 61.5 % respectively with the subsequent renaming of the company to Putu Iron Ore Mining (PIOM) Inc. Mano River Resources has since evolved into several companies including African Aura Mining Inc. when it merged with Africa Aura Resources and Afferro Mining in 2010 and its gold wing became a company in its own right. Afferro Mining has since sold its 38.5 % shares in PIOM to Severstal making them the sole owner of PIOM through their subsidiary company Lybica Holding B.V. To date over 60,000 m has been drilled at PIOM.

1.4 Geometallurgy of iron ores

Geometallurgical analysis can never be ignored in any project. All projects gain from these analyses and in many cases they have been responsible for saving projects from major errors (Ashley and Callow, 2000). The trend for integrating a geometallurgical approach as early as possible in the exploration cycle is particularly relevant to BIF-hosted iron ore deposits. There are multiple mineralogical, geochemical and physical parameters/characteristics of material types present within a potential iron ore body. These characteristics underpin the determination of industry standard indexes such as how fast the rock/product falls apart during transport (tumble, abrasion, decrepitation), or reduces within a blast furnace (Clout, 2003). Research which focuses on understanding a potential ore body from this broader perspective should enhance the ability of the deposit owner to develop a more efficient mine design and allow a more consistent control of the product(s). Two restricting factors could be the ability of an exploration team to gather relevant day-to-day data and also the deposit owners' understanding of what the downstream market requires.

1.4.1 What is and why geometallurgy?

Lamberg (2011b) gives a review on what is geometallurgy, why it is necessary in any project and how it should be conducted. He explained the traditional approach to mine development and highlighted the problems associated with it. The traditional approach comprises drilling of an ore deposit, interpreting the drill results and creating models which can be used for mineral resource

estimation. The next steps involve estimating the ore reserves, designing the mine, proposing a mining sequence and production schedule and finally evaluating the economy of the project. Some of the problems he pointed out include the fact that the ore reserve data does not include information on the spatial variation on metallurgical parameters and that ore boundaries are based on grades only. He also mentioned incomplete resource utilisation and poor risk management. According to Lamberg (2011b) "Geometallurgy combines geological and metallurgical information to create spatially-based predictive models for mineral processing plants."

Factors other than the absolute grade of the deposits obtained from chemical analysis of drill cores can seriously affect the economics of a project. These factors include recovery, physical competence and metallurgical variability which may have no relationship to the grade. A combination of all of this in a geometallurgical framework provides a basis for testing of all these parameters leading to well defined mineral domains and zones. Early in an exploration programme, when the core is only used for geochemical analysis, testing consumes between half and 2 g of material per test and a 1 or 2 kg sample may be sufficient to be representative. However analysis later in the project needs more sample. Metallurgical testing consumes 2.5 - 25 kg/test and typically 10 - 75 kg is requested (Forrest, 2009). Projects have failed because of lack of understanding of how the geology and mineralogy can affect metallurgical responses and thus cash flow.

In any feasibility through to exploitation program, it is important to have a clear understanding about what is termed the geometallurgy of the deposits. Steve Williams, President of GeoMet Tech Ltd (2010), defines geometallurgy as "the study of the drivers of metallurgical response that lie in the geology and mineralogy of the rock that is exploited". According to the geometallurgy branch of Société Générale de Surveillance (SGS) group of companies (2011), it is defined as the "geologically informed selection of a number of test samples to determine metallurgical parameters and the distribution of these parameters through an ore body using an accepted geostatistical technique to support metallurgical process modelling". These metallurgical parameters clearly lie in the geology and mineralogy of the deposits and their definitions has to include

the spatial distribution of the values. Understanding these is essential in developing a mining and treatment plan. The deposits have to be characterized based on zones with similar mineralogical, geological and metallurgical responses. Unlike grades, both proxies and absolute measures of geometallurgical variables are not necessarily linear or additive and therefore require very careful geostatistical consideration (Dunham and Vann, 2007).

Geometallurgy is an emerging field aimed at identifying either direct measures or proxies for throughput (hardness, grindability), recovery (liberation, mineral shape/texture, etc) and concentrate quality from easily collected macro, meso and microscopic data (Dunham and Vann, 2007). Developing the metallurgical testing program to define the geometallurgy of the deposit and select the optimum treatment scheme involves the utilization of all of the available information on geology, mineralogy, chemistry, and metallurgy. The physical and chemical aspects associated with the mineralogy and textures of the ore are the fundamental drivers of the metallurgical performance of that ore.

According to Williams and Richardson (2004), a geometallurgical mapping approach consists of several steps:

- Developing a geometallurgical matrix (geomatrix) using the geological model of the deposit,
- Using the geomatrix to guide sampling and compositing for further testing,
- Characterizing the ore samples or composites for a selection of geological, analytical, geotechnical, mineralogical, metallurgical and physical characteristics,
- Adding this data to the overall 3D model used for mine planning and economic projections.

Table 1.1 gives a summary of the important parameters according to Williams and Richardson (2004) from the various disciplines necessary for ore characterisation and the possible testing methods involved. Most of these tests are done on drill core samples and reverse circulation (RC) chips from the study areas.

Table 1.1 Tests that quantify various parameters important in ore characterization (Williams and Richardson, 2004).

Discipline	***Parameter***	***Testing possible***
Geology	Field relationships	Field mapping, drilling and drill core logging
Chemistry	Grade	Assays
Mineralogy	Zonation, mineral identification, association, size, texture and liberation	QEMSCAN® , X-ray diffraction, reflected light microscopy, scanning electron microscopy, energy or wavelength-dispersive X-ray microanalysis
Physical Properties	Hardness (Grinding)	Bond Work Indices, the JK Drop-Weight test, Sag Power Index (SPI), MacPherson 18'' mill test
Metallurgical Response	Recovery	Flotation kinetics, locked-cycle tests, GRG gold, sink/float tests, bottle rolls
Geotechnical Measure	Site preparation, Environmental review	Soil density, ground water flow, slope stability

SGS has proposed a six stage "geometallurgical framework" to group such activities (SGS, 2011). They are:

- Stage 1; Multivariate spatial domain definition – domains of like characteristics selected,
- Stage 2; Sample selection – based on geological data,
- Stage 3; Parameter determination (testing) – metallurgical data collected,
- Stage 4; Multivariate model definition – using geostatistics to distribute data collected in stage 3,
- Stage 5 – Multivariate spatial model generation using the block model or mine plan,
- Stage 6 – Joint mining and mineral processing optimization.

They have also proposed the following requirements for a geometallurgical program:

- Technical publications – Digital copies of existing technical reports and published papers regarding the geological, geotechnical, geophysical, geochemical, tectonic, mineralogical and textural information.
- Drill hole database – Digital copy of the existing drill hole database containing collar, survey, geological, geotechnical, geophysical and geochemical information along with any other relevant data.
- Plans, cross sections and perspectives – Digital copies of any existing plans, cross sections and perspectives including geological, geotechnical, geophysical, geochemical, tectonic, mineralogical and textural information in addition to any other relevant data.
- Spatial interpretations and models – Digital copies of the existing spatial interpretations (strings) and models.

Lamberg (2011b) acknowledged 8 steps in a geometallurgical program:

1. Collection of geological data
2. Ore sampling for metallurgical testing
4. Establishing geometallurgical domains
3. Metallurgical laboratory testing
5. Model to derive metallurgical parameters
6. Establishing process model for simulation
8. Model calibration
7. Plant simulations

Coward et al. (2009) proposed a “Primary-Response framework” for the classification of geometallurgical variables. These variables include recovery, grindability, throughput, power consumption, mineralogy and content of deleterious materials. Their framework divides the variables into primary (reflects intrinsic attribute of the rock) and response (the response of a variable to measurement process) and was designed to assist with developing sampling approaches and identifying the most appropriate spatial modelling approach. The proposed framework can also help identify the risks associated with the designing, sampling and modelling of both types of geometallurgical variables.

1.4.2 Sampling for Geometallurgy

In most cases, small amounts of samples are needed for mineralogical investigations and as such the sampling techniques and sampling statistics are crucial if samples are to be representative of the body. Samples should not only be representative of the bulk chemistry but also of the size and textural characteristics of the body being investigated (Williams, 2010).

Samples should be selected based on a thorough understanding of the geology, the chemistry and mineralogy of not only the ore zones but also the un-mineralized zones. This is to ensure that the full variability of the ore is being sampled as they need to reflect the geology and metallurgy of the deposit. Samples need to reflect the "significant" domains within the deposit i.e. anything that represents more than 10 % of the deposit known volume (Williams, 2010) but could also include smaller percentage volume domains if there were some particular, unique feature in that domain. Uniform ores would require less quantity of samples than ores containing randomly distributed valuable constituent.

Barratt and Doll (2008) presented examples of protocols for sample collection and preparation from drill cores that simultaneously returned comminution datasets suitable for tests designed by three different companies i.e. Bond Work Index based method (DJB Consultants), an a × b dataset (JK SimMet), and a set of Sag Power Index (SPI) results (Minnovex). By carefully collecting data for all three methods, high quality geometallurgical datasets can be created for three commonly used comminution models. The results of the three models may then be compared during a feasibility study. Although three of the most commonly used grinding circuit throughput calculations require different test work protocols, it is possible to sample a set of drill core in such a manner as to provide comparable data sets for all. In addition, results may be obtained that are suitable for resource assay, operating cost estimates, and a geotechnical parameter. Locations of selected samples should be discrete i.e. individually separate and distinct, as eventually a geometallurgical model would have to be created based on their spatial distribution. The amount of sample studied will depend on the stage of the project. For this kind of conceptual research it will be

smaller than that required for a feasibility study. Table 1.2 gives the possible amount of samples needed for specific tests in a geometallurgical mapping program as suggested by Williams and Richardson (2004).

Table 1.2 The possible amount of samples needed in a geometallurgical mapping program (Williams and Richardson, 2004).

Types of Test	*Number of Samples*
Assays	> 10,000
Mineralogy	> 1000
Grinding	100 - 300
Metallurgical Tests	100 - 300

1.4.3 Current Research in Geometallurgy

Organisations actively involved in geometallurgy includes, amongst others, the Australian Mineral Industries Research Association Limited (AMIRA), the Australasian Institute of Mining and Metallurgy, the University of Queensland, Australia, SGS, University of Tasmania, Australia, Luleå, University of Technology, Sweden, GeoMet Tech Ltd, the University of Johannesburg and CSIRO.

AMIRA is currently working on the P843A GeMIII (***Ge***ometallurgical ***M***apping and ***M***ine ***M***odelling) project with 21 companies. P843A is an extension of the P843 project and was initiated in 2009 with an expected life span of four years. The P843 project developed methodologies and tools to deliver predictive measures of processing performance which can be embedded in resource models and exploited in mine planning and optimization. The P843A project is conducting research in geometallurgy which “is recognized as a high-value activity that can deliver demonstrated operational improvements based on increased ore body knowledge”. In June 2010, JKTech, the Queensland, Australia-based technology transfer company for the Julius Kruttschnitt Mineral Research Centre officially opened a new geometallurgical testing facility at Sumner Park in Brisbane, Queensland. The 5,000 m^2 laboratory houses state of the art equipment and will be the main characterization testing facility for geometallurgical projects as part of the AMIRA P843A project. The new facility

will also allow JKTech to carry out commercial testing and provide industry-based training for sponsors of the project.

In mid July 2010, JKTech reported the launch of its new ore breakage characterization tool, the JK Rotary Breakage Tester (JKRBT). The JKRBT is claimed to rapidly generate highly repeatable ore breakage data for use in the design of autogenous (AG) and semi-autogenous (SAG) mills and crushers for new projects or for existing plant optimization projects. This data also has value for geometallurgical applications such as contributing to resource valuation and mine planning.

CSIRO in collaboration with some of its partners are presently involved in "the Minerals Down Under National Research Flagship project" (CSIRO, 2010). The aim is to develop technologies that will keep the Australian minerals industry globally competitive. For iron ore producers, these technologies include:

- Processes to halve the phosphorus content of high-phosphorus iron ores,
- Processes to remove or mitigate the effects of other impurities such as kaolinite and alumina,
- A new database that provides a clear picture of the nation's main iron ore reserves, their tonnage and chemical features.

As a result, Australia's ore reserve inventory is growing through sub-economic mineral resources becoming economically viable ore reserves. These deposits have already been discovered but their value cannot be realised due to technical or environmental limitations.

The University of Tasmania, Australia has a geometallurgy project, in collaboration with the Environment and Sustainability Institute, University of Exeter, that has quite a wide scope including "Predictive environmental indicators in mining" to measure and prevent environmental parameters such as acid mine drainage. This sub-project is titled "Theme 1 (P4A1) Predictive environmental indices" and according to the University of Tasmania "provides

early predictive information of intrinsic rock characteristics likely to impact on environmental performance and management during mineral processing, product manufacture and waste disposal. The underlying aim is to develop the foundations for a more predictive (and proactive) approach to early environmental characterisation that supports more effective management and valuation during mineral processing, and subsequent storage of waste" (University of Tasmania, CODES – ARC Centre of Excellence in Ore Deposits, 2013).

Geometallurgy research being carried out at Luleå, University of Technology includes establishing a geometallurgical program for the Malmberget iron ore deposit, northern Sweden (Lund et al., 2013). An element to mineral conversion technique has been developed using data from electron microprobe (EPMA), X-ray fluorescence (XRF) and SATMAGAN analyses. Bulk samples and size fractions were analysed with XRF, the amount of divalent iron was analysed with wet chemical titration and the amount of magnetic material was determined with a SATMAGAN magnetic balance. Element to mineral conversion is based on a set of linear algebraic equations where the bulk chemical composition of a sample is converted to mineral grades using a set of least-squares equations (Lund et al., 2013). The technique was validated using QEMSCAN®.

1.5 Aims and objectives of the research

This study aims to improve the mineralogical understanding of these deposits in order to predict their metallurgical responses. To achieve this, field work was conducted at Nkout and a total of 52 mineralised samples including quarter cores from 35 drill holes, grab and outcrop samples were studied in the field and brought back to the UK for laboratory studies which included whole rock geochemistry by XRF, EPMA, Scanning Electron Microscopy (SEM) and semi-quantitative XRD. Eleven half drill cores and nine crushed core samples representative of the Putu deposit were sent by the PIOM Chief Geologist at the time to Camborne School of Mines, University of Exeter for analysis.

With the knowledge gained from these analyses, the Nkout fieldwork exercise and knowledge acquired working as a geologist/geophysicist for Afferro Mining and PIOM, the subsequent main objectives of the research were as follows;

1. To determine micro scale detailed mineralogy and chemical data to understand the location and distribution of deleterious elements such as aluminium, phosphorus and silicon. Such knowledge could not only lead to the analysis of metallurgical parameters such as lump/fine ratios and ore grade, but forms the basis of impurity removal and beneficiation of the ore. A complete mineralogical and geochemical analysis of the samples will improve understanding of the mineral deposits and the knowledge gained will be used to predict metallurgical responses of the ore. Mineralogy in this context refers to the study of the behaviour of minerals during processing with the aim of assessing and, if possible, predicting metallurgical performance on the basis of the mineralogical information (Schouwstra and Smit, 2011). Other terms used by other workers to refer to the study and practice of the behaviour of minerals during processing includes applied mineralogy, ore-dressing and process mineralogy. The geochemistry part looks at the geochemical trends associated with the mineralogical changes from the magnetite itabirite to the enriched material.
2. To develop a method of ore characterisation using QEMSCAN® automated mineralogical analysis that distinguishes the key iron oxides and iron hydroxides; mainly magnetite, hematite and goethite.
3. To conduct metallurgical testing on the samples analysed in order to verify the results of the QEMSCAN® study as the recovery of the iron minerals is usually a function of the ore mineralogy. The metallurgical tests will be both low and high intensity magnetic separation.

1.6 Thesis Layout

The layout of this thesis is such that chapters 1 to 3 are considered to be introductory chapters. Chapter 2 gives a review of the global distribution of banded iron formations and iron ore deposits. Emphasis is placed on the processing of iron ores including processing options, smelting for iron and steel

and metallurgical testing. Chapter 3 describes the geology of the study areas from a regional, national and deposit point of view based on literature.

Chapter 4 summarises the results of the field work carried out at Nkout and takes a detailed look at the geology of the Nkout deposit partly based on interpretation of a ground magnetic survey I conducted on the Nkout deposit. The material type classification that was used at Nkout at the time of the field work was analysed and the proposed classification used in this research presented.

Chapter 5 explains the analytical methods of XRF, SEM/EDS, optical microscopy and EPMA used in this research including the general sample preparation.

Chapter 6 and 7 document the mineralogy and geochemistry of the Putu and the Nkout iron ore deposits respectively. Sample locations were not considered for Putu as the samples are not sufficient to make conclusions based on locations even though they are representative of the deposit.

Chapter 8 details the QEMSCAN® work including differentiating the iron oxides, i.e. goethite, hematite and magnetite. A huge part of the variability that a deposit may show will be in its mineralogy across the deposit and as such quantitative mineralogy lends itself to the research environment because it adds the capability to manipulate and assess massive datasets derived from mineralogical relationships. The complete identification of the modal mineralogy, mineral phases present and particle sizes in relation to degree of liberation and mineral associations are presented.

Chapter 9 documents the low and high intensity magnetic separation metallurgical tests carried out and synthesizes the results with those obtained from the QEMSCAN®.

Chapter 10 discusses the main findings of the research, how this work may be applied to other deposits in the world, lists the conclusions and suggests future work that could be done.

Appendix 1 details the XRF results for all the samples studied whilst Appendix 2 gives the EPMA data used in this thesis. Appendix 3 gives the QEMSCAN® data which includes modal mineralogy, mineral association, liberation and theoretical grade recovery charts for the samples. Appendix 4 gives the paper "Quantitative mineralogical and chemical assessment of the Nkout iron ore deposit, Southern Cameroon" published in Ore Reviews Journal and the extended abstract "A comparative automated mineralogical analysis of the Nkout (Cameroon) and Putu (Liberia) iron ore deposits" which was an oral presentation at the 12th SGA Biennal Meeting, Uppsala, Sweden. Both papers are based on the research reported in this thesis. Appendices 1 to 3 are copied to a CD accompanying this thesis.

Chapter 2

Review of Iron Ore Properties, Processing, Metallurgical Tests and some Global Deposits

2.1 Definitions

The first widely accepted definition of an iron formation was by James (1954) who defined it as “a chemical sediment, typically thin-bedded or laminated containing 15 percent or more iron of sedimentary origin commonly but not necessarily containing layers of chert”. This definition was modified by Trendall and Morris (1983) and then by Klein (2005) by not restricting the iron percentage to a minimum of 15 %. According to Klein, the principal chemical characteristic of an iron formation is an anomalously high content of iron, with anomalous meaning higher than contemporaneous volcanic rocks.

An ore is defined as “A metalliferous mineral or an aggregate of metalliferous minerals, more or less mixed with gangue, which from the standpoint of the miner can be won at a profit, or from the standpoint of the metallurgist can be treated at a profit. Economically mineable aggregates of ore minerals are termed ore bodies, oreshoots, ore deposits or ore reserves” (Evans, 2009). As such an accumulation of iron bearing minerals that can be suitably mined commercially is referred to as an iron ore deposit.

2.2 Properties of iron ore

2.2.1 Introduction

The main oxides present in iron ore are hematite, magnetite, goethite and to a lesser extent limonite. Iron ore consisting entirely of hematite is referred to as pure iron ore and contains a maximum of about 70 wt % iron. The maximum contained iron in magnetite and goethite ores are about 72 wt % and 63 wt % respectively. Direct shipping ore (DSO), which is usually hematite ore, used to be > 65 wt % Fe but nowadays many projects classify DSO as approximately 60 wt % Fe, which is about 85 % Fe_2O_3. Other iron bearing minerals that could be present are the silicates and carbonates of iron. The presence of additional

minerals reduces the amount of recoverable iron. Table 2.1 gives the chemical formulae and percentage iron of the common iron ore minerals.

Table 2.1 Iron bearing minerals in iron ore (formulae from Deer, Howie and Zussman, 1992).

Group	*Mineral*	*Chemical Formula*	*Weight % Fe*
Oxides/ Hydroxides	Hematite	Fe_2O_3	69.94
	Magnetite	$Fe^{2+}Fe_2^{3+}O_4$	72.36
	Goethite	$FeO(OH)$	62.85
	Limonite	$FeO(OH).n(H_2O)$	62.85
Silicates	Stilpnomelane	$(K,Ca,Na)(Fe^{2+},Mg,Fe^{3+})_8(Si,AL)_{12}(O,OH)_{27}.n(H_2O)$	29.54
	Minnesotaite	$(Fe^{2+},Mg)_3Si_4O_{10}(OH)_2$	30.48
	Grunerite	$Fe_7(Si_8O_{22})(OH)_2$	39.03
	Chamosite	$(Fe^{2+},Mg)_5Al(AlSi_3O_{10})(OH)_8$	29.43
Carbonates	Ankerite	$Ca(Fe^{2+},Mg,Mn^{2+})(CO_3)_2$	16.24
	Siderite	$FeCO_3$	48.20
	Ferroan dolomite	$CaFe(CO_3)_2$	16.24
Sulphide	Pyrite	FeS_2	46.55
Iron Titanium Oxide	Ilmenite	$FeTiO_3$	36.81

The value of a low grade ore depends on factors such as the composition of the ore minerals, transport costs and distance to market. They need to be beneficiated which incurs costs in infrastructure and other operating costs. Iron ore concentrates must meet certain sales specifications, especially with respect to deleterious elements such as silica/quartz (SiO_2), phosphorous (P_2O_5), aluminium (Al_2O_3) and also weight loss-on-ignition (LOI) which mainly relates to the abundance of carbonate, goethite and clays. Alkalis such as potassium and sodium are also deleterious to the iron making process. With technological improvements, sales specifications vary from customer to customer so figures given here are just for a general scenario. SiO_2 is almost always present in iron ore but typically needs to be below 3.0 wt %. Phosphorus should be less than 0.08 wt % as above this quantity, iron becomes brittle and very high concentrations of phosphorus render the iron unusable. Al_2O_3 should be less than 2.5 wt % as it increases the viscosity of the slag and this slows down the

furnace operation. K_2O and Na_2O must all be kept as low as possible as they are also present in other raw materials used in the sinter and iron making processes. They accumulate in blast furnace in the form of carbonates, intercalation compounds of carbon and complex silicates and these compounds decompose in the lower part of blast furnace to give metallic alkali which consume high heat and reduce the same in colder region during condensation (Sarkar and Subrahmanyam, 2009). Clout and Simonson (2005) gives a more detailed look on the effect of deleterious gangue and minor and/or trace elements on downstream process performance.

The physical and metallurgical behaviour of an iron ore during mining, processing, transport and the production of iron and steel are also critical to its value. The markets require that iron ore must be within certain tolerances and exhibit consistency in particle size, mechanical strength, reducibility and permeability. Particle sizes from 6.30 mm to 31.50 mm are classified as lumps and up to 6.30 mm as fines for sinter agglomeration (Clout and Simonson, 2005). Pellets range in size from 8.0 mm to 18 mm and are produced by beneficiated feeds of less than 1 mm.

2.2.2 Mineralogical types

There are three principal types of BIF hosted iron ore deposits. These are high grade hematite ores containing 60 to 68 wt % iron, martite-goethite ores containing 56 to 63 wt % Fe and magnetite ores containing about 15 – 40 wt % Fe. Hematite pseudomorph after magnetite is referred to as martite. The high grade hematite could be divided into itabirite derived residual and microplaty hematite replacement (Clout and Simonson, 2005). Itabirites are metamorphosed BIF and hence can have a distinct mineralogy from the BIF protolith which could be any of the associated rocks such as the meta-sedimentary rocks or granites.

Itabirite is a term that originated from the province of Itabirito (Pico de itabirito), in the state of Minas Gerais in Brazil which hosts major banded quartz hematite magnetite metamorphosed oxide facies BIF. The quartz has been recrystallized into megascopic quartz and the iron can exist in the form of hematite, martite

goethite and magnetite. This region of Brazil hosts major deposits, encompassed by the Quadrilatero Ferrifero, and was once linked to the Congo Craton (Tohver et al., 2006) and West African Craton which host similar deposits in West and Central Africa. The Nkout and Putu deposits are oxide facies iron formations similar to those in Brazil in terms of their geological setting, chemical and mineralogical setting. This relationship can be explained using plate tectonics as it is postulated that both areas were once together before the drifting apart of the continents (Figure 2.1).

Figure 2.1 Paleogeographic reconstruction of Africa and South America at 180 Ma (modified from Zanaga iron ore, 2010). Sizes are relative and the patches represent single or group of deposits.

Hematite ores consist of crystalline hematite and martite with usually less than 15 wt % goethite and less than 0.06 wt % phosphorus (Morris, 2002). Microplaty

hematite could also be present. Direct shipping ore exploitation is currently dominated by Australia, South America and Asia. Extremely friable, high grade hematite iron ore powders occurring in nature are referred to as blue dust and they are common in India (Roy et al., 2008).

Martite-goethite ores could also require some amount of beneficiation to increase the iron content and get rid of penalty elements. Approximately 90 % of BIF hosted ores in the Hamersley province are of the goethite–martite type (Harmsworth et al., 1990). Goethite content is usually greater than 50 % and is responsible for higher phosphorus content (0.07 – 0.17 wt %).

There are various forms of magnetite deposits. These include itabirites magmatic / volcanic, alluvial accumulations from volcanic formations, skarn and hydrothermal deposits and magmatic accumulations of massive magnetite. Magnetite ore usually contains less penalty elements and could be beneficiated to grades higher than those for a hematite DSO.

2.3 Processing of iron ore

2.3.1 Introduction

Iron ores are processed so that they will meet the requirement of clients in preparation for smelting and also to maximise the recovery and yield of iron minerals. It is necessary to upgrade lower grade ores before selling to markets around the world and this is often done in sites close to the mine in order to save transportation costs of the raw material. This process of upgrading the ores is called beneficiation and has been defined as follows; “Concentrating the mineral content of an ore by ore-dressing, smelting and pelletizing” (Mayhew, 2004). Beneficiation techniques include washing, sizing of particulates, and concentration. Concentration involves the separation of valuable minerals from the other raw materials received from a grinding mill. The crushed ore is screened to various size fractions. Ore dressing involves concentrating the iron rich phases into small bulks by removing the gangue minerals. Distinguishing properties of the iron rich phases compared to the gangue or waste e.g., magnetism, wettability, density, size, are used to concentrate the ore.

Smelting is the means by which iron metal is separated from the iron rich minerals and it is done by heating the ore to a high temperature in a furnace in the presence of a reducing agent and a fluxing agent.

2.3.2 Comminution (crushing, grinding), scrubbing and screening

The aim of comminution is to liberate the iron-bearing minerals from the gangue. The iron bearing mineral goes to the concentrate and the gangue to the tailing product. Comminution involves a single or multistage process of crushing of the run-off-mine (ROM) accompanied by grinding to a particular particle size which should have been predetermined by mineralogical studies. Crushing is usually done to about 6 - 14 mm and grinding down to micrometer sizes. The crushed material is composed of not only well liberated iron bearing minerals and gangue but also particles that contain both mineral and gangue referred to as middling particles. These middling particles are selected according to their mineral content and could be classified as one of three options: concentrates, tailings or separated for further grinding to enable further liberation.

This liberation particle size differs from deposit to deposit. Optimum liberation is necessary for the physical separation of the iron rich minerals and the gangue minerals. It is therefore important to get this particle size right as over-grinding does not only lead to excess power consumption raising processing cost, but may have a negative effect on the different separation processes (Wills, 1977). At the same time, poor liberations lead to poor recoveries of the iron rich minerals and results in a poor quality final product.

There are usually several stages of crushing of the ROM. Primary and secondary crushing these days are done mainly by Jaw, Gyratory, Kawasaki and Cone crushers. In the 19th century, Cornish stamps were used to break tin ore. Jaw, Gyratory and Kawasiki crushers can handle soft to very hard materials and are common features in heavy mining projects. Cone crushers are suitable for medium hard to very hard materials. Crushers consist of a set of manganese steel jaws in which one is fixed and the other moves in a back and forth motion relative to the fixed jaw. The size of the material is progressively

reduced as it travels through the crusher until they are small enough to escape at the other end. Cone crushers and High Pressure Grinding Roll (HPGR) are mainly used for tertiary crushing. Breakages produced by HPGR are mainly along mineral boundaries which lead to less energy consumption and better liberations.

Grinding systems are a major and critical component of any mineral processing facility. They apply force to reduce the sizes of the mineral grains so that the valuable mineral is liberated. There are two main types of grinding; Autogenous (AG) and Semi-Autogenous (SAG). For autogeneous grinding the feed material itself is used as the grinding media in a tumbling mill whereas for semi-autogenous grinding there is a supplementary grinding media which are usually steel balls in addition to the feed material in the mill. Both types of mills are used to grind ROM ore directly or products from primary or secondary crushers. This is determined by the size of the feed to the mills which has to be restricted to sizes that can be conveyed and supplied to the mill. The products of the mills could either be ready for further processing or sent for further grinding in a ball mill or pebble mill. Ball mills can grind ores to 35 µm or finer. Its feed can come from products of crushing and screening but also from primary AG and SAG grinding. For hard ores, the normal feed size is about 6 mm or finer whereas for soft ores it is 25 mm or finer.

Even though DSO material type typically has Fe ≥ 60 wt %, deposits may contain gangue elements/minerals concentrations over the customers' specifications. Quartz, Al oxyhydroxides and clay minerals are the main gangue found associated with DSO material (Clout and Simonson, 2005). After the crushing and grinding stages of the ROM, the next stage is referred to as scrubbing and is accompanied by the use of water to rinse the material as it is being scrubbed. Scrubbing is more suitable for ore that will be sold as lumps rather than fines. The main reasons for scrubbing are to get rid of the gangue and to separate the lumps from the fines. In the case of low grade material, simple washing and scrubbing cannot upgrade the iron content to a satisfactory level (Das et al., 2007). Fines are generated from secondary crushing and during the scrubbing process. Desliming is the process used to separate the finest fractions which are not required amongst the lumps. Scrubbing prior to

screening is also important in achieving acceptable screening efficiencies (Maxton et al., 2003). The alumina and silica content are expected to be lowered while the iron content increases proportionally (Timbillah, 2007). However, according to Singh et al. (2010), washing (scrubbing and screening) helps in removal of adhering clay and quartz to produce free flowing lumps and sand but the alumina content of lumps was not significantly lowered for the samples they worked with.

There are two main types of scrubbers; rotary scrubbers and attrition scrubbers, and they are particularly useful for lateritic iron ores. According to Mclanahan (2014), attrition scrubbers, (also known as attrition cells), are used to liberate deleterious material and remove it from competent aggregate material. Attrition scrubbers produce a high shear environment wherein the ore particles scrub against themselves to scour their surfaces and liberate deleterious materials. Rotary or drum scrubbers are robustly built steel structures with a rotary drum made out of steel plates. The rotary scrubbers rotate on carrier rollers made up of hardened steel and the ore to water ratio is adjusted as desired but is usually 1:2, respectively.

Laboratory scale scrubbers are used for metallurgical test work. Laboratory scrubbers can have dimensions of 0.5 m diameter and 1 m length, or 0.75 m diameter and 1.5 m length (SGS, 2014). Scrubbing and screening facilities are designed to process ore material in tonnes per hour (tph). For example in Maxton et al. (2003), a 3 m diameter by 7.6 m long rotary drum scrubber, along with the screening facility, was designed to process 800 tph of ore material.

Screening is the simplest process used to separate particles into various size fractions, known as sizing. The particles are passed through a number of screens with various aperture sizes. In ore bodies with high moisture and clay content, crushing and screening can be difficult and it may be economical to send them directly into AG or SAG mills (Dunbar, 2012). These mills can grind not only to similar sizes as crushers and screening will achieve but also to those produced in rod mills and ball mills. Using the AG/SAG mills instead of crushers, rod and ball mills could significantly lower operating and maintenance costs.

2.3.3 Mineral separation

Processing of an iron ore depends to a large extent on the type of deposit. After the comminution and screening phases, a DSO will be split into lumps and fines. Lumps are generally richer in iron and contain less penalty elements compared to fines. This is because the Al_2O_3 and SiO_2 tend to be associated with the finer clay particles (Howard et al., 2005).

It is necessary to know the amount and variation of magnetite to hematite present in a particular iron ore deposit as they require different roots for beneficiation. In fact this knowledge is critical to getting some ideas about not only the process that will be involved in the beneficiation but also give an idea of the costs involved. The proportions of magnetite to hematite are responsible for varying capital and operational cost as magnetite can be removed using less expensive low intensity magnetic separation whilst removing hematite requires high intensity magnetic separation which is relatively more expensive. Magnetite is ferromagnetic and hematite, paramagnetic resulting in magnetite being more magnetic than hematite hence hematite requires much stronger magnets than those required for magnetite separation.

The method used for processing hematite is dependent on the particle size under consideration. For lumps and fines greater than 1 mm, the most effective methods are dense media separation (DMS) or jigging which is based on the specific gravity of the materials being processed. Dense media separation is a form of gravity concentration but unlike gravity separation which uses only water or air as the main medium, DMS as the name implies requires a dense medium. The media may be dense organic liquids but are now mainly suspensions of ferrosilicon (FeSi) in water. Even though DMS has a higher operating cost than jigging, it results in a much more efficient separation which leads to optimum recovery and lower tailings grade.

For hematite fines less than 1 mm, one of or a combination of the following processes can be used; Spirals, Teeter Bed Separator (TBS), Wet High Intensity Magnetic Separation (WHIMS), SLon Magnetic Separation and Flotation (King, 2009). Spirals separate components in slurry (wet spiral

separators) based on differences in particle density and hydrodynamic properties. The larger and heavier particles will sink to the bottom of the sluice faster than the lighter ones where they experience more drag and hence move slowly and concentrate toward the centre of the spiral. The lighter particles remain in the outside of the spiral with the water and reach the bottom of the spiral faster where they are separated using adjustable bars, channels or slots.

Teeter bed separators (TBS) are classifying vessels with an evenly distributed upward flow of water in which the feed settles. When water is introduced, the minerals teeter. When the velocity of the falling particles equals that of the upward flow of water, the particles will not fall to the bottom of the vessel. The denser grains will then move to the bottom of the column whist the lighter ones move to the top where they are discharged to an overflow. The specific gravity of the minerals is the basis for this separation process.

During magnetic separation, the particles are moved in a magnetic field. Separation can be based on the magnetic field strength or the magnetic field gradient. The different techniques which may be operated in a wet (W) or dry mode include; high intensity magnetic separation (HIMS), high gradient magnetic separation (HGMS) and low intensity magnetic separation (LIMS). In order for WHIMS to be effective, there should be a significant difference in magnetism between hematite and the gangue minerals and the gangue should not be paramagnetic. A matrix such as grooved metal plates or filamentary materials is introduced into a circuit of magnetic separators to generate disturbances enabling fine and weakly magnetic materials to be separated. The matrix acts like a filter which collects magnetic particles and allows non-magnetic minerals to pass through. The combination of the magnetic field and the matrix leads to areas of rapidly changing high intensity magnetic field i.e. high gradient. The difference between HGMS and HIMS is that HGMS processes materials by batch while HIMS is a continuous process.

SLon magnetic separation was developed in China (Xiong, 1994, Svoboda and Fujita, 2003) to overcome multiple disadvantages with the WHIMS technology which has long been available for the separation of paramagnetic materials, but traditionally has encountered inefficiencies with finer feeds (< 100 μm). The

basic difference between WHIMS and the SLon is that in SLon, the slurry within the matrix is exposed to the forces of gravity and hydrodynamic pulsations resulting in better separation in the magnetic field. The non-magnetic particles pass through the matrix pile into the tailings box (Hearn and Dobbins, 2007).

Flotation is mainly used to add additional recovery, especially getting rid of quartz which can still be higher than the customers' requirement even after upgrading using other techniques. The process makes use of differences in hydrophobicity of the iron ore minerals and the gangue i.e. the extent to which they can be dissolved or mixed easily with water. This property can be increased by the use of surfactants and wetting agents which alter the surfaces of the particles so that they are either repelled or attracted by water. Wetted particles will sink to the bottom whilst un-wetted will attach themselves to the air bubbles, float in the froth and are removed. There are two types of flotation; reverse and forward. Forward flotation is used to float fine sized iron oxide whilst reverse flotation float the gangue e.g. quartz. Quartz is made hydrophobic and attaches to air bubbles in a stable froth using an anionic collector for silica separation and overflows the flotation cell (Zou, 2007). The enriched iron is collected at the bottom of the cell.

Magnetite is separated mainly using wet LIMS and TBS (King, 2009). Flotation is used for fines less than 75 µm for additional recovery and the removal of quartz which tends to be concentrated in fines. Magnetite can be concentrated to greater than 65 % Fe and then used to make pellets which command high prices in the iron ore markets because they are used as direct feeds in smelting plants. Pellets are formed by mixing the ground ore with a binder and fired in a grate kiln. Pelletisation was developed in India to utilise ultra fine concentrates including "blue dusts" that are generated in beneficiation plants. Blue dusts refer to very fine, soft powdery hematite which has a steely blue-grey colour. Unlike fines which restrict air flow during smelting, air can pass between the pellets decreasing the resistance of air flows during smelting.

2.4 Smelting for iron

2.4.1 Introduction

Smelting is defined as the process of separating a metal from its ore by heating the ore to a high temperature in a suitable furnace in the presence of a reducing agent, such as carbon, and a fluxing agent, such as limestone. Iron ore is smelted in this way so that the metal melts and, being denser than the molten slag, sinks below the slag, enabling it to be removed from the furnace separately.

2.4.2 Blast furnace

Reduction of iron ore in a blast furnace is the most advance method of iron ore smelting. Figures 2.2 illustrate a traditional blast furnace (Cope, 2008). The blast furnace is fed with a mixture of iron ore, charcoal or coke and limestone at the top with hot air blasts at the base. The iron ore can be in the form of lumps or agglomerated pellets or sinter fines (Goldring, 2003, Firth and Boucher, 2007). Lumps and pellets are direct feeds whilst agglomerated sinter is mixed with carbonate. The coke reacts with air to form carbon monoxide (CO) and heat which drives the smelting process. The limestone decomposes forming CO_2 and removes impurities and gangue minerals forming slag ($CaSiO_3$). The CO_2 reacts with more coke forming more CO. The ratio CO/ CO_2 must be kept at about 1:1. A greater ratio will produce soot whilst if lesser, there will be excess C forming CO. The ratio by weight of iron ore to coke to limestone is approximately 2 : 1 : 0.3.

As the iron ore feed descends down the furnace chamber, the temperature is increased resulting in the reduction of hematite to magnetite at temperatures of less than 900 ^oC and then first to wüstite (FeO) at temperatures above 900 ^oC. Molten iron is formed at temperatures of approximately 1200 ^oC and is deposited in the hearth zone at the base of the furnace below the hot air flow zone. Gangue elements such as Al, Ca, Mg, Mn and Si are reduced by C and are mixed with the slag which forms on top of the molten iron preventing it from being oxidised. If these gangue elements are not retained in the slag, they could

vaporise as reflux and condense on the linings of the furnace causing damage even when their initial concentration in the iron ore was small.

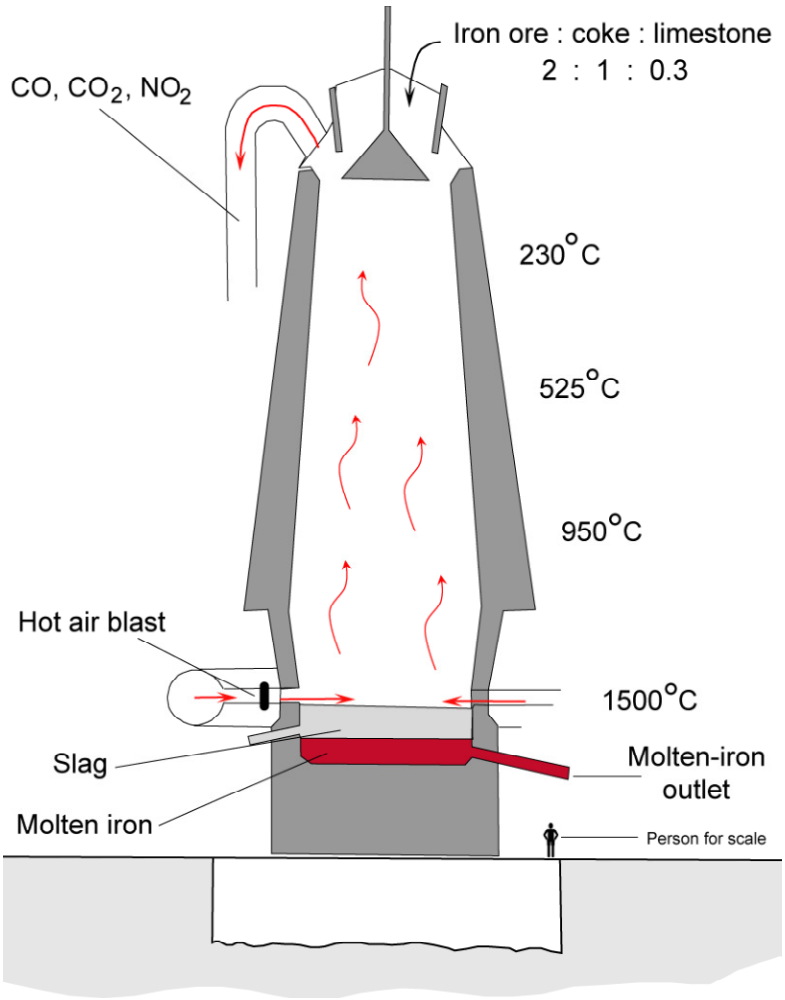

Figure 2.2 A traditional blast furnace (after Cope, 2008).

The final product of iron ore smelting is known as pig iron and is removed from time to time during the process. It normally contains amounts of carbon (~ 5 %), phosphorus and sulphur (~ 2 %). Pig iron is used directly as feed for steel smelting or sold. The relationship between steel and iron makers and their suppliers is usually long term with supply contracts of 15 to 20 years. This is because furnaces are designed to perform consistently for iron ores that meet the customers' specific requirements. This maximises the efficiency and productivity of the furnace.

2.4.3 Other iron making technologies

Other methods of obtaining iron from iron ore have been sought because blast furnaces are relatively expensive to install run and maintain. The feed for a blast furnace has to be in the form of lumps, sinter or pellets. This means that iron ore fines need to be converted to one of these forms increasing costs. Research into using the fines directly in the iron making process was therefore necessary. Furthermore coal has to be converted to coking coal for it to be used in a blast furnace. The process of sintering and coke making not only adds to operating costs but increases environmental pollution and this has lead to research into using coal directly. Finally, blast furnaces are designed to operate non-stop and are difficult to start and to switch off. The current other iron making technologies could be divided into two broad groups. These are those producing non-liquid iron and those producing liquid iron.

2.4.3.1 Non-liquid Iron - Direct Reduced Iron (DRI)

The main non-liquid iron making process is the direct reduced iron process. In this method, the iron ore is directly reduced in the solid form at temperatures from about 800 to 1050 ^{o}C. It can use lumps, pellets and fines and the reducing agents are H_2, CO or coal. The operating costs are lower compared to that of a blast furnace and this technology has been commercialized. The product of DRI is referred to as sponge iron. The disadvantage of using DRI is that the sponge iron is susceptible to oxidation and rusting if left unprotected. Furthermore hot DRI forms hydrogen when in contact with water and this can lead to fatal explosions. As such they are normally quickly processed to steel requiring the iron and steel making facilities to be close-by to overcome these potential problems.

2.4.3.2 Liquid iron - HIsmelt process

Rio Tinto and its partners (Nucor, Mitsubishi and Shougong groups) have developed a novel process of converting iron ore fines and waste iron bearing minerals into pig iron with an iron content of approximately 96 %. This process is called the ***H***igh ***I***ntensity ***Smelt***ing process i.e. HIsmelt process (Figure 2.3).

The HIsmelt method differs from other blast furnaces in that iron ore, coal and limestone are not fed at the top of the furnace but the process uses a metal bath with dissolved carbon as the main reaction medium (HIsmelt cooperation, 2008). Dissolved carbon leads to much faster smelting rates. As the feed is poured directly into a liquid bath, it results in a strong turnover of the liquid which minimises the temperature gradient in the bath. The process fuel is ground non coking coal eliminating the need of making coke. The feed can be flexible and does not have to be agglomerated fines or pellets. Energy consumption is less than other blast furnaces resulting in lesser environmental emissions.

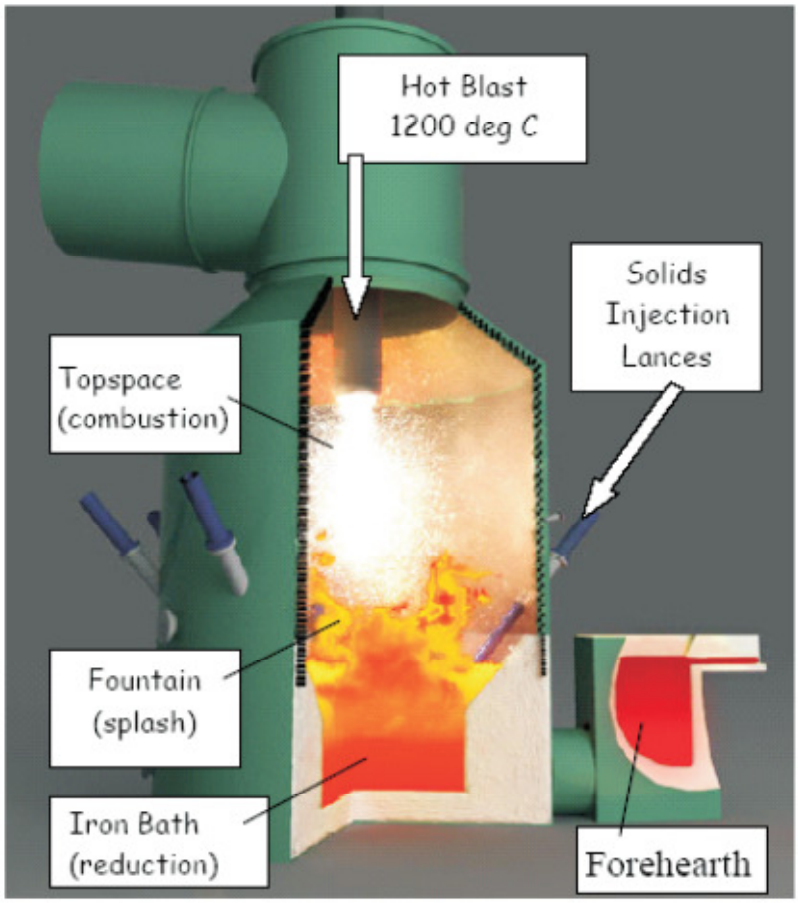

Figure 2.3 The HIsmelt technology (HIsmelt cooperation, 2008).

2.4.3.3 Liquid iron – COREX and FINEX

These technologies are from Siemens VAI for the COREX and a collaboration between Siemens VAI and Research Institute of Industrial Science and Technology, Korea, in the case of FINEX. A major difference between these

technologies and the HIsmelt process is that they require two vessels and two stages; the reduction and smelting occurs in different vessels. Emissions are low meaning that they have a lower environmental impact and they have flexible operations in terms of production output. Even though they are the most successful smelting and reduction (SR) technologies, the COREX cannot use fines directly and these need to be converted to sinter feed or pellets. In addition the volatile matter in non-coking coal is maintained at ~ 25 %. The FINEX is a subsidiary to the COREX process that uses iron ore fines directly.

2.5 Smelting for steel

Steel can be made using amongst others, the Basic Oxygen Steelmaking (BOS) furnace or the Electric Arc (EA) method. Pig iron is the feed for BOS whilst EA can use both pig iron and scrap metal and EA requires high energy (Goldring, 2003). As with iron ore smelting, limestone is added to form slag with deleterious elements such as silicon and phosphorus. Silicon and phosphorus react with oxygen to form acidic oxides which reacts with limestone to form compounds such as calcium silicate and calcium phosphate which are removed in the slag. Pig iron contains dissolved carbon and sulphur which are removed by blowing oxygen through the molten iron. Controlled amounts of carbon are added to increase strength and hardness, nickel and chromium are added as coating to form stainless steel. Depending on the final product, other alloying elements could be added.

2.6 Metallurgical testing

2.6.1 Metallurgical properties

Several standard industry tests are available to quantify metallurgical properties of iron ore including clustering, reducibility, thermal breakdown and swelling (Varajão et al., 2002). These tests include abrasion index (AI), tumble index (TI), decrepitation index (DI), drop tower test, reduction degradation index (RDI) and reducibility index (RI) (Clout, 2003).

Abrasion index and tumble index are used interchangeably and they are a measure for evaluating the resistance of iron ores to size degradation by impact

and abrasion. This impact and abrasion occurs during mining, handling and transport to the markets. Decrepitation index is a measure of the potential of lumps to crack due to rapid heating when fed into the furnace. The test portions are further screened to different grain size in order to determine the DI based on the different mass ratios. Reduction degradation index indicates how fast this occurs purely as a result of progressive reduction whilst reducibility index gives an indication of the ease of reduction of iron ore lumps. The tumble strength test provides a measure of the behaviour of the burden material under load, subject to impact and abrasive forces.

2.6.2 Drop Tower test

The Drop Tower test is becoming an integral part of an iron ore test work program, and is used to predict the final lump/fine split and particle size distribution expected from the blasting and processing of an ore. The drop tower (Figure 2.4) is manufactured by MARC Technologies (formally known as MARC Environmental Solutions), an Australia based company, and is a fully automated piece of equipment designed for performing drop testing of material samples such as iron ore. It has the capacity of dropping 50 kg to 100 kg of samples from heights of 2 m to a maximum of 15 m selectable in 100 mm increments. The accuracy in height is down to a few millimetres. The process can be repeated numerous times as required before the samples are delivered back to the operator for further analysis. Since it is fully automated the system is 100 % repeatable and accurate results are obtained each time a test is done and the number of drops and exact height of each drop is maintained every time.

The sample ID, number of drops and the height of the drops can be input into the programmable logic controller (PLC) via a personal computer (PC) with integrated ethernet connection. The operator loads the test sample into a special bin and all other commands are through a touch screen panel via a series of sensors. The machine ensures all prompted items are completed prior to running the test and that there is a bin in the out feed location. The sample material is automatically loaded into the unit and transferred to the drop bucket and raised up the tower to the pre-programmed height. When dropped, the

sample is either re-loaded into the drop bin for an additional drop in the cycle, or transferred to the out-feed bin for analysis. Cycle time for a 15 m drop is approximately 6 minutes (MARC Technologies, 2010). The drop tower has integral dust collection, installed at all major dust points ensuring a dust free environment. All panels and access doors are also safety interlocked to prevent any possibility of access to the mechanism whilst a drop cycle is in progress.

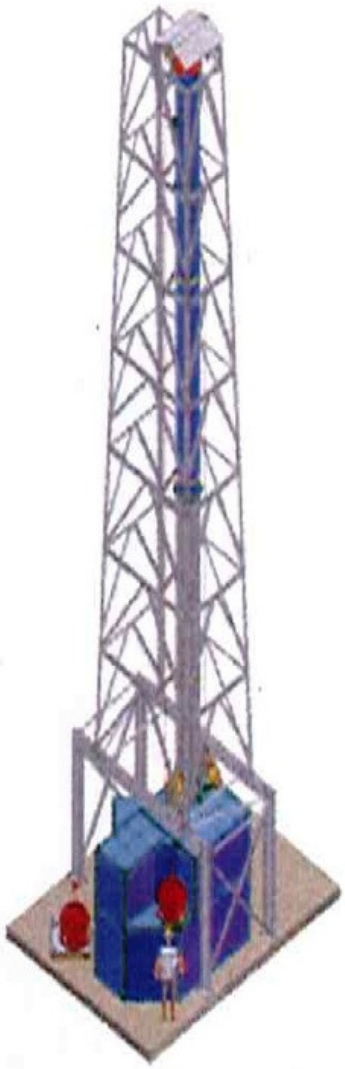

Figure 2.4 AMMTECS Drop Tower (MARC Technologies, 2010).

2.6.3 Other drop tests

Drop tests including critical drop height tests, cushioning tests, different types of impact surface tests, different sample size tests, stabilization tests, weathering tests and volume breakage index tests are routine in iron ore testing programs

but the fully automated drop tower is a relatively new piece of equipment and as such literature on it is scarce.

Several workers including Waters and Mikka (1989) have concluded that drops from higher heights should be avoided and replaced by smaller drops which reduce the fines generated. They conducted experiments which proved that the amount of lump iron ore degradation due to a single drop from 30 m was higher than the degradation caused by smaller drops with sum equal to the same total height (6 drops at 5 m or 10 drops at 3 m). They suggested that drop heights more than 3 m should be avoided and replaced by smaller drops. For repeated drops, the fines produced from earlier drops offers a cushioning effect on the lump iron ore degradation and it has been shown that an initial 30 % fines with lump iron ore reduced fines generation by 40 % (Sahoo, 2007). Larger lump sizes produce higher percentages of fines than smaller sizes (Waters and Mikka, 1989). Furthermore, larger particles are more likely to contain larger cracks and thus are more susceptible to breakage.

The mineralogical and textural characteristics of rocks could be proxies for their physical and mechanical properties. Various ore types could be subjected to mineralogical and petrographic studies using QEMSCAN®, XRF, XRD and the same samples could also be subjected to testing for physical properties using the drop tower tests, tumble tests and bond work indices. Statistics, mainly regression analysis could be used to work out the relationships between the physical properties and the petrographic and mineralogical properties.

2.6.4 Degradation tests

The degradation characteristics of various iron ores due to particle breakage have been studied by a number of researchers to determine the causes of degradation and its prevention during the handling process from mines to end users (Sahoo, 2007). Teo et al. (1990) defined degradation as the reduction of a given size fraction to a smaller size fraction through the range of final products expressed as a percentage of the whole.

The grade differences between lump and fines, together with the lump percentage, are referred to as the 'lump algorithm' (Howard et al., 2005). Different ore types can be expected to have systematically different lump algorithms. It has been found that weighted-least-squares (WLS) multiple regressions can be used to ascribe lump algorithms to different ore types, provided sample periods have sufficiently varied ore type mixes.

The product-size distributions on which the standard strength indices for the drop tower and tumble strength tests are based and the breakage rate constants are dependent on other factors other than the strength of the lumps (Dukino et al., 1997). Teo et al. (1980) worked on the degradation of iron ore lumps and showed that the lump size materials could be reduced by two mechanisms; fracturing of individual lumps and surface breakage due to abrasion. The two mechanisms are distinguished by the size distribution of the degradation products shown in Figure 2.5.

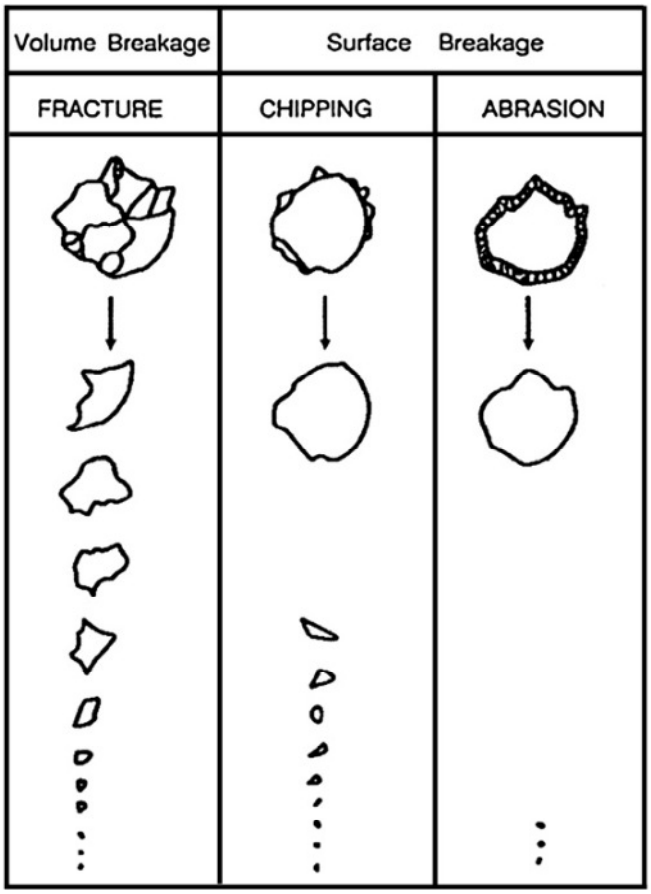

Figure 2.5 Mechanisms of three breakage phenomena (Sahoo, 2007).

The conclusion of their work was that size degradation of the sample tested in a tumbler drum is due to both volume and surface breakage, and a drop test method is best able to overcome the limitations of tumbler drum tests which are more applicable to handling of iron making materials such as sinter and coke (Sahoo, 2007). In the tumble test the following can happen to the samples: abrasion of the particles as they roll in the drum and rub against each other, as they roll against the surface of the drum, and the generation of fines due to collisions as the samples drop from lifters and impact the rotating drum (Sahoo, 2007).

2.7 Distribution and characteristics of major and selected iron formations and deposits of the world

2.7.1 Types of banded iron formations

Iron formations deposited during the Archean to Proterozoic are known to contain the greatest volume of iron compared to those deposited during other geologic times such as the non-cherty and oolitic iron formations of the Phanerozoic. Figure 2.6 shows the relative abundances of some major banded iron formations (BIF) deposition through the Archean to Neoproterozoic.

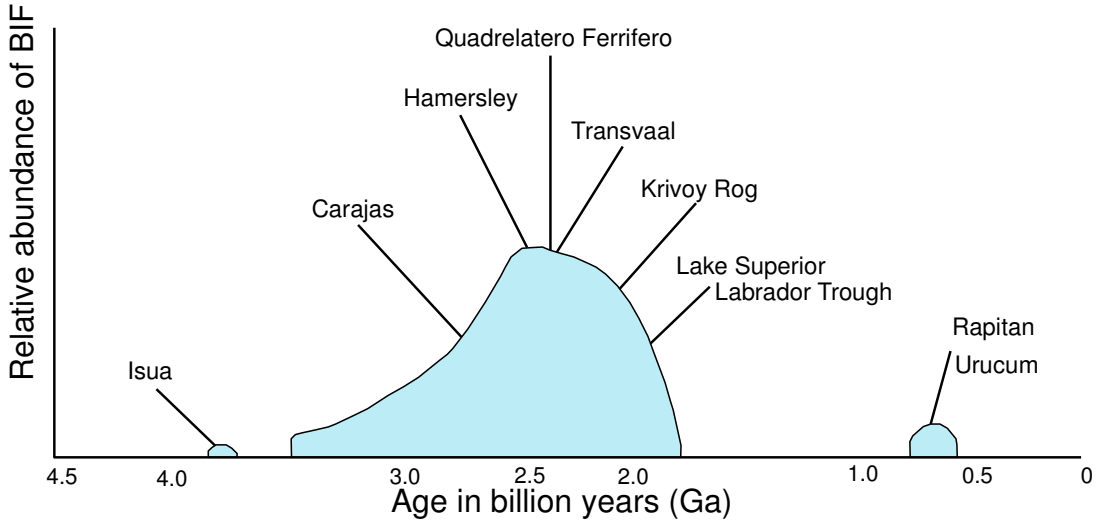

Figure 2.6 Relative abundances of Archean to Proterozoic BIFs (modified after Klein, 2005).

Archean-Proterozoic BIFs are commonly divided into three main categories according to their age of deposition and inferred depositional setting (Gross, 1965, 1973). These are termed the Algoma, (Lake) Superior and Rapitan types

and they range in age from Archean (~ 3.5 to 2.6 Ga) through Paleoproterozoic (2.6 to 1.8 Ga) to Neoproterozoic (~ 0.8 to 0.6 Ga), respectively (Klein and Beukes, 1993). There are also younger Phanerozoic iron formations which are non-BIF such as oolitic iron stones (Young, 1989).

Algoma-type BIFs were deposited principally during the Archean and exhibit a volcanic arc-greenstone belt association (Goodwin, 1973). They are relatively thin (< 100 m thick) and of limited areal extent (< 100 km^2) and have high iron oxide and silica content. They are characterised by thin banding or lamination with no oolitic or granular textures. The associated rocks include shale, greywacke and volcanics.

In terms of size, the Superior-type BIFs dominate the three BIF categories. The name is a reflection of their abundance in the Lake Superior region of USA and Canada. These thick (> 100m), and laterally extensive (> 1000 km^2) BIFs were deposited during the Paleoproterozoic and represent the major period of iron deposition in earth's history. The Superior-type BIFs generally consist of fine-grained iron oxides, silicates, carbonates or sulphides present in planar mm to cm scale bands, usually alternating with similar scale bands of chert. Lithological textures may also be dominated by coarser-grained oolitic or rounded granules within poorly defined mineralogical bands. The major superior BIFs are those in the Hamersley in Australia, Quadrelatero Ferrifero in Brazil and the Transvaal in South Africa.

Rapitan-type BIFs are generally thin, aerially restricted, chert-poor bodies. Most are of Neoproterozoic age. They occur mainly in the Northwest Territories, Yukon in Canada from where they got their name from the Rapitan Group in the Mackenzie Mountains. Iron formations deposited elsewhere in the world around the time the Rapitan type BIFs were deposited include those from the Urucum in Brazil (Figure 2.6).

The Kiruna type iron formation is not regarded as sedimentary in origin as these rocks exhibit a strong magmatic association and typical magnetite-hematite-apatite mineralogy (Nystrom and Henriquez, 1994). They are often genetically and spatially associated with iron oxide-copper-gold deposits (Hitzman et al.,

1992). Examples include those known in northern Sweden (Kiruna and Malmberget) and central Chile (the Iron Belt and El Laco).

Sedimentary Minette-type iron ores occurs in many part of the world, including the Lorraine basin in France and the Peace River district in Alberta, Canada (Petruk et al., 1977). According to Siehl and Thein (1989), Minette-type ironstones are “detrital sediments containing typically ooids, pisoids and clasts of silica-rich aluminous goethite, hematite, Al-rich berthierine / chamosite or a combination of these”. The term “Minette” also refers to a mica-rich lamprophyre but was adapted to sedimentary iron ores by French miners because it could be translated to mean “little mine” due to its relatively poor iron content (28 – 34 wt % Fe).

2.7.2 Distribution

Figure 2.7 illustrates the global distribution of some major and selected BIFs and iron ore deposits including the Putu and Nkout deposits. Factors other than enrichment of the chemistry of an iron deposit can dictate whether an iron ore is mined of not. These could be political, social but are mainly commercial. For commercial exploitations, some of the most important issues are, recoverable iron content, physical and metallurgical properties of the ore, transport infrastructure and regional/national political stability. Current iron ore deposits in the world are dominated by Archean to Proterozoic iron-formations as they satisfy the requirements of quantity, chemistry and metallurgy of recoverable iron. Table 2.2 lists major and selected iron deposits from Africa including tonnage/grades, material types, processing methods and operating companies.

2.7.2.1 Africa

Apart from South Africa, other leading iron ore producing countries in Africa include Mauritania, Morocco and Algeria. In southwest Cameroon the Paleoproterozoic Nyong Group hosts a discontinuous belt of BIFs (Lerouge et al., 2006) amongst which is the Nkout deposit. Several Paleoproterozoic BIFs are located within the West African craton, including the Nimba Group which is dominantly in Liberia but also in the Ivory Coast and Guinea. The Faleme skarn

deposits in south eastern Senegal (Schwartz and Melcher, 2004) and those occurring in several schist belts in western Nigeria (Mücke, 2005) are West African iron ore formations of Birimian age (~ 2.1 Ga). The Congo craton of central Africa hosts a number of BIFs including those within the Paleoproterozoic Kibali Group of northeast Democratic Republic of Congo (DRC) and their extensions into the Central African Republic (CAR).

Figure 2.7 Global distribution of major and selected BIFs and districts including the Putu and Nkout deposits (world map from ESRI, locations of BIFs modified after Klein, 2005).

The Transvaal Supergroup on the Kaapvaal craton are the main BIFs in southern Africa and these are of a comparable size to those of the Hamersley province, Australia. Other South African BIF's includes the Barberton greenstone belt on the Kaapvaal craton and the Belingwe greenstone belt on the Zimbabwe craton.

2.7.2.2 Asia

The states of the former Soviet Union host the main BIFs in Asia. Prominent amongst them are the BIFs within the Krivoy Rog, the Kremenchung basins, those in the Kursk area and the Odessa-Brusilov belt (Alexandrov, 1973). They

are all located within a general N-S belt extending from the Ukranian Shield up to the Kola Peninsula and are generally considered to be superior type BIFs.

The major BIFs within the Indian sub-continent are located in the Bihar-Orissa district of north-eastern India, the Central Provinces and the schist belts of the Dharwar Craton in southwest India and are mainly Archean in age. They include the Noamundi which is of Algoma type (Majumder et al., 1982), and the Kiriburu which is of superior type (Ghosh and Mukhopadhyay, 2007).

China has several iron formations including Anshan, Dalizi, Dengfeng, E. Hebei, Huoqiu, Qingyuan, Taishan, Wutai-Lüliang, Yinshan iron formations. These are mainly Archaen to early Proterozoic in age. Even though China is the world's largest producer of iron ore, especially magnetite iron ore, all their production is for domestic consumption. The iron ore deposits in China are mainly low grade with some containing high proportions of phosphorus. As such China has invested heavily in research on beneficiation techniques so that they could unlock some of their uneconomical deposits.

2.7.2.3 Australia

The Hamersley province of the Pilbara Block, Western Australia is the most important BIF in Australia. Other iron ore formations include the Yilgarn Block in Western Australia and the Middleback Range of South Australia. Covering over 50,000 km^2, the Hamersley group represents the largest iron ore formation on Earth (Barley et al., 1997) with the main formations being the Boolgeeda, Brockman, Marra Mamba and Weeli Wolli formations. Western Australia in general accounts for over 90 % of the country's iron ore exports and about a quarter of global production.

2.7.2.4 Europe

The most important iron formations in Europe are in Sweden. The Kiruna-type deposits are dominant in northern Sweden, whilst smaller Superior type deposits occur within the Bergslagen district of south-central Sweden. Ten deposits of apatite iron have been mined in northern Norrbotten, Sweden and

the two largest deposits; Kiirunavaara and Malmberget are still being mined. The Skellefteå Belt of north-central Sweden hosts a number of small iron formations. Sweden produces about 90 % of Europe's iron ore.

2.7.2.5 North America

The iron formations in the USA and Canada are mainly Granular Iron Formations (GIF). The USA hosts the Lake Superior region and smaller greenstone associated formations such as those in the Wyoming-Montana area. Neoproterozoic BIFs are found in the Rapitan districts of the Northwest Territories of the USA. The Labrador trough and the Abitibi greenstone belts (Algoma-type BIFs) are found in Canada.

2.7.2.6 South America

The most important iron formations in South America are found in Brazil and include the Quadrelatero Ferrifero in southeast Brazil, the Urucum district in western Brazil and the Carajas district in northeast Brazil. Other BIFs in South America include the Imataca group of eastern Venezuela and the Chapare group of eastern Bolivia. Tectonic links have been established between tectonic plates underlying South America and West Central Africa using geochronology, paleomagnetism and lithofacies (Zhao et al., 2002). These include between the Brazilian Sao Francisco-Sao Luis-Amazon cratons and the West African craton and between the Congo Craton and the Sao Francisco cratonic link. The headquarters of the world largest iron ore producer i.e. Vale, is in Brazil.

Table 2.2 Major and selected iron ore deposits in Africa.

Country	***Iron Ore Deposit***	***Tonnage/Grade (Indicated)***	***Material Type***	***Processing***	***Company***	***References***
Cameroon	Mbalam	775 Mt / 57 % Fe	DSO / hematite itabirite	Grinding / reverse flotation	Sundance resources Ltd	Lerouge et al., 2006 Suh et al., 2009 Nforba et al., 2011 Anderson et al., 2014
	Ngovayang	300 - 500 Mt / 16 - 40 % Fe	magnetite BIF	Grinding / LIMS	Jindal Steel and Power	
	Nkout	1.6 Bt / 33.3 % Fe 64.3 Mt / 54.5 % Fe	Martite – goethite, magnetite BIF	attrition scrubbing / mag. separation	International Mining & Infrastructure Corporation plc ("IMIC")	
Central African Republic	Bakala-Bambari	64.38 % Fe	DSO	Expl stage	AXMIN Inc.	
Côte d'Ivoire	Mount Nimba Mount Kalayo	3 Bt / 40% Fe	Hematite - magnetite BIF	Expl stage	Société pour le Développement Minier en Côte d'Ivoire	Foster, 2003; Schmidt and Kennedy, 1983
Republic of Congo	Mayoko	33 Mt / 55.6 % Fe	DSO / Hematite - magnetite BIF	Grinding / mag separation	African Iron (80%) / Equatorial Resources (20%)	Woodtli, 1961
	Avima	690 Mt / 58 % Fe 580 Mt / 60 % Fe	DSO / itabirite hematite		Core Mining	Suh et al., 2008
Gabon	Belinga	1 Bt / 60 % Fe	DSO / Magnetite BIF		China Machinery Engineering Corporation	Feybesse et al., 1998
	Mebaga	90 - 150 Mt / 35 - 65 % Fe 540 – 900 Mt / 25 - 40 % Fe	DSO Magnetite BIF	Expl stage	Ferrex Plc (Equatorial Resources)	

Mt – million tonnes, Bt – billion tonnes, Expl – Exploration, DSO – direct shipping ore, LIMS – low intensity magnetic separation

Country	*Iron Ore Deposit*	*Tonnage/Grade (Indicated)*	*Material Type*	*Processing*	*Company*	*References*
Gabon	Kango	98 - 750 Mt / 30 - 60 % Fe	Hematite itabirite, magnetite BIF	Expl stage	Volta Mining	Soto-Viruet, 2010
	Mékambo	40 – 67 % Fe	DSO Hem itabirite	Expl stage	Waratah Resources	
Guinea	Faranah	25 – 40 % Fe	Magnetite BIF	Expl stage	Guinea Iron Ore Limited	
	Gaoual	5 Bt / 59 % Fe	DSO		Guinea Iron Ore Limited	
	Simandou (Pic de Fon)	8 Bt / > 60 %	DSO		Rio Tinto Vale/BSGR	Cope et al., 2005
	Nimba	178.4 Mt / 60 -63 % Fe	DSO		Sable Mining Africa Ltd	
Liberia	Mount Nimba Yekepa		DSO		ArcelorMittal	Berge, 1974 Billa et al., 1999
	Western cluster	3.5 Bt / > 60 % Fe	DSO		Vedanta-Group Sesa Goa	Fitzhugh, 1953 Lersch, 1966 Berge, 1971
	Bong Range	290 Mt / 35 - 45 % Fe	Magnetite BIF		Union/Wisco	
	Goe Fantro Range	35 – 40 % Fe	Hematite itabirite		BHPB	
	Totor Range					
	Putu Range	3.24 Bt / 45 - 62 %	DSO Magnetite itabirite	Grinding/mag separation	Severstal	
Mauritania	Guelb el Rhein	926 Mt / 36.2 % Fe	Magnetite BIF		Société Nationale Industrielle et Minière de Mauritanie (SNIM)	Bronner & Chauvel, 1979
	El Agareb	1 Bt	Magnetite BIF		SNIM/ArcelorMittal	
	Guelb el Aouj	3 Bt			SNIM/ Sphere Investments	

Mt – million tonnes, Bt – billion tonnes, Expl – Exploration, DSO – direct shipping ore

Country	***Iron Ore Deposit***	***Tonnage/Grade (Indicated)***	***Material Type***	***Processing***	***Company***	***References***
Namibia	Ondjou Hammerhead	2.0 – 3.4 Bt / 20 – 30 % Fe	Magnetite BIF			Beukes, 1973
Nigeria	Agbaja	2 Bt / 45 – 54 % Fe	Magnetite BIF	Expl stage	National Iron Ore Mining Company	Mucke, 2005 Adekoya, 1998 Anike, 1993 Adekoya et al 2012
	Itakpe	200 – 300 Mt / 38 – 45 % Fe	Magnetite BIF			
	Muro Hills	25 – 35 % Fe	Magnetite BIF			
Republic of Congo	Avima,	690 Mt / 58 % Fe	DSO	Expl stage	Core Mining	
	Badondo	200 to 300 Mt / 40 - 65 % Fe 1.1 to 1.9 Bt 30 % - 45 % Fe	DSO Magnetite BIF	Expl stage	Equatorial Resources Ltd	
	Zanaga	6.8 Bt / 32 % Fe	Magnetite BIF	Expl stage	Jumelles / Xstrata and Zanaga Iron Ore Company	
	Nabeba	472.0 Mt / 57.9 % Fe	DSO	Expl stage	Sundance Resources	
		1.7Bt / 33.9 % Fe	Magnetite BIF			
Senegal	Faleme	750 Mt / 43 % Fe	Skarn	Work suspended	ArcelorMittal	Schwartz and Melcher, 2004
Sierra Leone	Bagla Hills	838 Mt / 32 % Fe	Magnetite BIF	Forest Reserves		
	Marampa	1Bt @ 31.1% Fe	banded quartz-hematite schists		London Mining	Marmo, 1956 Williams, 1978
		680 Mt / 28.2 % Fe			Cape Lambert	

Mt – million tonnes, Bt – billion tonnes, Expl – Exploration, DSO – direct shipping ore

Country	***Iron Ore Deposit***	***Tonnage/Grade (Indicated)***	***Material Type***	***Processing***	***Company***	***References***
Sierra Leone	Tonkolili	126.5 Mt / 58.1	DSO		African minerals	
		12.8Bt / 35%Fe	Mag BIF			
South Africa	Sishen-	918.9 Mt / 65 % Fe	DSO	Mine	Anglo American/ Kumba resources	Pickard, 2003 Carney and Mienie, 2003
	Beeshoek	117.5 Mt / 63.7 % Fe	DSO	Mine	Assmang Limited	Gutzmer et al., 2005
	Thabazimbi	62% Fe	DSO		Anglo American	
South Africa						Beukes, 1973 Bontognali et al., 2013
Uganda	Muko	30-50 Mt / 68% Fe	DSO		Muko Iron Ore Development Co. Ltd (MIDECO)	
	Sukulu	50 Mt / 55% Fe				

Mt – million tonnes, Bt – billion tonnes, Expl – Exploration, DSO – direct shipping ore

Chapter 3

Literature Review of the Geology of the Study Areas

3.1 Introduction

In this chapter, an overview of the regional geology of the West and Central Africa sub region is discussed including the potential of the age differentiated principal rock units for iron ore. The geology of Cameroon and Liberia are then discussed in more detail as they are the host countries of the deposits being studied. The geology of the Nkout and Putu iron ore deposits are then reviewed based on literature. Very little literature has been published specifically on the geology of these deposits and most of what is described here has been obtained from company reports and documents from previous exploration phases.

Unless stated otherwise, the regional geology presented here are from two sources: Milesi et al. (2006) and Wright et al. (1985). It should be noted that the study regions, like others, are made up of geological provinces which transcend national boundaries. Different authorities place geological boundaries in different places and as such maps from different countries will not always agree in detail. The regional geology is considered with respect to age provinces and Figure 3.1 (modified from Taylor et al., 2009, USGS) which summarises the principal geological units of West and central Africa.

3.2 Regional Geology of West and Central Africa

3.2.1 Archean Craton (> 2,500 Ma)

The West African Archean is characterised by a granite-greenstone association. The granite component of this association comprises both the gneiss-migmatite basement and the intrusive granites. The supracrustal belts are the greenstone component. The name comes from the green colour of the chlorite and hornblende in metamorphosed basic volcanic rocks. These typically predominate in the lower parts of greenstone belt sequences; the upper parts being dominated by metasediments.

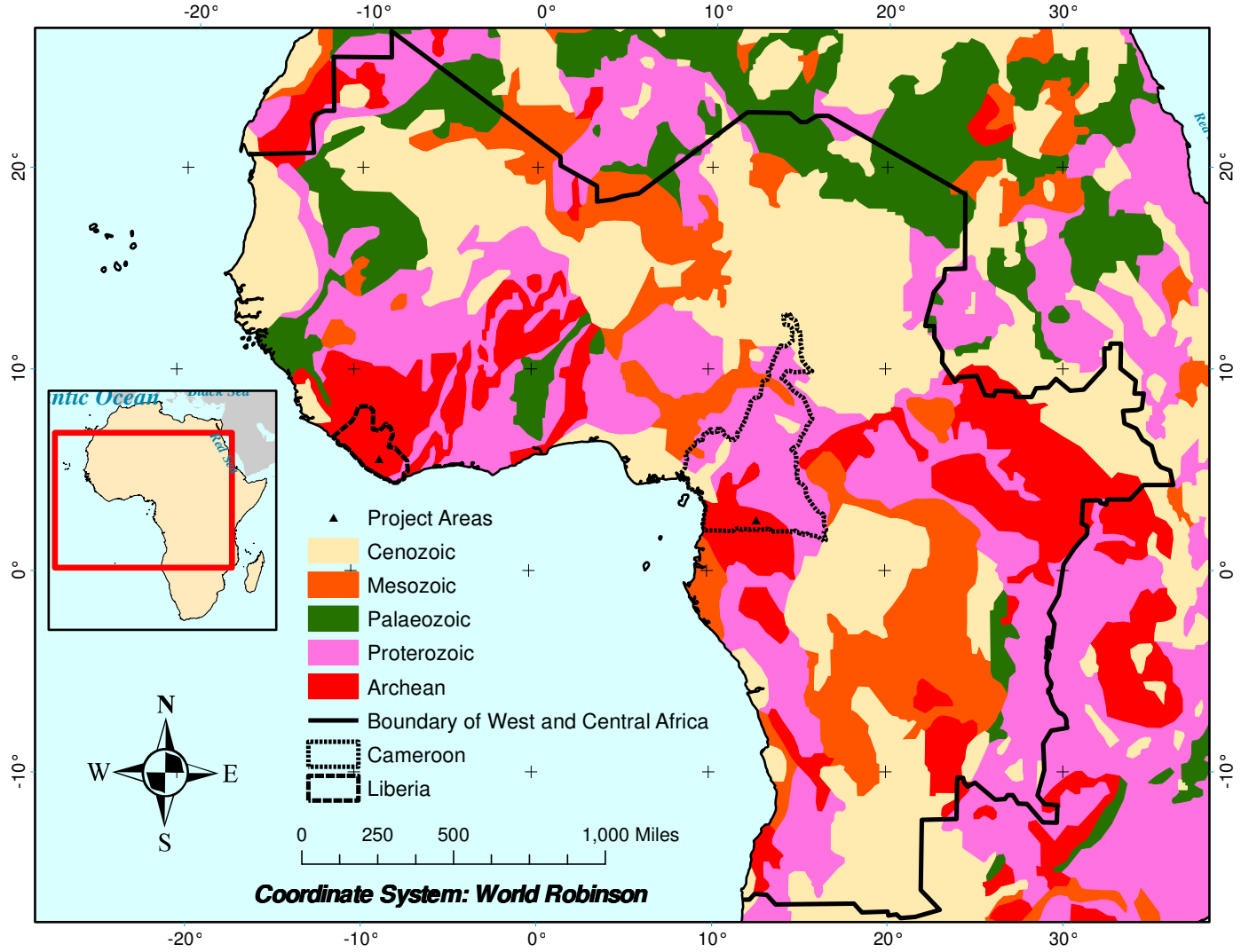

Figure 3.1 Simplified regional geological map of West and Central Africa (modified from Taylor et al., 2009, USGS).

All the supracrustals are generally considered to belong to the last cycle of sedimentation and volcanism in the Archean of this region and were deformed and metamorphosed in the Liberian (2700 Ma). It is not certain that the basement is everywhere older than the supracrustals; some of the gneiss and migmatites may represent parts of the supracrustal sequence that have been granitised. The Archean nucleus of the West African craton underlies much of Guinea, the extreme west of Ivory Coast, and most of Liberia and Sierra Leone.

In Central Africa, the Archean nuclei are composed of gneissic and anatectic complexes, and partly preserved greenstone belts and the associated magmatism. In Central Africa, four main Mesoarchean–Neoarchean blocks have been mapped:

- The ‘‘West Central Africa’’ craton (Ntem in Cameroon, Equatorial Guinea, Gabon Massif and Congo), is tectonically overlain by Paleoproterozoic rocks. It contains: (i) Trondhjemite–Tonalite–Granite (TTG) and banded gneiss (ii) meta-sedimentary rocks and greenstone belts, including BIF and mafic-ultramafic rocks, that were deformed up to medium pressure granulite facies metamorphism; (iii) intrusive rocks, including TTG charnockites and associated greenstones; and (iv) late magmatic rocks (ultramafites, K-richgranitoids, syenogranites).
- The northern Archean Democratic Republic of Congo (DRC) – Central African Republic (CAR) craton contains: a) various granite-gneiss complexes, b) BIF-bearing Mesoarchean greenstone belts overlying the granite–gneiss complex which is divided into the lower and upper Kibalian greenstone belts. The ‘‘Lower Kibalian’’ (DRC), comprises mesozonal to catazonal rocks (paragneiss, amphibolites, amphibole–garnet ± muscovite ± biotite ± sillimanite ± cordierite bearing gneisses and scarce BIF). The ‘‘Upper Kibalian’’ of DRC constitutes narrow troughs that contain folded terranes (quartzite, BIF, greywackes, volcano-sedimentary rocks, and basal mafic volcanic rocks) cross cut by granitoids.
- The ‘‘Central Shield’’ of western Angola comprises Archean rocks of a granite (granite to tonalite)–gneiss–migmatite complex intruding a possible gabbro–norite–charnockite complex (gabbro, norite, anorthosite, enderbite, mafic rocks, charnockite, scarce granulite).

- The “Kasai-Lomani-Luanda” Neoarchean-Mesoarchean craton the poorly exposed “Cuango Shield”, Angola, comprise a younger granite-gneiss-migmatite complex and an earlier gabbro-norite-chanockite complex.

3.2.1.1 Iron ore potential of the Archean Craton

Iron ore is the most important mineral resource of the Archean in both West and Central Africa. In West Africa, the major deposits are in the eastern supracrustal belts, which are dominated by banded iron formations. The BIFs are interbedded with mafic schists and amphibolites, quartzites and phyllites. Gold is also important in the Archean of Central Africa and they are spatially associated with volcanic rocks and BIF-bearing formations (greenstone belts; e.g. Kilo-Moto, Isiro, Gorumbwa, Ituri-Uetele, DRC and Belinga, Gabon). From Figure 3.1 it can also be seen that the Archean craton dominates the geology of Liberia and the southern part of Cameroon where Nkout is located.

3.2.2 Proterozoic (2,500 – 540 Ma)

Lower Proterozoic rocks representing the time span from about 2500 to 1800 Ma form the major part of the West African craton (Guinea Rise). The Birimian sediments and volcanic accumulated after the Liberian event, over an area that covered what is now Ghana and Ivory Coast, much of Burkina Faso and parts of northern Guinea, south western Mali, south eastern Senegal, western Niger and south eastern Liberia. They may extend north (beneath the younger sedimentary cover) as far as Morocco.

The area of crust affected by the 2000 Ma Eburnian thermotectonic event is about 1000 km wide from eastern Ghana to eastern Liberia. The regional trend of the rocks within the area is similar to that of the Liberian event i.e. between N-S and NE-SW. The whole region is underlain by lower Proterozoic Birimian supracrustals and older basement affected by regional deformation, metamorphism and granite emplacement in the Eburnian event is also known as the Baoulé–Mossi domain. The eastern boundary of the Baoulé–Mossi domain with the younger Pan African domain to the east is marked by the thrust

zones of the Togo belt. In the west, the boundary with the older Kenema-Man domain is less well defined, except along the Sassandra Mylonite Zone.

In Central Africa, Paleoproterozoic belts have been locally overprinted by the Pan-African event (and probably by the Kibaran in Zambia). Three different belts are discussed below:

1. The first Paleoproterozoic belt extends west of the Congo craton from Angola to SW Cameroon and is known as the West Central African Belt (WCAB). The crustal evolution is dominated by an Archean inheritance recorded in metasediments and metaplutonic rocks. The rocks are generally well-preserved but are locally strongly deformed by the West Congolian Neoproterozoic belt.

2. The second belt, probably a northern prolongation of the WCAB is developed in central and northern Cameroon. This belt is oriented NE–SW and is lithologically similar to the WCAB, but with a significant presence of Paleoproterozoic juvenile material. It probably extends into eastern Nigeria.

3. The third possible belt is located at the northern periphery of the Congo basin between Archean blocks complex in Cameroon and Bomu complex in Central African Republic and the Pan-African thrust nappes (Yaounde´ and Gbayas) to the north.

Mesoproterozoic to the early Neoproterozoic formations have been identified in Central Africa and they comprise four belts:

1. The NNE–SSW ‘‘Kibaran belt’’, located in eastern DRC, is marked by an inner and a foreland domain. Mafic-ultramafic rocks emplaced between the inner and foreland domains delineate a westward curvature north of DRC. The foreland domain is composed of volcano-sedimentary formations that include detrital sedimentary rocks (conglomerate, sandstones and pelite), and interbedded basic to dacitic volcanics and sills. The belt may be correlated with rock suites in NW Tanzania.

2. From geochemical, geochronological and metallogenic considerations the Choma-Kalomo block of Zambia is included in the Kibaran domain. This block is composed of orthogneisses, granitoids and gneiss. They are crosscut by granitoids and late Sn–granitoids.

3. The Mesoproterozoic Irumide belt, Zambia, oriented NE–SW, is composed of gneisses, high-grade granulites, charnockitic complexes and granitoids. Some pre-Irumide granitoids (ca. 1650 Ma) and relicts of Neoarchean or Paleoproterozoic rocks have been identified.

4. Several sedimentary formations (Liki-Bembien, Ituri Group), crop out near the frontiers of Central African Republic, Congo Brazzaville and DRC. These detrital rocks (conglomerate, sandstone, quartzite, pelite and argillite) change laterally to possible turbidites and calcareous sediments (limestone, calcschist). They locally display a contact metamorphism (Cu–Fe–skarn, Ca–hornfels).

3.2.2.1 Iron ore potential of the Proterozoic

Although on a global scale Proterozoic iron formations are generally thicker and more extensive than those of the Archean, iron ores are a great deal more widespread in the Archean nucleus of the West Africa craton than in the lower Proterozoic Birimian terrane, where their place seems to have been taken by manganiferrous sediments. The large Falémé deposit in easternmost Senegal may be of this type, however. There appears to be a continuation of this deposit across the border in south westernmost Mali. Banded iron formation rocks in southwestern Ivory Coast – for example, the Monogaga deposit near Sassandra have been classed as being of Birimian age, but these deposits occur within the reactivated part of the cratonic nucleus. They are therefore older than Birimian and belong with the Archean supracustals. Deposits of lower Proterozoic iron ores occurs in norites and gabbros in various places. They are probably all magmatic segregations, dominated by titaniferous magnetite, sometimes with significant vanadium enrichment, as in northern Burkina Faso. Near Takoradi, in southern Ghana, a deposit of such ores is estimated to be 8 km long and a few hundred meters across, and samples have yielded 55 % Fe and 12-22 % Ti.

The potential of the Central African Paleoproterozoic belts seems underestimated by comparison with their equivalents in West Africa and NE Brazil. In some geological and metallogenic aspects, they are comparable to West Africa as they display stratiform mineralisation including Mn & Fe (including BIF), Au–pyrite associated with the early stages of the orogeny. The eastern extension of the belt through the Republic of the Congo, Central African Republic and then DRC has been less explored, although it hosts grouped or isolated lithologically and structurally controlled occurrences of Au, Nb–Sn, Fe and Ti (ilmenite > rutile). The southeastern belt (DRC–Zambia) hosts mainly Fe–Mn deposits.

3.2.3 The Pan African (Neoproterozoic-Cambrian, 1000 – 450 Ma)

The Pan African orogeny or thermotectonic event is represented in West Africa by the relatively narrow Rokellide belt and the southern part of the Mauritanide belt in the west and by the extensive Togo-Benin-Nigeria swell in the east. The two domains are separated by the West African Craton. The term Pan African refers to the major and wide-spread orogenic or thermotectonic event that affected most of the rocks outside the cratons, between about 650 and 450 Ma ago. It involved the last major reactivation of basement rocks in Africa, and was the final stage in the formation of the African shield. After it, the so-called mobile belts (younger orogens) became as tectonically stable as the cratons themselves. The sole exceptions were the northern parts of the Mauritanides and the Alas Mountains in the north west and the Cape Fold belt in the extreme south. Apart from these comparatively small areas, the only deformation to affect the continent following the pan African event was faulting and gentle (epeirogenic) crustal warping.

In the large eastern Pan African domain, there are many low-grade supracrustal belts whose size and general NNE-SSW trend is similar to that of supracrustals in the cratonic nucleus. However, they are largely confined to a broad belt in the western half of Nigeria, except for scattered outlying ridges of mainly quartzitic rocks nearer to the craton margin, in Benin and southern Togo. The basement has a history of reactivation going back at least to the Liberian and it experienced its last major reactivation in the Pan African. The supracrustals

have been strongly deformed, being almost everywhere isoclinincally folded with a steep foliation that parallels the trend of the belts. Metamorphism is generally in the greenschist to amphibolite facies.

Pan-African belts in Central Africa are characterized by the juxtaposition of recycled and juvenile domains. Four major belts are recognized north, west, east, and south of the Congo craton.

1. The belt north of the Congo craton is oriented NE–SW to ENE–WSW. It is characterized by the presence of NE–SW shear zones (e.g. Adamawa and Sanaga faults) and by the southward thrusting of its southern limit onto the Congo craton. The belt comprises polycyclic (Adamawa-Yade in Cameroon, Central African Republic and Chad) and monocyclic domains (e.g. Yaounde and Poli in Cameroon and Gbayas in Central African Republic, Lere in Chad). All of the rocks in these belts are metasedimentary and volcano-sedimentary (various kyanite schists and gneisses, migmatites, amphibolites and quartzites) and metaplutonic rocks (gabbro, garnet–pyroxene-bearing diorite and granitoid). They were metamorphosed under amphibolite to granulite facies between 640 and 600 Ma.

2. The NNW–SSE West Congolian belt and its ‘‘foreland’’ sedimentary deposits were built during a three-phased evolution: (i) a 1000–910 Ma rifting stage (also suggested by the study of mafic dykes) followed by (ii) the deposition of passive margin platform deposits (pre-Pan-African), and (iii) Pan-African deformation that began at ca. 600 Ma and ended at 566 Ma. The major structures in the belt verge to the east. NNE - SSW sinistral shear zones have also been mapped in Cameroon.

3. The ‘‘Copper Belt’’, developed in Zambia and DRC between the Congo and Kalahari cratons, is part of the ‘‘Katangan Belt’’. The Copper Belt belongs to the Lufilian Arc, an arcuate thrust and fold belt developed in northern Zambia and southeastern DRC during the Neoproterozoic transcontinental Damara–Lufilian–Zambezi Orogeny. This orogenic system separates the Mesoproterozoic terranes of DRC, Rwanda and Burundi (‘‘Kibaran’’) from those of Zambia and Mozambique (‘‘Irumides’’ and ‘‘Choma-Kalomo block’’).

4. N-S trending Neoproterozoic grabens extending for about 160 km along strike. These grabens contain a lower group of black schists, siltstones and tillites, and an upper group of conglomerates, sandstones and schists. They occur in the east of the map area (eastern DRC), parallel to the western Great Lakes Rift.

3.2.3.1 Iron ore potential of the Pan African

Relatively few mineral deposits of importance appear so far to have been discovered in the Rokelide-Mauritanide belt of southern West Africa, but this is not to say that more do not exist. Those that have been found, occur in and near eastern Senegal and include copper near Bakel, uranium near Kedougou and iron ore (magnetite) near Goto. The Neoproterozoic belts are host to the rare breccia-hosted iron-oxide-rich deposits of probable iron oxide–copper–gold type at Mumbwa, Zambia. Iron ores are the only other metallic minerals that can be presently considered of economic interest in this age province. In some supracrustal belts (e.g. the Maru belt) there are banded quartz–hematite rocks, sometimes magnetite–bearing, associated with garnet-grunerite-schist, amphibolites, phyllites and quartzites. They resemble the banded iron formations (itabirite) of the Archaen terrane but are much smaller and leaner, with average grades not exceeding 40 % Fe at best. A certain amount of supergene secondary enrichment has occurred in the surface weathering zone, but this is not deep, and the deposits cannot be regarded as a promising economic prospect.

Similar considerations may apply to deposits of banded iron formation type in rocks of both the Buem and Togo Formations in the northern part of the Togo belt. In the region around Dako, magnetite-hematite (-limonite) ores grading 40-45 % Fe are associated with quartzites and mica-schists, some of which contain chlorite, garnet and epidote. However there are richer and purer itabirite-type ores interbedded among basement gneisses and forming prominent ridges near Okene (south-east of kabba) in southern Nigeria. These are probably older metasediment relics and they could be as old as Archean (and perhaps can be correlated with the iron ores of Liberia and Guinea.

3.2.4 Paleozoic–Mesozoic basins (542–65 Ma)

An older and a younger group of sedimentary basins can be distinguished in West Africa, and the basins are of two main kinds. Intracontinental basins are relatively broad and shallow with a thin sediment fill, generally not much more than 5 km thick. Coastal basins are normally rather narrow and deep, with sediments up to 10 km thick or more. The younger basins developed mainly in the Mesozoic. The large and subcircular Iullmedden and Chad Basins are intracontinental, and so are the more linear Bida Basin and Benue Trough, though the latter is a rifted basin and something of a special case. Continental margin basins include the Senegal Basin and Niger Delta, along with the smaller coastal basins. The seas retreated from the intracontinental basins early in the Tertiary, as the Alpine orogeny commenced in southern Europe. There was regression in the coastal basins at the time, but sedimentation continued in them offshore.

A sedimentary basin formed on the Congo Craton, now broadly termed the Congo Basin, is a prominent feature of the Central Africa region. It contains Paleozoic (Carboniferous–Permian) marine sediments and continental coal-bearing and glaciogenic-sediments are present in some troughs. Mesozoic (Karoo, Jurassic–Cretaceous) sediments (lacustrine and fluviatile deposits) and Late Cretaceous continental sequences (Kwanga Group, DRC) are also represented. In the northern part of Central Africa, early Cretaceous rifting in for example north Cameroon and south Chad occurs in response to both a submeridian extensional regime and dextral strike-slip movement, producing pullapart basins along the Central Cameroon Shear zones.

Sedimentary formations were deposited from the late Neoproterozoic to the Paleozoic in the Congo Basin and in small troughs developed on the Precambrian basement. Clastic and/or carbonate-bearing sequences were deposited in Gabon, Angola and DRC (Bushimay, Lulua). The central Congo Basin contains Paleozoic–Mesozoic formations. They comprise clastic–carbonate lacustrine and fluviatile deposits and Late Cretaceous continental clastic sedimentary formation. The Karoo Supergroup (mainly sandstones and mudstones) e.g. Zambia, was deposited from Carboniferous to Jurassic. The

lowest part of Karoo contains glaciogenic clastic sediments; the middle part is represented by sandstones containing coal; and the upper part is represented by Jurassic mudstones and sandstones with interlayered basalts.

The coastal basin comprises mainly marine clastic–carbonate formations that overlie the Proterozoic rocks and were deposited from the Cretaceous to the Pleistocene. Mesozoic fluviatile and lacustrine clastic (conglomerates, sandstones and shales) and carbonatic sediments were deposited from early to late Cretaceous in restricted troughs located in Cameroon.

3.2.5. Cenozoic (65 Ma – Present)

Cenozoic volcanism in West Africa is of alkaline affinities and is virtually confined to Pan African areas east of the craton. On the Jos Plateau, early Cenozoic volcanism produced the Fluvio-Volcanic Series of intercalated sediments and basaltic lavas. Many basalts contain megacryst and upper mantle inclusions. The Cameroon line forms the major part of the Gulf of Guinea province with lrgeshield volcanoes and basalt plateaus, and plugs of phonolite, trachyte and rhyolite. There was minor Cenozoic volcanism in the Daker region of Senegal. Most of the Cenozoic magmatism occurs in long established areas of crustal doming or uplift and cannot realistically be related to fixed hot spots in the mantle. In Central Africa, Cenozoic formations comprise:

- Continental sedimentary cover: the central basins of Congo and Angola are mostly filled with Eocene to Upper Neogene sandstones of Lower and Upper Kalahari age and with the ‘‘Formation des Cirques’’ (or Upper Quelo). In Chad this cover developed from the Upper Paleogene to the Quaternary and overlies Paleocene and Maastrichtian deposits.
- Coastal and offshore basins: in Cameroon, marine sedimentary formations of Cenozoic age form part of a passive-margin basin. Marine sediments overlie Mesozoic deposits in other coastal basins (e.g. Gabon and Angola).
- Volcanism developed along the western rift in the Middle Miocene to Holocene in the Virunga Massif, DRC, and along the 1500 km NNE–SSW trending Cameroon Volcanic Line (Paleocene–Eocene granitoid and syenite

ring-complexes; recent and active alkaline volcanism such as Mount Cameroon and Lake Nyos).

- Lateritic profiles (Paleogene to Quaternary) are developed in the tropics (e.g. Central Africa Republic, central Cameroon and Angola), but incomplete, truncated profiles occur in equatorial areas (Gabon, south Cameroon).
- Quaternary alluvial–eluvial deposits (alluvium, sands, and gravels) have formed along river valleys or depressions.

3.2.5.1 Iron ore potential of the Cenozoic

The iron ore potential of the cenozoic rocks in both West and Central Africa is limited and restricted to secondary enrichment: Fe in Archean BIF in Isiro district and Ituri-Uele, DRC; Zanaga, Republic of Congo and Bélinga, Gabon.

3.3 Geological Setting of Cameroon

According to Vicat et al. (1997), the geology of Cameroon can be divided into five geotectonic units. These are; the Craton, the Craton Cover, The Pan-African Chain, the Sedimentary Basins and the Cameroon Volcanic Line.

The craton, located in southern Cameroon consists of Archean to Proterozoic cratonic basement (2500 to 600 Ma) which extends across parts of several west-central African countries. It forms part of the northern extension of the Congo craton and comprises the Ntem formation which is composed of the Ntem Complex (NC), the Dja Series (DS) and the Nyong series (NS) (Tagne-Kamga, 2003) (Figure 3.2). These rocks have been metamorphosed and include quartzites, schists, amphibolites, charnockites, greenstones, granulites and gneiss. Rocks of the Ntem Complex are the oldest in Cameroon.

The craton cover could be found in the south eastern part of the country where it borders the Central African Republic and the Republic of Congo. It includes the Dja series, the Bélé-Libongo tillite complex, the Boulou and Mouloundou arkoses, conglomerates, sandstones and shale series of the lower Dja and the Lobeke dolerite dyke and sills which occurs with pillow lavas and occasional syenite plutons.

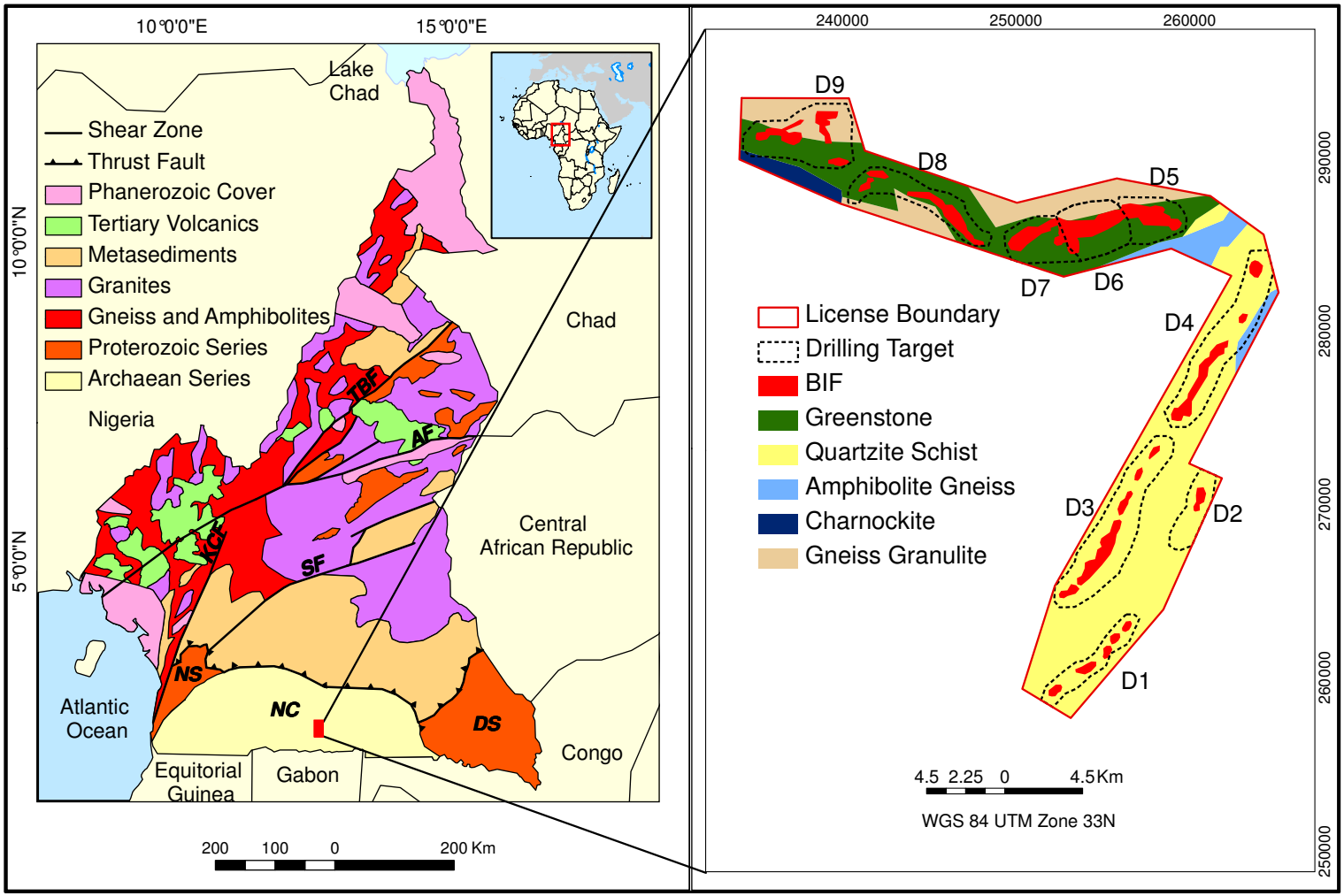

Figure 3.2 Simplified geological map of Cameroon and the Nkout License (modified from Ngnotue et al., 2000, Tagne-Kamga, 2003 and various internal reports). Ntem Complex (NC); Dja Series (DS); Nyong series (NS); Adamaoua fault (AF), Kribi-Campo fault (KCF), Sanaga fault (SF); Tchollire-Banyo Fault (TBF).

The Neoproterozoic Pan-African mobile belt, which is also referred to as the North Equatorial Fold Belt, underlies the central and northern parts of Cameroon. It includes crystallophyllian and magmatic formations which are cut by NE-SW trending mylonitic shear zones, the Sanaga Fault and the Central Cameroon Shear Zone. It is generally accepted that this fold belt resulted from convergence and collision between the Sao Francisco craton (South America), the West African craton, the Congo craton and a Pan African mobile belt. In Cameroon, the fold belt represents the southernmost extension of the Pan-Africano-Braziliano belt (Nforba et al., 2011).

Two types of sedimentary basins have been identified in Cameroon. They are the Palaeozoic and the Cretaceous basins. The Palaeozoic basins are considered to be made up of volcanic detrital deposits of Devonian to Ordovician age and they overly the Pan-African. The Cretaceous basins include fluvio-lacustrine deposits with Aptian Cenomanian and Turonian sandstone, the coastal basin deposits which are Eocene and Miocene in age and contain oil and gas reserves and the Quaternary basins which are related to the sedimentation of Lake Chad.

The Cameroon Volcanic Line (CVL) is a peculiar intraplate tectono-magmatic corridor trending N30^{o}E and stretching over 1600 km, from the Annobon Island in the Gulf of Guinea, to Lake Chad, in the continental interior of West Africa (Tamen et al., 2007). The CVL comprises volcanic structures which are still active today and includes sixty anorogenic plutons with gabbros, granites, diorites and syenites.

Cameroon has experienced three main orogenic cycles and three main extensional phases. The orogenic cycles are the Liberian cycle (2.5 Ga), the Ebunnean or Transamazonian cycle (2.5 – 1.8 Ga) and the Pan-African (1000 - 600 Ma) (Mbarga, 2009). The Ntem complex was formed during the Liberian cycle and both the Nyong and Dja series during the Eburnean cycle. The extension phases comprise the lower Palaeozoic period, the Cretaceous and the Tertiary. Continental erosion and recent alluvial deposits typifies the Quaternary period.

Two main structural features are dominant in Cameroon. These are a generally E - W trending thrust fault which marks the northern limits of the Congo Craton and a series of SW - NE parallel and sub-parallel strike slip faults (Figure 3.2). The strike slip faults include the Adamaoua Fault (AF), Kribi- Campo Fault (KCF), Sanaga Fault (SF) and Tchollire-Banyo Fault (TBF) and forms part of the regional structure referred to as Central African Shear Zone system (CASZ).

The BIFs in the region are Archean in age (4000 to 2500 Ma), hosted by greenstones, associated with granites and gneiss of similar age and located at the northern extent of the Congo craton. Owing to the metamorphosed nature of the rocks and the outcrop density of about 5 %, there is some ambiguity in distinguishing and dating of the lithologies. Deposits have been developed or are being mined in Gabon, Congo Republic, Democratic Republic of Congo, Equatorial Guinea and Central African Republic.

3.4 Geology of the Nkout License

The Nkout deposit is underlain by the Archaen Ntem Complex (Figure 3.2) and early Proterozoic Nyong series rocks at the northern end of the Congo Craton. The deposit forms part of a 150 km long greenstone belt discovered by the BRGM (Chapter 1) from ground observations of airborne magnetic signatures. The Archean to Proterozoic rocks includes BIFs, quartzites, schists, granites, amphibolites, gneisses (greenschist to upper amphibolite facies), itabirites, greenstones, granulites and both charnokitic and non-charnokitic metagranitiods, all of which are widely affected by NNW-SSW and E-W shear zones. Figure 3.2 also illustrates the geology of the Nkout's iron ore license.

Nkout East (D5) (Figure 3.2) forms the eastern most hills at Nkout. The deepest hole drilled up to the field work period shows about 50 m of martite-goethite cap associated with metasediments, gneiss and granite. The granites in the area are usually basement granites and from the logging of the hole may indicate the presence of structural features such as folds and/or faults as granites have been found on top of magnetite rich rocks in drill cores.

Nkout Centre (D6) comprises a series of east-west striking hills. The BIF conforms roughly to areas of elevated topography and this is consistent with the interpretation of the ground magnetic surveys (Chapter 4). The western most hills in this central Nkout region are the highest topographically and also showed the highest concentration of high grade BIF grab samples.

The Nkout West hills, proved similar to the central Nkout hills. The one large BIF outcrop found shows bedding striking roughly east-west and dipping to the south at 45^{o}. Visual estimates show this outcrop contains approximately 50 % magnetite + hematite (Norton, 2009).

Unlike D5 to D7 (Figure 3.2) which have a roughly east west trend, D3 has a NE – SW trend and is hosted by quartzite schists rather than greenstones as in the others. The quartz content of its BIF is also higher than that of the other areas and this may be the reason why work was suspended there at a relatively early stage to focus on Nkout East, Centre and West.

3.5 Geological setting of Liberia

Liberia is underlain by Precambrian (Archean to late Proterozoic) rocks of the West African Craton which are mainly igneous and metamorphic rocks e.g. gneiss, granite and schists. The Precambrian basement in Liberia can be divided into 3 main age provinces: The Liberian Province (2700 million years), The Eburnean Province (2100 million years), and the Pan African (600 million years). The Liberian province occurs mainly in the northern parts of Liberia (Figure 3.3) but also occurs in the central and western parts of the country. The Liberian province comprises the Archean basement gneiss (granite-gneiss terrain) and the Archean supracrustal schist belts. The schist occurs within the greenstone belts which have an E-W and NE structural trend. The Eburnean age province occurs in the central to southern part of the country (Figure 3.3) and consists of Paleoproterozoic volcanic, sedimentary and plutonic rocks. The boundary between the Liberian and Eburnean provinces is not well defined.

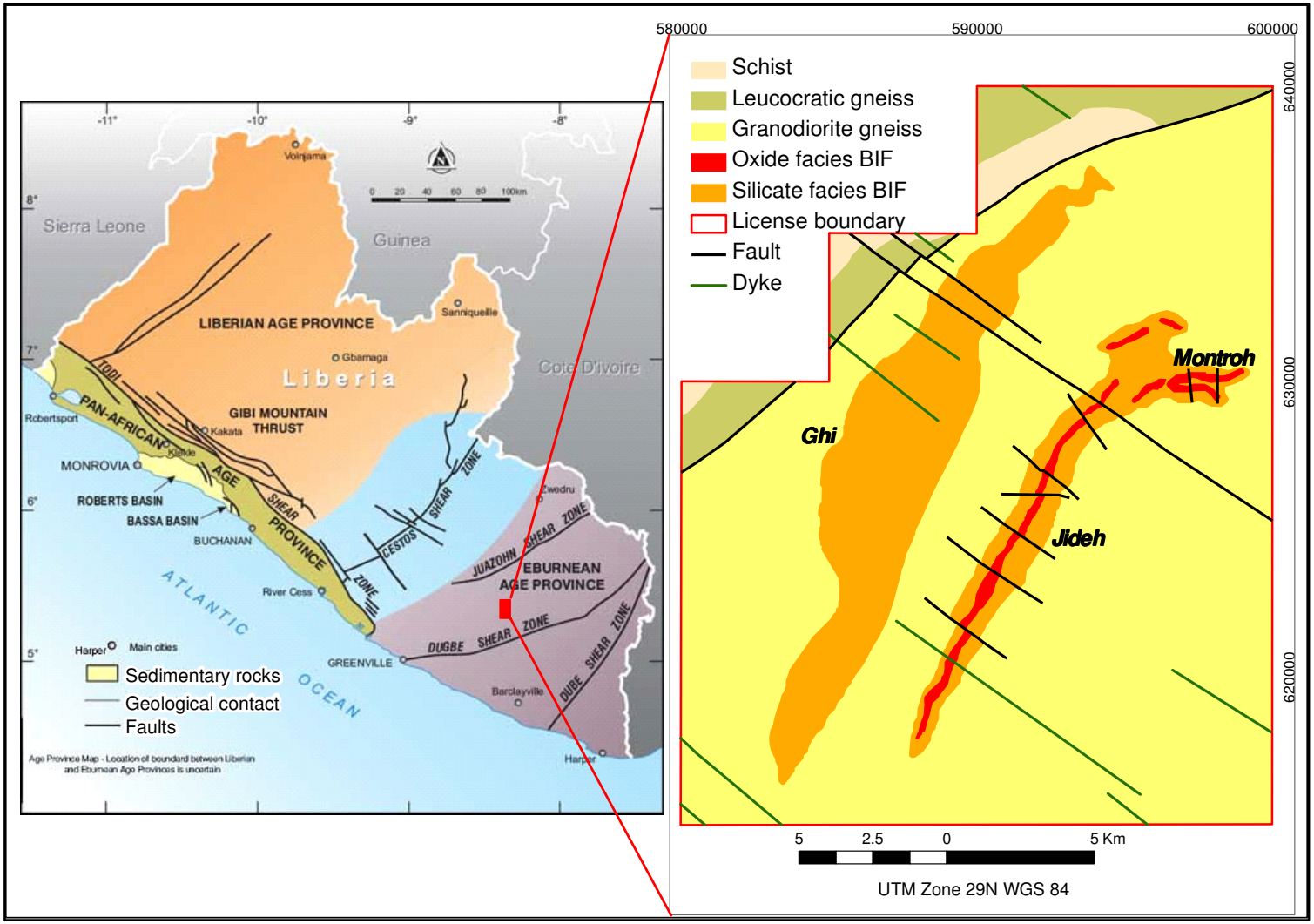

Figure 3.3 Age Provinces of Liberia and simplified geology of the Putu Licence (Modified from Afferro-Mining, 2010 and Amlibgroup, 2013).

The Pan African province occurs in the north western part of the country and is composed of Precambrian and supracrustal rocks. The dominant trend of metamorphic rocks in the Liberian and Eburnean Provinces is NE - SW whilst for the Pan-African rocks the dominant trend is NW - SE. The Pan-African Province is separated from the Liberian province by the Todi Shear Zone which has a NNW-SSE trend (Figure 3.3).

The rock types in the northern and western parts of Liberia are mainly gneiss units with siliceous banded iron formations (itabirites) and schist which are Liberian (2.7 Ga) in age (Figure 3.3). The eastern and southern parts are Proterozoic in age and dominated by greenstones, meta-greywacke and syn-kinematic granites. Sandstone beds lie along the coast line (Figure 3.3) with a few crystalline outcropping rocks which include high grade metamorphic rocks comprising mafic granulites, granite gneiss, pegmatites and kyanite-sillimanite schist. They are Pan-African in age (500 Ma). Other rock types present include dykes, and unconsolidated deposits. Northwest trending Jurassic dolerite dykes and sills cut across all the age provinces forming dyke swarms present all over the country. The West African shield has been subjected to several intense deformations resulting in numerous folding, faulting, unconformities and metamorphism. These structures have a N - E trend and are steeply dipping with vertical or lateral displacement. Some of these faults represent extensions of major structures from the neighbouring West African states of Guinea, Ivory Coast, Niger and Sierra Leone for e.g. the Cestos Shear Zones (Figure 3.3).

3.6 Geology of the Putu License

The licenses occur in the central part of the Juazohn Quadrangle which is underlain by crystalline metamorphic and igneous Precambrian rocks. The metamorphic rocks are mainly metasedimentary in origin of amphibolite facies. The dominant rock type in the area is the granodiorite gneiss and foliation in the gneiss is commonly faint and defined by oriented biotite and locally tabular quartz grains and by dips at moderate angles.

The Putu Iron Ore deposit forms part of the Precambrian Putu mountain ranges which have a general NNE-SSW trend. The deposit is divided into two mountain

ranges with different trends; Jideh has a NNW – SSE trend and Montroh an E – W trend (Figure 3.3). A third mountain range called Ghi which is not part of the deposit being drilled at the moment is comprised of silicates facies iron formation as oppose to the oxides facies iron formation found in Jideh and Montroh. The main economic deposit at Putu is that present at the Jideh Mountain.

The itabirites are mainly fine grained and composed or quartz, iron oxides and minor silicates. Even though the bulk of the deposit is made up of magnetite itabirite, drilling has shown that there is a hematite itabirite in the lower and western portions. Jideh in particular is known to have a hematite cap up to 80 m thick with DSO potential. The iron silicates of the Ghi Mountain are fine grained and are associated with quartz-hornblende or actinolitic hornblende-plagioclase (oligoclase)-magnetite–biotite iron silicate rocks. Both Jideh and Ghi are flanked by leucocratic rocks of gneissic to dioritic to granodiorite composition which are medium to coarse grained.

Jideh Mountain was interpreted by the previous license owners, i.e. BMC/DELIMCO, to be a tight steeply dipping syncline with soft ore at the top which grades into an itabirite transitional zone and ultimately into magnetite itabirite with a decrease in weathering and an increase in competency of the rocks with depth (Tysdal, 1978). Recent drilling has suggested that the structure is more likely to be an antiformal structure rather than a synformal structure as suggested by BMC/DELIMCO reports. Both models however indicate that the deposit sits within steeply dipping limbs.

The deposit at Jideh Mountains is estimated to have a 10 km strike length and is divided into 3 sections separated by minor faults. These are the northern, central and southern sections. The itabirite of the Jideh Mountain is hosted by the granodiorite gneiss and it is the only iron ore deposit of economic significance in the Juazohn quadrangle (Tysdal, 1978).

Itabirite outcrops at Jideh are sporadic and those studied have steep to vertical dips with a roughly N - E strike. The deposit at Montroh covers about 1.5 km with a strike of about 010^{o}. The itabirites at Montroh have shallower dips and

shorter strike lengths compared to Jideh. A thick layer of hematite-itabirite lies over the magnetite-itabirite in the Jideh mountain range but this has not been proven in the Ghi Mountains NW of Jideh. The Ghi mountain range has few outcrops which include iron cap boulders and weathered limonitic soil. A major NE – SW trending fault is present close to the NW boundary of the license. Several NW trending faults offset the NE - SW faults and several cut across Jideh Mountain (Figure 3.3). The faults at Montroh are mainly N - S trending.

Chapter 4

Detailed Geology of the Nkout Iron Ore Deposit: Material Types, Ground Magnetics and Stratigraphy

4.1 Introduction

This chapter summarises the field procedures employed during the fieldwork exercise at Nkout and the sample classification scheme that was being used there at the time. The new sample classification scheme adopted for this research for both the Nkout and Putu samples are discussed to avoid repetition in various chapters. A summary of the report on a ground magnetic survey I conducted at Nkout is also presented. During the field work exercise at Nkout, access was granted to the existing drill core database and this has been used to reconstruct the probable stratigraphy and to create chemical/grade domains. Figure 4.1 shows a digital terrain model of the drill (D) targets.

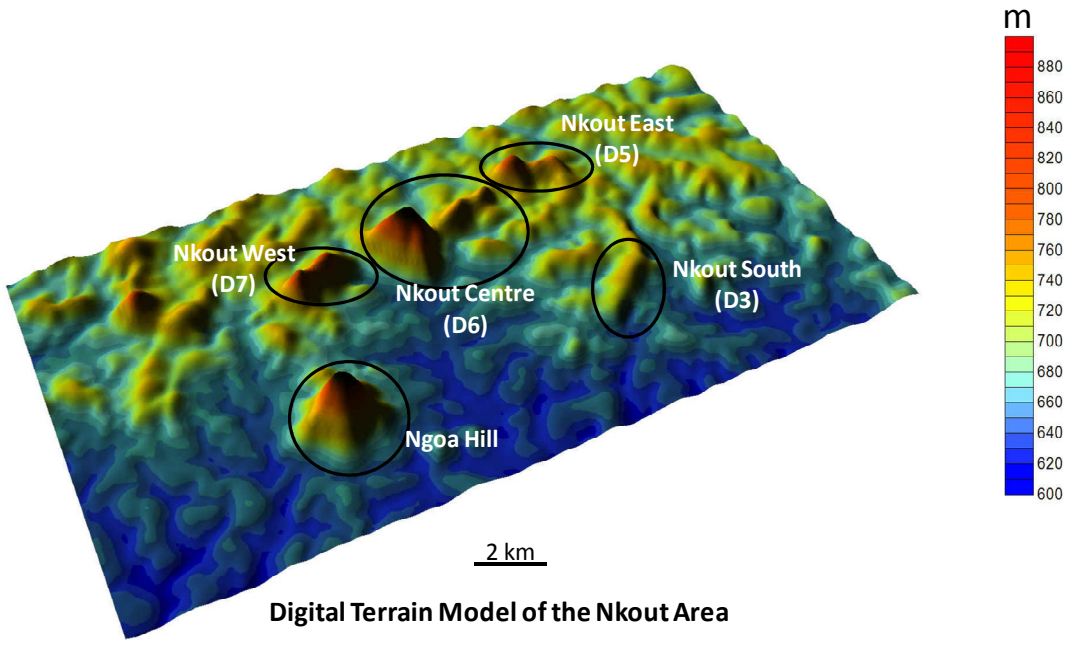

Figure 4.1 Digital terrain model of hills drilled (Afferro-Mining, 2010).

The drill cores were sampled at 2 m intervals for whole rock geochemical analysis, which was done by XRF at ALS Laboratories Ltd, Ireland. At the time of the fieldwork exercise, XRF results were available for 13 drill holes from Nkout east (D5), 73 from Nkout centre (D6) and 9 from Nkout west (D5) although results for Nkout south (D3) and the Ngoa Hill were not available. The locations of the drill collars were measured using a hand held global positioning

system (GPS) and so are accurate to ± 5 m. It should be noted that some inferences and interpretation drawn from the data used in this research may have to be modified due to further drilling.

4.2 Field work at Nkout

The main aim of the fieldwork exercise was to collect representative samples of the rock types in the following project areas; Nkout South (D3), Nkout East (D5), Nkout Centre (D6) and Nkout West (D7) and to study the geology of the area. The samples comprised saprolite, fresh banded iron formation (BIF), grab and outcrop samples. The samples were labelled using the following convention; the first two letters of the sample numbers is an indication of its location e.g. NC for Nkout centre, NW for Nkout west and the third letter indicates whether it is a saprolite sample i.e. S or BIF sample i.e. B. Grab samples have the suffix "G" and the outcrop samples have "Out" as their suffix. The number indicates the sequence in which they were collected with reference to the first three letters described above.

Drilling in the project areas was planned to intersect two targets: saprolite (chemically weathered rock still possessing weakly discernible structures) and BIF (banded siliceous, hematite/magnetite deposit formed by chemical-organic sedimentation processes). Whilst the drilling at D5 and D6 targeted both saprolite and BIF, drilling at D3 and D7 were exclusively for saprolite for the duration of the field work. The rationale was to get a preliminary mineral resource estimate for the direct shipping ore as quickly as possible. Deep holes (> 200 m) are therefore only present at D5 and D6. In order to capture the full variability of the lithologies present, the drill core database was studied and representative samples of all lithologies present were collected. The methodology employed during the fieldwork exercise could be summarised as follows:

- Study of the Nkout database with emphasis on lithology, assay results, structures and geotechnical data.
- Collection of representative quarter core saprolite and fresh BIF samples from each lithology present in the different drill targets. Both mineralised

and host rock samples were collected in order to sample the full variability of all rock types present.

- Field mapping (restricted due to very few outcrops), description and collection of grab samples and samples from in-situ outcrops.
- Photographs of all samples, outcrops and structures.
- Search for literature on Nkout and related deposits from Afferro Mining's in house literature collections.

4.3 Ground magnetics survey

The ground magnetic data was collected using three Overhauser GEM magnetometers (version GSM – 19W v6.06). Overhauser systems have the advantage of lighter batteries and faster sampling rates compared to other types of magnetometers, owing to the fact that electron-proton coupling can happen as measurements are taken. Omni-directional sensors were used for the survey and this eliminated the need to face north when taking readings.

Two magnetometers were used along the lines (one at a time) in a continuous walking mode and the other as a base magnetometer. With the continuous walk mode, readings were taken at approximately every 1 m in gentle terrain and less than 1 m in difficult terrains. They were all cycled at 2 second intervals meaning readings were automatically recorded every 2 seconds. The base station was selected such that it is central to the grid as the same base station was used for the entire survey. The base sensor was tied to a big tree at a constant marked height from the ground to minimise if not completely eliminate the effects of wind. The "walk mode" magnetometers were attached to a series of straps with the sensor securely attached to a backpack using a couple of screws. This ensured that it was easier to carry the console and sensor in difficult terrain. The position of every 25m peg and reading were stored in the magnetometer and used to link the magnetic data to the grid as explained below. Even though the magnetometers had inbuilt GPS systems, these were not used as the area was forested and reasonably accurate GPS readings could not have been collected at the walk pace and the 2 second sampling interval. The line and station locations were collected separately with the aim of obtaining GPS coordinates with an error of ± 5 m. At the end of each day's

work, the base magnetometer was connected to the walk magnetometers using a RS232 cable and the walk magnetometer readings were corrected for diurnal variations and the data downloaded to a laptop. The data downloaded include base data, raw and corrected walk magnetometer data. As the magnetic data were collected using local grid coordinates i.e. line and station, at the end of the day, the UTM coordinates including station elevations were merged into the data during the processing stage of the corrected data.

Twenty lines were surveyed at Nkout with the total distance covered being 39,875 m with line spacing of 400 m. L0 was not surveyed in the Nkout block as it was close to a main road and other areas of logging activities with heavy machinery; this may have resulted in false anomalies. It was necessary to extend some lines in order to define incomplete anomalies based on the original recommended lengths. The surveys for such extensions were started 200 m within the old survey so that there was sufficient overlap between measurements taken on different days. This area of overlap ensured that the old data could be tied in with the new one along the same line.

The corrected walk magnetometer data were then processed so that they could be imported and archived into Geosoft's gdb database. Grids of the total magnetic intensity (TMI) and elevation contours (created from station elevations) were made using Geosoft's "Target" mapping software. X-ray fluorescence results for multi-element analysis of grab samples taken within the survey areas were made available during the magnetic survey and samples with assay results for hematite and iron were extracted from the database. These new data were overlain on the magnetic grids so that they could aid their interpretation.

An insight to the geology of Nkout East, Centre and West i.e. D5 – D7, was obtained using the interpretation of the ground magnetic survey along with the grab, hematite and Fe data. Figure 4.2 shows the elevation contours overlain on the total magnetic intensity grid. The distinct features of the grid are areas of relatively high (pink) and of low (blue) magnetic intensity. The high magnetic area indicates magnetite rich BIFs and they occur mainly on the southern side

of the hills with a strike length of approximately 7 km strike length trending 72° to UTM north and steeply dipping towards SSE.

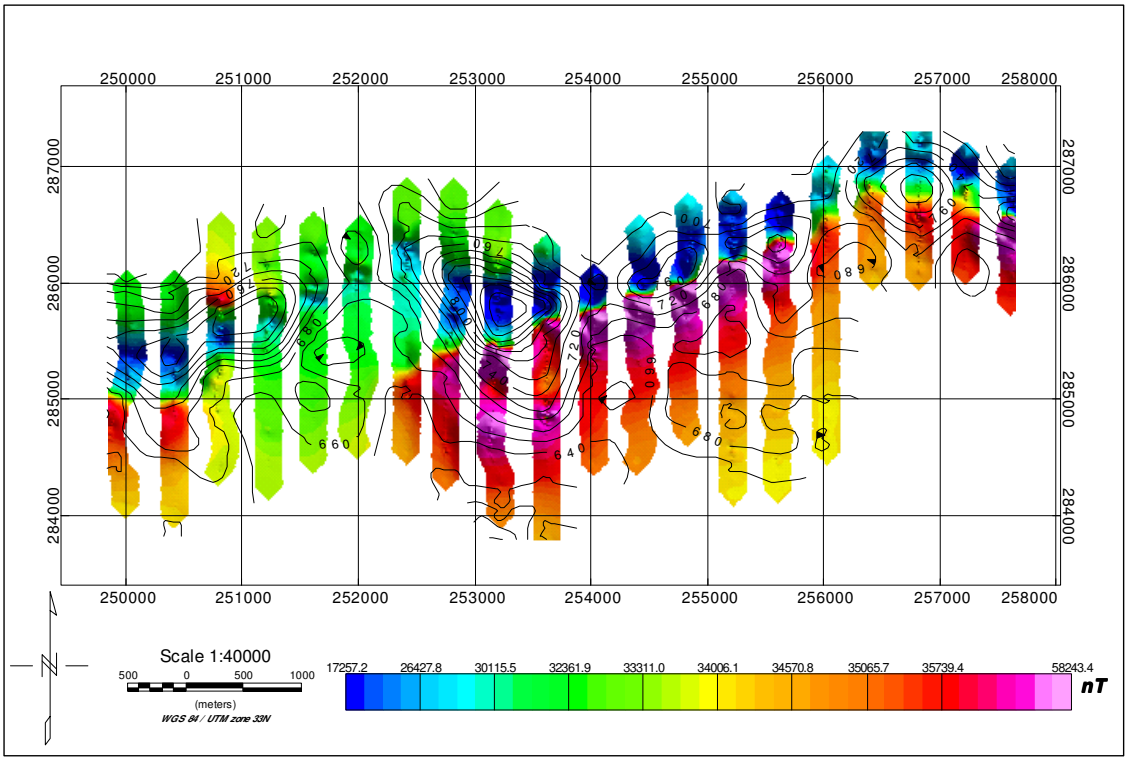

Figure 4.2 Elevation contours overlain on Total Magnetic Intensity Grid, Nkout Iron Ore Project (D5 - D7). The scale represents magnetic intensity in nano tesla (nT).

The peaks of the hills and the adjoining northern slopes are coincident with low magnetic values as can be seen from the elevation contours (Figure 4.2). The first impression one has is that the blue areas represents a different lithology. However when the percentages of hematite (Figure 4.3) present in the grab samples were overlain on the TMI grid, it was seen that the blue areas represent enriched BIFs in a magnetic dipole. Furthermore, two out of the four largest BIF outcrops in the area are located in areas with low magnetic intensity. It was proposed that the blue areas represent enriched material with the potential of DSO for approximately 6 km strike length. The assumption is that there is enriched material cap over the magnetite rich BIF. This sequence has been tilted slightly towards the north and that is why the low magnetic areas occur at the peak and northern side of the hills.

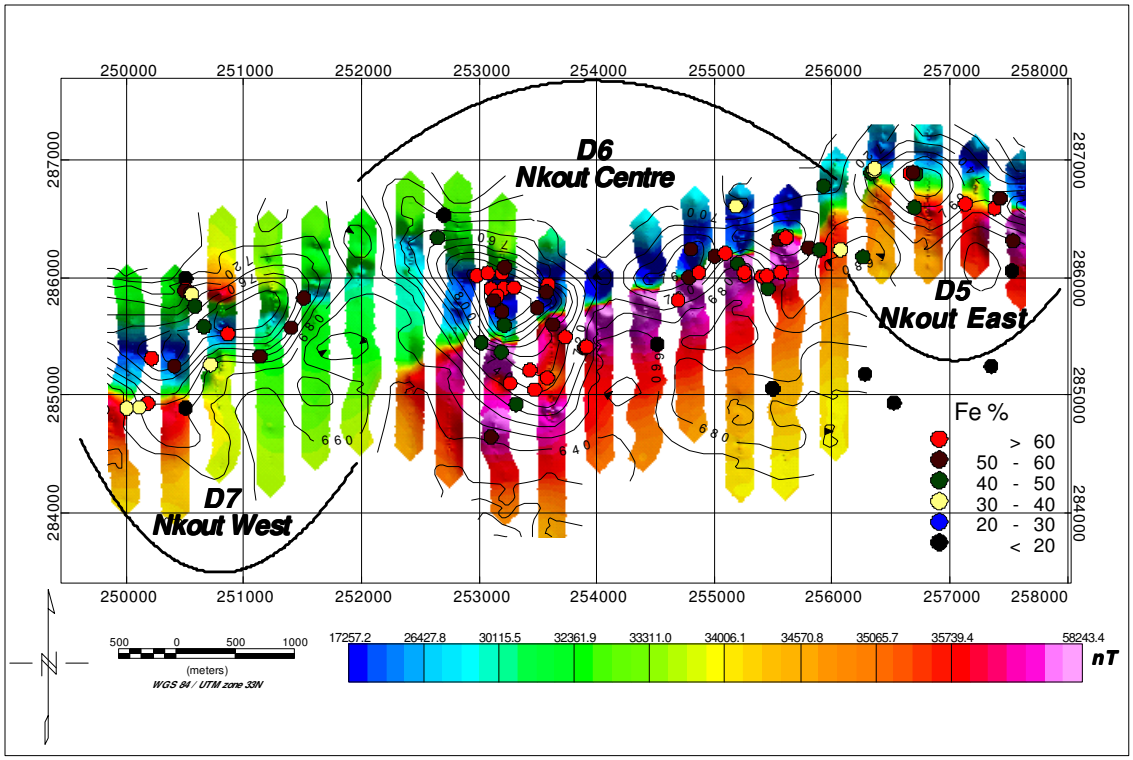

Figure 4.3 Total magnetic intensity grid for D5 - D7 showing anomalous zones, Fe content of grab samples, drill collars and elevation contours.

4.4 Classification of material types

4.4.1 Previous classification scheme at Nkout

Drill core samples were collected using the classification scheme that was used on site at Nkout during the field work. The codes, lithologies and descriptions used in this classification are given in Table 4.1. This was based on visual estimates of major minerals present in the various lithologies or as in the case of coarse magnetite BIF (CMB) and fine magnetite BIF (FMB), the size of certain textures on the drill cores e.g. bands. This classification may be suitable for the host or associated rocks but not for the iron ore deposit itself. For example, differentiating hematite-magnetite BIF (HMB) and magnetite-hematite BIF (MHB) was based on the colour of the cores and hence subjective, i.e. based on the perception of the geologist doing the logging. Furthermore, no measurement was made to differentiate CMB from FMB and with additional categories such as BIF, laterite, saprolite and saprolite rock, similar material types were put under different categories depending on who was doing the logging.

Table 4.1 Afferro Mining's material types classification scheme used at Nkout.

Code	***Lithology***	***Description***
Amp	Amphibolite	Medium- to coarse grained metamorphosed basic igneous rock with feldspars, biotite, quartz, epidote, amphibole
BIF	Banded Iron Formation	Banded siliceous, hematite/magnetite deposit formed by chemical-organic sedimentation processes
BQGn	Biotite Quartzite Gneiss	Biotite and quartzite grains dominant in gneiss
Cl	Clay	Fine-grained (< 0.002mm) earthy material primarily of hydrated silicates of aluminium
CMB	Coarse banded Magnetite BIF	Coarse banded (alternating Fe-bearing / siliceous) banded iron formation
FMB	Fine banded Magnetite BIF	Fine banded (alternating Fe-bearing / siliceous) banded iron formation
GGn	Garnetiferous Gneiss	High concentration of garnet in gneiss
GMB	Garnetiferous Magnetite BIF	High concentration of garnet in magnetite BIF
Gn	Gneiss	Generally coarse-grained, high grade metamorphic rock. At Nkout, gneiss protolith is basement granite
Grt	Granite	Coarse-grained, quartz-rich igneous rock with feldspar, micas. Accessory magnetite, apatite
HMB	Hematite Magnetite BIF	Banded Iron Formation with greater hematite than magnetite
Lat	Laterite	Weathering product of rocks composed mainly of hydrated Fe & Al oxides and hydroxides and clay minerals. No structural remnants
MHB	Magnetite Hematite BIF	Banded Iron Formation with greater magnetite than hematite
MS	Metasediment	Fine to medium-grained, mottled, low grade metamorphosed rock with traces of mineral alignment
Peg	Pegmatite	Very coarse grained (>250mm) igneous rock of granitic composition
Qtz	Quartzite	metamorphic rock composed predominantly of quartz (protolith: quartzitic sandstone)
QV	Quartz Vein	Vein of quartz >1m in thickness
Sap	Saprolite	Chemically weathered rock still possessing weakly discernible structures
SapRk	Saprolite rock	Chemically weathered rock possessing strongly discernible structures, although still a product of chemical weathering
Sc	Schist	Medium grade metamorphic rock with smaller grain size than Gn (though >1mm) displaying schistosity

4.4.2 Proposed classification of material types

The samples were divided into 4 main groups based on the whole rock Fe content determined by XRF analysis and the degree of weathering determined by visual estimation. The groups are enriched material (EM), weathered magnetite itabirite (WMI), transitional magnetite itabirite (TMI) and magnetite itabirite (MI) (Table 4.2, Figure. 4.4). The magnetite itabirite group is divided into 2 sub-groups; high-grade (HMI) and low-grade magnetite itabirite (LMI).

Table 4.2 Classification scheme adopted for this research.

Code	*Material Types*	*Fe content and degree of weathering*
EM	Enriched material	≥ 60 wt %, WI = 2 to 6
WMI	Weathered magnetite itabirite	50 wt % ≤ Fe < 60 wt. %, WI ≥ 4
TMI	Transitional magnetite itabirite	15 wt % ≤ Fe < 50 wt %, WI = 3 or 4
HMI	High-grade magnetite itabirite	Fresh itabirite, 30 wt % ≤ Fe < 60 wt %, WI = 1 or 2
LMI	Low-grade magnetite itabirite	Fresh itabirite, 15 wt % ≤ Fe < 30 wt %, WI = 1 or 2

Fe contents determined by XRF. Arbitrary weathering index (WI) of 1 to 6 in which 1 represents fresh itabirite and 6 is highly weathered material.

The physical characteristics of the ore grade materials have been classified using their intensity of weathering based on a weathering index (WI) on a scale of 1 to 6. One and two represent hard materials such as fresh itabirite or hard massive hematite and BIF outcrops (Figure 4.4, e, f), 3 and 4 medium hard materials (Figure 4.4 a, d, g and h) and 5 and 6, friable biscuity or lateritic material (Figure 4.4 b, c, j & l). Enriched material and WMI materials at Nkout are dominated by friable biscuity, laterite and saprolite material although at least one hard hematite/goethite outcrop is present (Out01, Figure 4.4k) and was studied. These groups were chosen to represent processing requirements and characteristics rather than geological origin.

The enriched material (EM) group consists of all samples with Fe contents ≥ 60 wt %. Material types that meet this threshold are usually considered to be direct shipping ores (DSO) provided other deleterious elements are within the customer's specifications. The weathered magnetite itabirite by definition will require minimal processing to meet the DSO specifications. Materials containing lower concentrations of Fe and at an earlier stage of weathering compared to

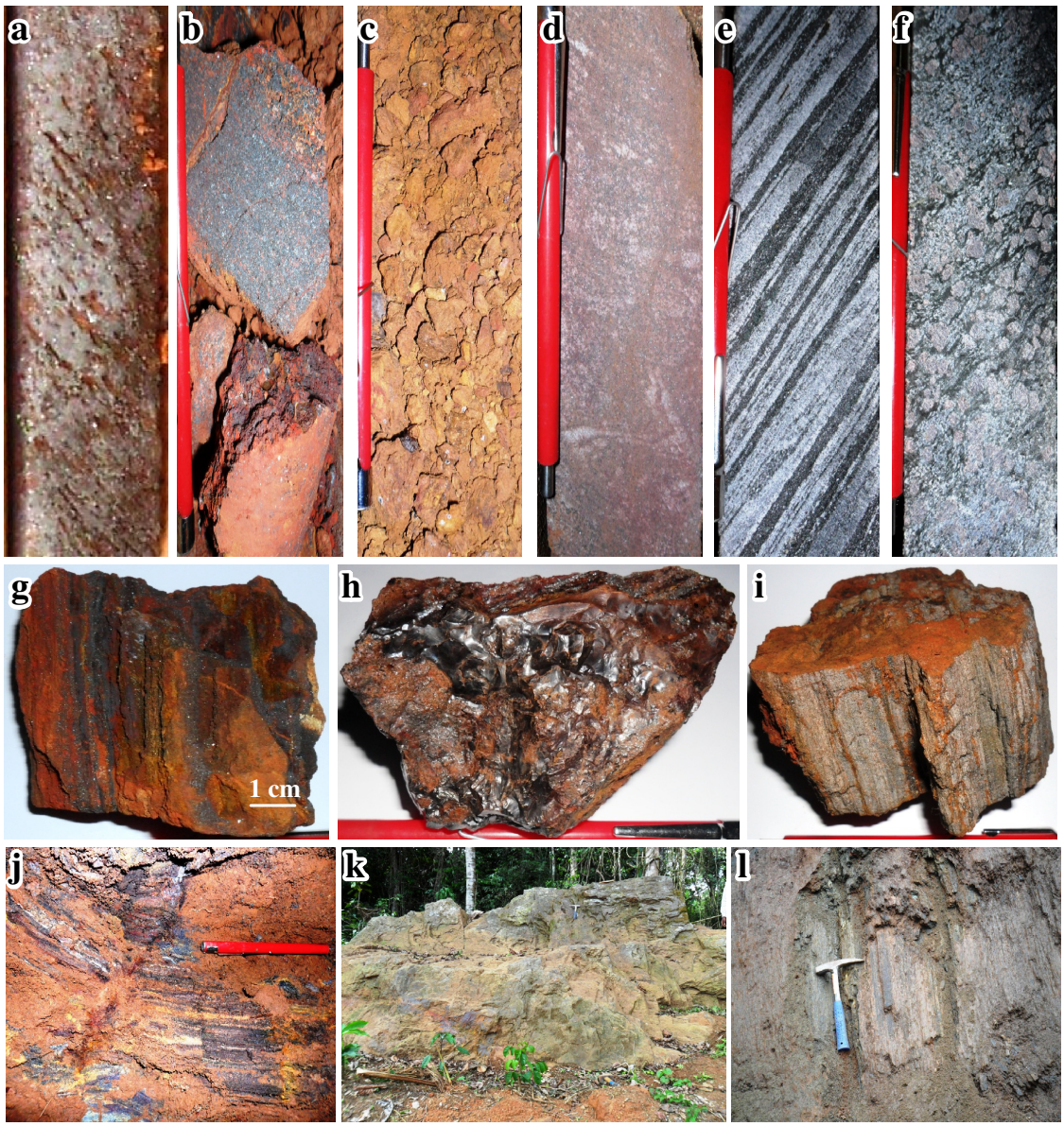

Figure 4.4 Examples of material types a) Enriched material with silver-grey hematite crystals; drill hole NKHC040, 12.6m WI = 4, (Sample NCS09), (b) Weathered magnetite itabirite with black magnetite and red hematite; drill hole NKEHC007, 6.3m WI = 5 (Sample NES04), (c) Lateritic weathered magnetite itabirite containing yellowish limonite/goethite; drill hole NKHC020, 20m WI = 6 (Sample NCS08), (d), Transitional magnetite itabirite showing initial stage of weathering of fresh itabirite; drill hole NKEHC008, 28.35m WI = 3 (Sample NES05), (e) High-grade magnetite itabirite with alternating bands of magnetite, quartz and silicates; drill hole NKWHC002, 73.00m, WI = 1 (Sample NWB02), (f) Low-grade magnetite itabirite with round pink garnet grains; drill hole NKWHC001, 85.60m WI = 1 (Sample NWB01), (g) Grab sample with blue/black hematite/magnetite and yellow goethite minerals, WI = 3 (Sample G02), (h) Magnetite and goethite rich grab sample with glassy texture; WI = 3 (Sample G01), (i) Siliceous grab sample WI = 4 (Sample G03), (j) Saprolite outcrop WI = 6 (Sample Out02), (k) Hard massive outcrop WI = 2 (Sample Out01). (l) Silica rich saprolite outcrop WI = 6 (Sample Out03).

EM and WMI are classified as transitional magnetite itabirite (TMI). The low-grade magnetite itabirite in Figure 4.4f is garnetiferous; the garnet being almandine (Chapter 7). The EM constitutes a minor part of the deposit and is mainly found at Nkout East and Centre whilst the magnetite itabirite (MI) forms the bulk of the deposit.

4.4.3 Associated rock types

From the drill core logs, it was noted that the rock types listed in Table 4.3 are also present within the deposit. The metasediments and granite gneiss could be found intercalated with the magnetite itabirite though the granite gneiss mainly occurs as the basement rock. Some gneiss and metasediments have been found to be garnetiferous. Quartz bands and veins are found within the granite gneiss layers. They could also be found within the weathered profile, which is an indication that they are a direct result of leaching of silica during the enrichment process. Relatively few intersections of amphibolites and schists were cut during drilling.

Table 4.3 Rock types associated with the deposit.

Code	*Lithology*	*Description*
Amp	Amphibolite	Medium- to coarse grained metamorphosed basic igneous rock
GGn	Garnetiferous Gn	Garnet bearing Gn
GMS	Garnetiferous MS	Garnet bearing MS
Gn	Biotite Granite Gneiss	Biotite bearing granite or gneiss, includes charnockites
MS	Metasediments	Metamorphosed sedimentary rocks, mainly phillites,
QB	Quartz Band	Includes quarz vein and quartzite
Sc	Schist	Laminated, flaky micaceous metamorphic rock

4.5 Stratigraphy of the Nkout Deposit

4.5.1 Methodology

The drill collar, geology, lithology, survey and assay files were imported into Geosoft's Target software as comma separated value (CSV) files. With the exception of the lithology file, all the other files included columns for the hole and sample IDs which were used to link all of them. In addition, the collar file includes the sample ID, azimuth, dip, hole coordinates (x, y), elevation (z), depth to which the holes were drilled (end of hole) and the proposed dips and

azimuth of the holes. The geology data which comprised lithologies logged based on the existing system at Nkout, were reclassified to the adopted material types used in this research based on their iron content and the weathering index (WI). The geology file gives the lithologies logged based on the depth from where a particular lithology starts to where it ends i.e. from–to data, in addition to the weathering index. The lithology file includes the lithology codes and descriptions which could be used in the legend of maps. The assay files give from–to data for assays, in this case, XRF data. The assay file gives amongst other assay results the Fe, SiO_2, Al_2O_3, P_2O_5 and loss on ignition (LOI) percentages for the drill cores and also includes the sample ID. The from-to data, sample ID and hole ID were used to merge the XRF results and material types to the drill hole logs.

Plan maps of the collars for holes drilled up to the time of the field work exercise were created and used to display surface views of drill hole collars, coordinates, drill hole traces and other grids such as in this case, the ground magnetic data based on their coordinates. As the bulk of the drilling was focused on Nkout Centre, a 3D ltihology map was also created for Nkout centre. Selected drill cores from Nkout Centre were then used to produce section maps. The section maps provide cross sectional views of drill hole traces, coordinates, assay values, material types and can also help to establish subsurface drilling coverage. Holes were selected so that they are mainly in the E – W direction and with minimal overlaps. The elevation data was used to create a topography profile in the E – W direction and this was overlain on the section maps to give the relationship between the core classification and topography. Section maps could also be displayed with the assay values of the cores but this will result in a clustered map. As an example to see how this could be done and how effective it could be, a strip log of the deepest hole was made along with the weathering index and assay values for Fe, SiO_2, P_2O_5, Al_2O_3 and LOI.

4.5.2 Stratigraphic reconstruction

The drill holes used in this research are shown in the plan map in Figure 4.5. It is clearly seen that most of the drilling was focussed on Nkout Centre. Since the trend of the Nkout hills is east-west, the sections have also been constructed in

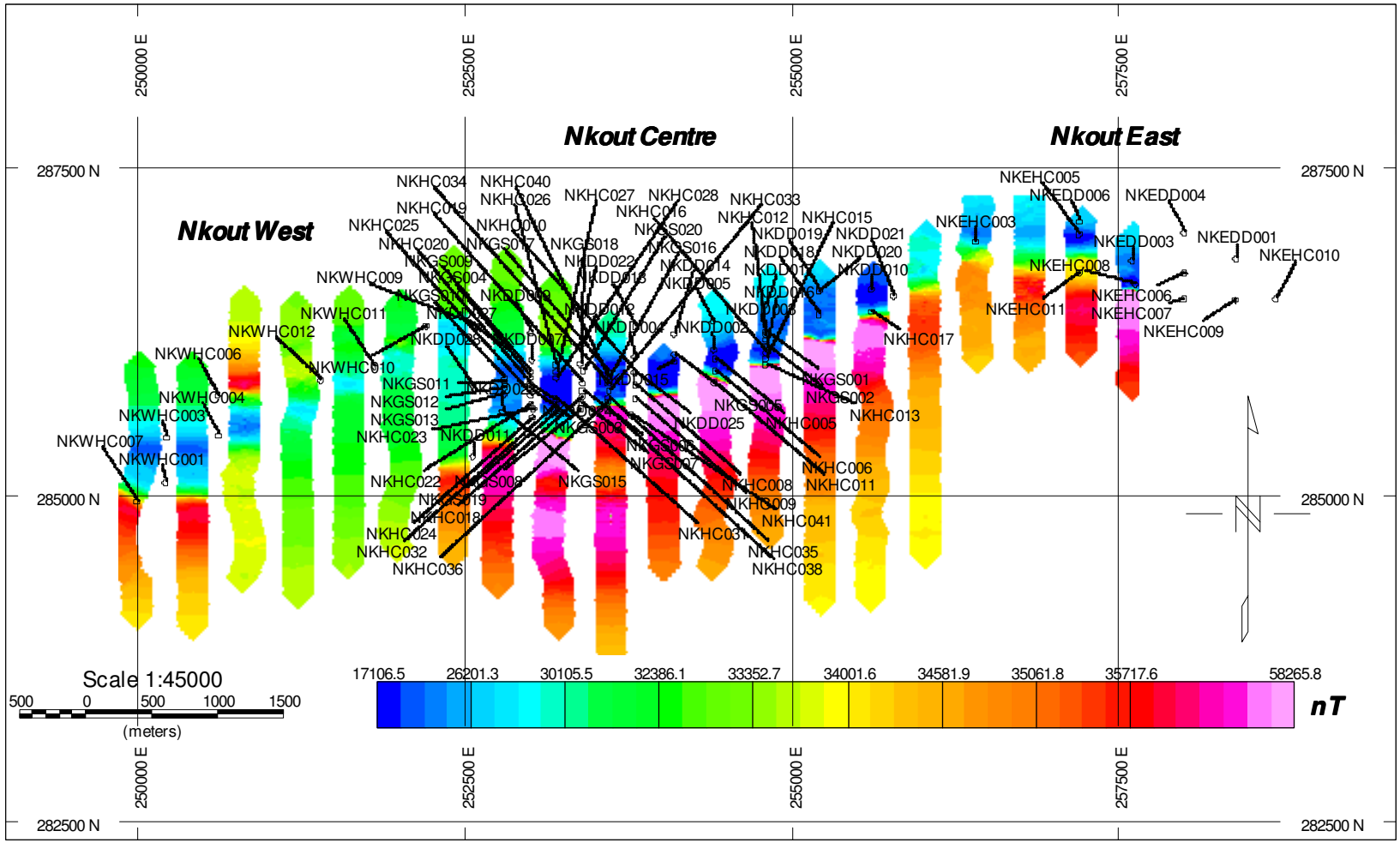

Figure 4.5 Location of drill hole collars overlain on total magnetic intensity grid. The bulk of the holes have been drilled at Nkout centre because it has the greatest potential for DSO material.

the W-E and E-W directions. Metamorphism leading to strong deformation has made it difficult to reconstruct a detailed stratigraphy by joining similar material types from adjacent drill holes. As such, the drill data was studied along with the local and regional geology to come up with a proposed or possible stratigraphy. A possible stratigraphy from top to bottom could be summarised as follows:

Enriched Material - This material type which represent the potential DSO material at Nkout are mainly found at Nkout Centre and to a small extent at Nkout East but have not been shown to be present at Nkout West or South. They have been assigned weathering index (WI) of 2 to 6. Weathering index of 4 relates mainly but not exclusively to materials with recrystallized hematite whilst WI of 5 to 6 indicates lateritic, biscuity and powdery hematite / goethite / magnetite material. It has been shown by QEMSCAN® (Chapter 8) that some of these material types contain significant amounts of magnetite and goethite. They are generally about 2 to 10 m below the surface and have been shown to have thicknesses of up to 60 m.

Weathered Magnetite Itabirite - These are materials with DSO potential but which need processing to reduce the aluminium and, in some cases, the silica content and thereby increase the Fe content. The aluminium content is related to clays and to some extent goethite. They include lateritic material and saprolite. Laterite is formed by intensive and prolonged tropical weathering intensified by high rainfall and high temperatures. As the BIF transforms to laterite, there is an increase in the iron content and a decrease in silica above the parent rock. The initial products are called saprolite and are essentially kaolinized or in general, clay-rich rocks showing the structure of the original rock. Iron is not as strongly concentrated in the saprolite as in the laterite and they occur at depths deeper than the laterite.

Transitional Magnetite Itabirtie – This type represents the dominant weathered ore material in the weathering profile and is mainly found on top of the fresh itabirite. Closer to the surface it is characterised by high Al, magnetite and goethite concentrations with magnetite and goethite in higher concentrations than hematite in most cases. They are however in most cases found at depths

greater than that of the WMI. They have WI of 3 to 6, are common to all 4 drill targets and represent the initial stages of weathering as the fresh magnetite itabirite is upgraded to the enriched material.

Magnetite Itabirite – This type represents the dominant ore type in the area and even though it is mainly fresh BIF, in a few cases some samples have undergone some weathering owing to the mobilisation of fluid through deep lying structural features. They have been divided into high grade and low grade magnetite itabirite as defined in Table 4.2. This type can be massive or banded, with banding considered as coarse if $\geq$ 3 mm or fine if less than 3 mm. The bands are mainly made up of magnetite and quartz. The quartz may be recrystallized and megascopic as shown in Figure 4.6 and the bands may be folded or straight. At Nkout west and the western part of Nkout centre, some magnetite itabirite contains a significant amount of garnets, mainly almandine but andradite is also present (Chapter 7).

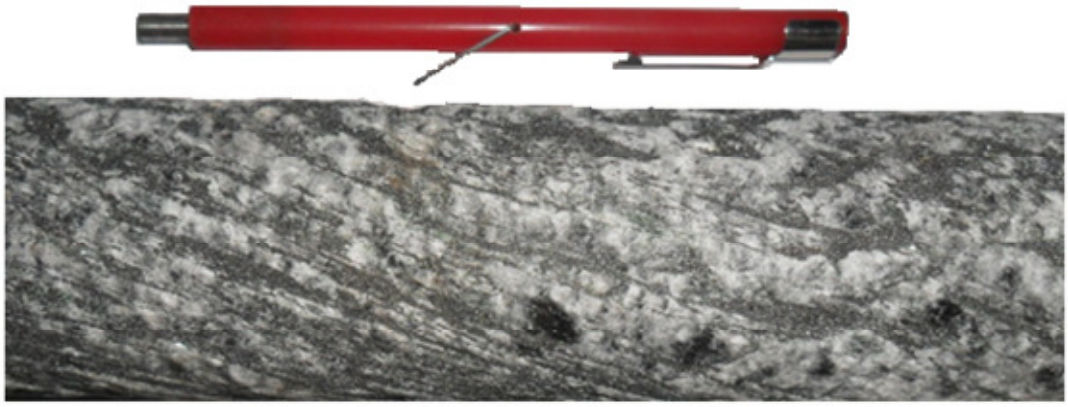

Figure 4.6 Fresh itabirite with megascopic recrystalized quartz rich bands.

Metasediments - These are mainly phyllites and chlorite schists. They are found intercalated with the magnetite itabirites and have their greatest thickness in the east with a decrease toward the west. Grain sizes vary from fine to medium and colours are greenish or greenish grey to dark grey.

Basement granite gneiss - Even though this has been termed as basement, these rocks are found intercalated with the magnetite itabirite. In some drill holes they have been found to occur on top of the itabirites. Biotite and quartz are the dominant minerals and the quartz exists as quartzite, quartz bands and veins. In the Congo Craton these rocks are referred to as charnockites.

The limited surface exposure makes it difficult to effectively map the area but drill core logs have been used to create a 3D map showing a constructed surface and below surface lithology for Nkout Centre in both the East-West and West-East directions (Figure 4.7). Nkout Centre was chosen for the 3D lithological map because it has the most drill coverage including deep holes i.e. holes greater than 200m. The map was constructed using the minimum curvature gridding method. Gridding in general is an interpolation scheme which estimates values for areas with no data using nearby known data values. The minimum curvature surface is the smoothest possible surface that will fit the known/measured data values. The descriptions of the units described above were partly based on this interpretation of the subsurface lithology. These lithological units could well be regarded as geological domains which could be used for mine planning. For the enrichment profile however, it is concluded that alteration and stratigraphy are the main controls on the mineralisation. Supergene upgrade by gangue leaching in the weathering zone was marked by martitization and replacement of magnetite by goethite. Gangue leaching is plausible because with the exception of the surficial material which could be clay rich, the iron content decreases with depth from EM to WMI to TMI to MI. From the sections, it is seen that Nkout Centre has the greatest potential for the enriched material which occur at the crest of the hills.

It can be seen from Figure 4.7 that the enriched material and the weathered magnetite itabirite are to be found at the crest or flanks of the highest peak at Nkout Centre. Even though there are a few gneiss and metasedimentary outcrops, the dominant surficial material is the transitional magnetite itabirite which extends right through the length of Nkout Centre. This lithological description is the same for Nkout West and Nkout East. Figure 4.8 shows a section constructed form selected drill cores from Nkout Centre. The trends of the hills that comprise the Nkout deposits are in an E - W direction and this is therefore the orientations of the sections in Figure 4.7.

The general spacing of the drill holes is 200m and the topography is included in the sections i.e. the E-W black line on top of the sections. All attempts to join

similar lithologies have proved futile and the BIF mineralised zones occur as stacks which bear no direct stratigraphic relationship.

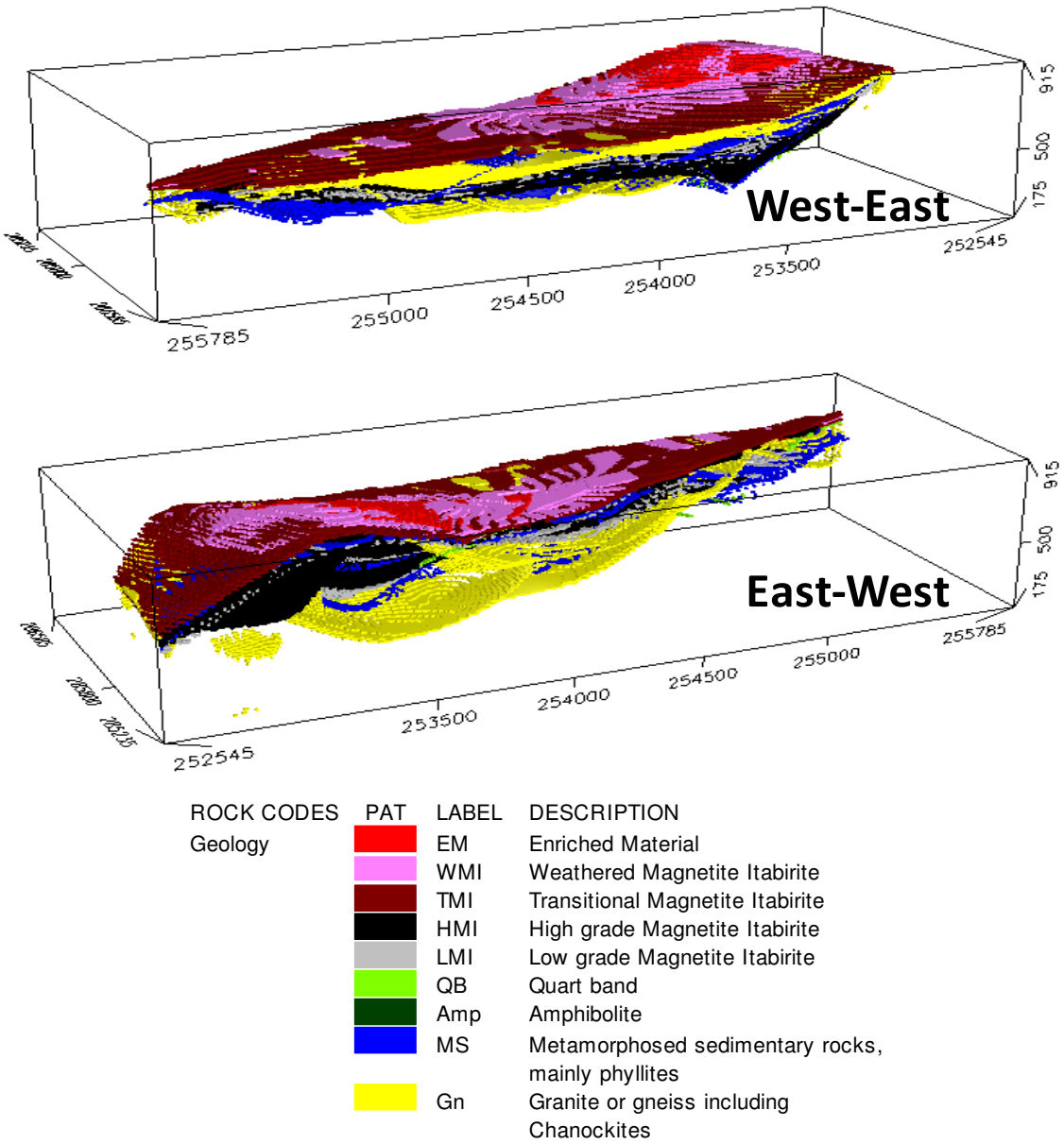

Figure 4.7 3D Lithological maps for Nkout Centre, constructed from 73 drill holes using the minimum curvature method on Geosoft's Target software.

A closer look at the section of the selected drill holes from Nkout Centre (Figure 4.8) shows that some amount of folding and faulting has occurred resulting in the basement gneiss being on top of the magnetite itabirite in holes NKDD027, NKDD013 and NKDD014. These structural features have also affected the metasediments as can be seen in drill hole NKDD024. Even though structures were not studied in this research, it is important that their presence be taken into consideration.

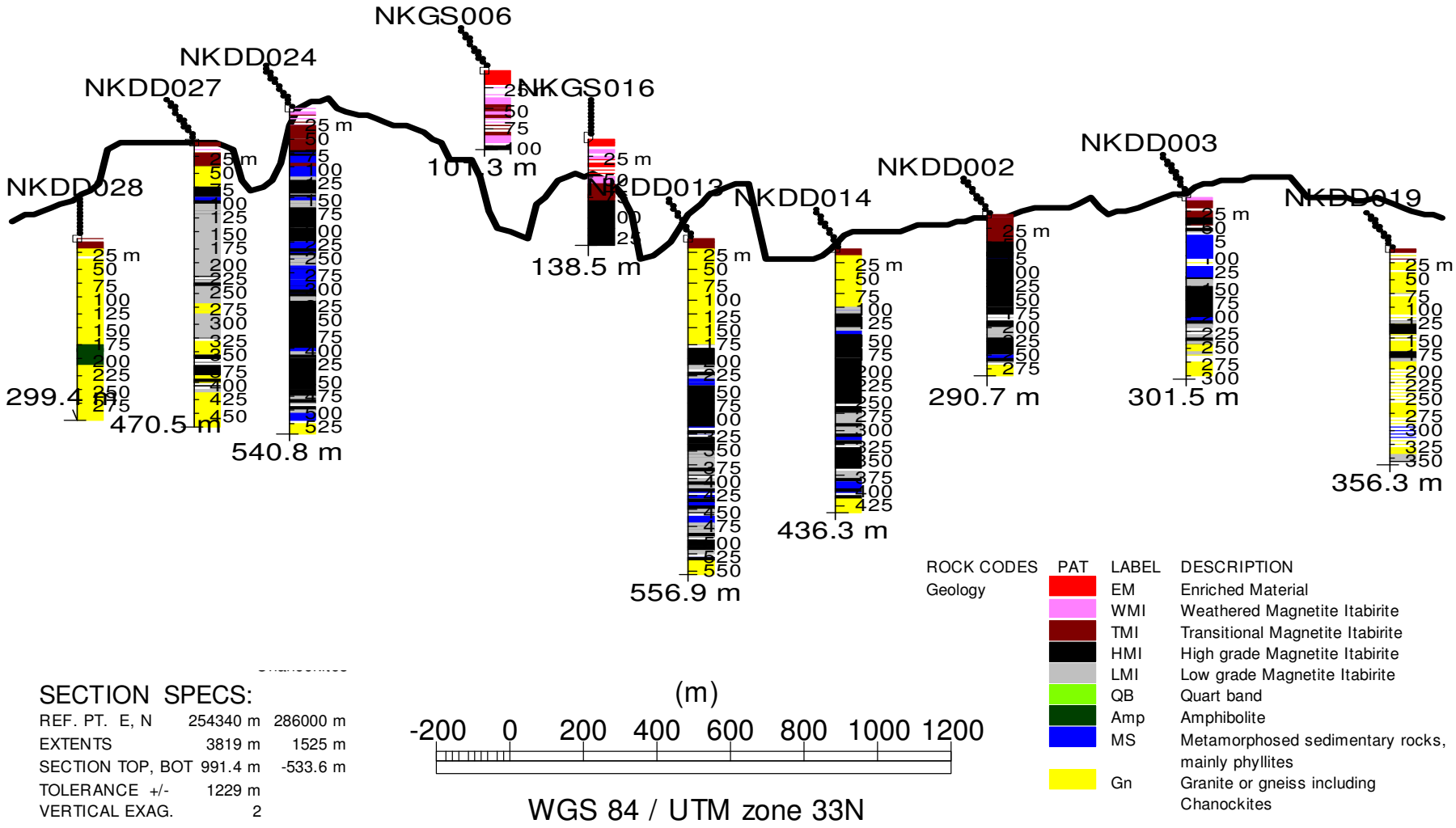

Figure 4.8 W - E section constructed from selected drill holes from Nkout Centre.

For example, drilling a new hole that intersected gneiss might give the impression that the basement has been reached but in reality the gneiss might just be part of a folded limb.

This folding has also affected drill core NKDD022 which is the deepest hole and the core selected for the strip log (Figure 4.9). This folding is indicated by the gneiss being found just below (about 10 m) the transitional magnetite itabirite. Note that the Fe % for the high grade magnetite itabirite and the transitional magnetite itabirite are similar being between 30 to 40% (Fourth column on Figure 4.9). The difference is in the weathering index which is 6 for the TMI but 1 for the HMI. The lowest Fe values are for the granites and to a lesser extent, the metasediments. The granites on the contrary have the highest SiO_2 and Al_2O_3 concentrations due mainly to the aluminosilicates present in them. Phosphorus is < 0.05 % for most lithologies but most importantly for the HMI which is good for the quality of the iron ore. The highest loss on ignition as expected is for the TMI which is weathered and potentially contains goethite.

4.5.3 Distribution of Fe, LOI, Al, P and Si domains within the Nkout deposit

Creating domains is essential in mineral resource evaluation and processing. Homogeneous geological domains are created based on differentiating characteristics such as age, chemistry, mineralogy, alteration, lithology, geophysical properties, etc. (Ortiz and Emery, 2006). Domains are created based upon sound knowledge of the ore body obtained mainly from drill hole data. In most cases, different domains may have differing recoveries of ores within these distinctive geological properties. Geostatistical tools such as variograms and kriging are used to populate areas with no data in domains (Rao et al., 2014). This may require infill drilling to limit the distances between known data points and so increasing reliability of the predictions. According to Ortiz and Emery (2006), the definition of the boundaries between geological domains can be problematic due to the following factors;

- Several interpretations are possible as the domain definition is based on the geologist's knowledge and interpretation of the ore body and hence subjective.

- Sample information may be limited resulting in zones and boundaries of uncertainty which are created based on geostatistical techniques rather than true values.
- Domain boundaries are often considered to be hard i.e. data from across the boundaries are disregarded when estimating the grades within a given domain. If there is a significant spatial correlation of the domain property across the domain boundaries, the assumption that the boundary is hard can affect the quality of the estimates made. The geological mechanisms that result in ore formation are in most cases transitional or “soft”.

In this study, due to the limited amount of samples available, the limited areal coverage of the magnetic data, and the fact that the mineralogy logged for the drill cores based on the original rock classification used at Nkout has been changed to the material class classification used in this thesis, only chemical domains showing the distribution of Fe and the major deleterious elements were created. The domain boundaries have been set to the legend for the distribution of the particular element considered (Figure 4.10). Furthermore domains were created using the material types classification used in this thesis (Figure 4.7). These material classes can be considered as metallurgical domains because they might require different processing routes based on their different mineralogical and chemical compositions. For example the EM might only require crushing (if necessary), scrubbing and screening whist the WMI and TMI might require in addition, both low and high intensity separation as they contain magnetite along with the less magnetic hematite and goethite. The HMI and LMI might only require low intensity magnetic separation.

The main elements used to determine the chemical properties of an iron ore are iron, silicon, phosphorus and aluminium. Others such as sulphur, titanium and the alkali elements can be important if present in high concentrations but this is not the case at Nkout. Loss on ignition which is related to the presence of volatiles is also important in determining the qualities of an iron ore as it devalues its cost due to a potential reduction of volume during smelting. The effects of these deleterious gangue minerals and LOI have been discussed in

Chapter 2. Voxel gridding has been used to create 3D grids based on the grade/concentration of these elements and LOI and these are shown in Figure 4.10.

The range of values for the Fe image has been ordered in intervals of 10 % so that we can clearly see where the DSO material i.e. Fe % ≥ 60 % is located. The DSO material is concentrated at Nkout Centre and surrounded by Fe % ≥ 50 % which has been described as WMI and has the potential of being easily upgraded to DSO requirements. The bulk of the remaining surficial material contains Fe between 30 % and 50 %. There is then a general decrease in Fe concentration with depth indicating supergene upgrade by gangue leaching in the weathering zone.

The high Al_2O_3 % could be found at the top and bottom of the deposit which according to the lithology map coincides with the EM, WMI and TMI at the top and the granites and/or metasediments at the bottom. The middle areas with relatively lower Al content correspond to that of the magnetite itabirite. It is proposed that the high LOI at the top of the deposit could be explained by the presence of clay minerals such as gibbsite and to some extent Al present within goethite. Loss on ignition in general decreases as we go deeper into the deposit which is an indication of the presence of fresh materials such as the magnetite itabirite and the granites/gneiss at depth.

The distribution of phosphorus would have being considered as being random if not for its highest concentration coinciding with the high Fe material. At the surface, high phosphorus could not be due to apatite and other phosphorus minerals as they have not been found to be present in the weathered materials of EM, WMI and TMI. At depth, it is due to the presence of apatite within magnetite itabirite. It is proposed that the high phosphorus at the top central part of the deposit is due to phosphorus locked within goethite which could be a major cause of concern in terms of processing. Even though research is being conducted on removing phosphorus locked within goethite (AMIRA project) it is still one of the greatest challenges to mineral processors due to the amorphous nature of goethite (AMIRA, 2009).

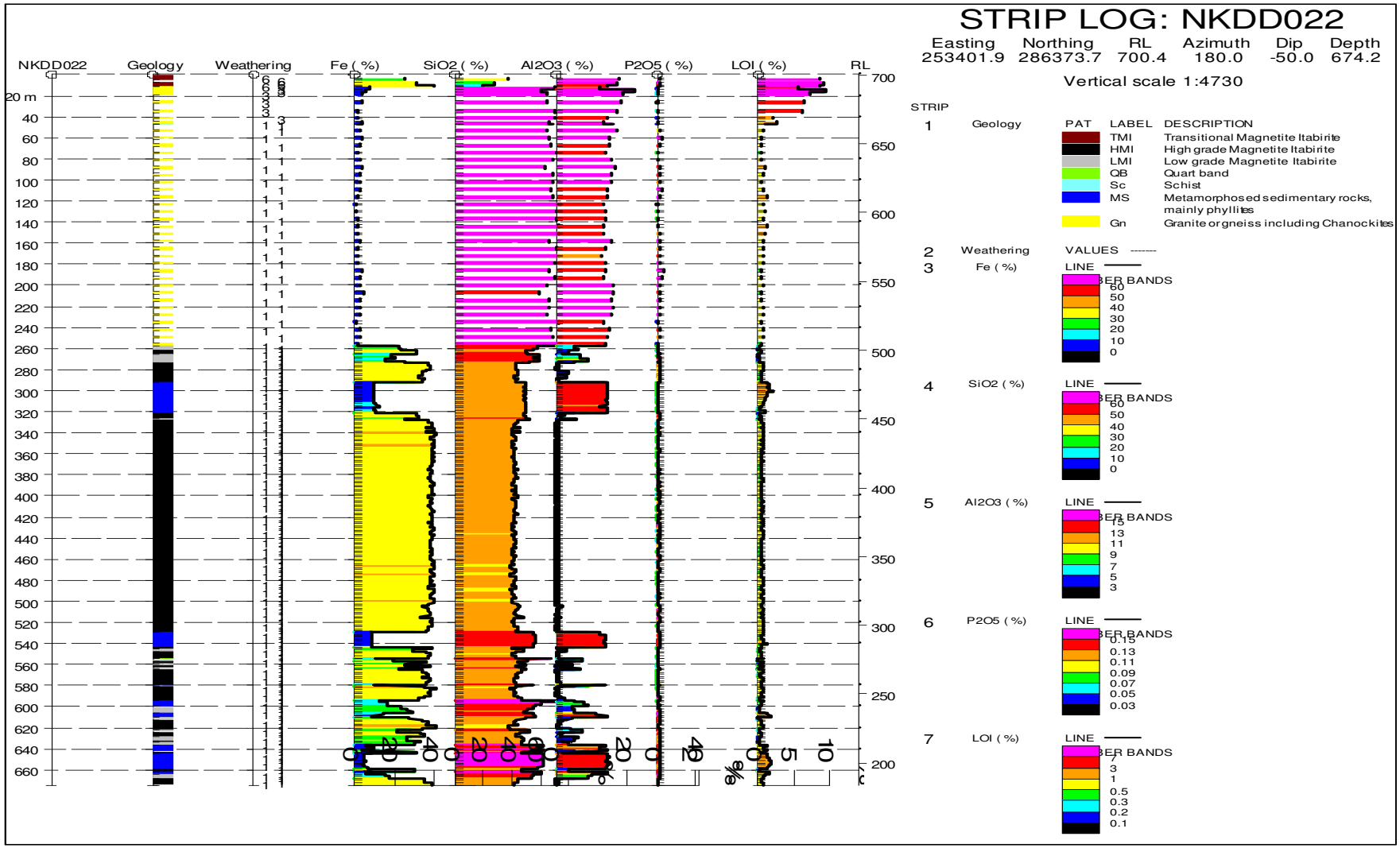

Figure 4.9 Strip log for Drill Hole NKDD022.

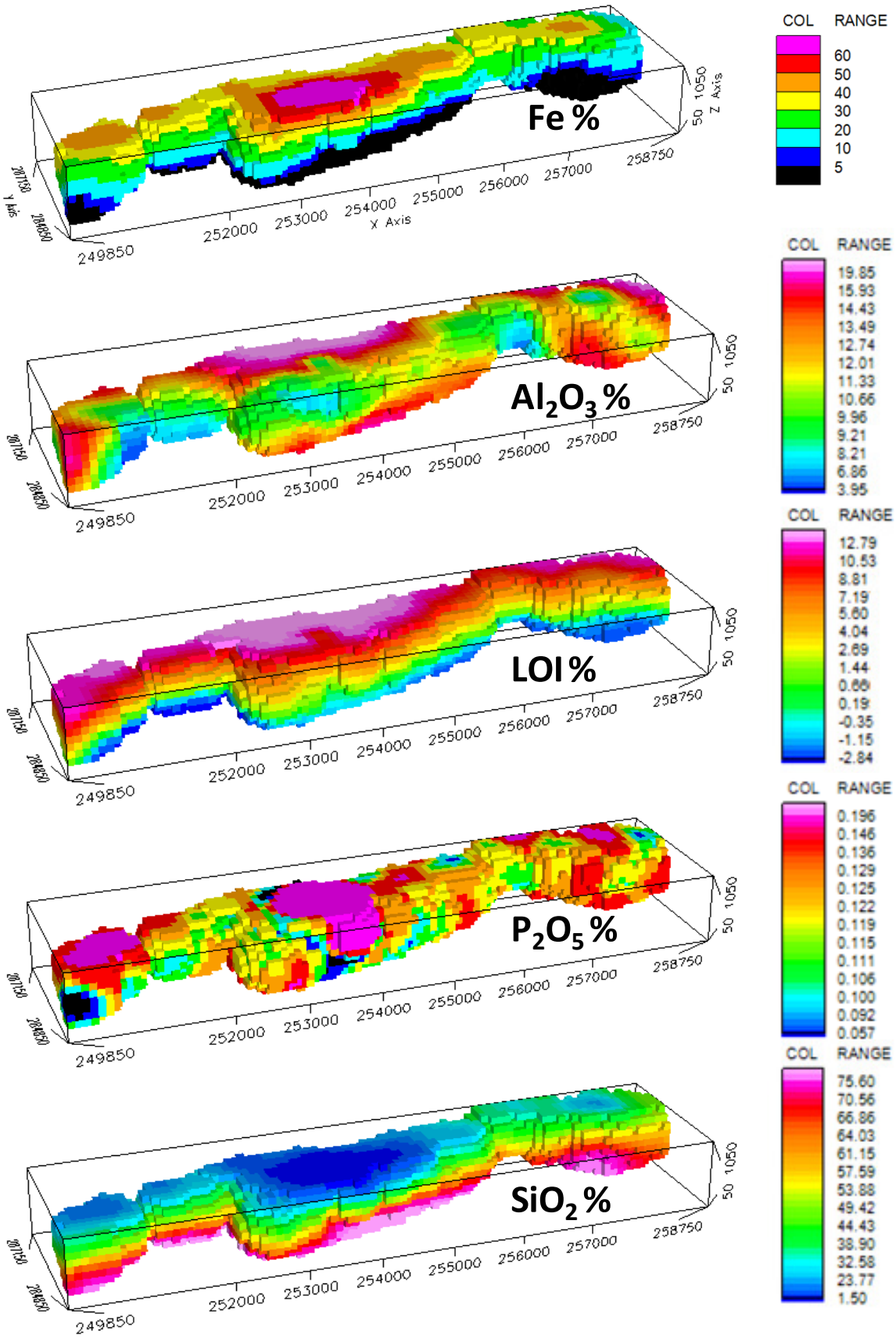

Figure 4.10 The distribution of Fe, loss on ignition, and the main deleterious elements in 3D for the Nkout Deposit.

The distribution of silicon is more straightforward with the least concentration being found in the surficial material which is rich in iron. The Si concentration increases deeper into the deposit, as expected, due to the high Si concentrations of the magnetite itabirite and the granites/gneiss.

4.6 Conclusions

The project areas have undergone extensive deformation during metamorphism which has resulted in a disruption of the expected stratigraphic sequence of rocks in which the granites/gneiss are basement rocks. This sequence is proposed to be from top to bottom – weathering profile (EM – WMI – TMI), high grade magnetite itabirite, low grade magnetite itabirite, metasediments, granite/gneiss basement. Garnets are found within all of these units, mainly in minor quantities, but occasionally present in concentrations of up to 30 %.

From Figure 4.8, it can be seen that this ideal stratigraphic sequence is not always present with for example, granite and metasediments found at relatively high levels in the sequence in some logs. The surficial materials are in general clay rich and the Fe content decreases with depth indicating that the enrichment profile is being formed by supergene upgrade by gangue leaching in the weathering zone, accompanied by martitization and replacement of magnetite by goethite. This upgrading is directly related to elevation with enriched materials being found on the highest peaks. Mineralisation follows the topography closely and is related to surficial weathering and oxidation. The enrichment profile is not overly thick with the greatest depth of weathering being about 70m.

The proven DSO potential follows the topographic elevations closely with Nkout Centre (with the highest mountain peaks) having the greatest DSO potential. With decreasing average elevation we also have decreasing proven DSO potential in the following order: Nkout Centre, Nkout East and Nkout West. The LOI and elemental 3D images do not take into consideration the rock types present and as such Figure 4.10 is a more suitable tool for mine planning as it shows the location of the iron rich material types of the EM, WMI, HMI and LMI.

Chapter 5

Analytical Methods to determine Mineralogy and Chemistry

5.1 Introduction

This chapter serves to explain the analytical methods used in subsequent chapters in order to avoid repetition of the descriptions of the main techniques. All but the QEMSCAN® and metallurgical techniques, which have dedicated chapters, are discussed.

Mineralogy is the main control on metallurgical response, in particular the mineralogical species, micro and macro textures, associations and also the chemical aspects of the mineralogy. Several workers (Fandrich et al., 2006; Ramanaidu et al., 2008; Hoal et al., 2009) have sought to bring to the attention of the iron ore industry the value of applying techniques such as the use of reflectance spectroscopy, XRD, raman spectroscopy, SEM, EPMA, and proton induced X-ray emission analysis (PIXE) in the characterization of iron ore deposits. According to Ramanaidu et al. (2008), "microchemical analyses using SEM, EPMA and PIXE emphasize the mineralogical relationship and distribution of deleterious elements such as P, Al, and Si that underpins the development of downstream processing upgradability and exploitation of iron ore deposits".

Table 5.1 summarises the disciplines, parameters and tests that were used in this research. Emphasis has been placed on the chemical and mineralogical characterisations but these are combined with low and high intensity magnetic separations to see the correlation of the mineralogy and metallurgic response. With the exception of the XRF analysis which was outsourced to the ALS Laboratory, Loughrea, Ireland, all other mineral chemistry and mineralogical analyses were conducted in the laboratories of the Camborne School of Mines (CSM), Penryn Campus, Cornwall, UK. Low and high intensity magnetic separations were conducted in the CSM mineral processing lab.

In this research, QEMSCAN® was used to characterise the Nkout iron ore deposit and Putu Iron Ore project with respect to process mineralogy. Process mineralogy is defined as "the application of mineralogical information to

understanding and solving problems encountered during the processing of ores, concentrates, smelter products and related materials" (University of Cape Town centre for minerals research, 2013). It is a cross between mineral processing and mineralogy and incorporates aspects of geology, geo-statistics, mathematics and sampling theory.

Table 5.1 Tests used for the characterisation of the Nkout and Putu deposit (modified from Williams and Richardson, 2004).

Discipline	***Parameter***	***Testing Done***
Chemistry	Grade, multi-element, trace elements	XRF
Mineralogy	Mineral identification, association, size, texture and liberation, distribution of deleterious elements,	Quantitative mineralogy (QEMSCAN®), XRD, SEM-EDS, EPMA, optical microscopy
Geology	Field relationships (mineralised and host rocks)	Field mapping Ground magnetic survey
Metallurgical Response	Grade, Recovery	Low (Davis tube) and high intensity magnetic separation.

The details of the samples from Putu and Nkout will be discussed in their respective chapters. An introduction is however given here with respect to the sample preparation for analysis.

5.2 General sample preparation

A total of fifty-one samples, comprising 42 samples from 31 drill holes, three grab samples, and six outcrop samples from Nkout were analysed using the methods in Table 5.1. The drill core samples were carefully selected so that they were representative of the deposit based on detailed core logging and include saprolite, laterite and fresh BIF samples. Iron rich grab and outcrop samples were collected during detailed mapping of the area and nine of these were selected for analysis. Other rock types were also collected in order to sample the variability of rock types present. Nine coarse rejects samples

representative of the Putu deposit were selected by the chief geologist at the time and sent along with eleven representative half BIF drill cores for analysis. The weights of samples from both study areas ranged from 100 to 500 g. Physical properties of the half/quarter drill cores and outcrops were described and photographed including microphotographs.

The outcrop, grab and core samples were crushed using a Retsch steel jaw crusher (to - 3 mm), then milled using a tungsten-carbide Tema mill so that various size fractions necessary for other techniques could be produced. They were then divided using a Jones Riffle into three parts. One part was milled into powder (- 45 µm) for XRF analysis, loss-on-ignition (LOI) and powder XRD studies, another part was sieved with a Ro-Tap shaker into various size fractions for EPMA and QEMSCAN® and the third set reserved. Sand or glass beads were used to clean the tungsten-carbide mill between samples. The -250/+180 µm, -125/+90 µm, and -63/+45 µm size fractions were studied using QEMSCAN® and optical microscopy. In addition to these size fractions, the -180/+125 µm was also studied using SEM and EPMA. These size fractions were chosen as time and cost had to be considered for the project and they represent every other size fraction (after - 45 µm) in order to cover the range of size fractions. Since the samples comprise different minerals with different densities and sizes, to avoid bias, the samples were subdivided using a rotary microriffler.

5.3 X-ray fluorescence (XRF), and loss on ignition (LOI)

Geochemical data derived from XRF forms the basis for the classification of the material types in both Putu and Nkout. The classification is based on the iron content of the samples and a weathering index, as explained in Chapter 4. XRF and LOI data constitute an integral part of the research and are widely accepted by the iron ore industry. XRF provide elemental and chemical data for samples using the borate fusion sample preparation method, which reduces effects associated with particle size, mineralogy and matrix and is robust, repeatable and provides accurate and precise results across the full range of iron oxide types (Ramanaidu et al., 2008). Loss on ignition provides a better understanding of the presence of volatiles and consequences for processing

behaviours. For example, goethite contains the OH group and as such can be responsible for elevated LOIs.

Figure 5.1 illustrates the basic principle of the XRF method. The sample must be finely ground and fused before being analysed and as such XRF yields an average bulk elemental or oxide composition of the sample. The characteristic X-ray spectra of the elements in the sample are excited by high energy continuous spectrum of an X-ray tube and are detected using wavelength (as illustrated) or energy dispersive techniques. The instrument is calibrated using standards of known composition.

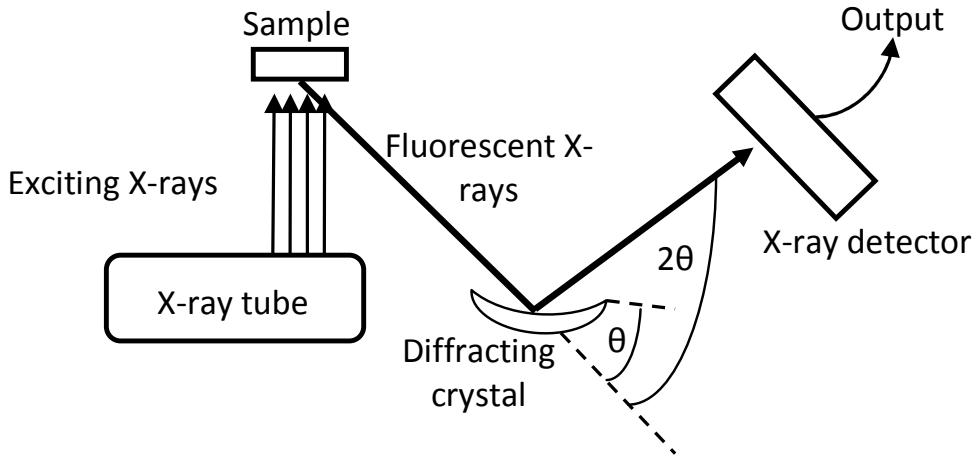

Figure 5.1 A simplified X-ray florescence Spectrometer (Modified from Nesse, 2000).

Sixty-seven samples were initially sent to ALS geochemical laboratories, Loughrea, Ireland which is part of the Stewart Group of Labs specialising in geochemical assay. Approximately 30 g of each sample were sent and they comprised 7 samples from Putu, 51 from Nkout, 1 European certified reference material i.e. Euronorm-crm No. 682-2 iron ore and 3 blank (glass beads) and 5 duplicate samples. ALS's package (code ME-XRF21u) for iron ores was selected in which the following elements and oxides are analysed for; Al_2O_3, As, Ba, CaO, Cl, Co, Cr_2O_3, Cu, Fe, K_2O, MgO, Mn, Na_2O, Ni, P, Pb, S, SiO_2 Sn, Sr, TiO_2, V, Zn and Zr, was used. Fe_2O_3 was calculated and reported as part of the result. Loss on ignition (code OA-GRAO5x) at 1000 ^oC was also done by thermo gravimetric analyses. After the magnetic separations were conducted, 30 samples comprising 3 size fractions of 10 concentrates were sent to ALS for the same iron ore analysis. The raw XRF data for all the XRF analyses are given in Appendix 1.

Analytical accuracy was tested using the European certified reference material (ECRM) i.e. Euronorm-crm No. 682-2 iron ore. In addition to this, ALS analysed the following certified reference materials: GIOP-18, SARM-1, SARM-3, SCH-1, ECRM 680-1. An accuracy of ± 10 % from reference value was obtained for all the elements and element oxides discussed in this thesis. Analytical precision was tested with the 5 blind duplicate samples and 3 blank samples (glass beads). ALS also analysed 4 duplicate samples and 4 blank samples of their own. The analyzed elements and element oxides (above detection limits) discussed in this thesis showed a reproducibility of ± 90 %.

5.4 Powder X-ray diffraction (XRD)

This was done in order to have an idea of the bulk mineral assemblages in the samples. The analysis done was qualitative wherein identification of minerals and estimation of abundance is based on their crystalline structure and relative peak heights, respectively. The instrument used was a Siemens D5000 X-ray diffractometer. The XRD was run at a voltage of 40 kV, current of 30 mA and samples run from 2^{o} to 70^{o}, 2θ.

The detection limit of XRD is about 5 % but it is also dependent on the crystallinity of the minerals being identified. For example, weakly crystalline or amorphous minerals such as goethite do not give distinct peaks and produce noisy profiles. The raw data was smoothed for some samples in order to aid the interpretation which used the JCPDS PDF-2 (2004) database and Bruker EVA software V.10.0.1.0. The software links to the international centre for diffraction data (ICDD) where it matches the profile obtained for a sample to the powder diffraction file database of possible minerals. Knowledge of the possible minerals in the project areas was useful in cases of ambiguity in suggested minerals.

5.5 Scanning electron microscopy with energy dispersive X-ray spectrometer (SEM-EDS)

This technique was used in order to provide high resolution imaging of the surfaces of polished blocks and to study their elemental compositions.

Backscattered electron (BSE) images based on average atomic number were taken to identify mineral phases and also to give the mineralogical relationships of deleterious elements such as P, Al and Si. SEM-EDS was also used as a guide in deciding which elements were to be analysed for using EPMA.

The equipment used was a JEOL JSM-5300LV Low Vacuum SEM. Analyses were undertaken in high vacuum mode and as such the samples were carbon coated. Imaging was undertaken at an acceleration voltage of 25 kV and in backscattered electron mode. The EDS X–ray detector was linked to an Oxford ISIS system for qualitative chemical analysis. Information about the distribution of different elements in a sample can be obtained due to the fact that the intensity of the BSE signal is strongly related to the atomic number of the elements in the sample. As such heavy elements (high atomic number) backscatter electrons more strongly than light elements (low atomic number), and will appear brighter in the image.

5.6 Optical microscopy

Quantification of hematite, goethite and magnetite or their ratios is necessary for the characterisation of the deposit as these minerals provide vital information on ore grade and geometallurgical properties such as processing routes. The mineralogical characteristics of the samples were studied using polished thin sections under transmitted and reflected light microscopy and by photomicrographs taken using a Nikon Eclipse E600 Pol with instant image capture through a Nikon Digital Sight 5MP camera. Results are correlated with those of the QEMSCAN®.

5.7 Electron probe microanalysis (EPMA)

EPMA, undertaken in a JEOL JXA-8200 superprobe, was used for the quantitative analysis of minerals on the surfaces of polished blocks. Knowledge gained from fieldwork, XRD, optical mineralogy and SEM were used to select elements to be determined. Experimental conditions were as follows; beam current: 15 nA, accelerating voltage: 15 kV, spot size: 5 µm. A ZAF matrix

correction routine was used. The results were quantified with reference to primary synthetic and mineral standards (see Table 5.2).

In order for sample surfaces to be made electrically conductive and electrically grounded to prevent accumulation of charges at the surface, they were coated with an ultrathin layer of ~ 20 nm carbon by high vacuum evaporation. Non conductive specimens tend to develop charges on their surface and this causes streaking and other image distortions during scanning. Coating can also increase signal to noise ratio of samples with low atomic number.

Table 5.2 List of oxides and elements determined along with the standards used.

Oxide Analysed	***Standard Used***
SiO_2	Olivine
Na_2O	Jadeite
CaO	Diopside
FeO	Hematite
P_2O_5	Apatite
Al_2O_3	Almandine
K_2O	Orthoclase
MnO	Rhodonite
MgO	Olivine
Cl	Tugtupite
Cr_2O_3	Chromium metal
F	Apatite
ZrO_2	Zirconia
SO_3	Barite
BaO	Barite
TiO_2	Rutile
Cd	Cadmium metal

Minerals with similar cations for example hematite and goethite will show different backscattered behaviour because of their different cation densities (Andersen et al., 2009). Hematite has a higher backscatter coefficient than goethite and hence appears brighter. Magnetite appears brighter than hematite but the difference is subtle and is mainly identified after recalculation of the total EPMA oxide percentage which is expected to range from 98 % to 100 % whilst

hematite will have between 90 to 95 %. Goethite normally sums up to between 80 to 90 % but could be lower as is the case for limonite (hydrated goethite) as it usually contains other elements apart from Fe. The lower percentages are a reflection of the presence of species such as the OH group which are not analysed for. The hematite, identified by their relatively lower total EPMA oxide percentages when calculated using the expected number of 4 oxygens for magnetite were then recalculated using 3 oxygens for hematite and the totals rose from the 90 to 95 % obtained before to between 98 to 100 %.

Twenty-two samples from Nkout and Putu were selected for this part of the study based on their mineralogy identified using XRD, their location and type i.e. saprolite/laterite, BIF, outcrop and grab samples. The chemical formulae of minerals were calculated using methods described by Droop (1987) and Deer et al. (1992). Their methods could be summarised as follows:

a) Divide the oxide weight percentages by the molecular weight of the oxide concerned to obtain the molecular proportions of the various oxides.
b) Multiply by the number of oxygen atoms in the oxide concerned to get a set of numbers proportional to the numbers of oxygen associated with the elements concerned.
c) Sum up the numbers.
d) Re-cast the oxygen atom proportions so that they total the number of oxygen X in the formula of the mineral whose formula is being calculated. This is achieved by dividing the expected numbers of oxygens by the total obtained in (c) above and multiplying all by the result. This ensures that the number of oxygen atoms total the expected provided the correct mineral is being calculated for.
e) Divide the value obtained in d) by the number of oxygens in the oxides to obtain the number of cations associated with the oxygen.

All elements with values less than 0.10 were left out of the calculated chemical formulae as they are not expected to make significant contributions to the identification of the minerals. The EMPA analysis gave iron content in terms of Fe^{2+} i.e. FeO and the amount of Fe^{3+} i.e. (Fe_2O_3) if present in minerals such as hematite, was estimated using the method proposed by Droop (1987). In this

method, the number of Fe^{3+} ions per X oxygen atoms in the chemical formula of a particular mineral, F, is given by;

$$F = 2X\left(1 - \frac{T}{S}\right)$$

Where T = ideal number of cations per formula unit, and S is the observed cation total per X oxygen calculated assuming all iron to be Fe^{2+}. Table 5.3 gives the values for X and T used in the calculation of formulae for minerals identified in the EPMA. The oxide wt % list was adjusted for those that were found to contain Fe^{3+} resulting in an increase in the total wt %.

$$\text{The new wt. \% FeO} = \frac{\text{old wt. \% FeO} \times Fe^{2+}}{(Fe^{2+} + Fe^{3+})}$$

$$\text{The new wt. \% } Fe_2O_3 = \frac{1.1113 \times \text{old wt. \% FeO} \times Fe^{3+}}{(Fe^{2+} + Fe^{3+})}$$

Table 5.3 Number of oxygen and ideal number of cations used in the calculation of mineral formulae and Fe_2O_3 content of minerals identified in the EPMA (Deer et al, 1992, Droop, 1987).

Mineral	***Oxygen (X) in formula***	***Cations in formula (T)***
Magnetite	4	3
Hematite	3	2
Calcic Amphiboles	23	13
Fe, Mg Amphibole	23	15
Pyroxene	6	3
Apatite	26	12
Alkali feldspar	32	12
Chlorite	28	20
Andradite	23	16
Micas	22	16
Ilmenite	6	3
Kaolinite	22	20

Minerals such as quartz, calcite and gibbsite were identified based on the percentages of SiO_2 (≥ 95 %), CaO (approx. 55 %) and Al_2O_3 (≥ 80 %)

respectively and the fact that all other elements and/or oxides in them occurred in trace quantities.

Chapter 6

Mineralogical and Geochemical Characterisation of the Putu Iron Ore Deposit

6.1 Introduction

Eleven half drill cores and nine crushed half core samples from the Putu Iron Ore Mining (PIOM) deposit have been studied. The half drill cores and four of the crushed cores came directly from Liberia whilst the remaining five crushed cores came from Amdel Mineral Laboratories, Perth, Australia. The crushed half core samples originally in 1 m lengths had been crushed to -19 mm. A 5 kg split of each interval was taken and these were blended to make the ore type composites. Sub-samples of each composite were then crushed to - 3.35 mm and used for testwork. Precise sample locations were not taken into consideration in this research as there were too few samples available to make conclusions based on locations. The samples were rather carefully selected by Hector Galam, the chief geologist at PIOM at the time to be representative of all the Fe minerals and the major gangue minerals present within the deposit. According to Hector, the samples are representative of both the Jideh and Montroh mountain ranges. Samples which had Fe content greater than 15 wt % based on XRF analysis were considered to be mineralised, whilst samples with less than 15 wt % were classed as un-mineralised. The four crushed cores from Liberia were classified into mineralised (LB01, LB02) and un-mineralised (LB08, LB09). Details of the samples are given in Table 6.1. Samples LB01 and LB09 are from Jideh whereas samples LB02 and LB09 are from Montroh. The samples from Amdel, Australia are composite crushed core samples which were chosen so that they included magnetite-rich material, hematite-rich material and samples transitional between the two extremes.

In this chapter, the half drill cores and crushed core samples are described based on visual analysis and the results of various geochemical and mineralogical analyses are presented and discussed. XRF, SEM/EDS and EPMA were the chemical and mineral chemistry methods used. XRD and optical microscopy were also carried out to determine the mineralogy of the samples.

Table 6.1 Details of samples from the Putu Iron Ore Project.

Hole ID	*ID*	*Length (m)*	*Field Description*	*Sample Type*	*Comments*
PDD038	LB01		Magnetite Silica BIF	crushed core	Mineralised
PDD062	LB02		Magnetite Silica BIF	crushed core	Mineralised
	LB03		Magnetite sample	crushed core	Mineralised
	LB04		Magnetite sample	crushed core	Mineralised
	LB05		Magnetite hematite sample	crushed core	Mineralised
	LB06		Hematite magnetite sample	crushed core	Mineralised
	LB07		Hematite sample	crushed core	Mineralised
PDD062	LB08		Quartz Chlorite Magnetite	crushed core	Unmineralised
PDD038	LB09		Amphibole Chlorite Magnetite	crushed core	Unmineralised
PDD038	1	0.3	Magnetite Silica BIF	Half-core	Mineralised
PDD038	2	0.2	Magnetite Silica BIF	Half-core	Mineralised
PDD038	3	0.15	Quartz Chlorite Magnetite	Half-core	Unmineralised
PDD038	4	0.18	Amphibole Chlorite Magnetite	Half-core	Unmineralised
PDD038	5	0.25	Magnetite Silica BIF	Half-core	Mineralised
PDD038	6	0.21	Magnetite Silica BIF	Half-core	Mineralised
PDD038	7	0.15	Amphibole Chlorite Magnetite	Half-core	Unmineralised
PDD038	8	0.25	Amphibole Chlorite Magnetite	Half-core	Unmineralised
PDD038	9	0.3	Quartz Chlorite Schist	Half-core	Unmineralised
PDD038	10	0.2	Quartz Chlorite Schist	Half-core	Unmineralised
PDD038	11	0.25	Amphibole Chlorite Magnetite	Half-core	Unmineralised

Fe wt % > 15 % - mineralised, Fe wt % < 15 % - un-mineralised

6.2 Description of half cores

The half cores were divided into four main lithologies by the team at Putu based on the perceived major mineral content by visual inspection and reflecting both the mineralisation and gangue mineralogy. They are: magnetite silica BIF, quartz chlorite magnetite, amphibole chlorite magnetite and quartz chlorite schist. Samples of these are shown in Figure 6.1. This subjective classification was subsequently changed to the classification scheme described in Chapter 4. In these descriptions, the terms fine grained is used for material up to 250 µm, ‘medium grain > 250 µm < 0.5 mm and coarse grain > 0.5 mm.

The magnetite silica BIF (Figure 6.1, sample 2.0) is characterised by alternating layers of magnetite intercalated with layers of quartz. It is a coarse grained metamorphic rock with grains of quartz and magnetite distinguishable by eye. The average thickness of the layers is 1 to 2 mm. Chlorite and pyrite are accessory minerals occurring as bands parallel to the quartz and magnetite layers. The quartz chlorite magnetite sample is light coloured due to the high proportion of quartz. Note the chlorite infills in the lower half of the core (Figure 6.1, 3.0). Magnetite occurs mainly as micro crystals and the quartz as thin layers (less than 1 mm). It has a grain size ranging from fine to medium.

Figure 6.1 The four main lithologies at the Putu deposit. (2.0) magnetite silica BIF, (3.0), quartz chlorite magnetite, (8.0) amphibole chlorite magnetite, (9.0) quartz chlorite schist. All half cores are from drill hole PDD038.

The greenish colour of sample 8.0 in Figure 6.1 is a reflection of its mineral content i.e. amphibole and chlorite. Sulphides, mainly pyrite, are present, occurring in random orientation. Grain size ranges from fine to medium and magnetite occurs as an accessory mineral. Micro folds are also present. The quartz chlorite schist is fine grained, has a brownish green colour and flaky appearance due to the chlorite present (Figure 6.1, sample 9.0). Pyrite is

present in a random orientation. Figure 6.2 shows magnetite and some of the gangue minerals present.

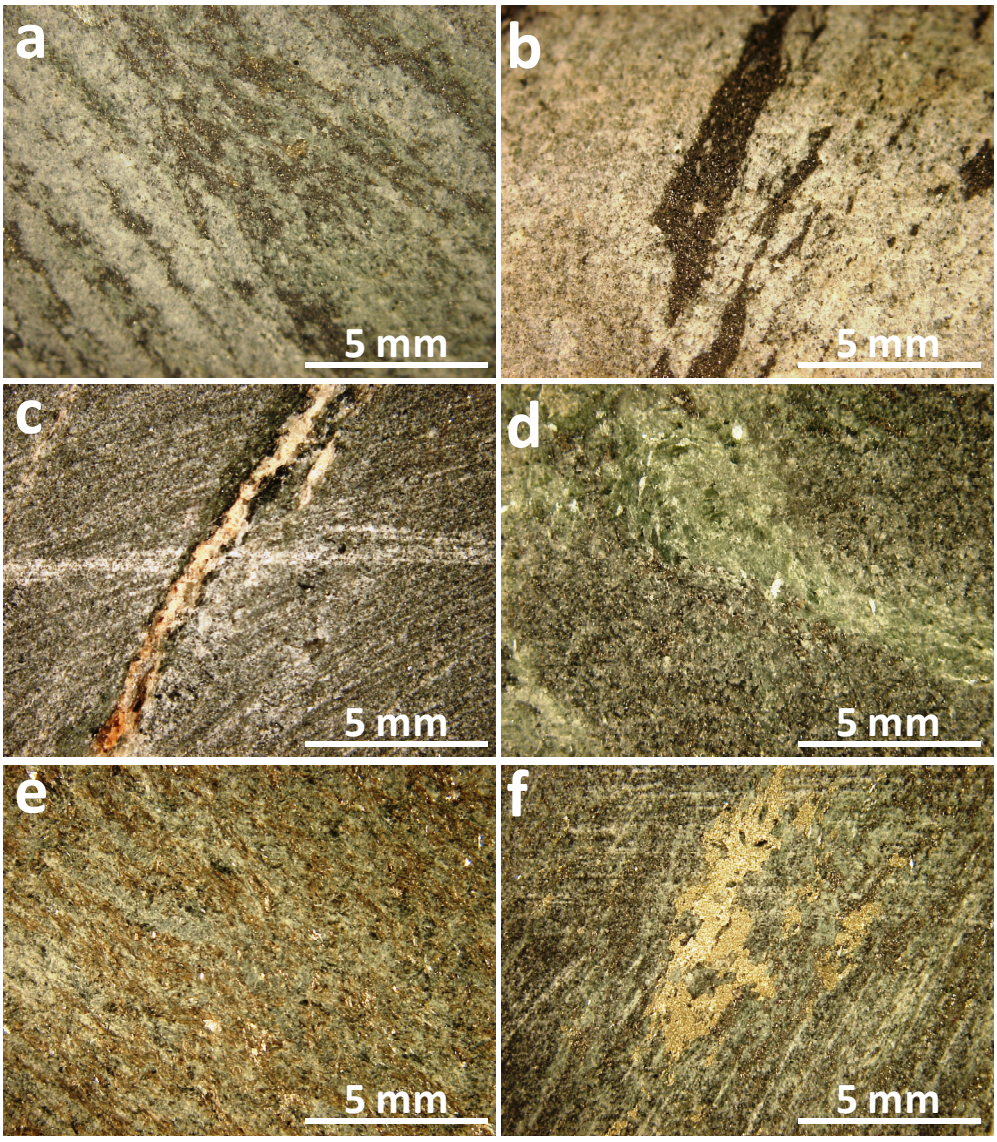

Figure 6.2 Photomicrographs in reflected plane polarised light showing magnetite and some gangue minerals present in drill core PDD038. (a) and (b) show examples of magnetite in the BIFs, (c) quartz vein (quartz is the main gangue mineral), (d) chlorite grain ocurring with granular magnetite, quartz and other gangue minerals, (e) quartz chlorite schist, (f) coarse pyrite grain. Figures 6.2 a and b show the main forms in which magnetite can occur as a major mineral in the drill cores. Figure 6.2a shows magnetite (black) occurring in alternating bands with quartz and feldspars and b shows magnetite occurring as coarse grains. In both cases, pyrite occurs as an accessory mineral. Figure 6.2c shows a quartz vein that cuts through magnetite quartz and chlorite bands; quartz is the main gangue mineral. Figure 6.2d shows coarse chlorite grains (green) occurring with granular magnetite, quartz and other gangue. Figure 6.2e shows the main host rock for the itabirites that is quartz chlorite schist. Note the parallel arrangement of the medium sized mica grains occurring in bands with the quartz, feldspar and amphibole grains. Pyrite occurs mainly as an accessory mineral but in some instances may occur as coarse grains as seen in Figure 6.2f.

6.3 Analytical results for crushed cores

6.3.1 Description of crushed cores

Figure 6.3 shows the crushed core samples for the magnetite-rich sample LB01 (magnetite BIF) and the magnetite-poor (unmineralised) samples: LB08 (quartz chlorite magnetite) and LB09 (amphibole chlorite magnetite). The subtle difference in their colouration gives an indication of not only the types of minerals present but also of the quantities in which the minerals are present. For example, LB01 is darker than LB08 and LB09 because of its higher magnetite content whilst LB08 has a lighter colour compared with LB09 due to its higher concentration of quartz. LB09 also has a slight greenish tint due to the presence of amphibole and chlorite. The high grade magnetite samples of LB03 and LB04 are not shown but they are magnetite rich samples and appear similar to LB01.

Figure 6.3 also shows the enriched samples LB05, LB06 and LB07. LB05 contains more magnetite than goethite and hematite and appears dark brown in colour. The LB06 sample has a yellow-brown look due to its higher goethite/limonite and hematite concentration. LB07 appears red due to its content of hematite and red andradite. The general variation in colour is a direct result of weathering and alteration. As these progress, the black magnetite gradually alters to yellow-brown limonitic goethite and then to the red hematite. Note that the descriptions from Putu for samples LB06 and LB07 did not take into consideration the presence of goethite and andradite respectively. This further justifies the reclassification of the samples from their original classification which was based on the identification of the three most abundant minerals by the geologist logging the cores.

6.3.2 XRF

Table 6.2 shows a simplified version of the results of the XRF analysis conducted at ALS global geochemistry labs for the various mineralised material types from Putu. The table gives the average chemical composition in percentage of some oxides and elements for the samples sorted into material types based on the classification system outlined in chapter 4. Figure 6.4 is a

plot of these results. The complete XRF results for the Putu samples are given in appendix 1.

Figure 6.3 Crushed core samples for LB01, LB05, LB06, LB07, LB08 and LB09. LB08 and LB09 are magnetite poor BIF samples whereas LB01 is a magnetite rich sample. Note the difference in colour between the magnetite rich and poor samples. The magnetite hematite sample (LB05), hematite magnetite sample (LB06) and hematite sample (LB07) show colour variations which are due mainly to the alteration of magnetite through to goethite and then to hematite.

Table 6.2 Simplified XRF results (wt %) for the various material types from Putu.

Material Type	SiO_2	TiO_2	Al_2O_3	Fe_2O_3	Mn	MgO	CaO	Na_2O	K_2O	P	S	LOI 1000^{0}C	Total
EM	8.25	0.030	2.280	85.86	0.011	0.060	0.010	<0.005	<0.001	0.113	0.011	3.530	100.35
TMI	32.20	<0.010	0.195	62.38	0.018	0.770	3.945	<0.005	<0.001	0.069	0.001	0.910	100.65
HMI	33.30	<0.010	0.647	62.24	0.031	2.380	2.337	0.323	0.080	0.084	0.001	-1.023	100.64
LMI	66.80	0.120	3.030	22.64	0.051	3.570	2.970	0.571	0.782	0.048	0.132	0.100	101.30

EM – enriched material, TMI – transitional magnetite itabirite, HMI – high grade magnetite itabirite, LMI - low grade magnetite itabirite. Negative loss on ignition for HMI is due to weight gained from hydration when the samples were allowed to sit out to cool before weighing. The other material types were not affected.

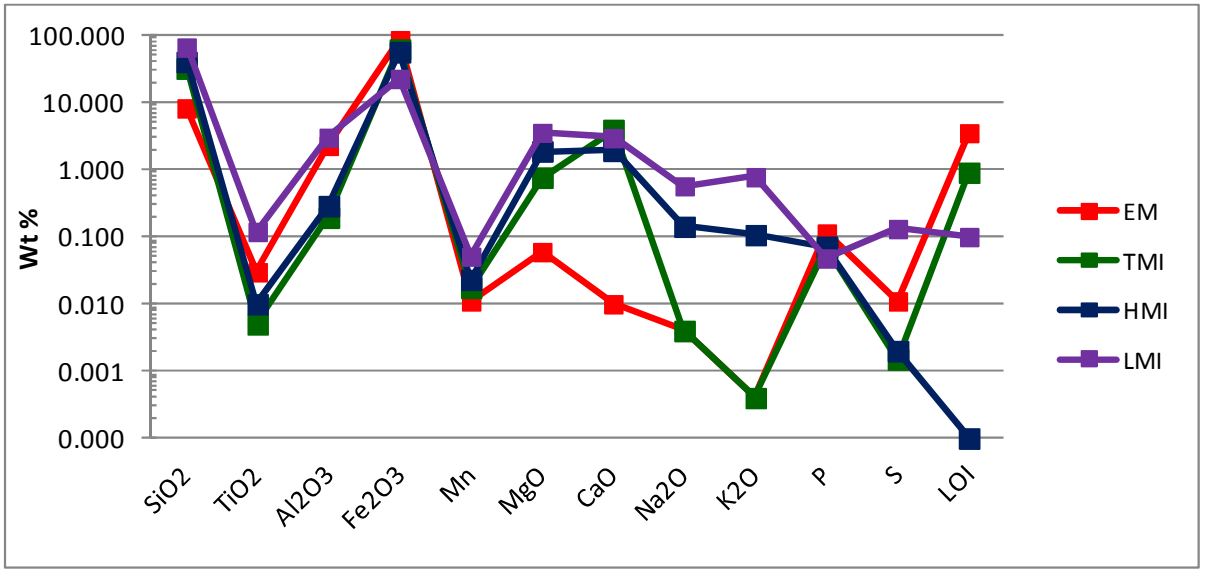

Figure 6.4 Plot of average chemical compositions determined by XRF for the various material types from Putu. See Table 6.2 for explanation of abbreviations.

These samples were received as crushed cores and, therefore, weathering indices could not be assigned with certainty. This meant that the classification scheme could not be applied directly. However the loss on ignition whole rock chemistry results gave an indication of the degree of weather. Negative and low LOI (e.g. 0.100 %) could with confidence be used as an indication of fresh i.e. unaltered/weathered BIF as they indicate lack of water and other volatiles expected in weathered materials. As such those samples with LOI being negative or < 0.1 % have been assigned to HMI and LMI based on the Fe percentages. LB05 and LB07 have been assigned to the TMI group based on their relatively higher LOI, Fe % and their colour. The enriched material has the highest LOI (3.53 %) which is due to the presence of volatiles in minerals such as goethite. None of the Putu samples fit into the WMI material type as described in chapter 4 owing to the fact that the samples considered to be weathered did not have enough Fe % to fit into the WMI group. As such the WMI group is absent in the Table 6.2 and Figure 6.4.

The calculated Fe_2O_3 wt % content of the TMI and HMI groups are about the same. The EM material type has the least SiO_2 wt %, Mn wt %, MgO wt %, CaO wt % concentrations and the highest Fe_2O_3 wt %, P wt % and LOI wt % concentrations. The high P wt % for the EM material type is unlikely to be due to the presence of apatite, the main phosphorus bearing mineral present in the deposit. Apatite is known to be present in the fresh magnetite itabirite and not the EM. It is proposed that the P is present within the goethite and this group is expected to have the highest concentration of goethite indicated by its highest LOI %. The Na_2O and K_2O percentages for the TMI group are much lower compared to that of the HMI group. This is an indication of minerals such as alkali feldspars present in the BIFs but absent in the weathered TMI sample. The HMI has a higher MgO and Al_2O_3 percentage which is mainly due to the presence of mafic aluminosilicates in the BIFs. The LMI material type has the highest SiO_2, TiO_2, Al_2O_3, Mn, MgO, Na_2O, K_2O and S concentrations which are indicative of a higher aluminosilicate mineral concentration. LMI has a higher Al_2O_3 percentage than EM but whilst the Al_2O_3 in the LMI is due to the aluminosilicates, that of the EMI is due to Al oxides and hydroxides such as gibbsite.

There is a negative correlation between Fe_2O_3 and SiO_2 (Figure 6.5a). With the exception of the LMI group, there is also a negative correlation between SiO_2 and Al_2O_3 (Figure 6.5b) but a positive correlation between Fe_2O_3 and Al_2O_3 (Figure 6.5c). The Al_2O_3 concentration of the LMI group cannot be related to weathering, as is the case for the TMI and EM groups but is the result of the presence of aluminosilicates in the fresh BIF. It is clear that enrichment was due to the leaching out of Si, which resulted in an increase in Fe content and as such SiO_2 now exists as an independent phase. The enrichment proceeded with weathering and alteration, leading to the formation of Al rich phases as indicated by the positive correlation of Fe_2O_3 and Al_2O_3. The strong negative correlation between Fe_2O_3 and SiO_2+Al_2O_3 (Figure 6.5c) suggests the presence of silica and alumina phases such as kaolinite.

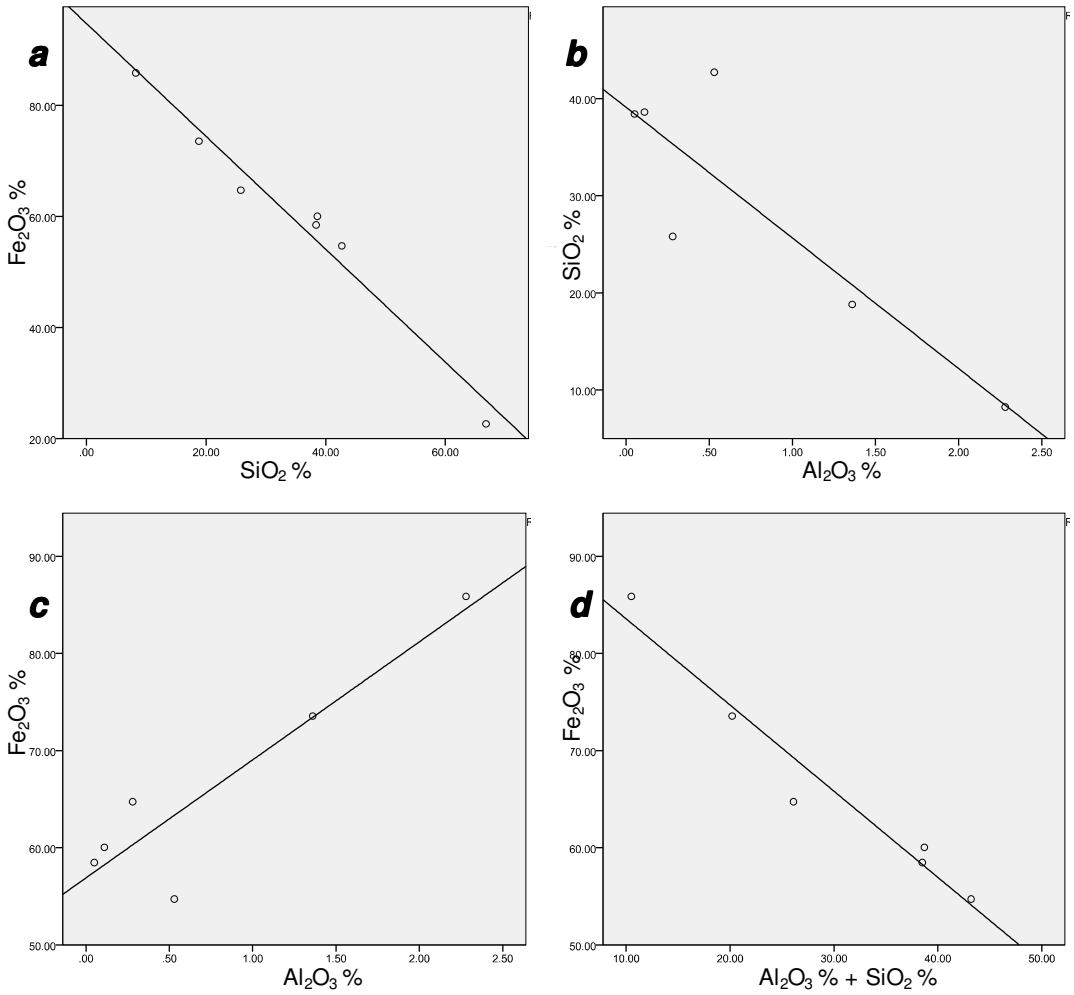

Figure 6.5 Plots showing correlations between the Fe_2O_3, SiO_2 and Al_2O_3 concentration of the crushed core samples. (a) Plot of Fe_2O_3 vs SiO_2 showing a negative correlation, (b) Plot of SiO_2 vs Al_2O_3 showing a negative correlation (c) Plot of Fe_2O_3 vs Al_2O_3 showing a strong positive correlation, (d) Plot of Fe_2O_3 vs Al_2O_3 showing a positive correlation.

6.3.3 XRD

As expected quartz and magnetite are the major minerals in the magnetite itabirite samples LB01, LB02, LB03 and LB04. Hematite becomes important in the transitional magnetite itabirite and enriched material samples. The major minerals identified for the samples are given in Table 6.3 and profiles for two transitional magnetite samples are shown in Figures 6.6 and 6.7. Note how hematite and andradite are shown to be major minerals in LB05 and LB07 respectively.

Calcic amphiboles, hornblende and tremolite are the dominant amphiboles whilst biotite and phlogopite are the main micas in these samples. Albite is also one of the major minerals in the un-mineralised sample LB09. Almandine and andradite garnets are present in LB08 and LB07, respectively. The XRD analysis confirms the description given for the samples from Putu because the mineralogy changes from LB05 through to LB06 and LB07, involving the alteration of magnetite through goethite to hematite. Hematite is dominant in the samples described as hematite magnetite, i.e. LB06 and the hematite sample LB07. Both contain quartz and goethite. The team at Putu did not however mention the goethite present in both of them and the garnets in LB07 and LB08 in any previous reports.

Table 6.3 Major minerals identified using XRD.

Material Type	*ID*	*Minerals Identified using XRD*
EM	LB06	Hematite, quartz, goethite, magnetite
TMI	LB05	Quartz, hematite, magnetite
	LB07	Hematite, quartz, andradite
HMI	LB01	Quartz, magnetite, tremolite, phlogopite
	LB03	Quartz, magnetite, hornblende, phlogopite
	LB04	Magnetite, hematite, hornblende, quartz, epidote
LMI	LB02	Quartz, magnetite, hornblende, phlogopite
Un-mineralised	LB08	Quartz, biotite, almandine
	LB09	Albite, quartz, biotite, magnetite, tremolite

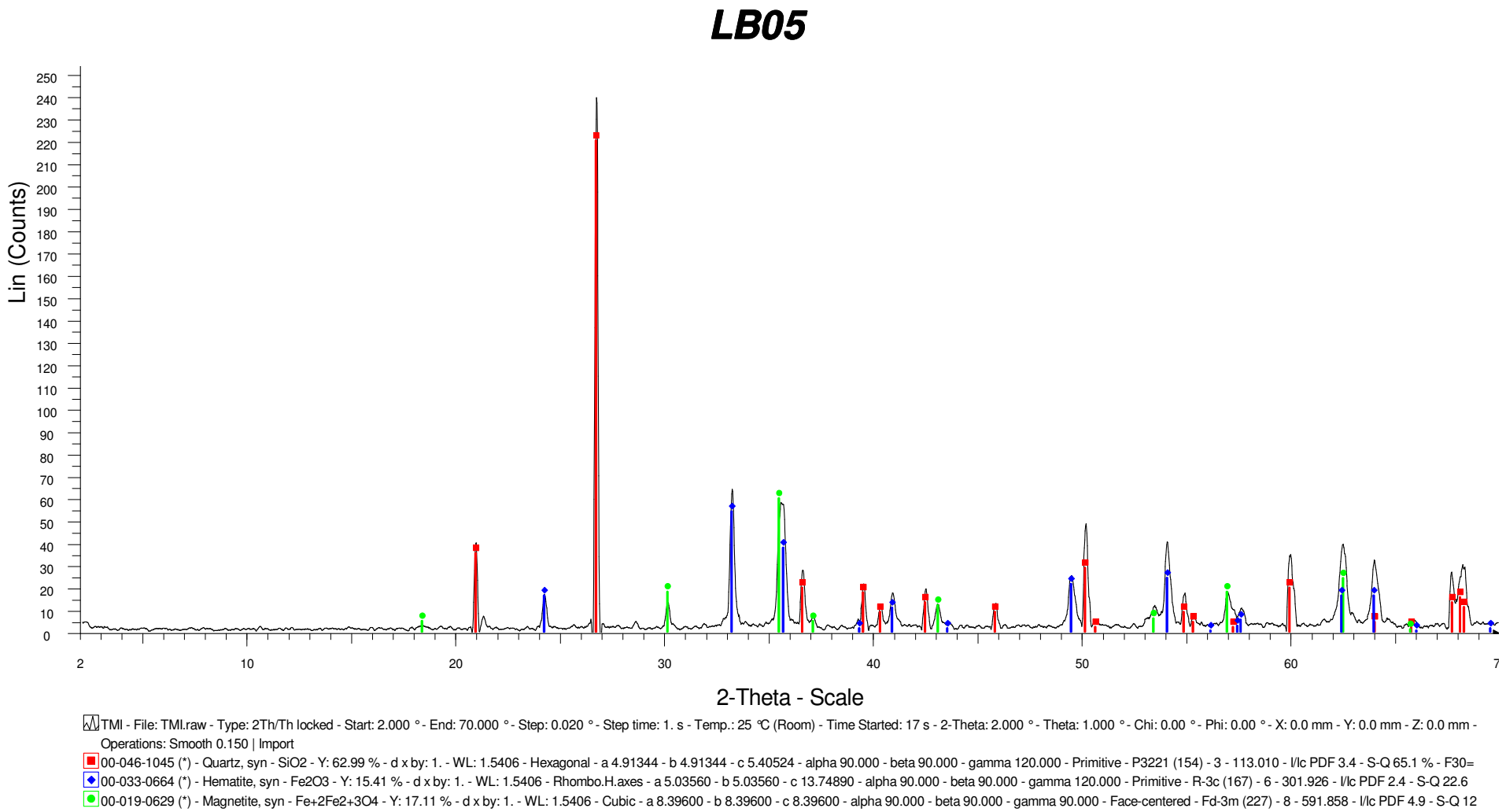

Figure 6.6 XRD profile for the transitional magnetite itabirite sample LB05.

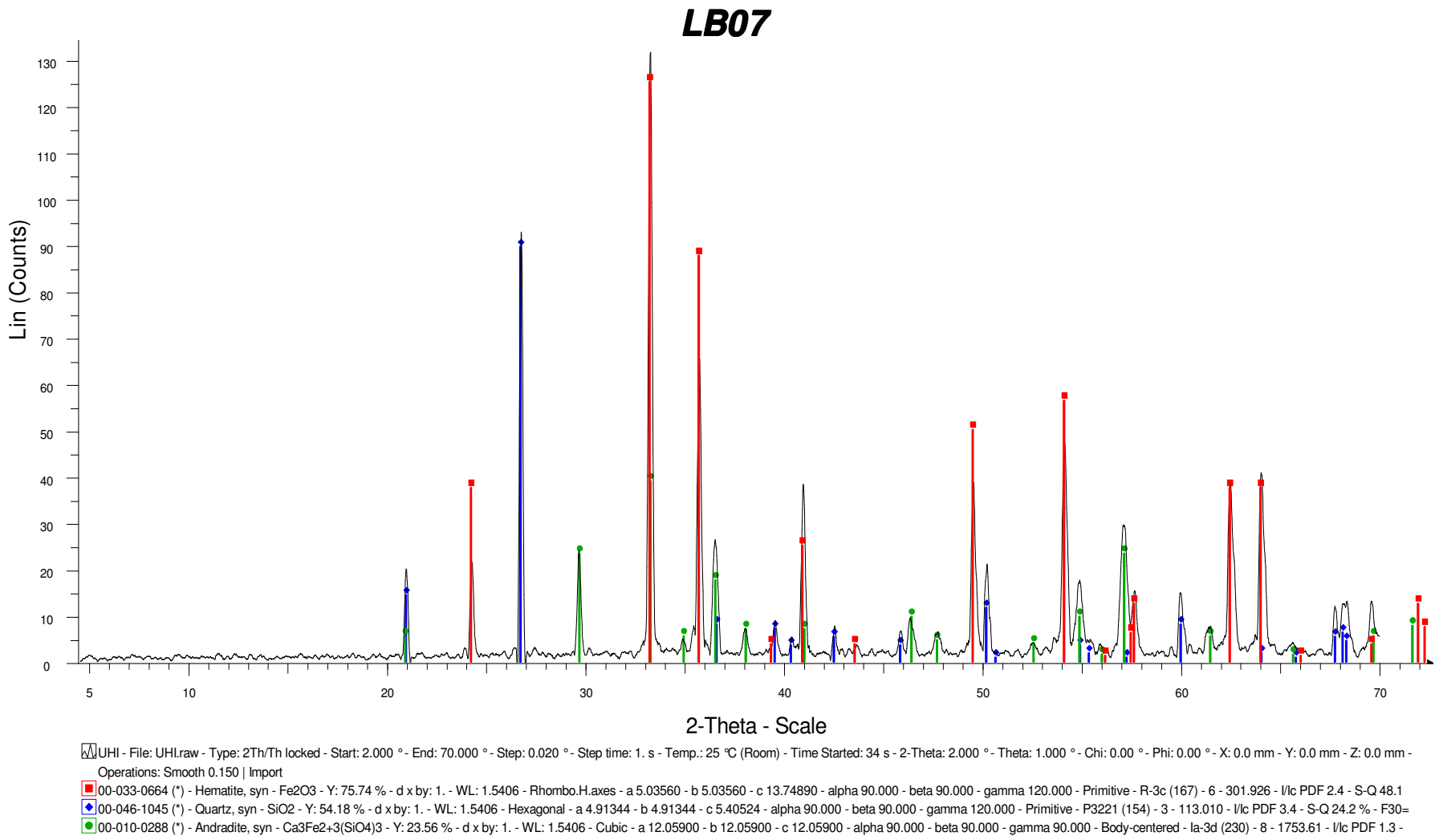

Figure 6.7 XRD profile for the transitional magnetite itabirite sample LB07.

Only a few major minerals (maximum 4) were identified with certainty using the XRD technique because the detection limits of the technique are about 5 modal %. Important deleterious elements may be present in minerals below this limit. The high detection limits and lack of quantification during this study are drawbacks of this method. With appropriate software and standards, it is possible to produce quantitative XRD results for iron ores (McCusker et al., 1999) but these would still suffer from the same relatively high detection limits.

6.3.4 SEM/EDS

This method was used early on in the research to aid the selection of elements to be analysed for by EPMA. Further details of the method are given in Chapter 5. As the SEM/EDS analyses conducted were qualitative, they provided information on the elements present according to the EDS X-ray spectra but could not definitively identify the minerals. For example magnetite and hematite will both show peaks for Fe and O. Heavy elements (high atomic number) backscatter electrons more strongly than light elements (low atomic number), and appear brighter in a backscattered electron image in the SEM. However as the images are in grey scale, identification of many different scales with the naked eye can be problematic. Based on the contrast and brightness settings used for this analyses, the brightest (usually white on images) common minerals in these samples were iron oxides, mainly magnetite but, also hematite with goethite being consistently darker.

The higher backscattered electron coefficient of the Fe-oxides and their EDS spectra with only Fe and O (Figure 6.8a) means they were easy to identify, as was quartz (Si and O Figure 6.8b) with its low backscatter coefficient and pyrite (Fe and S, Figure 6.8c). Other minerals were not so easy, for example the mineral in Figure 6.8d could be any one of a number of aluminium-silicates. Figure 6.9 shows examples of the SEM images obtained. From Figures 6.9 a, b and c it can be seen that the main association of the Fe-oxides is with quartz. Figure 6.9d shows a probable clay mineral e.g. kaolinite with numerous small fragments of magnetite/hematite and other larger silicates (light grey). Figures 6.9d and e show other gangue minerals. In Figure 6.9f, based on their respective EDS spectra (not shown), the light grey mineral is pyrite and the

medium grey mineral is an amphibole with the main elements being Si, Al, Na, Ca and K and the dark grey is quartz.

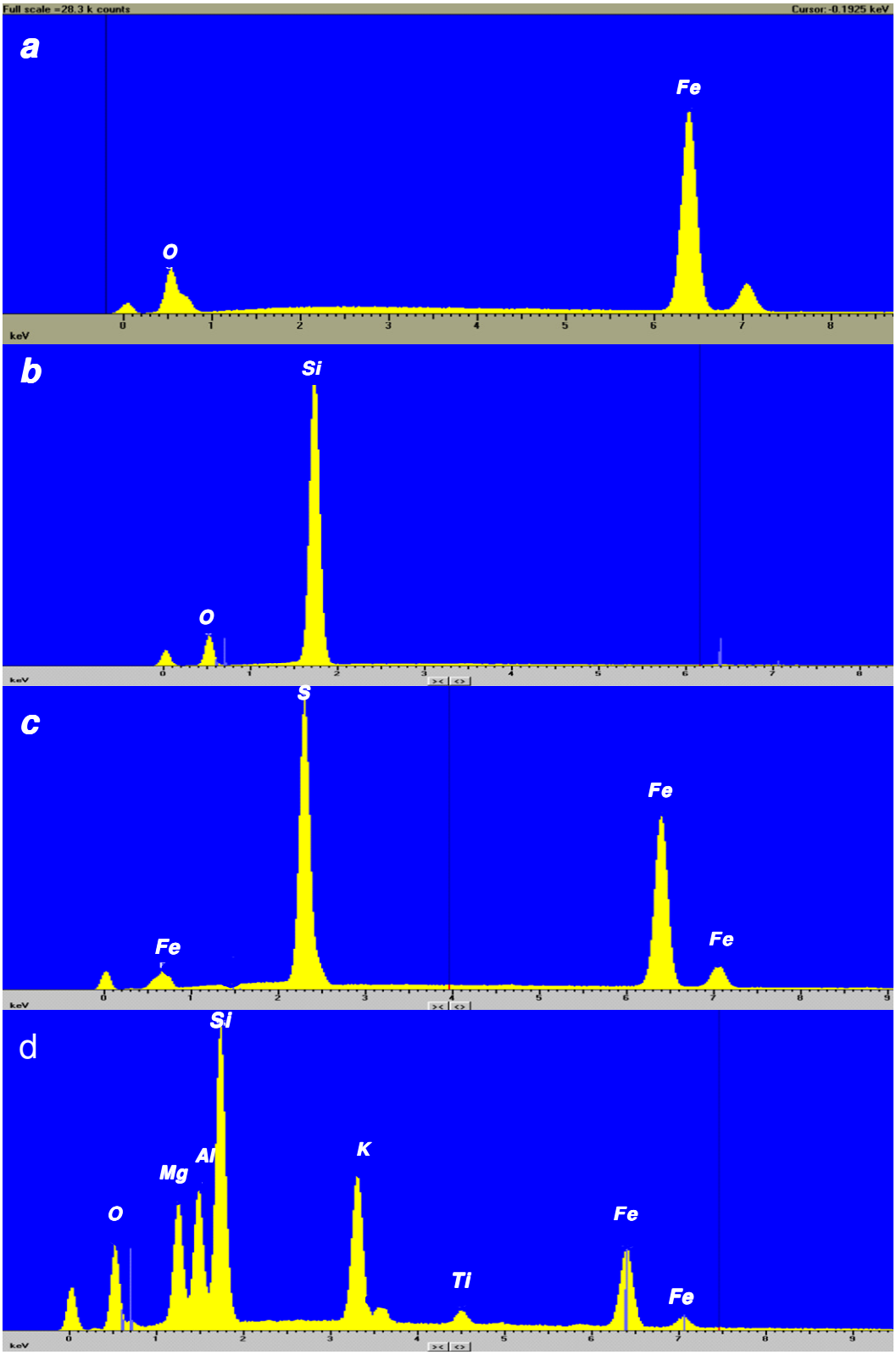

Figure 6.8 EDS spectra of gangue minerals in sample LB08. a - magnetite, b - quartz, c - pyrite, d – phlogopite (not shown in Figure 6.9).

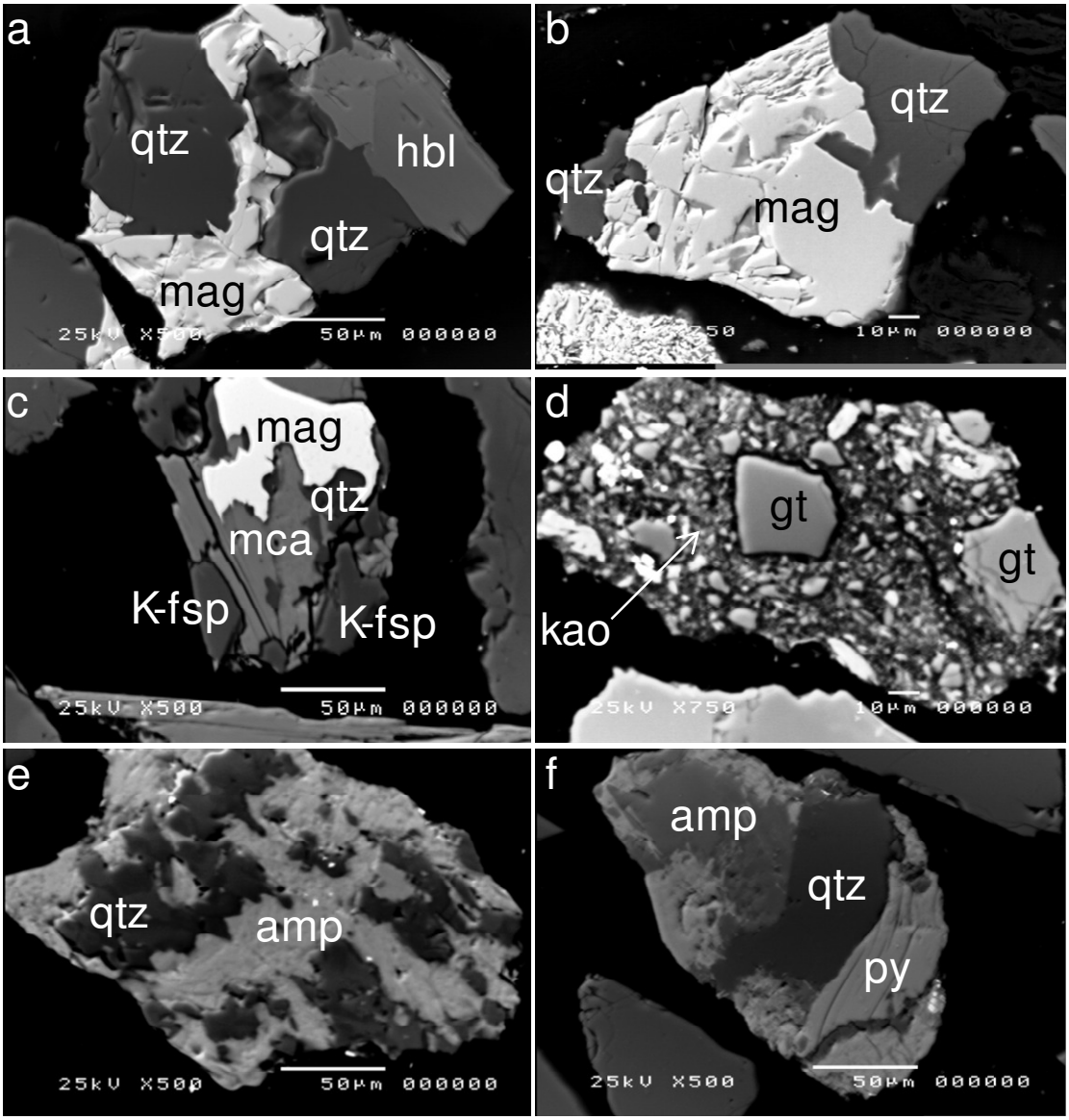

Figure 6.9 Backscattered electron images (BSE) showing various mineral associations amp – amphibole, gt- goethite, hbl – hornblende, kao – kaolinite, K-fsp – K-feldspar, mag – magnetite, py – pyrite, qtz – quartz.

6.3.5 EPMA

Figure 6.10 shows backscattered electron (BSE) images of some of the iron oxides and gangue mineral associations representative of the Putu samples analysed. Tables 6.4 and 6.5 give the compositions of the iron oxides and gangue minerals labelled in Figure 6.10. Magnetite is the main iron oxide in the high grade magnetite samples LB01 and LB03. The main gangue minerals associated with the magnetite are quartz, pyroxene, actinolite and clinochlore, with apatite, calcite and K-feldspars occurring in small quantities. Quartz is present in all the samples. Calcite ($CaCO_3$) is the only carbonate mineral

encountered and is present in sample LB08. The EMPA could not analyse for carbon and the identifcation was made according to the mineralogy database (http://www.mindat.org) which gives the ideal composition of calcite as CaO = 56.037, CO_2 = 43.963. One analysis contained 14.67 wt. % MnO. It is not uncommon for Mn to replace some of the Ca in calcite.

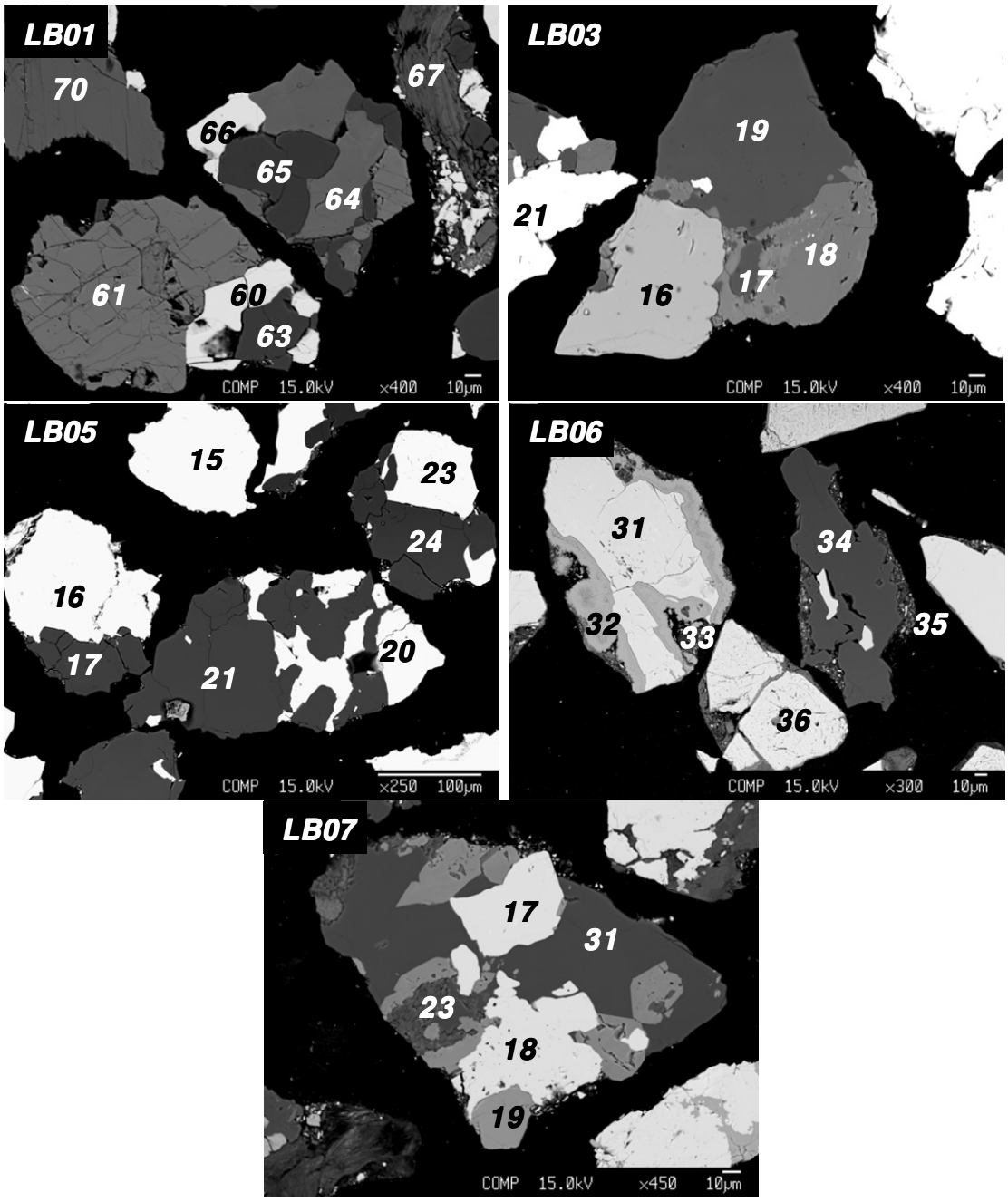

Figure 6.10 Representative BSE images (taken using the electron microprobe, see Chapter 5) showing some of the Fe-oxide and gangue mineral associations present in the Putu samples.

Four apatite grains were encountered; three in LB03 and one in LB07. They all have higher F than Cl; OH cannot be determined by EPMA. They are therefore

mainly fluorapatite, which is part of the isomorphous series with end members being fluorapatite, $Ca_5(PO_4)_3F$, hydroxylapatite, $Ca_5(PO_4)_3OH$, chlorapatite, $Ca_5(PO_4)_3Cl$ and carbonate-apatite, $Ca_5(PO_4,CO_3,OH)_3(F,OH)$.

Table 6.4 Composition of the iron oxides in Figure 6.10.

Mineral	*Analysis ID*	*SiO_2*	*Al_2O_3*	*Fe_2O_3*	*FeO*	*P_2O_5*	*Total*
Magnetite	LB01-60	bdl	bdl	68.95	30.95	bdl	99.90
Magnetite	LB01-66	bdl	bdl	69.47	31.23	bdl	100.70
Magnetite	LB03-21	bdl	bdl	68.87	30.86	bdl	99.73
Magnetite	LB05-15	bdl	bdl	69.11	31.12	bdl	100.23
Hematite	LB05-16	0.35	0.11	98.28	0.42	0.19	99.35
Magnetite	LB05-20	bdl	bdl	69.43	31.17	bdl	100.60
Hematite	LB05-23	bdl	bdl	101.00	bdl	bdl	101.00
Hematite	LB06-31	bdl	bdl	98.94	bdl	bdl	98.94
Goethite	LB06-32	0.54	0.93	82.97	bdl	1.36	85.80
Hematite	LB06-36	0.14	0.19	98.42	0.09	bdl	98.84
Hematite	LB07-17	bdl	bdl	100.08	bdl	bdl	100.08
Hematite	LB07-18	bdl	bdl	100.28	bdl	bdl	100.28

Analyses by EPMA, see Chapter 5 for analytical details. bdl – below detection limit. Fe_2O_3 calculated using the method of Droop (1987).

The feldspars are mainly albite, microcline and orthoclase. Biotite and phlogopite are the dominant micas whilst the pyroxenes are dominantly from the diopside-hedenbergite series. Even though the amphiboles present are dominantly Ca-amphiboles, a few Mg, Fe amphiboles such as cummingtonite were identified in sample LB08. Chamosite (Fe rich) is the dominant chlorite in the iron rich samples, LB06 and LB07, but in the Fe-poor samples such as LB01, the chlorite present is the Mg–rich variety clinochlore. The magnetite hematite sample, LB05, has magnetite, goethite and hematite as the iron oxides present with quartz being the major gangue mineral. The major difference between this sample and the hematite magnetite sample, LB06, is that LB05 contains more magnetite and quartz than LB06 which has more goethite and hematite. The goethite present in WMI in general contains more aluminium than those in TMI which might be a reflection of the position in the weathering profile with WMI being closer to the surface. Sample LB07 contains hematite as its dominant iron oxide with quartz and andradite as the main gangue minerals. Phosphorus occurs mainly in the form of apatite.

Table 6.5 Composition of the gangue minerals labelled in Figure 6.10.

Mineral	*Analysis ID*	*SiO_2*	*TiO_2*	*Al_2O_3*	*Fe_2O_3*	*FeO*	*MnO*	*MgO*	*CaO*	*K_2O*	*Na_2O*	*P_2O_5*	*F*	*Total*	*Formula*
Augite	LB01-61	53.07	bdl	0.50	3.71	3.33	bdl	14.38	23.61	bdl	0.91	bdl	bdl	99.51	$(Ca_{0.96}Na_{0.05}Mg_{0.81}Fe^{2+}_{0.12}Fe^{3+}_{0.07})(Si_{1.99}Al_{0.01})$
Quartz	LB01-63	97.25	bdl	0.12	bdl	bdl	bdl	bdl	bdl	bdl	Bdl	bdl	bdl	97.37	$Si_{0.97}O_2$
Actinolite	LB01-64	54.11	bdl	2.28	3.26	6.56	bdl	17.99	12.39	0.11	0.50	bdl	bdl	97.20	$Ca_{1.88}Na_{0.14}Mg_{3.80}Fe^{2+}_{0.78}Fe^{3+}_{0.35}Si_{7.67}Al_{0.38}O_{22}(OH)_2$
Quartz	LB01-65	100.78	bdl	Bdl	bdl	bdl	bdl	bdl	bdl	bdl	Bdl	bdl	bdl	100.78	SiO_2
Clinochlore	LB01-67	31.52	0.38	17.55	bdl	12.64	1.82	22.65	0.35	1.49	Bdl	bdl	bdl	88.40	$(Mg_{3.33}Fe_{1.04}Al_{1.14}Ti_{0.03}Mn_{0.15}Ca_{0.04}K_{0.15})(Si_{3.10}Al_{0.90})O_{10}(OH)_8$
Actinolite	LB01-70	57.28	bdl	0.21	0.35	5.48	bdl	20.46	12.89	bdl	0.20	bdl	bdl	96.87	$Ca_{1.93}Na_{0.06}Mg_{4.26}Fe^{2+}_{0.64}Fe^{3+}_{0.03}Al_{0.03}Si_8O_{22}(OH)_2$
Actinolite	LB03-18	57.56	bdl	0.36	3.66	4.21	bdl	19.52	10.29	bdl	1.68	bdl	bdl	97.28	$Ca_{1.53}Na_{0.45}Mg_{4.05}Fe^{2+}_{0.49}Fe^{3+}_{0.38}Al_{0.06}Si_{8.01}O_{22}(OH)_2$
Quartz	LB03-21	101.87	bdl	Bdl	bdl	bdl	bdl	bdl	bdl	bdl	Bdl	bdl	bdl	101.87	SiO_2
Apatite	LB03-16	bdl	bdl	Bdl	bdl	0.27	bdl	bdl	54.96	bdl	Bdl	40.24	1.39	96.86	$Ca_{5.14}P_{2.97}O_{12}(OH_{0.62}F_{0.38})$
Calcite	LB03-17	bdl	bdl	Bdl	bdl	0.36	0.22	bdl	58.01	bdl	Bdl	bdl	bdl	58.59	$CaCO_3$
Quartz	LB05-17	101.26	bdl	Bdl	bdl	bdl	bdl	bdl	bdl	bdl	Bdl	bdl	bdl	101.26	SiO_2
Quartz	LB05-21	101.04	bdl	Bdl	bdl	bdl	bdl	bdl	bdl	bdl	Bdl	bdl	bdl	101.04	SiO_2
Quartz	LB05-24	100.85	bdl	Bdl	bdl	bdl	bdl	bdl	bdl	bdl	Bdl	bdl	bdl	100.85	SiO_2
Chamosite	LB06-33	14.04	bdl	13.93	0.49	30.55	bdl	0.12	bdl	bdl	Bdl	0.31	bdl	59.44	$Fe^{2+}_{4.47}Mg_{0.03}Al_{1.33}Fe^{3+}_{0.06}Si_{2.46}Al_{1.54}O_{12}(OH)_{16}$
Quartz	LB06-34	99.94	bdl	Bdl	bdl	0.34	bdl	bdl	bdl	bdl	Bdl	bdl	bdl	100.28	SiO_2
Chamosite	LB06-35	15.27	bdl	11.60	11.69	34.46	bdl	bdl	0.14	bdl	Bdl	0.29	bdl	73.45	$Fe^{2+}_{4.29}Mg_{0.02}Al_{0.30}Fe^{3+}_{1.31}P_{0.04}Si_{2.27}Al_{1.73}O_{12}(OH)_{16}$
Apatite	LB07-19	dbl	bdl	Bdl	bdl	bdl	bdl	bdl	56.60	bdl	Bdl	40.77	1.06	98.43	$Ca_{5.20}P_{2.96}O_{12}(OH_{0.71}F_{0.29})$
Quartz	LB07-20	100.59	bdl	Bdl	bdl	0.84	bdl	bdl	bdl	bdl	Bdl	bdl	bdl	101.43	SiO_2
Clinochlore	LB07-23	31.47	bdl	16.22	bdl	12.46	0.13	25.35	0.14	bdl	Bdl	bdl	bdl	85.77	$(Mg_{3.77}Fe_{1.04}Al_{1.05}Mn_{0.01}Ca_{0.02})(Si_{3.14}Al_{0.86})O_{10}(OH)_8$

Analyses by EPMA, see Chapter 5 for details of the method. bdl – below detection limit. Formula calculated using method described in Deer et al. (1992).

6.4 Conclusions

The mineralogy and chemistry of the Putu Iron Ore deposit was characterised using SEM-EDS, XRF, XRD and EPMA. The XRF analyses were used to classify the samples into material types, the SEM/EDS gave an indication of the elements and hence possible minerals present, the XRD gave the major minerals present and the EPMA identified not only the major and minor minerals but also their compositions. Some of the minerals identified in the EPMA were not seen in XRD patterns because of the detection limit of the XRD which is about 5 % (McCusker et al., 1999).

The description that accompanied the samples from Putu, provided by their Chief Geologist, has been found to be correct, except for sample LB07 which was assumed to contain the highest Fe percentage because its main iron oxide is hematite. It has however been found to contain andradite as a major mineral and since it is also red in colour it was misidentified as hematite. It has been observed that the major iron minerals are magnetite, hematite and goethite whilst the major gangue minerals are quartz and amphibole. Other gangue minerals present are apatite, calcite, epidote, alkali feldspar (orthoclase, albite) pyroxene (diopside-hedenbergite), amphibole (hornblende, actinolite, tremolite, cummingtonite) and mica (biotite, phlogopite). There is no evidence of the presence of any iron silicate or iron carbonate minerals.

Minor differences have been observed between the two main areas at Putu; apatite and quartz seem to be the main gangue in the Jideh area whilst calcite and quartz are prominent in the Montroh range. In addition, micas are the main Al bearing phases at Putu. Apatite and calcite are the main P and Ca bearing minerals.

These techniques have been used by several workers to test the linking of iron ore types to beneficiation requirements (Roy et al., 2007, Ramainaidu et al., 2008, Rao et al., 2009). The mineralogy, grain size and textures of ores can be used to improve process efficiency in an iron ore mine (Johnson et al., 2007). For example, carbonate minerals require calcinations during the formation of

pellets and this implies additional heat which will slow down the indurations process and reduce throughput.

The nature of the iron minerals and associated gangue minerals decides the method of beneficiation to be adopted. Magnetite-bearing iron formations are generally conducive to beneficiation by low intensity magnetic separation at reasonable cost. According to Rao et al. (2009), as long as alumina and silica phases are not too fine grained and the ore is composed of magnetite/hematite with coarse grained quartz, the magnetic route is the most effective means of beneficiation.

Chapter 7

Mineralogical and Geochemical Characterisation of the Nkout Iron Ore Deposit

7.1 Introduction

This chapter presents results from mineralogical and whole rock geochemical analysis of samples from the Nkout Iron Ore deposit. Mineralogical information was sought from optical microscopy and XRD whilst mineral chemistry was studied using EMPA. The geochemistry section using major and minor elements determined by XRF looks at the geochemical trends associated with the mineralogical changes from the magnetite itabirite to the enriched material. The average chemical compositions of the various material types are also shown.

7.2 Samples

The location of the outcrops and drillhole collars of the cores sampled from Nkout West to East are given in Figure 7.1, which shows them overlain on the total intensity magnetic map (Chapter 4). Exposures in the area are few and all the known ones were sampled. Even though un-mineralised rocks associated with the deposits were also sampled, with the exception of two samples (clay and granite samples), only mineralised samples were analysed. Forty-two samples from 31 drill holes (27 from Nkout West to East and 4 from Nkout South), 3 grab samples and 6 outcrop samples were analysed. Nkout Centre, which has been drilled the most, has four out of the six outcrops, with one each at Nkout East and West. Table 7.1 gives the project areas, drillhole IDs, samples numbers and type of samples.

The physical properties of the samples were studied and they were divided into two sets. One set was reserved and the other screened to prepare various size fractions for analysis using Optical Microscopy, XRD, XRF, SEM, EPMA and QEMSCAN®. The results of the QEMSCAN® analysis are presented and discussed in Chapter 8.

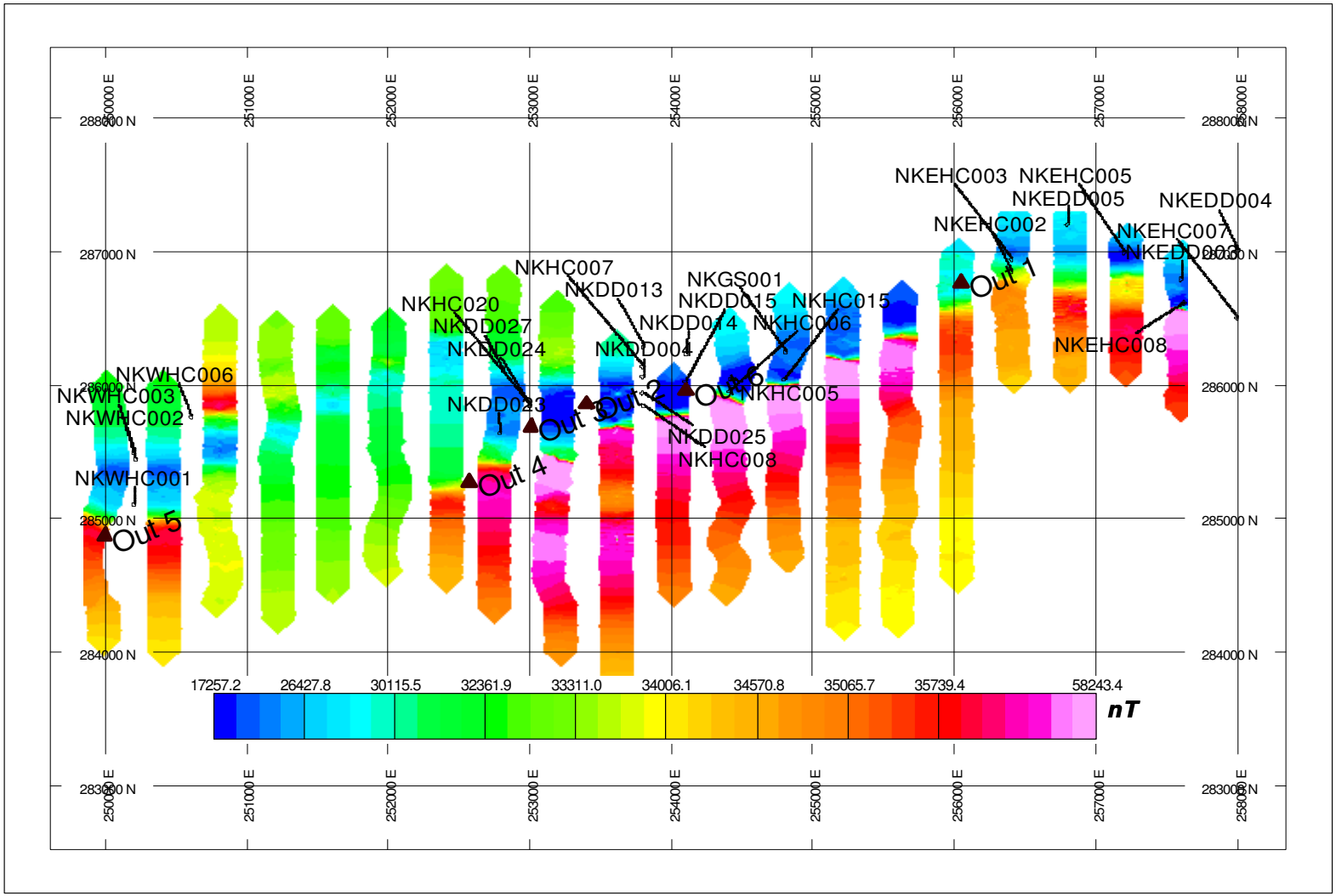

Figure 7.1 Location of outcrops and drill collars of cores sampled at Nkout East, Nkout Centre and Nkout West.

Table 7.1 Details of the samples analysed.

Material Type	*Hole ID*	*Sample ID*	*Sample Type*
EM		G02	Grab
	NKHC007	NCS04	Saprolite/Laterite
	NKEHC007	NES04	Saprolite/Laterite
		OUT 02	Outcrop
WMI		G01	Grab
	NKHC006	NCS03	Saprolite/Laterite
	NKHC020	NCS07, NCS08	Saprolite/Laterite
	NKEHC002	NES01	Saprolite/Laterite
	NKWHC002	NWS03	Saprolite/Laterite
		OUT 01	Outcrop
		OUT 3	Outcrop
TMI		G03	Grab
	NKGS001	NCS01	Saprolite/Laterite
	NKHC005	NCS02	Saprolite/Laterite
	NKHC008	NCS05	Saprolite/Laterite
	NKHC015	NCS06	Saprolite/Laterite
	NKEHC003	NES02	Saprolite/Laterite
	NKEHC005	NES03	Saprolite/Laterite
	NKEHC008	NES05, NES06	Saprolite/Laterite
	D3HC006	NSS01	BIF
	D3HC007	NSS02	Saprolite/Laterite
	D3HC010	NSS03	BIF
	NKWHC001	NWS01	Saprolite/Laterite
	NKWHC002	NWS02	Saprolite/Laterite
	NKWHC003	NWS04	Saprolite/Laterite
HMI	NKDD004	NCB01	BIF
	NKDD015	NCB04, NCB05	BIF
	NKDD023	NCB06	BIF
	NKDD027	NCB09	BIF
	NKEDD003	NEB01, NEB02	BIF
	NKEDD005	NEB04, NEB05	BIF
	D3HC005	NSB02	BIF
	NKWHC003	NWB02, NWB03	BIF
		OUT 04	Outcrop
		OUT 05	Outcrop
		OUT 06	Outcrop
LMI	NKDD013	NCB02	BIF
	NKDD014	NCB03	BIF
	NKDD025	NCB08	BIF
	NKEDD004	NEB03	BIF
	D3HC005	NSB01	BIF
	D3HC007	NSB03	BIF
	NKWHC001	NWB01	BIF
Clay	NKWHC006	NWS05	
Granite	NKDD024	NCB07	

7.3 Mineralogy

7.3.1 XRD studies

The major minerals identified in the weathered zone along with their formulae are given in Table 7.2. The minerals identified in the BIF samples and their ideal formulae are given in Table 7.3. Representative profiles showing the major minerals in both the weathered profile and the fresh BIF are shown in Figures 7.2 – 7.4.

Whereas the three iron oxides i.e. magnetite, hematite and goethite were identified in all the material types, the major iron bearing mineral in the HMI and LMI of the four project areas was magnetite. The major gangue minerals identified in the weathered profile were quartz, kaolinite and gibbsite whilst quartz and aluminosilicates such as amphiboles, feldspars and micas were the major gangue minerals in the BIF. Amphiboles were the dominant silicate minerals, with the calcic amphiboles dominant over the iron magnesium amphiboles. The major calcic amphibole was hornblende but actinolite, and sodic varieties such as edenite and pargasite were identified. The main Fe, Mg amphiboles identified were cummingtonite, anthophylite and its sodic variety arfvedsonite was identified at Nkout Centre. Note that all the amphiboles identified are characteristic of metamorphic terrane confirming that the study areas have being metamorphosed (Jacobson and Sorensen, 1986). The feldspars identified were albite, labradorite and anorthite; all plagioclase. The micas identified were the Al, Fe and Mg varieties, muscovite, annite and phlogopite respectively. Other silicates identified include epidotes and chlorites including the Fe-rich variety chamosite. Almandine (garnet) was present in some of the HMI and LMI.

Table 7.2 Minerals identified in the saprolite / laterite zones using XRD.

Group	*Mineral*	*Formula*
Silica minerals	quartz	SiO_2
Clay minerals	kaolinite	$Al_2Si_2O_5(OH)_4$
Fe-(hydr)oxides	goethite	$FeO(OH)$
	hematite	Fe_2O_3
	magnetite	$Fe^{2+}Fe_2^{3+}O_4$
Sulphide	pyrite	FeS_2
Al-hydroxides	gibbsite	$Al(OH)_3$
Sheet silicate	chlorite	$(Mg,Fe^{2+},Fe^{3+},Mn,Al)_6(AlSi)_4O_{10}(OH)_8$

Formulae from Deer et al. (1992)

Table 7.3 Minerals identified in the fresh BIF zones using XRD.

Group	*Mineral*	*Formula*
Fe Oxide	magnetite	$Fe^{2+}Fe_2^{3+}O_4$
Silica minerals	quartz	SiO_2
Amphibole	actinolite	$Ca_2\ (MgFe^{2+})_5(Si_8O_{22})(OH,F)_2$
	pargasite	$Na,Ca_2(Mg,Fe^{2+})_4Al(Al_2Si_6O_{22}(OH)_2$
	arfvedsonite	$Na_3(Fe_4^{2+}Fe^{3+}Si_8O_{22}(OH)_2$
	fluoro-edenite	$NaCa_2(MgFe)_5AlSi_7O_{22}(F,OH)_2$
	ferrohornblende	$Ca_2(Mg,Fe^{2+},Fe^{3+}Al,)_5(Al,Si)_8O_{22}(OH)_2$
	cummingtonite	$(Mg,Fe)_7Si_8O_{22}(OH)_2$
	anthophylite	$(Mg,Fe^{2+})_7Si_8O_{22}(OH)_2$
Feldspar	albite	$Na(AlSi_3O_8)$
	labradorite	$(Ca,Na)Al(Al,Si)Si_2O_8Ab_{30}$-$An_{70}$
	anorthite	$CaAl_2Si_2O_8$
Mica	phlogopite	$KMg_3(AlSi_3O_{10})(F,OH)_2$
	annite	$KFe^{2+}{}_3\ (AlSi_3O_{10})(OH,F)_2$
	muscovite	$KAl_2(Si_3AlO_{10})(OH)_2$
Epidote	epidote	$Ca_2(Fe^{3+},Al)_3(SiO4)(Si_2O_7)(O,OH)_2$
Chlorite	chlorite	$(Mg,\ Fe,\ Al)_6(Si,Al)_4O_{10}(OH)_8$
	chamosite	$Fe_3^{2+}(Fe_2^{2+}Al)(Si_3AlO_{10})(OH)_8$
Garnet	almandine	$(Fe^{2+}Mn)_3Al_2(SiO_4)_3$

Formulae from Deer et al. (1992)

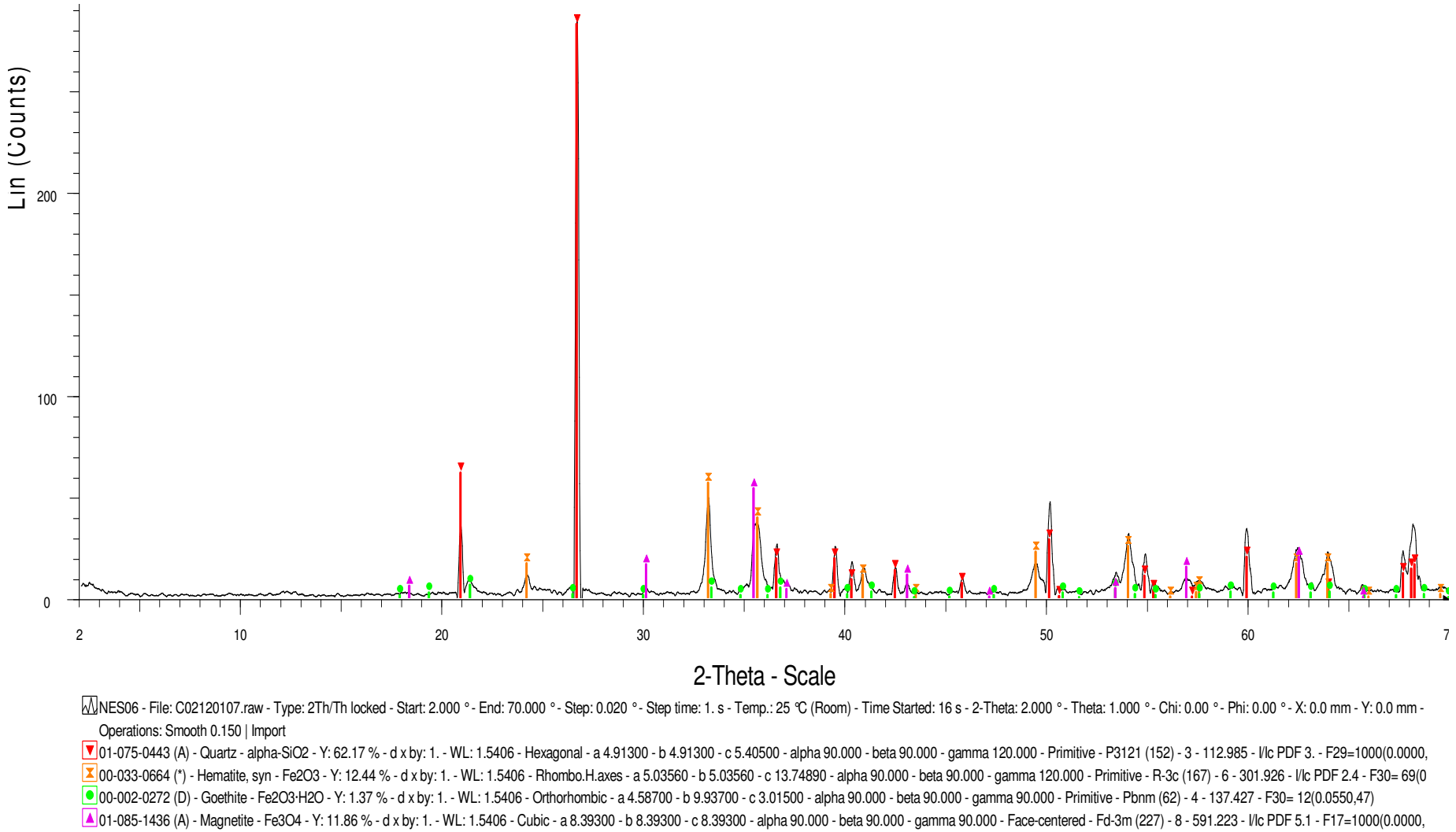

Figure 7.2 XRD Profile for NES06 with showing the main Fe oxides and quartz, the main gangue.

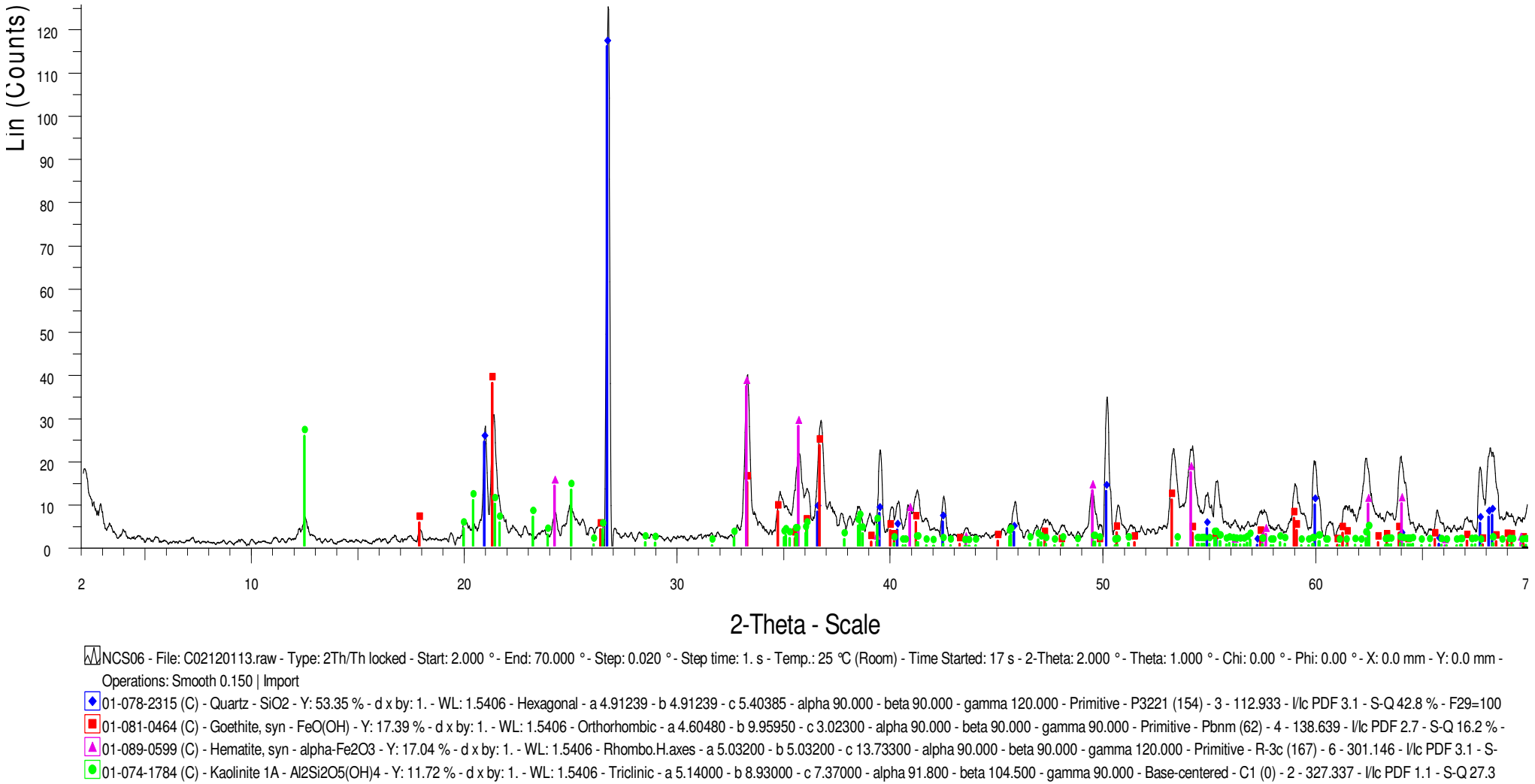

Figure 7.3 XRD Profile for NCS06 showing hematite and goethite as the main Fe oxides and quartz and kaolinite as the main gangue minerals.

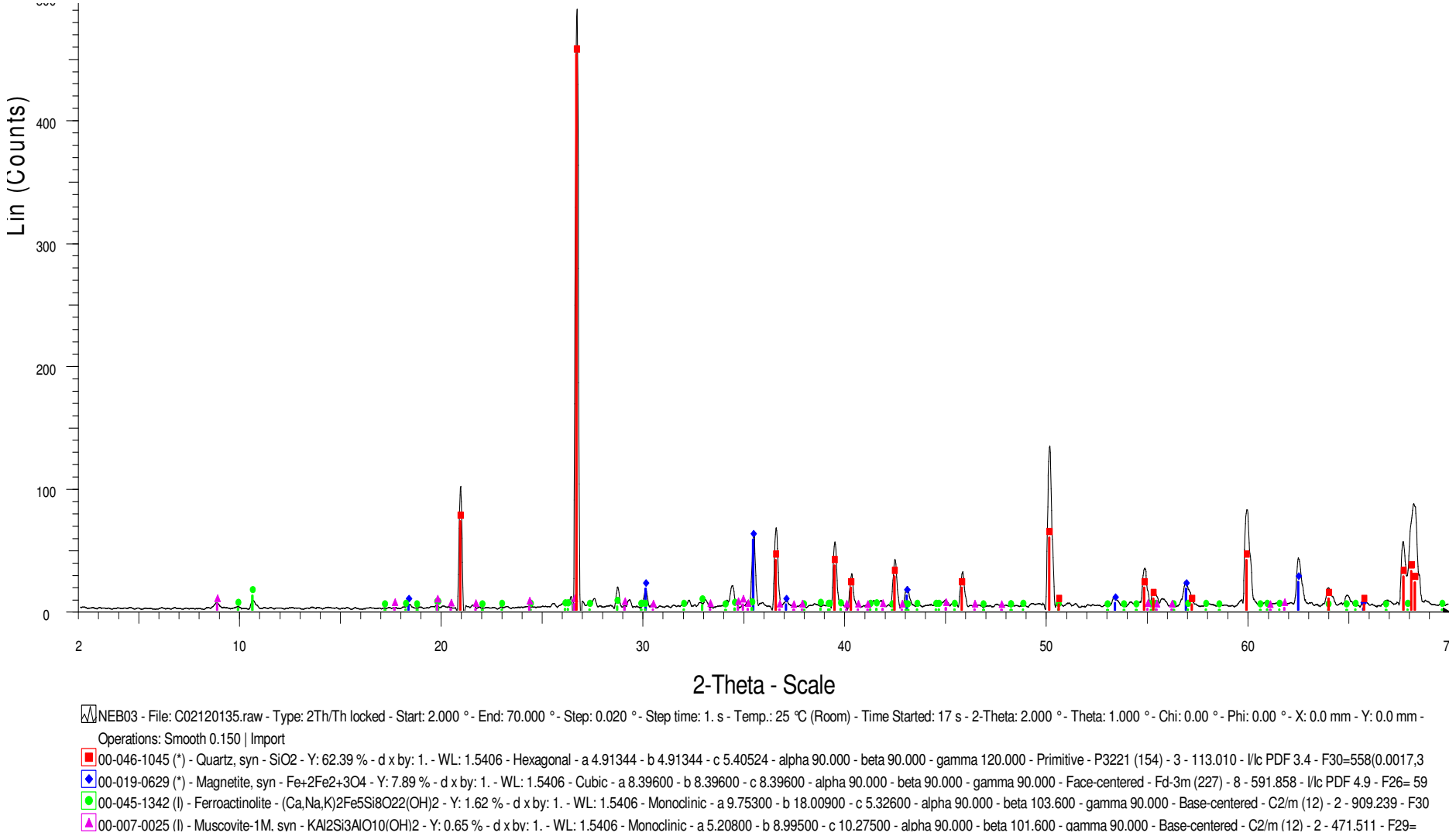

Figure 7.4 Representative BIF profile showing magnetite as the Fe oxide and quartz, actinolite (amphibole) and muscovite (mica) as gangue minerals.

7.3.2 EPMA studies

Twelve samples representative of the various material types were selected for EPMA studies and 318 point analyses were made.

7.3.2.1 Magnetite and hematite

There is a slight compositional variation in magnetite, the main ore mineral at Nkout, between the different material types. The magnetite in the WMI carries up to 0.05 wt % SiO_2 and this concentration increases to up to 0.12 wt % in the TMI and HMI groups. Those in the LMI carry the highest SiO_2 (up to 0.50 wt %). TiO_2, MgO, CaO, Na_2O, P_2O_5 and SO_3 all occur in trace quantities in the WMI, TMI and HMI whilst MnO occurs in up to 0.20 wt % in the WMI. The concentration of these oxides increases in the LMI to up to 0.46 wt % as in the case of TiO_2. Al_2O_3 on the other hand occurs in trace quantities only in the HMI material type (up to 0.05 wt %). In the others it occurs in minor quantities up to 0.31 wt % in WMI, up to 0.12 wt % in TMI and highest in LMI (up to 0.70 wt %).

Apart from iron, the other oxide concentrations are in general higher in hematite than those in magnetite. In particular Al_2O_3 occurs up to 1.57 wt % in the WMI, up to 3.00 wt % in TMI, up to 0.36 wt % in HMI and 0.25 % in the LMI. Even though the dominant composition is Fe_2O_3 (up to 100.29 wt % in TMI), minor amounts of FeO occur up to 1.38 wt % in the WMI, up to 0.78 wt % in TMI and 0.33 wt % in the HMI.

7.3.2.2 Goethite group minerals

It is known that goethite can contain various elements such as Al, Si and P in its lattice resulting in varying compositions (Ramanaidu et al., 2008). Based on the EPMA results (Table 7.4), two categories of goethite were made, namely goethite/limonite and aluminium-bearing goethite (goethite (Al)). An arbitrary concentration of 3 wt % Al_2O_3 was set as a cut off point with goethite (Al) containing > 3 wt % Al_2O_3 and goethite/limonite containing < 3 wt % Al_2O_3. A plot of FeO vs Al_2O_3 (Fig. 7.5a) for all the goethite analysed shows the division into goethite/limonite and goethite (Al).

Table 7.4 EPMA average compositions (Avg) including standard deviations (StDev) for goethite analysed.

	Goethite (Al)				***Goethite/limonite***					
	WMI		***TMI***		***WMI***		***TMI***		***HMI***	
	Avg wt%	StDev	Avg wt%	StDev	Avg wt%	StDev	Avg wt%	StDev	Avg wt%	StDev
SiO_2	1.13	1.27	3.16	2.22	2.29	1.24	1.24	1.98	2.30	4.14
TiO_2	0.41	1.11	0.33	0.33	0.22	0.72	0.10	0.13	bdl	bdl
Al_2O_3	7.88	3.60	6.76	2.57	1.98	0.85	0.67	0.99	0.40	0.63
FeO	70.54	4.31	71.53	6.56	75.42	5.50	80.42	4.23	75.02	3.49
MnO	0.02	0.06	0.01	0.02	0.06	0.08	0.08	0.05	0.01	0.02
P_2O_5	1.84	1.20	0.41	0.31	0.37	0.38	0.13	0.25	0.38	0.64
SO_3	0.17	0.21	0.16	0.11	0.21	0.23	0.03	0.06	0.08	0.05
Total	81.99		82.36		80.55		82.67		78.19	1.54

bdl = below EPMA detection limits of < 0.01 wt %. Material types WMI, TMI and HMI are as defined in Chapter 4. Total Fe as FeO. Fe-oxides with totals between 70% - 90% when recalculated for magnetite were assigned as goethite. Goethite with Al concentration ≥ 3 wt. % is classified as goethite (Al).

The EPMA results did show that some of the goethite contained > 3 wt % Al_2O_3 and that > 95 % of the Si content observed in the goethite was below the 3 % threshold and as such a goethite (Si) category was not included (Table 7.4). Goethite/limonite occurs mainly in the TMI and HMI material types but is also present in the WMI. Goethite (Al) is confined to the WMI and TMI groups. Lack of goethite (Al) in the magnetite itabirites is consistent with them being fresh BIF. The Si content in both goethite (Al) and goethite/limonite increases from WMI to TMI to HMI and the Al_2O_3 content is highest in the WMI group.

There is a negative correlation between FeO and Al_2O_3 (Fig. 7.5b) for the goethite (Al) especially those in the WMI category where goethite (Al) is most abundant. Higher Al content in the goethite causes a decrease in backscattered electron coefficient as would be expected from the decreasing mean atomic number (Figure 7.5c).

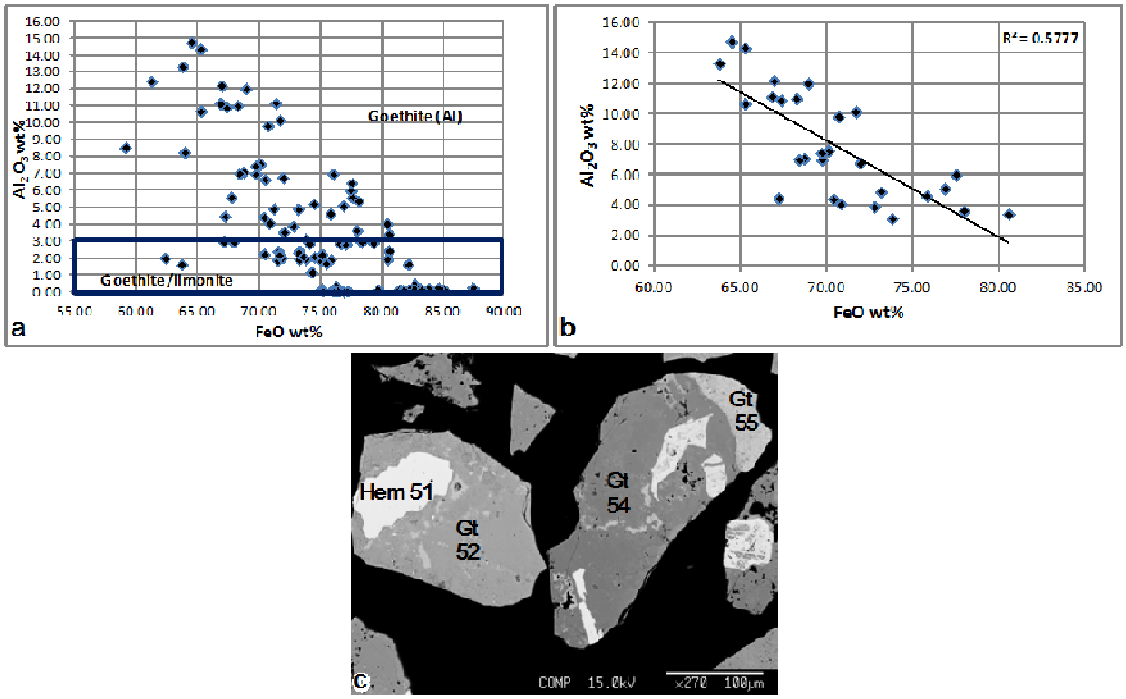

Figure 7.5 Compositional variation of the goethite at Nkout. (a) All goethite analysed (b) Goethite (Al) from the WMI category showing negative correlation between Al_2O_3 and FeO. (c) Sample G01 showing hematite (Hem) and goethite (Gt) showing variation in backscattered coefficient due to varying Al concentration. All the goethite belongs to the goethite (Al) category with Gt-55 containing 4.61 wt % Al_2O_3, Gt-52 contains 7.45 wt. % and Gt-54 contains 14.75 wt. %. Note the change in BSE with increasing Al_2O_3 concentration.

7.3.2.3 Fe-oxide textures

The Fe-oxides are highly intergrown. In most cases, hematite replaces magnetite and goethite replaces both magnetite and hematite. Alteration of hematite to goethite seems to start at the periphery of the grains and also through voids, cracks and other fissures within the hematite and may be due to hydration (Figure 7.6a, b and c). The grains therefore display both intragranular texture i.e. the voids are filled with goethite, and intergranular texture i.e. the goethite occupies the interstitial spaces between the hematite / magnetite grains. Goethite also has rims of Al-rich minerals such as gibbsite or kaolinite. Hematite forms lamellae within the magnetite (Figure 7.6c, d, e, and f). The goethite has cracks looking like 'mud cracks' which are an indication of the fine grained nature of the sample (Figure. 7.6e and f). Hematite replacing magnetite can appear porous, with its pores now filled by goethite. Chamosite can occur associated with clay minerals such as kaolinite, cements goethite/limonite, hematite and magnetite grains (Fig. 7.6g and h).

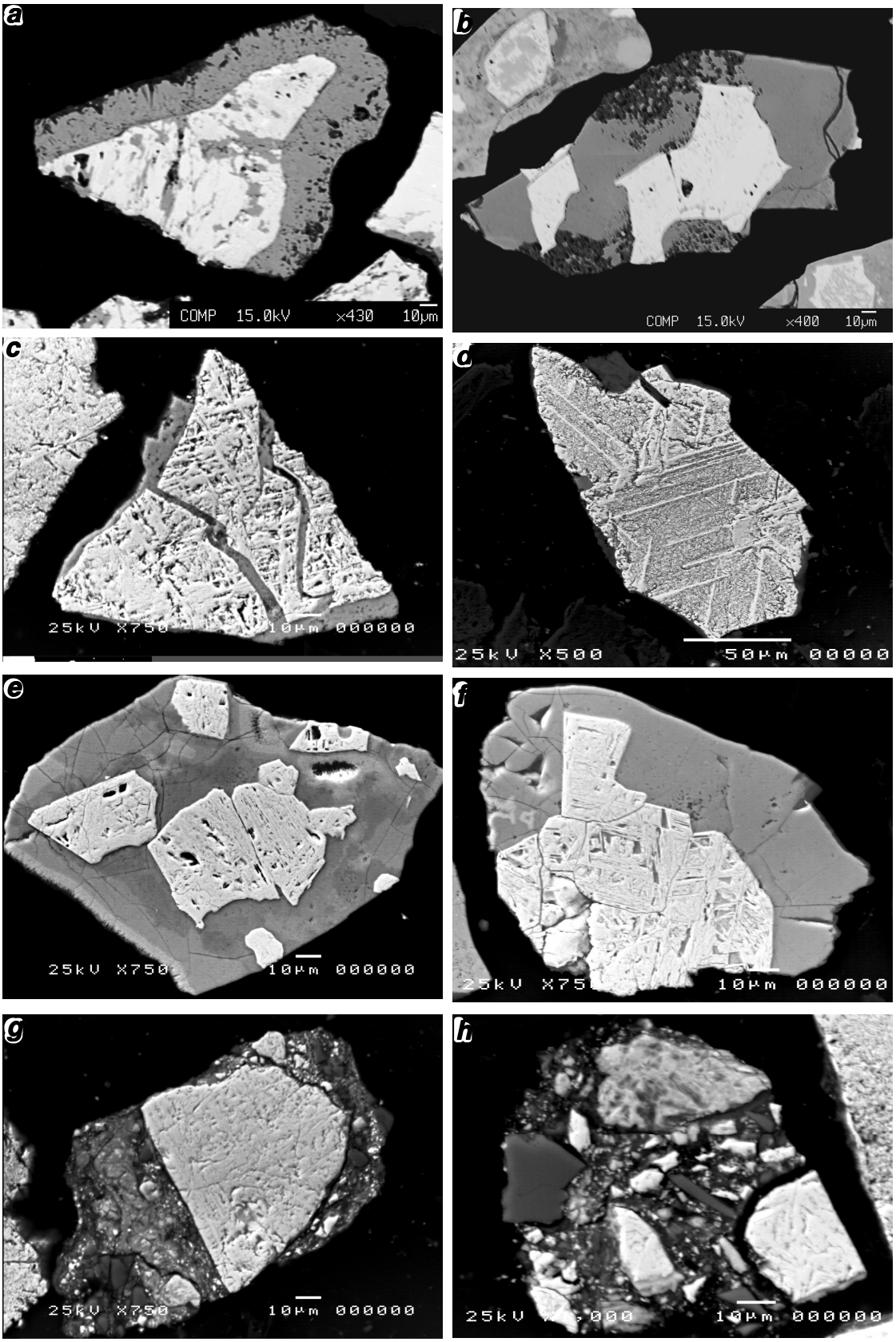

Figure 7.6 Fe oxide textures present.

7.3.2.4 Chlorite and gangue minerals

Chlorites are renowned for their substantial, varied and often continuous cation substitution making it difficult to assign specific names (Deer et al., 1992). Simple nomenclatures for the Mg-rich, Fe-rich and Mn-rich chlorites are clinochlore, chamosite and pennantite, respectively. Optical microscopy and EPMA analysis confirmed the presence of both clinochlore and chamosite, in the study area. They occur as weathered aggregates and chamosite in particular is closely associated with the Fe-oxides (white coloured minerals in Figure 7.7a), Figure 7.7b shows chamosite under reflected light microscopy. Table 7.5 gives their average composition and standard deviations within the WMI and TMI material groups.

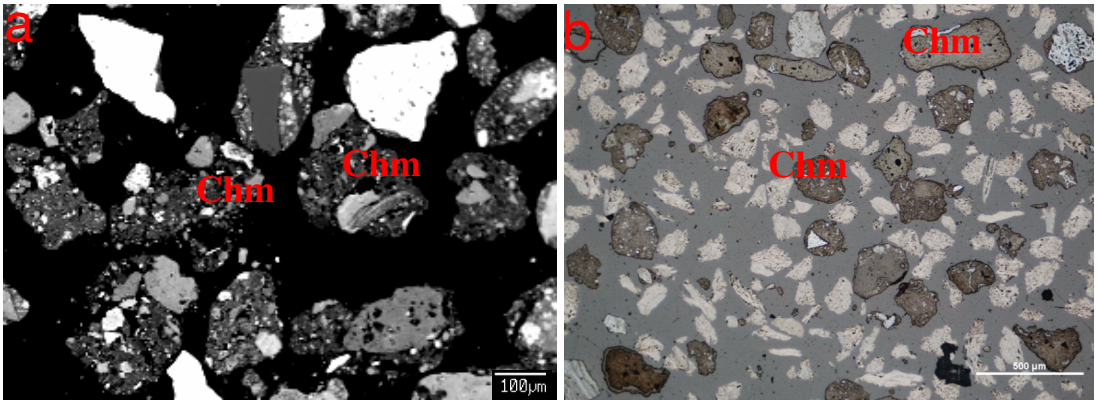

Figure 7.7 (a) BSE image and (b) reflected light micrograph showing chamosite (Chm) present at Nkout. The chamosite is mainly associated with the Fe-oxides.

Table 7.5 Average compositions (Avg) and standard deviations (StDev) for chamosite.

	WMI		***TMI***	
	Avg wt %	***StDev***	***Avg wt %***	***StDev***
SiO_2	17.77	3.66	19.09	4.04
TiO_2	0.16	0.27	0.49	0.19
Al_2O_3	15.53	3.37	20.57	2.73
Fe_2O_3	17.02	9.81	5.62	6.24
FeO	41.39	4.65	38.75	3.92
CaO	0.08	0.02	0.05	0.01
Na_2O	0.06	0.02	0.05	0.02
P_2O_5	0.09	0.02	0.16	0.10
SO_3	0.06	0.08	0.07	0.07
Total	92.16		84.85	

FeO / Fe_2O_3 proportions were calculated using the method of Droop (1987).

Table 7.6 gives representative compositions of the gangue minerals. The main gangue minerals in the WMI and TMI are the Al oxides and hydroxides, mainly gibbsite. Quartz and to a lesser extent kaolinite were also present whilst quartz and aluminium silicates are dominant in the magnetite itabirite. The amphiboles in the HMI are mainly Ca Mg amphiboles in the tremolite-actinolite series. In the LMI, Fe Mg amphiboles such as cummingtoninite-grunerite are dominant. The micas (mainly lath shaped) in the HMI and LMI have similar compositions with the FeO, Al_2O_3 and K content of the LHI being higher than those of other material types. Pyroxenes were encountered in the LMI and show varying Fe, Ca, Al and Mg concentrations. Both plagioclase and K-feldspar were identified in the magnetite itabirite. Fluorapatite is a minor to trace mineral in the magnetite itabirite.

7.3.2.5 Representative BSE images and composition of the sample types

Representative BSE images of the samples discussed in this section are shown in Figure 7.8 and some of the mineral grains are labelled. In the text, the labelled grains are referred to by their sample numbers followed by their number on Figure 7.8. The data for the labelled grains have been divided into two tables, one for the iron oxides (Table 7.7) and another for chamosite and the gangue minerals (Table 7.8). The discussion below considers grab samples, outcrop samples and then drill core samples which are themselves divided into saprolite/laterite samples and fresh BIF samples.

Grab samples

This sample was selected because of its glassy crystals (Figure 7.9), assumed to be hematite. However, the EPMA result concurred with that of the XRD and gave hematite and goethite in roughly equal proportions. The composition of the goethite indicates that it has P, Al and Si in its lattice. For example in Figure 7.8, grain G01-67, contains 2.85 wt % P and 10.15 wt % Al_2O_3 and even though the highest SiO_2 weight percent given is for grain G01-64 i.e. 0.18 wt %, the goethite in the area can contain between 2 and 3 wt % SiO_2.

Table 7.6 Representative compositions of the gangue minerals at Nkout analysed by EPMA.

Mineral	*SiO_2*	*TiO_2*	*Al_2O_3*	*Fe_2O_3*	*FeO*	*MnO*	*MgO*	*CaO*	*Na_2O*	*K_2O*	*P_2O_5*	*SO_3*	*F*	*Total*
Ap	0.05	bdl	0.01	0.17	bdl	0.14	bdl	55.06	0.02	bdl	44.08	0.02	1.37	100.92
Ap	0.05	bdl	0.02	0.20	bdl	0.10	bdl	55.32	0.02	bdl	44.08	0.01	1.14	100.94
Ca Amp	54.19	bdl	2.72	4.10	8.55	0.32	15.56	11.64	0.52	0.19	0.08	bdl	0.16	98.03
Fe Amp	51.02	0.02	0.23	bdl	39.10	0.83	6.33	0.66	0.07	bdl	bdl	bdl	bdl	98.26
Gbs	0.04	bdl	81.81	bdl	0.14	bdl	bdl	0.01	bdl	bdl	0.01	bdl	0.06	82.07
Kao	46.21	0.05	38.36	bdl	0.99	0.02	0.02	0.06	0.09	0.12	bdl	0.04	bdl	85.96
Kao	42.69	bdl	33.82	bdl	0.96	0.02	0.02	0.07	0.11	0.01	0.04	0.12	0.01	77.91
K-Fsp	51.59	bdl	31.22	bdl	1.58	0.14	0.50	0.26	1.67	8.60	bdl	0.01	0.02	95.59
Pl Fsp	58.20	bdl	26.10	bdl	0.33	bdl	bdl	8.71	6.53	0.19	0.03	bdl	bdl	100.09
Mca	36.89	1.61	17.21	bdl	18.85	0.01	11.12	0.06	0.42	8.78	bdl	0.01	0.03	94.99
Mca	36.44	1.92	16.79	bdl	19.01	bdl	10.69	0.02	0.41	8.86	bdl	0.05	0.07	94.26
Pyx	42.92	0.05	7.53	10.45	20.36	0.23	3.68	10.00	1.52	1.38	0.05	0.01	bdl	98.19
Pyx	38.63	0.02	20.87	bdl	34.11	0.41	2.63	3.71	0.01	0.02	bdl	bdl	bdl	100.41
Qtz	101.57	bdl	0.02	bdl	0.12	bdl	bdl	0.01	0.01	bdl	bdl	bdl	bdl	101.73

Notes: bdl = below detection limit. X = no. of oxygen, T = no. of cations used in mineral formulae calculations. Amp = amphibole, Ap = apatite, Gbs = gibbsite, Fsp = feldspar, K = alkali, Pl = plagioclase, Kao = kaolinite, Mca = mica, Pyx = pyroxene, Qtz - quartz.

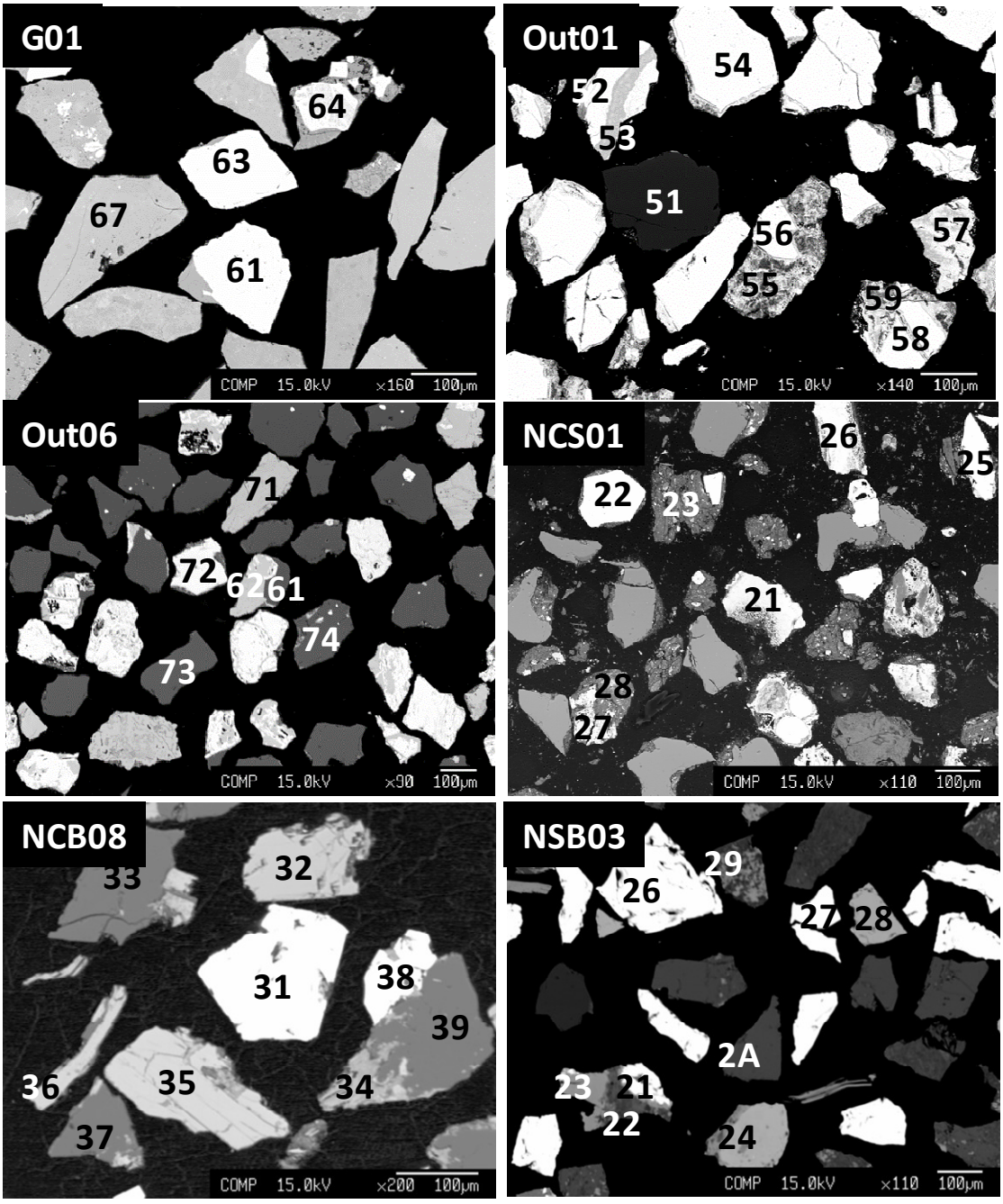

Figure 7.8 Representative BSE images for grab, outcrop, saprolite and BIF samples.

Note the difference in Al_2O_3 composition between goethite G01-64 (3.41 wt %) and G01-67 (10.15 wt %) (Table 7.7) and the resulting difference in backscattered electron coefficient with G01-67 (higher Al_2O_3 %) being darker. The almost isometric shape of the hematite grains (G01-63, 61) confirms that they are martite i.e. a pseudomorph after magnetite (Figure 7.8).

Table 7.7 Representative EPMA data (wt %) for the Fe oxide grains labelled on Figure 7.8.

Mineral	*Analysis ID*	*SiO_2*	*TiO_2*	*Al_2O_3*	*Fe_2O_3*	*FeO*	*P_2O_5*	*SO_3*	*Total*
Hematite	G01-61	0.02	0.02	0.49	95.91	0.63	0.34	0.01	97.43
Hematite	G01-63	0.01	0.04	0.03	99.49	bdl	bdl	bdl	99.57
Gt(Al)	G01-64	0.18	0.01	3.41	86.09	bdl	0.99	0.04	90.72
Gt(Al)	G01-67	0.15	0.39	10.15	75.65	bdl	2.85	0.06	89.25
Goethite	Out01-52	2.24	0.01	1.63	82.14	bdl	0.09	0.03	86.26
Gt(Al)	Out01-53	1.15	0.05	6.97	69.74	bdl	1.44	0.06	79.57
Hematite	Out01-54	0.14	0.04	0.23	98.94	0.20	0.06	bdl	99.68
Magnetite	Out01-56	0.01	0.02	0.17	67.90	30.71	bdl	bdl	98.88
Gt(Al)	Out01-57	3.79	0.20	3.63	77.98	bdl	0.35	0.04	86.17
Magnetite	Out01-58	0.04	0.02	0.09	68.17	30.77	bdl	bdl	99.18
Goethite	Out01-59	3.31	2.70	2.85	76.61	bdl	0.67	0.03	86.35
Goethite	Out06-62	0.54	bdl	0.02	82.08	bdl	0.04	0.11	82.79
Goethite	Out06-71	1.52	0.01	1.69	80.45	bdl	0.93	0.04	84.64
Hematite	Out06-72	0.01	0.01	0.05	98.64	bdl	bdl	bdl	98.71
Gt(Al)	NCS01-21	2.77	0.13	4.91	75.46	bdl	0.61	0.30	84.22
Magnetite	NCS01-22	0.04	bdl	0.10	68.38	30.86	0.01	0.01	99.41
Magnetite	NCS01-25	0.05	bdl	0.04	68.36	30.83	bdl	bdl	99.31
Hematite	NCS01-26	0.14	bdl	0.22	100.36	bdl	bdl	bdl	100.75
Gt(Al)	NCS01-27	5.20	1.26	3.53	75.92	bdl	0.75	0.12	86.94
Magnetite	NCB08-31	0.11	bdl	0.05	68.06	31.00	0.01	0.01	99.24
Magnetite	NCB08-38	0.11	0.01	0.06	67.74	30.93	bdl	0.01	98.97
Hematite	NSB03-21	0.16	0.07	0.03	95.32	0.01	bdl	0.01	98.96
Magnetite	NSB03-26	0.02	0.03	0.17	68.46	30.98	bdl	bdl	99.7
Magnetite	NSB03-27	0.05	bdl	0.14	68.75	31.01	bdl	bdl	100.06

bdl – below detection limit. Gt(Al) – aluminium rich goethite (Al_2O_3 > 3 wt %)

Outcrop Samples

Two outcrop samples were selected for EPMA analysis not only because of their extreme positions; Out01 in the east and Out06 in the west, but mainly because of their mineralogy identified by XRD. Out01 is hematite-rich and contains very little quartz whist Out06 is quartz-rich. Out01 also has significant amounts of the Fe rich chlorite, chamosite. Magnetite is a minor mineral in the outcrop Out01 where it is mainly associated with hematite, goethite (Out01-58, 59) and to a lesser extent chamosite (Out01-55, 56, Table 7.8). Magnetite is a major mineral in Out06. Hematite has a similar association with magnetite and goethite. The grains of Out01 have cracks and are porous with goethite and chamosite being the infill minerals. The iron oxide minerals are relatively

liberated (not associated with any other mineral grains) in sample Out06 but few are associated with quartz (Out06-61, 62, Figure 7.8, Table 7.7 and Table 7.8).

Figure 7.9 Grab sample G01. It was initially thought to be re-crystallised hematite because of its glassy texture but found to contain significant amounts of goethite.

Saprolite / Laterite samples

Sample NCS01 contains all three Fe oxides minerals (NCS01-21, 22, 26, Table 7.7) and the main gangues in the saprolite / laterites i.e. quartz (NCS01-24), kaolinite (NCS01-23, 28, Table 7.7) and gibbsite. Goethite occurs in quantities comparable to hematite confirming the findings of the XRD that the deposit is mainly a martite – goethite deposit. Goethite in general occurs in all the saprolite / laterite samples to varying degrees. Chamosite also occurs in this sample as with most of the other samples occurring in the weathered profile. Chamosite should be classified as a gangue even though it is an iron rich chlorite mineral with around 30 % Fe. According to the whole rock geochemistry (Section 7.4), sample NES03 contained 37.64 % Fe which is as high as could be expected from the high grade magnetite itabirite, and as such might imply that chamosite should be considered as part of the ore mineral assemblage. However, as is seen in Chapter 8, the deleterious effect of chamosite outweighs its potential as an ore mineral.

Table 7.8 Representative compositions determined by EPMA for chamosite and other gangue minerals labelled on Figure 7.9.

Mineral	*ID*	*SiO_2 %*	*TiO_2 %*	*Al_2O_3 %*	*FeO %*	*Fe_2O_3 %*	*MnO %*	*MgO %*	*CaO %*	*Na2O %*	*K2O %*	*P_2O_5 %*	*SO_3 %*	*Cl %*	*F %*	*Total %*
Chamosite	Out01-55	17.73	bdl	13.19	41.13	20.52	bdl	bdl	0.09	bdl	bdl	0.10	bdl	bdl	bdl	93.64
Kaolinite	NCS01-23	21.78	0.83	18.33	13.61	bdl	bdl	0.04	bdl	bdl	0.05	0.17	0.13	bdl	bdl	54.94
Kaolinite	NCS01-28	33.17	0.10	25.68	11.2	bdl	bdl	0.05	bdl	bdl	bdl	0.11	0.18	bdl	bdl	70.49
Omphacite	NCB08-32	42.92	0.05	7.53	20.36	10.45	0.23	3.68	10.00	1.52	1.38	0.05	bdl	0.14	bdl	98.31
Biotite	NCB08-34	33.93	0.40	13.14	31.83	bdl	0.10	4.48	0.14	0.57	8.33	bdl	bdl	0.27	0.02	93.46
Grunerite	NCB08-35	51.02	0.02	0.23	39.10	bdl	0.83	6.33	0.66	0.07	bdl	bdl	bdl	0.02	bdl	98.28
Biotite	NCB08-36	32.77	0.45	12.57	35.29	bdl	0.11	5.05	0.08	0.14	7.15	0.01	bdl	0.27	0.02	94.06
Augite	NSB03-23	38.29	0.42	21.91	12.68	bdl	0.16	bdl	23.35	0.02	0.02	0.13	bdl	bdl	bdl	96.97
Apatite	NSB03-24	0.05	bdl	0.01	0.15	bdl	0.14	bdl	55.06	0.02	bdl	44.08	bdl	0.18	1.37	101.07
Apatite	NSB03-28	0.05	bdl	0.02	0.18	bdl	0.10	bdl	55.32	0.02	bdl	44.08	bdl	0.11	1.14	101.02
Augite	NSB03-29	39.18	bdl	22.24	12.07	bdl	0.34	dbl	22.27	0.05	0.01	0.14	bdl	bdl	bdl	96.30
Labradorite	NSB03-2A	58.20	bdl	26.10	0.33	bdl	bdl	bdl	8.71	6.53	0.19	0.03	bdl	bdl	bdl	100.09

bdl – below detection limit

BIF samples

Magnetite is the major iron oxide mineral in all but one (NSB03) of the BIF samples analysed. NSB03 has been assigned a weathering index of 3 meaning it is partly weathered which may account for the presence of hematite (NSB03-21). The magnetite grains for this size fraction are in general well liberated (Chapter 8). The dominant amphiboles in the east are calcic whilst in the centre they are iron magnesium amphiboles. Amphiboles were not encountered in the west and south. Micas are found in all but the south of the projects areas. They are mainly lath shaped and the micas in the centre are iron rich compared to those in the east and west. The pyroxenes found in the south are Ca rich varieties whilst those in the west and centre are Fe rich. Well-liberated apatite grains (i.e. they occur as grains with no association with other mineral grains) were found in the south (NSB03-24 and NSB03-28). Feldspars were only encountered in the south.

7.4 Whole rock geochemistry by XRF

The XRF data was analysed by looking at plots showing how the average composition varies between the different material types. Plots showing how Fe_2O_3 relates to the main gangue minerals of SiO_2 and Al_2O_3 were then made including plots of Fe_2O_3 against SiO_2, Fe_2O_3 against Al_2O_3 and Fe_2O_3 against SiO_2+Al_2O_3. The latter shows the relationship of iron and the aluminosilicates. A plot of SiO_2 against Al_2O_3 was also made which shows the relationship between quartz and Al oxide/hydroxide during the enrichment process which is accompanied by decrease in SiO_2 concentration.

7.4.1 Average XRF for the various material types

The average amount of iron varies in the sample types, decreasing in the order EM-WMI-TMI-HMI-LMI whilst SiO_2 increases as can be seen in Table 7.9 and Figure 7.10 whereas Table 7.10 shows the major element geochemistry (XRF) with depth through the enrichment profile of drill hole NKHC027. TiO_2 is in general low. The Al_2O_3 content decreases in the order LMI-WMI-TMI-EM-HMI and is mainly due to Al Ox(OH) such as gibbsite in the EM, WMI and TMI whilst

for HMI and LMI, it is hosted by aluminosilicates such as feldspar, pyroxene and amphibole. These aluminosilicates are also responsible for the relatively higher Mg, Ca, Na and K seen especially in the LMI but also the HMI compared to the EM, WMI and TMI material types. The highest Al percentage is recorded for the surficial material which is classified as WMI (Table 7.10) and is due to the presence of clays, Al Ox(OH), and/or goethite. Its corresponding P_2O_5 and LOI percentages are higher than those of the other material types indicating the presence of goethite which can have P and Al in its lattice. Phosphorus is highest in WMI followed by LMI, EM, TMI and HMI respectively. Whereas the P in the LMI, HMI and to a lesser extent TMI is due to apatite which occurs mainly as a minor mineral, that in the WMI and EM samples is mainly hosted in goethite. This result is not apparent from XRD and is made from the QEMSCAN® analyses (Chapter 8).

Table 7.9 Average major element geochemistry (XRF) for all material types.

Material Type	***EM***	***WMI***	***TMI***	***HMI***	***LMI***
SiO_2	2.57	8.65	28.13	45.48	58.1
TiO_2	0.06	0.12	0.35	0.17	0.24
Al_2O_3	2.29	4.12	6.79	0.84	7.96
$Fe_2O_3^*$	91.83	80.26	60.16	51.28	27.27
MnO	0.07	0.06	0.05	0.06	0.08
MgO	0.03	0.02	0.03	1.49	2.15
CaO	bdl	bdl	bdl	0.97	2.17
Na_2O	bdl	bdl	bdl	0.23	1.04
K_2O	bdl	bdl	0.04	0.17	1.35
P	0.09	0.23	0.05	0.03	0.13
S	0.01	0.03	0.02	0.39	0.1
LOI	2.93	6.91	5.03	bdl	0.17
Total	99.88	100.4	100.65	101.11	100.76

LOI=loss on ignition conducted at 1000 ^{0}C, bdl = below detection limit. * = total Fe as Fe_2O_3

7.4.2 Correlation of the major oxides

The saprolite/laterite samples analysed which fall within the categories of EM, WMI and TMI, are noted to in general have a higher Fe_2O_3 and hence Fe content compared to the BIF samples. This could be explained by the significant quantities of hematite and goethite present in them. Those with high LOI have been directly related to samples with high goethite content. These

samples also generally have lower SiO_2 content compared to the BIF samples but a higher Al_2O_3 content. Phosphorus levels of some of the samples, especially within the EM and WMI material types, are higher than the generally accepted maximum level of between 0.05 wt % and 0.08 wt % whilst Al levels are above the required < 2.5 wt %. Silica in the BIF, as expected, are well over the 3 wt % threshold which implies they will have to be processed to meet the standard requirements of customers (Chapter 2).

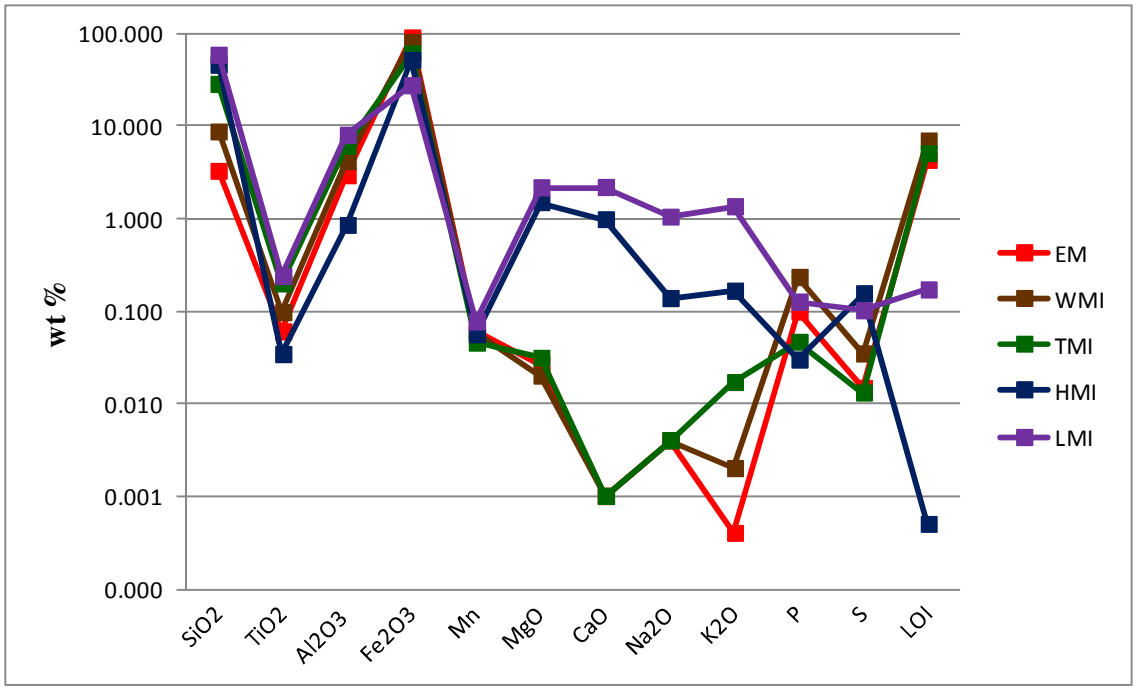

Figure 7.10 Plot of average chemical compositions for all material types.

Fe_2O_3 has a strong negative correlation with SiO_2 (Figure 7.11a) whilst Fe_2O_3 shows no correlation with Al_2O_3 (Figure 7.11b). An explanation for this is that most of the SiO_2 is present as a discrete phase, quartz, whereas Al_2O_3 may be in gibbsite and kaolinite and also substituting into the iron oxides (goethite in particular). The weak negative correlation between SiO_2 and Al_2O_3 (Figure 7.11c) suggests that they are not only related in aluminosilicate phases such as kaolinite but also exist in other phases. A plot of SiO_2+Al_2O_3 against Fe_2O_3 (Figure 7.11d) shows a very strong negative correlation which is an indication of the presence of aluminosilicate minerals: micas, pyroxenes chamosite and kaolinite. This is so because the aluminosilicates are mainly found in the fresh magnetite BIF which have relatively low Fe wt % compared to the weathered material i.e. an inverse relationship between Fe wt % and aluminosilicate concentrations.

Table 7.10 Major element geochemistry (XRF) with depth through the enrichment profile of drill hole NKHC027.

Depth (m)	Material Type	SiO_2	TiO_2	Al_2O_3	$Fe_2O_3^*$	Mn	MgO	CaO	Na_2O	K_2O	S	P	LOI	Total
3.60	WMI	2.12	0.18	5.59	83.37	0.04	0.03	0.01	0.06	0.01	0.02	0.18	7.50	99.12
8.10	WMI	0.77	0.09	6.06	86.61	0.05	bdl	bdl	bdl	bdl	0.02	0.18	7.22	101.02
12.60	EM	0.44	0.06	3.20	91.68	0.09	bdl	bdl	bdl	bdl	bdl	0.11	4.76	100.36
17.10	EM	0.51	0.03	2.01	92.74	0.08	bdl	bdl	bdl	bdl	bdl	0.18	5.43	101.00
27.60	EM	0.78	0.02	1.27	94.80	0.09	bdl	bdl	bdl	bdl	bdl	0.14	3.32	100.44
30.60	EM	0.44	0.01	0.50	95.30	0.11	bdl	bdl	bdl	bdl	bdl	0.08	3.06	99.53
39.60	EM	1.27	0.02	0.82	97.51	0.12	bdl	bdl	bdl	bdl	bdl	0.05	1.46	101.29
41.60	EM	2.19	0.01	0.63	96.22	0.15	bdl	bdl	bdl	bdl	0.01	0.04	1.44	100.73
46.10	EM	3.46	0.01	0.87	93.26	0.10	bdl	bdl	bdl	bdl	bdl	0.04	1.72	99.49
48.10	EM	8.76	0.02	0.46	89.68	0.09	bdl	bdl	bdl	bdl	bdl	0.03	1.46	100.53
50.10	WMI	22.52	0.01	0.55	74.66	0.08	bdl	bdl	bdl	bdl	bdl	0.03	1.38	99.25
54.10	TMI	29.54	0.03	1.14	67.57	0.03	bdl	bdl	bdl	bdl	bdl	0.02	0.72	99.06
56.10	TMI	42.43	0.06	2.33	52.68	0.02	0.01	bdl	bdl	bdl	bdl	0.03	1.98	99.54
58.10	TMI	38.77	0.04	1.57	57.32	0.02	0.01	bdl	bdl	bdl	bdl	0.03	0.92	98.69
60.10	TMI	45.98	0.04	1.57	50.47	0.04	bdl	bdl	bdl	bdl	bdl	0.02	1.02	99.15
62.10	TMI	34.59	0.02	1.12	62.64	0.02	bdl	bdl	bdl	bdl	bdl	0.05	1.16	99.62
64.10	WMI	27.98	bdl	0.26	71.63	0.08	0.02	bdl	bdl	bdl	bdl	0.03	0.90	100.92
66.10	TMI	35.73	bdl	0.30	63.20	0.04	0.03	bdl	bdl	bdl	bdl	0.04	0.30	99.65
68.10	HMI	41.74	bdl	0.14	55.35	0.04	1.33	0.85	bdl	0.03	bdl	0.03	bdl	99.52
70.10	HMI	42.19	bdl	0.13	54.83	0.05	1.79	1.27	0.08	0.03	bdl	0.03	bdl	100.41
70.10	HMI	42.22	bdl	0.15	54.47	0.05	1.75	1.22	0.06	0.04	bdl	0.04	bdl	100.01
72.60	HMI	41.95	bdl	0.10	53.76	0.05	1.76	1.09	0.09	0.03	bdl	0.03	bdl	98.87

bdl – below detection limit *= total Fe as Fe_2O_3

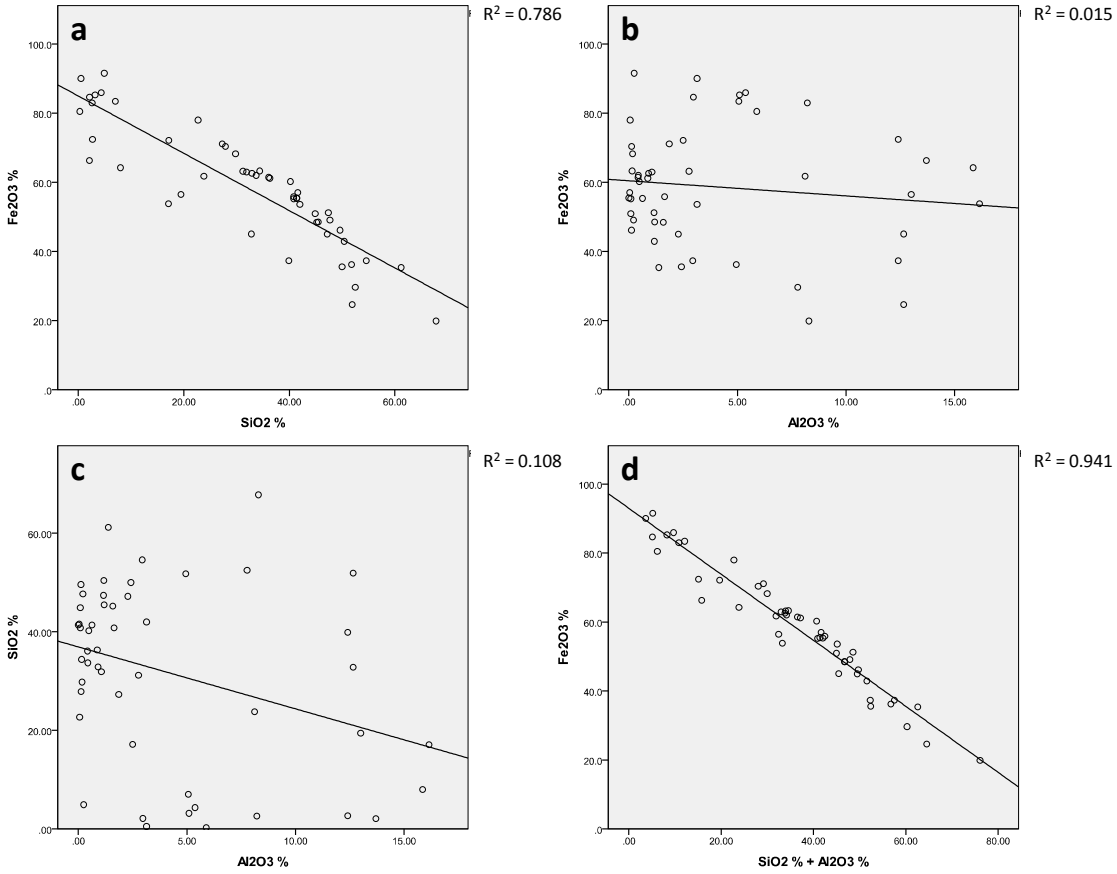

Figure 7.11 Correlation of the main oxides of Fe_2O_3, SiO_2, Al_2O_3. (a) Plot of Fe_2O_3 against SiO_2 showing strong negative correlation. (b) Plot of Fe_2O_3 against Al_2O_3 showing no correlation. (c) Plot of SiO_2 against Al_2O_3 showing weak negative correlation. (d) Plot of Fe_2O_3 against SiO_2+Al_2O_3 showing very strong negative correlation.

7.5 Conclusions

The Nkout deposits consist of iron oxides with no evidence of iron carbonate minerals. Iron sulphides are present mainly in the form of pyrite. Quartz is the major gangue mineral in the magnetite BIF and silicates such as amphiboles, mica and feldspars are also present. Phosphorus is hosted by apatite, which occurs as liberated grains likely to be easy to remove by grinding and further processing. In general, it is predicted that it will be relatively straight forward to process and upgrade the BIF deposit to form pellets. However in Out06, the iron oxides are associated with quartz in such a way that liberating the hematite in particular which is found associated with goethite and quartz (Out06-61 and Out 06-62, Figure 7.8) will involve grinding to fine size fractions (e.g. -63/+45 µm) which involves high energy consumption.

The BIF is the protore of the saprolite formed as a consequence of weathering. The bulk of the weathered material which was initially considered to be a hematite deposit (Suh et al., 2009) has been shown to actually be a martite – goethite ore. The main iron minerals in the enrichment profile are hence hematite, magnetite and goethite. Hematite occurs mainly in the form of martite. Goethite and hematite which are major minerals in the study areas are known to acts as efficient “sinks” for a wide range of minor and trace elements with a number of metal cations replacing Fe.

There are many types of goethite found in iron ore deposits including: 1) goethite pseudomorphs after gangue minerals such as quartz, carbonates and silicates 2) ochreous goethite or limonite which is soft to medium hard and microporous, yellow in colour with a chalky appearance and 3) vitreous goethite which is black to dark brown in colour with a conchoidal fracture (Ramanaidou et al., 2008). There is a shift towards smaller d-spacings of the diffraction peaks of natural goethite and hematite compared to pure ones. This shift is an indication of the presence of Al within their structures (Ramanaidu et al., 2008).

The major gangue minerals in the EM, WMI and TMI are quartz and clay minerals such as gibbsite and kaolinite. The east in particular has significant amounts of chamosite. A major potential problem in upgrading the martite goethite ore is getting rid of Al that EPMA has shown to be associated with goethite.

Chapter 8

Quantitative Mineralogy using QEMSCAN®

8.1 Introduction

Automated mineralogy is defined as "the unattended, repeatable measurement of inorganic samples to gather large datasets of texture and mineralogy" (Menzies, 2008). Quantitative process mineralogy is currently done by two main systems; quantitative X-ray diffraction using the Rietveld refinement and automated SEM based techniques such as Quantitative Evaluation of Minerals using a SEM (QEMSCAN®) and Mineral Liberation Analyser (MLA).

QEM*SEM was developed by Dr. Alan Reid of the Commonwealth Scientific and Industrial Research Organisation (CSIRO) in the late 1970's. In 1985, the system was sold commercially by CSIRO. In the 1990s, QEM*SEM was improved upon including the utilisation of Microsoft Windows which led to the production of the first QEMSCAN® system. QEMSCAN® is one of the earliest quantitative mineralogical assesment systems (Gottlieb et al., 2000). To date, it is the most advanced technology in mineralogical analysis. In the late 1990's to 2008, QEMSCAN® systems were produced by Intellection Pty Ltd in Australia and MLA systems by JKTech Pty Ltd and FEI. In December 2008, FEI Company acquired Intellection Pty Ltd.

QEMSCAN® compares acquired EDS X-ray spectra to a database of spectra and this facilitates mineral/phase identification. The database is referred to as the Species Identification Protocol (SIP) and is developed to suit the expected minerals or phases. QEMSCAN® is not routinely appropriate for the analysis of organic material, does not give an accurate chemical analysis (like an XRF or electron microprobe), nor does it see colour.

A huge part of the variability that a deposit may show will be variability of its mineralogy across the deposit and as such quantitative mineralogy lends itself to the research environment because it adds the capability to assess datasets derived from mineralogical relationships. The mineralogy and particle sizes in relation to degree of liberation, micro-textures and mineral associations at the Nkout and Putu deposits

have been studied. These are the key factors responsible for mineral processing problems during beneficiation of ores in the mining industry and provide guides in predicting process plant performance and product quality from ore reserves through to shipped products (Gottlieb et al., 2000). It therefore allows geologists, engineers and metallurgists to target improvements in grade, recovery and throughput.

A major problem with using QEMSCAN® in iron ore characterisation has been distinguishing the key iron oxides (magnetite, hematite and goethite) from each other because they have similar chemical composition and backscattered electron signals. It is common place for all of them to be classified as a group i.e. iron oxides instead of being identified individually. In addition to the characterisation of the deposits studied, this study aims to develop and validate methodologies for separation of these minerals using differences in the intensity of their back scattered electron and their X-ray spectra. This is important because the magnetite to hematite ratio in a deposit determines routes of processing and hence operational costs.

The Nkout and Putu samples were studied using optical microscopy, qualitative XRD, SEM and EPMA and in so doing, and based on ground knowledge of the study areas, the minerals to be included in the SIP were selected. The same SIP was used for both deposits and they were run under the same experimental conditions. Three size fractions of 51 samples from Nkout and 7 samples from Putu were analysed. These samples were selected because they were considered to be mineralized i.e. contained Fe wt % ≥ 15 %. Host rock samples were not analysed. The QEMSCAN® analysis was done in collaboration with Dr. Gavyn Rollinson who supported the whole process from sample preparation, polishing stages, SIP development, running the samples on the equipment and exporting the data for interpretation.

8.2 Instrumentation and measurement modes

The instrument used for this study is a QEMSCAN® 4300 which incoporates a Zeiss EVO 50 SEM platform with 4 light element Bruker silicon drift droplet (SDD) X-ray detectors which have detection limits to about 1 – 3 wt % (Rollinson, 2011). The maximum feature detection limit is usually set at 1 µm but could be as low as 0.2 µm (Rollinson et al., 2011). Its operation is similar to those of other SEM based

techniques which in this case uses a tungsten filament. See Chapman (1986) for more details on the SEM operation.

QEMSCAN® identifies mineral particles using image analysis of BSE maps. Within each defined area, X-ray spectra are emitted from the sample as it is scanned by an electron beam. The EDS spectra containing X-rays characteristic of all the elements excited are compared to the minerals in the SIP allowing mineral identifications (rather than the element identifications usually done by SEM/EDS or EPMA analysis). The X-ray spectra are usually limited to 1000 counts but can be varied. For routine work, this offers a compromise between measurement time and accuracy of mineral identification. A limitation of this approach is that minerals of similar chemical composition, in this case magnetite (Fe_3O_4), hematite (Fe_2O_3), and goethite (FeO(OH)), cannot be distinguished very effectively, or even not at all, using low count X-ray spectra (Maddren et al., 2007).

QEMSCAN® can be operated in different measurement modes; particle mineral analysis (PMA), specific/trace mineral search (S/TMS), bulk mineral analysis (BMA) and fieldscan images, (Pirrie et al., 2004, 2009, Pirrie and Rollinson, 2011). The -63/+45 µm and -125/+90 µm fractions were analysed using the PMA mode whilst the -250/+180 µm was analysed using the fieldscan mode. PMA is the optimal mode for geometallurgy work which includes particle based automated mineralogy. Using PMA mode, particles in a sample are divided into grids of pixels each with an analysis point. The result is a particle map showing the mineral compositions of the individual points of analysis corresponding to individual pixels. Fieldscans are used for textural and modal analysis. The sample field is broken down into pixels each with an analysis point. After analysis, the pixels are stitched together to create a map of the original sample field. The fieldscan images were particularly suitable for effective comparison of the QEMSCAN® results with other techniques such as optical microscopy.

The QEMSCAN® was run at an accelerating voltage of 25 kV and a beam current of 5 nA. The average number of particles analysed per sample was 6636 with a standard deviation of 2629. The average number of X-ray analysis points per sample was 1,328,826 with a standard deviation of 613,168. The X-ray pixel spacing for the

PMA analysis was 2 µm and 10 µm for the fieldscan analysis. The average measurement duration per sample was 2 hours 57 mins. The iMeasure v.4.2 software was used for data acquisition and iDiscover v. 4.2 was used for the spectral interpretation and data processing. The data from each analysis point was automatically compared with the SIP database of minerals and mineral phase spectra to identify the minerals present.

According to Donskoi et al. (2011), edge effects may be "caused by surface penetration of the electron beam at the edges of particles and pores such that the excitation volume is not fully within the same phase". Edge effects results in areas of misidentification which can result in biased results. These effects can be more pronounced in small particles and results in the edge of particles having a different mineral to that present within the main body of the particle. Edge effects change across particle boundaries and at times could be absent. Donskoi et al. (2011) also suggested that edge effect variations depend on the inclination of the particle surface under the surface of the epoxy resin. Edge effects were reduced by high quality polishing of the samples and post-processing filters in the iDiscover software. For details on the basic QEMSCAN® methodology and analytical modes see Gottlieb et al. (2000) and Pirrie et al. (2004).

8.2.1 Accuracy of QEMSCAN® analysis

Ideally the accuracy of the QEMSCAN® analysis should be tested using quantitative XRD, as is the case in the work of Ayling et al. (2012). They acknowledge the fact that there will never be a 100 % agreement between the two techniques because of the differences in the analytical procedures. Whereas QEMSCAN® in this research analysed sized fractions on the surface of moulds, XRD in general is used to analyse bulk crushed samples. Notwithstanding these differences, there should be a broad agreement between the two methods as can be seen in Table 8.1 from Ayling et al. (2012). More on the difference between the two techniques can be found on Table 8.11. Qualitative rather than quantitative XRD was done in this research and as such we can only compare the minerals identified rather than their abundances (wt %).

Table 8.1 Comparison of QEMSCAN® and XRD for 6 samples (Ayling et al., 2012). XRD values reflect mass fractions as percentages; QEMSCAN® values reflect percentage of scan area.

	GEO-N2 3469 ft		***GEO-N2 3763 ft***		***GEO-N2 4348 ft***		***BCH-3 3902 ft***		***BCH-3 4253 ft***		***BCH-3 4711 ft***	
Mineral Name	***XRD***	***QEMSCAN***	***XRD***	***QEMSCAN***	***XRD***	***QEMSCAN***	***XRD***	***QEMSCAN***	***XRD***	***QEMSCAN***	***XRD***	***QEMSCAN***
Hematite	0.9	1.5	2.5	-	-	-	-	-	2	0.3	-	-
Quartz	-	0.6	3.6	4	17	14	9.5	2.5	37	23	69	64
Micas	-	1.2	-	-	-	1.7	5.3	5.8	12	10	21	11
Calcite	-	-	-	-	4	2.5	14	12	28	29	-	-
Alkali Feldspar	3.3	3.3	3	8.6	-	1	6.9	6.3	-	1.6	5.3	6.5
Plagioclase	59	54	66	56	26	24	43	46	4.3	2.9	-	1.7
Smectites	23	29	8	11.5	-	25	-	14	-	17	-	1.4
Illite	-	0.1	-	-	29	15	1.5	1.1	-	-	-	0.3
Pyroxene	13	4.2	17	7.7	-	-	3.7	-	-	-	-	-
Zeolites	-	-	-	-	-	2.4	-	2.3	-	2.1	-	7.4
Sulphate	-	-	-	-	3.5	3	-	-	-	-	-	-
Oxides	-	-	-	2.2	3.7	0.6	2.2	-	-	0.3	-	-
Dolomite	-	-	0.1	-	-	-	-	0.34	-	2	-	-
Sulphides	-	-	-	-	-	-	-	-	-	-	2.3	1.9
Other	-	6.1	-	6.2	-	8.8	-	9.4	-	5.5	-	4.7

Table 8.2 gives the 6 most abundant minerals or mineral phases identified for 12 samples using the QEMSCAN® and these are compared to those identified from the XRD and EPMA analysis of the same samples.

Table 8.2 Comparison of QEMSCAN®, EPMA and XRD for 12 samples analysed in this research. (6 from Nkout and 6 from Putu).

Sample	***Method***	***Minerals Identified***					
NSS02	QEM	Gt	Mag	Hem	Chm	Qtz	Kln
	EPMA	Gt	-	Hem	Chm	Qtz	-
	XRD	Gt	Mag	Hem	-	Qtz	Kln
NES01	QEM	Mag	Gt	Hem	Chm	Al Ox(OH)	-
	EPMA	Mag	Gt	Hem	Chm	Al Ox(OH)	-
	XRD	-	Gt	Hem	Chm	Al Ox(OH)	Kln
NCS01	QEM	Mag	Qtz	Chm	Gt	Kln	Hem
	EPMA	Mag	Qtz	Chm	Gt	-	Hem
	XRD	Mag	Qtz	-	Gt	Kln	Hem
NWS03	QEM	Mag	Gt	Qtz	Hem	Chm	Kln
	EPMA	Mag	Gt	Qtz	Hem	-	Kln
	XRD	-	Gt	Qtz	Hem	-	Kln
NWB01	QEM	Qtz	Alm	Mag	Bt	Pl Fsp	Gt
	EPMA	Qtz	-	Mag	Mca	Pl Fsp	-
	XRD	Qtz	Alm	Mag	Ann	Ab	-
Out06	QEM	Mag	Qtz	Gt	Hem	Fe Mg Sil	Chm
	EPMA	-	Qtz	Gt	Hem	-	-
	XRD	-	Qtz	Gt	Hem	-	-
LB01	QEM	Mag	Qtz	Gt	Ca Mg Fe Sil	Hem	Bt
	EPMA	Mag	Qtz	-	Ca Amp/Pyx	-	Mca
	XRD	Mag	Qtz	-	Tr	-	Phl
LB02	QEM	Qtz	Mag	Ca Mg Fe Sil	Gt	Bt	Pl Fsp
	EPMA	Qtz	Mag	-	Gt	Mca,	-
	XRD	Qtz	Mag	Hbl	-	Phl	-
LB03	QEM	Mag	Gt	Ca Mg Fe Sil	Fe Mg Sil	Ca Fe Al Sil	Qtz
	EPMA	Mag	-	Ca Am/Px	-	-	Qtz
	XRD	Mag	-	Mg Hbl	-	-	Qtz
LB05	QEM	Mag	Gt	Hem	Qtz	Fe Mg Sil	Ca Mg Sil
	EPMA	Mag	-	-	Qtz	-	Ca Ap/Px
	XRD	Mag	-	Hem	Qtz	-	-
LB06	QEM	Hem	Gt	Mag	Chm	Qtz	Fe Mag Sil
	EPMA	Hem	Gt	-	Chm	Qtz,	Px
	XRD	Hem	Gt	Mag	-	Qtz	-
LB07	QEM	Hem	Gt	Adr	Mag	Qtz	Ca Mg Fe Sil
	EPMA	Hem	Gt	Adr	-	Qtz	Ca Am / Px
	XRD	Hem	-	Adr	-	Qtz	-

Ab – Albite, Adr – andradite, Alm – almandine, Al Ox(OH) – Al oxyhyroxide, Bt – biotite, Chm – chamosite, Gt – goethite, Hbl – hornblende, Hem – hematite, Kln – kaolinite, Mag – magnetite, Mca – mica, Phl – phlogopite, Pl Fsp – plagioclase, Px – pyroxene, QEM – QEMSCAN®, Sil – silicate, Tr – Tremolite, Qtz – quartz

The minerals identified after recalculation of the EPMA oxides should also be in agreement with those identified using the QEMSCAN®. Six of the samples are from Nkout and the other 6 from Putu. In most cases at least three of the minerals from the QEMSCAN® were also identified using both the XRD and EPMA. In some instances some minerals that were not identified using XRD were identified using EPMA and vice versa. In general there is good agreement between the different techniques. The precision of the QEMSCAN® was 99 % in so far as the QEMSCAN® "others" group was ≤ 1 wt %, and therefore it was possible to give a mineral name to 99 % of the mineral phases present in the samples.

8.3 Sample preparation

Specialist sample preparation routines are required to prepare materials for mineralogical analysis using techniques such as QEMSCAN® (Stanley and Laflamme, 1998; Nentwich and Yole, 1991). For this study, polished epoxy resin blocks were produced.

The +180/-250 µm, +90/-125 µm, +45/-63 µm size fractions were selected for QEMSCAN® analysis as these are the assumed main size fractions for optimum liberation. Since the samples comprise of different minerals with different densities and sizes, it was essential to have a random sample to avoid bias. Random error depends on the size of the largest particles in the sampled lot and on the mass of the sample (Henderson, 1995). The larger the range in particle size and the mass of the sample, the lower will be the random error. The mass of the samples used was between 0.8 g – 1.5 g and a rotary microriffler was used to ensure they were randomly collected. The samples were placed into a hopper which when vibrating converts the sample to a continuous flow stream. Eight tubes attached to a rotary devise were used to collect the sub samples. These tubes rotate at a constant speed below the hopper and collects material randomly as they rotate yielding a constant volume increment for each subsample (Henderson, 1995). The weight of samples in each tube was calculated based on the original weight of the samples and this value determined the number of tubes whose samples are placed back into the hopper for further riffling to achieve the targeted weight range.

Five main steps were followed during the epoxy resin block preparation. These are logging the sample into the database, epofixing the sample (resin stage), labelling the sample blocks (30 mm diameter), topping up the mould with araldite epoxy resin and removing the sample from the mould. Polishing the samples was done using a water based process in which the first grinding stage uses water as lubricant and for cooling and the second and third grinding stages use diamond solutions and lubricants which also contains water. The polishing machines used were three Struers Tegrapol-21 base units with Struers Tegraforce 5 head units. Two of the machines were connected to Struers Tegradoser 5 units for computer controlled lubricant and diamond solution delivery. Specific cloths are assigned to the machines to prevent contamination and maintain a smooth and efficient process from the coarse to fine grinding stages. The quality of the polishing was checked by examining the blocks under reflected light microscope. The resin block preparation and polishing steps have been set out by in house CSM operating procedures (Rollinson, 2008i, 2008ii).

In order for the sample surfaces to be made electrically conductive to prevent accumulation of charges at the surface, the samples were coated with an ultrathin layer of graphite (carbon) by high vacuum evaporation (Chapter 5).

8.4 Method development

8.4.1 BSE instability

The chemistry of the different iron oxides and hydro-oxides is similar and hence separation using QEMSCAN® is based on subtle differences in the intensity of their BSE signal. The BSE values are based on the average atomic number of the different iron oxide minerals. Table 8.3 gives the main iron oxide minerals along with their formula, weight percent in terms of chemistry and the average atomic number of Fe in the formula.

BSE signal is however known to vary due to external factors resulting in overlaps in the identification of the iron oxides. This fact is illustrated in Figure 8.1 (Benedictus and Horsch, 2008), which shows variation of the mass percentage of magnetite, hematite and goethite with time.

The following factors can directly result in drifts in this position; a) polish quality, b) carbon coating quality, c) vacuum and beam stability, d) varying room temperature.

Table 8.3 Formula, weight percent by chemistry and average atomic number based on formula of the main iron oxide minerals (Benedictus and Horsch, 2008).

Mineral	*Formula*	*Chemistry (wt %)*	*Average Atomic No.*
Fe metal	Fe	Fe: 100.00	26.00
Wustite	FeO	Fe: 77.73; O: 22.27	17.00
Magnetite	Fe_3O_4	Fe: 72.73; O: 27.64	15.71
Hematite	Fe_2O_3	Fe: 69.94; O: 30.06	15.20
Goethite	FeO(OH)	Fe: 62.85; O: 36.01; H: 1.13	10.75

a) Good polish quality was achieved by a diamond solution grinding media and following procedures strictly as grinding moves from coarse grind to fine grind. Quality control (QC) checks after the polishing was done by examining the polished block under a microscope, and looks for scratches, plucking, uneven polishing and any other issues.

b) The correct amount of carbon coat should be applied to the blocks. The optimum thickness is 25 nm and this is indicated by a peacock blue colour on a brass stub coated with the samples. The height of the stub should be roughly equal to those of the samples and it should be thoroughly cleaned in between samples. In certain situations, when this peacock blue colouration was not achieved, the carbon coat on the sample block was removed by fine polishing and the process repeated.

c) QEMSCAN® analysis is usually started when vacuum in the sample chamber is in the range of $3.0^{-0.005}$ Torr. For the iron oxides, it was observed that a stable vacuum was achieved at $5.0^{-0.006}$ Torr and this takes about three hours to achieve. This amount of down time is not usually economic for commercial companies but leads to beam stability via a better vacuum and thus better analysis.

d) Constant room temperature was achieved by a good, stable and reliable air conditioning system. This is important as the boundaries between the different

oxides vary with changes in temperature. Temperature was maintained between 19 to 21 ^{o}C for the analysis in this study.

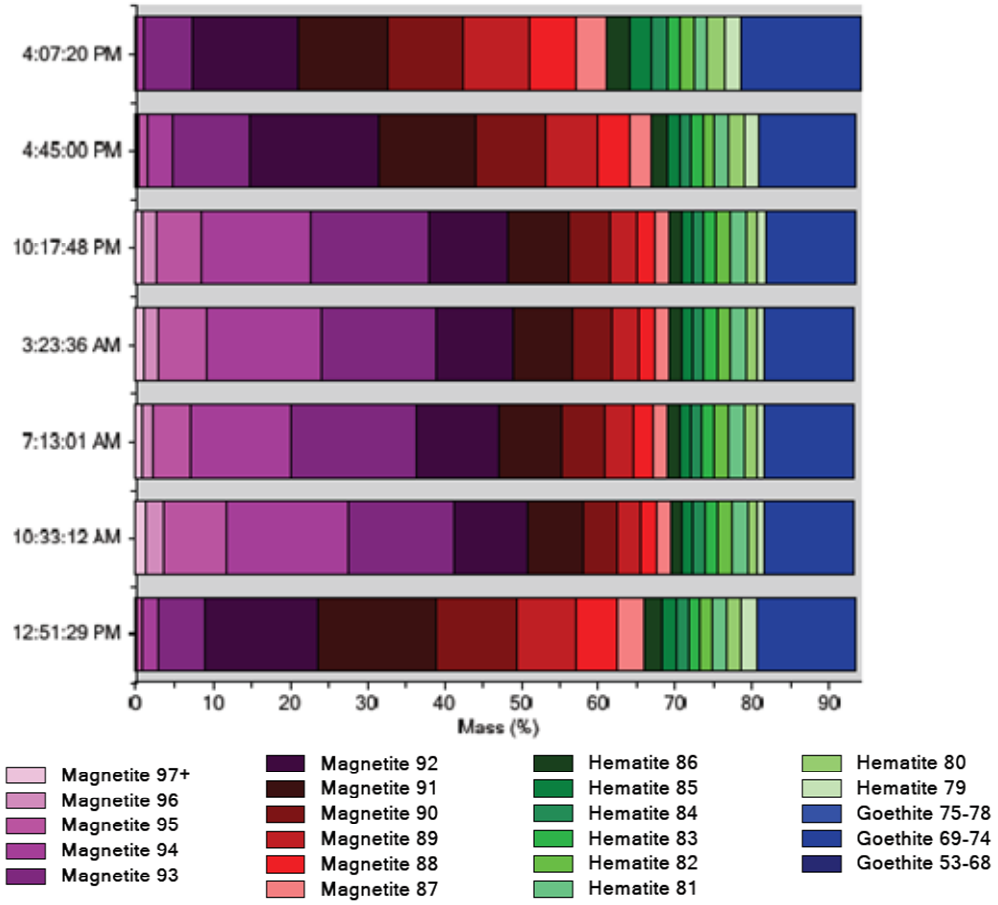

Figure 8.1 Effect of inherent SEM BSE instability on phase proportions over time (Benedictus and Horsch, 2008).

8.4.2 SIP database development

Optimum mineralogical characterisation of samples can only be done by the application of an appropriate mineral list which will be used by the QEMSCAN® system. This list must be verified using appropriate standards and customised to suite the aims of the analysis. The minerals allowed in a particular SIP entry can be based on ideal empirical formulae for their mineralogy or as was the case used in this research for magnetite and hematite, the analysis of standards. The QEMSCAN® operator limits the minerals that can be present in a particular SIP entry by selecting which elements are present in a particular entry. It is good to limit the number of elements in a SIP entry as these limits the number of non-unique interpretations of the X-ray spectra; QEMSCAN® has 72

elements available to choose from (Ayling et al., 2012). After this stage the equipment then looks at the mineral definitions that were input into the QEMSCAN® and includes wt % of elements, ratios of elements and or BSE differences. The “others” group results from the lack of mineral definitions in the SIP that are consistent with the measured spectra. They could also be due to boundary phases between mineral grains where the spectra for the two mineral grains have a contribution to the resulting spectrum which may not be consistent with the mineral definitions made. The iDiscover software has tools such as the boundary-phase pre-processor or the measurement de-bugger to help with boundary phase processing. Three important factors should be considered when developing a mineral list:

1) The possible minerals present in the samples or deposits.
2) The minerals that are important and directly impact the project under investigation. For example it should not only include the valuable minerals present but also the gangue minerals.
3) The detail to which the list should be developed, for e.g. is it sufficient to group calcite, dolomite and ankerite as carbonates, or group hematite, magnetite and goethite as iron oxides or rutile, titanite and ilmenite as titanium oxides or are the individual minerals important in their own right.

QEMSCAN® is supplied with its own “LCU5” SIP file which contains common minerals. This file provides a useful starting point but has to be modified to suit particular kinds of ore types. Modification can occur at the SIP level or SIP entries could be combined to form a primary list which can themselves be combined to form a secondary list depending on the required level of detail necessary for the investigation. Initial mineralogical knowledge of the samples under investigation were obtained from knowledge of the study area and using analytical techniques such as XRD, SEM/EDS, EPMA and optical microscopy (Table 8.4). These techniques can also be used to validate the QEMSCAN® results and aid their interpretation.

Some of the pertinent issues faced when developing the SIP for this research included:

Table 8.4 Mineral categories, abbreviations and descriptions as used in this research.

Mineral Category	***Mineral Description***
Andradite (Adr)	Any phase with Fe,Ca,Al,Si.
Al oxy-hydroxide (Al Ox(OH))	Any phase with Al, O. May include gibbsite and any other mineral with Al, O, or Al OH
Almandine (Alm)	Any phase with Fe, Al, Si, possibly trace Mg,Mn. (see SIP development for difference with chamosite)
Apatite (Ap)	Any phase with Ca P, O
Biotite (Bt)	Biotite and phlogopite mica, may include other mica
Ca Fe Al Silicate	Any Ca Fe Al silicates such as epidote and zoisite, may include ferrohornblende and hedenbergite
Ca Mg Fe Silicate	Any phase with Ca, Mg ,Fe, Si, (with or without Fe & Al) such as hornblende, diopside, tremolite, augite, actinolite, maybe amphiboles and pyroxenes
Calcite (Cal)	Includes calcite (Ca,O,C), with minor dolomite (Ca,Mg,C,O) and ankerite (Fe,Ca,Mg,O)
Chalcopyrite (Ccp)	Includes any phase with Cu,Fe,S such as chalcopyrite. May include trace amounts of bornite and Cu sulphides (chalcocite/covellite)
Chamosite (Chm)	Any phase with Fe, Al, Si, possibly low Mg
Chlorite (Chl)	Any phase with Fe, Al, Si, and Fe, Al, Mg, Si, such as chlorite / clinochlore, nontronite
Fe Mg Silicates	Any phase with Fe, Mg, Si such as the serpentine group (antigorite) and minnesotaite
Goethite (Al) (Gt(Al))	Any phase with Fe, O, and low Al (> 3 wt%). May contain trace Si, Al, P and Mn, and OH. Separated from hematite and magnetite by BSE - goethite BSE is lower due to hydration.
Goethite (P) (Gt(P))	Any phase with Fe,O, and low P(> 3 wt%). May contain trace Si, Al, Mn, and OH. Separated from hematite and magnetite by BSE - goethite BSE is lower due to hydration
Goethite /Limonite (Gt/Lm)	Any phase with Fe, O. May contain trace Si, Al, P and Mn, and OH. Separated from hematite and magnetite by BSE - Goethite BSE is lower due to hydration.
Hematite (Hem)	Any phase with Fe, O, adjusted to a hematite internal standard based on BSE and verified with XRD.
Ilmenite (Ilm)	Any phase with Fe, Ti, O (ilmentite). Also, includes Fe pyrophanite (Mn, Ti, Fe, O)
Kaolinite (Kln)	Includes kaolinite / halloysite / dickite and any other Al silicates such as kyanite / sillimanite / andalusite. Maybe trace topaz.
K-Feldspar (K-Fsp)	K-feldspars: any phase with K, Al, Si, O
Magnetite (Mag)	Any phase with Fe, O, adjusted to a magnetite internal standard based on BSE & verified with XRD.
Mn Phases	Includes Mn silicates (pyroxferroite), Mn oxides (pyrolusite), Mn Fe oxides and pyrophanite (Mn,Ti,O)
Muscovite/Illite (Ms/ill)	muscovite (K, Al, Si, O)
Plagioclase Feldspar (Pl Fsp)	Plagioclase feldspars: phases with Na, Al, Si, O to Ca, Al, Si, O
Pyrite (Py)	Includes pyrite/marcasite, boundary effects, minor pyrrhotite and trace jarosite
Quartz (Qtz)	Quartz and other silica minerals (Si, O)
REE phase	Includes mainly xenotime with trace monazite.
Rutile (Rt)	Any phase with Ti, O
Talc (Tlc)	Any phase with Mg,Si,O
Ti-Magnetite (Ti-Mag)	Any phase Fe, O, low Ti (0.1 – 5 wt %)
Titanite (Ttn)	Any phase with Ca, Ti, Si, O and minor Al, F, Fe.
Zircon (Zrn)	Any phase with Zr, Si, O
Others	Any other mineral not included above, edge effects. Includes trace sphalerite, galena, cassiterite, gypsum, cobaltite and contamination from grinding

Note: Abbreviations which are given in brackets next to the names of the mineral categories are from recommendations by Siivola and Schmid (2007) (International Union of Geological Sciences (IUGS) Sub-commission on the Systematics of Metamorphic Rocks).

a) Separation of magnetite and hematite,
b) Distinguishing compositional variants in the goethite group,
c) Investigating the Ca Fe silicate bucket i.e. developing the andradite group,
d) Separation of chamosite from other chlorites and almandine.

8.4.2.1 Separation of magnetite and hematite

Magnetite and hematite differ by about 3 wt % in their Fe content, which is not enough to allow them to be distinguished using the standard 1000 count X-ray spectra acquired during the QEMSCAN® analysis (Andersen et al., 2009, Rollinson et al., 2011).

From the EPMA analysis, it was noticed that minor element concentrations are in general higher in hematite than in magnetite. In particular Al_2O_3 occurs up to 1.57 wt% in the WMI, up to 3.00 wt% in TMI, up to 0.36 wt% in HMI and 0.25% in the LMI. Even though the dominant composition is Fe_2O_3 in TMI, minor amounts of FeO occur up to 1.38 wt% in the WMI, up to 0.78 wt% in TMI and 0.33 wt% in the HMI. However, there is no consistent difference that permits differentiation of the two minerals based on chemistry.

The most useful characteristic to enable separation of hematite and magnetite was found to be the small difference in the BSE signal (Figure 8.2). The BSE range is specific to the QEMSCAN® system used and will vary between different QEMSCAN® systems (Tonžetić and Dippenaar, 2011, Andersen et al., 2009). The system used was calibrated to quartz at the lower end (42) and gold at the higher end (232) of the grey scale.

Grains of well-characterised magnetite and hematite were set into a resin block and polished to form a standard block that could be used to set up and test the BSE range for each mineral. These were checked by XRD. This standard was used as a quality control before each QEMSCAN® measurement. The magnetite was found to range from 89 to 100 and hematite from 80 to 88 on this BSE scale; goethite was less than 80 and includes limonites at the lower range (about 50 or less). The limitations of this distinguishing technique include edge

effects, which cause the BSE signal to vary, if for example it is a mixture of the mineral with resin or neighbouring minerals, and changes in BSE brightness during the measurement process caused by variations in the chamber vacuum or room temperature change (Benedictus and Horsch, 2008). Edge effects were reduced by high quality polishing of the samples and post-processing filters in the iDiscover software. Temperature effects were reduced by stable air conditioning in the laboratory and the vacuum affects reduced by allowing the chamber vacuum to settle for a few hours after loading the sample so that a stable level was achieved before the measurement began (typically < 5.0^{-06} Torr).

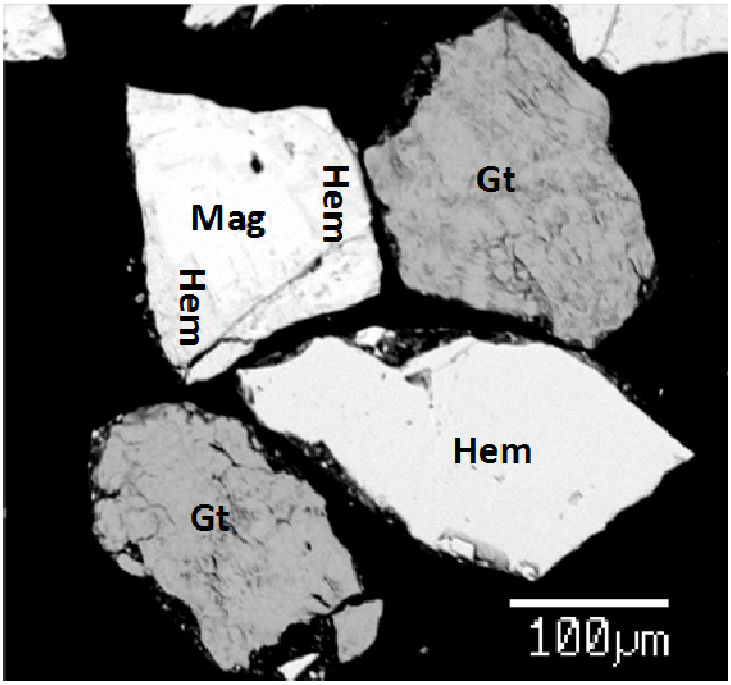

Figure 8.2 EPMA BSE image illustrating the variation in BSE of magnetite (Mag), hematite (Hem) and goethite (Gt). The magnetite is associated and partially surrounded by hematite. Although little difference between magnetite and hematite is observed by eye, there is sufficient contrast to be resolved in the digital signal (see text).

It should be noted that when working with spectra containing higher counts, as in the more usual SEM/EDS spot analysis, it is possible to separate Fe oxides using the Fe counts in the X-ray spectra. However, when mapping at higher count rates, the edge effect problems are still experienced and the mapping is too slow to have practical applications in acquiring the large amounts of data required for mineral processing applications.

8.4.2.2 Distinguishing compositional variants in the goethite group

Goethite was separated from magnetite and hematite, using differences in their BSE signal. It has a significantly lower BSE coefficient than either magnetite or hematite (Figure 8.2) because of its lower density. Goethite group minerals are known to vary in composition, thus a further aim of the research was to characterise this compositional variability using QEMSCAN®.

The automated mineralogy detection limit for elements in goethite is approximately 3 wt % for the QEMSCAN® system used (Andersen et al., 2009). EPMA results showed that some of the goethite contained > 3 wt % Al_2O_3 and that > 95 % of the Si content observed in the goethite were below the 3 wt % threshold and hence not detectable. Based on the EPMA results, two categories of goethite were created, namely goethite/limonite and aluminium bearing goethite (goethite (Al)). The detection limit of 3 wt % Al_2O_3 was set as an arbitrary cut off point with goethite (Al) containing > 3 wt % Al_2O_3 and goethite/limonite containing < 3 wt % Al_2O_3.

Owing to the automated nature of the QEMSCAN® which permitted the analysis of many thousands of particles compared to hundreds by EPMA, a third category named goethite (P) was identified during the QEMSCAN® analysis. The SIP therefore contains 3 goethite entries; goethite/limonite, phosphorus bearing (goethite (P)) and aluminium bearing (goethite (Al)) goethite. Goethite (P)) contains > 3 wt % P and < 3 wt % Al, Goethite (Al) contains < 3 wt % P and > 3 wt % Al whilst goethite/limonite contains < 3 wt % P and Al.

8.4.2.3 Investigating the Ca Fe silicate bucket; developing the andradite group

Garnets are abundant and visible with the naked eye in some of the itabirites in the study area. EPMA and XRD show that some of the garnets are andradites which have a similar formula to epidote and hedenbergite; both of which have also been shown to be present in some samples. Initially they were all placed in a bucket labelled Ca Fe silicate based on their formulae (see Table 8.5).

Table 8.5 Chemical formulae for andradite, epidote, hedenbergite and their average densities. (http://webmineral.com).

Mineral	*Formula*	*Average Density*
Andradite	$Ca_3Fe^{2+}{}_2(SiO_4)_3$	3.90
Epidote	$Ca_2Fe^{3+}{}_{2.25}Al_{0.75}(SiO_4)_3(OH)$	3.45
Hedenbergite	$CaFe^{2+}Si_2O_6$	3.55

Note that of the three, only epidote contains aluminium though in much lower quantity compared to Ca and Fe. The first task was to create a group for Ca Fe silicates that does not include Al. Since the quantity of Al in epidote is small (< 3 wt. %), it is possible that it will not be detected by the QEMSCAN®. All three have similar densities ruling out the use of BSE to differentiate them. As such it was decided to use the ratio of Ca to Si which is similar for epidote and hedenbergite (< 1) but different for andradite (≥ 1).

8.4.2.4 Separation of chamosite from other chlorites and almandine.

Chamosite is regarded as a low grade iron mineral and as such it was considered worth separating from the other chlorites and almandine. From Table 8.6 it is seen that chamosite has a much lower Mg content than clinochlore. Even though the Mg content might not be detected using the QEMSCAN®, the list was made tighter by excluding Mg for the chamosite group. This ensured that this group does contain chamosite even though there is a slight possibility the remaining chlorites might include chamosite.

XRD and EPMA confirmed that almandine (a garnet) is present in one particular sample i.e. NWB01 but not chlorite. The formula for almandine is given in Table 8.6. Note that it contains similar elements to chamosite especially since as stated above we have ignored the Mg content of chamosite in order to separate it from other chlorites. Ideally, almandine has a higher average density implying they could be separated based on their BSE signal. Upon investigation it was concluded that the actual density and Fe content of various grains of chamosite and almandine are very variable and that there were significant overlaps in composition. They could therefore not be separated based on chemistry or

BSE signal. Knowledge of this particular sample allowed us to duplicate the mineral list for the NWB01 sample but chlorite was renamed as almandine.

Table 8.6 Chemical formulae and average density for Mg, Fe, and Mn end member chlorites and almandine (http://webmineral.com).

Mineral	*Formula*	*Average Density*
Chamosite	$Fe^{2+}_3Mg_{1.5}AlFe^{3+}_{0.5}Si_3AlO_{12}(OH)_6$	3.20
Clinochlore	$Mg_{3.75}Fe^{2+}_{1.25}Si_3Al_2O_{10}(OH)_8$	2.65
Pennanite	$Mn^{2+}_5Al_2Si_3O_{10}(OH)_8$	3.06
Almandine	$Fe^{2+}_3Al_2(SiO_4)_3$	4.19

The categories in the mineral list have been validated to prevent any misclassification. This involved expanding each entry and checking the subcategories of the primary mineral list. The SIP list was then finalised including assigning specific colours to groups. All reprocessed data was checked again and the boundary phase processor applied as required. The data was then exported for further analysis and interpretation. Data processing also considered the issues discussed in Rollinson et al. (2011).

8.5 Interrogation of the Nkout QEMSCAN® data

8.5.1 Modal mineralogy determined by QEMSCAN®

As can be seen in Table 8.7 and Figure 8.3, magnetite is a major mineral in all of the material types at Nkout. The bulk of the weathered material comprising the EM, WMI and TMI material types, which was initially considered to be a hematite deposit (Suh et al., 2009) contains magnetite, hematite and goethite. Goethite/limonite and magnetite are the dominant minerals in EM and WMI whilst quartz and magnetite are dominant in the HMI and LMI material types. The transitional (TMI) ore contains magnetite and more or less equal proportions of goethite and quartz. Goethite (Al) occurs mainly in the weathered sample types and is highest in WMI. Concentrations are low in the itabirite sample types (HMI and LMI, Figure. 8.3, Table 8.7). There is a rather low (up to 2 wt %) but important concentration of phosphorus bearing goethite (Gt (P)) in the weathered EM and WMI material types in which this is the only P-bearing mineral. WMI in particular contains the highest P levels in the deposit due to its

goethite (P) content. There is no evidence of iron carbonate minerals at Nkout. Iron sulphides are present mainly as pyrite, which occurs as a minor mineral within the magnetite itabirite. Chamosite occurs in quantities greater than 30 wt % in occasional samples, as in the case of the TMI sample NES03 where it is the most abundant mineral. The TMI contains the highest average chamosite concentration of 17.27 wt %.

The main gangue minerals in the weathered materials types are quartz and the Al Ox(OH) phases mainly gibbsite. There is a significant increase in the quartz concentration from EM to WMI to TMI with the highest (10.02 wt %) in the -63/+45 µm fraction of the TMI. Al Ox(OH) is also highest in the -63/+45 µm fraction of this material type. Other gangue trace minerals in the EM group include kaolinite, Fe Mg silicates, Ti magnetite, chlorite and titanite. Minor gangue minerals present in the WMI that were not seen in the enriched material include Mn phases, plagioclase, biotite, pyrite and calcite. The other minor to trace gangue minerals present in the TMI that were not encountered in the previous two categories are muscovite/illlite, K-feldspar and zircon.

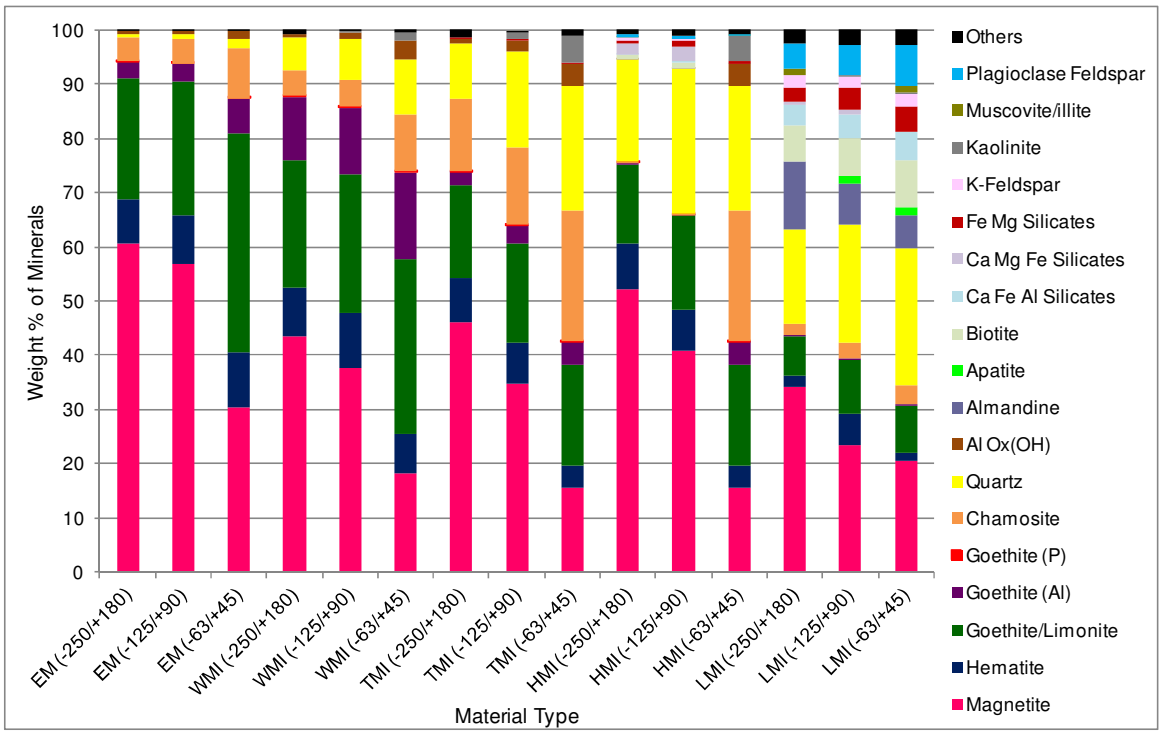

Figure 8.3 Average modal mineralogy (weight %) for the various size fractions (µm) analysed. Similar material types are placed side by side for easy comparison. The others category is larger than that in Table 8.7 as with the exception of goethite (P) only major minerals are included in this plot whilst the table contains minor and trace minerals in addition to the majors. See Chapter 4 for explanations of the material types.

Gangue minerals form between 55 to 63 wt % of the LMI samples. Throughout the itabirite sample types, quartz is the main gangue with the highest concentration being in the -63/+45 µm fractions. Al Ox(OH) is only present in the -63/+45 µm fraction of the HMI which also has the highest concentration of kaolinite (4.82 wt %). Almandine garnet can be present in the LMI up to 12.40 wt % in the -250/+180 µm fraction. Plagioclase is dominant over K-feldspar within the magnetite itabirite. Other gangue minerals include aluminosilicates, especially in LMI, including biotite, Ca Fe Al silicates, Ca Mg Fe silicates and clinochlore which occur in minor and trace quantities.

Table 8.7 Average mineralogical composition in weight percentage for the various material types.

	Enriched Material	***Weathered MI***	***Transitional MI***	***High grade MI***	***Low grade MI***
Magnetite	49.29	33.07	32.13	41.40	26.06
Hematite	9.08	8.8	6.63	6.10	3.01
Goethite/Lm	29.17	27.21	18.04	16.28	8.66
Goethite (Al)	4.27	13.33	3.40	0.17	0.28
Goethite (P)	0.03	0.16	0.01	bdl	bdl
Chamosite	6.13	6.80	17.27	0.28	2.84
Quartz	0.96	7.90	16.85	27.44	21.53
Al Ox(OH)	0.92	1.69	2.37	bdl	0.04
Fe Mg Silicates	0.03	0.06	0.35	1.49	3.81
Apatite	bdl	bdl	bdl	0.12	1.23
Ilmenite	0.01	0.01	0.10	0.01	0.27
Ti-Magnetite	0.01	0.06	0.08	0.03	0.16
Kaolinite	0.03	0.63	2.23	0.03	0.20
Pyrite	0.01	0.01	0.01	0.28	0.26
Biotite	bdl	bdl	0.02	1.19	7.43
Plag Feldspar	bdl	0.01	0.03	0.75	6.00
Ca Fe Al Silicates	bdl	bdl	bdl	0.27	4.54
K-Feldspar	bdl	bdl	bdl	0.36	2.25
Muscovite/illite	bdl	bdl	0.03	0.08	1.17
Ca Mg Fe Silicates	bdl	bdl	bdl	3.11	0.66
Others	0.02	0.22	0.41	0.56	9.60

MI - Magnetite itabirite. bdl – below detection limit. These averages were calculated using data from all three size fractions analysed.

There is significant variation in the modal mineralogy of the different grain size fractions. Magnetite content is in general highest in the coarsest -250/+180 µm fraction and decreases towards -63/+45 µm, the finest fraction analysed (Figure 8.3). Hematite is more evenly distributed at between 8 wt % to 10 wt % in all weathered size fractions and it is goethite in the weathered material that increases as the magnetite content decreases in the finer grained material. The other most noticeable grain size effect is that chamosite is in general highest in the -63/+45 µm fractions and lowest in the coarse -250/+180 µm fraction, and this is especially marked in the transitional magnetite itabirite material type (TMI) (Figure. 8.3).

8.5.2 Comparison of Fe weight % by XRF and QEMSCAN®

If the QEMSCAN® analysis is a precise measure of modal mineralogy and includes some mineral compositional information, a calculated value for Fe wt % using the QEMSCAN® results should be similar to that of the whole rock (XRF). The back calculated QEMSCAN® Fe wt % in general decreases with decreasing grain size (Figure 8.4) and is in general higher than that obtained using the whole rock XRF for the larger grain sizes (-250/+180 µm, -125/+90 µm) but lower for the -63/+45 µm fraction. An average composition of the three size fractions analysed using the QEMSCAN® is closest to the XRF Fe value (Figure 8.4). Explanations for this can be based on the mineralogy and sample preparation of the epoxy resin blocks for the QEMSCAN®. The QEMSCAN® analysis was not done on whole rock samples but on screened size fractions, selected from the following six size fractions made; +250 µm, -250/+180 µm, -180/+125 µm, -125/+90 µm, -90/+63 µm, and -63/+45 µm. QEMSCAN® analysis thus produces more precise data on the particular sized fractions considered and this always risks a non-representative sample compared to XRF analysis which was carried out on whole rock samples ground to - 45 µm.

Furthermore, the QEMSCAN® back calculations are done based on the mineral quantities exposed on the surface of the polished sections. These surface minerals may not be 100 % representative of the mineral quantities in the original sample not only due to mineral segregation during sieving but also due to mineral segregation during preparation of the sample blocks (Petruk, 2000).

Denser magnetite and hematite may settle to the bottom of the resin block mould i.e. the polished surface, faster than goethite, chamosite, gibbsite and quartz resulting in more of the Fe oxides on the surface than is actually present in the sample in terms of percentage. The result is that samples with high amounts of magnetite and hematite will give higher calculated Fe content whilst those with relatively low magnetite and hematite, but higher chamosite, gibbsite and/or quartz will give lower calculated Fe. Even though this effect is minimised by using graphite to improve particle separation, and minimise differential settling, it cannot be completely eliminated.

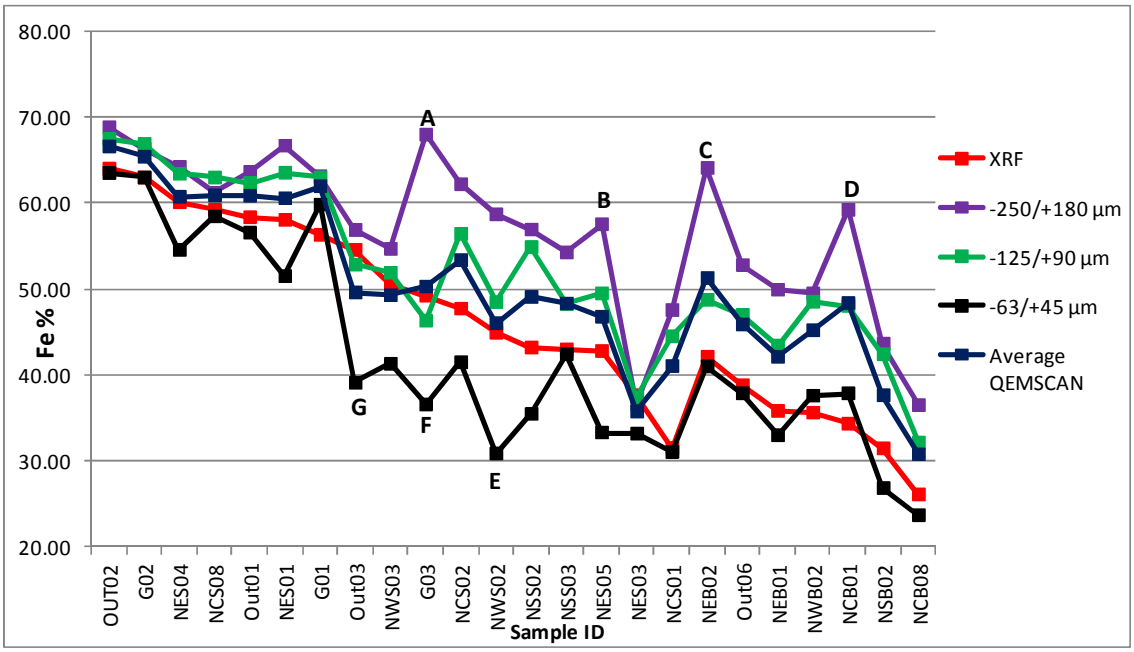

Figure 8.4 Comparison of the Fe wt % determined by XRF and Fe wt % calculated from the QEMSCAN® results.

An additional or alternative explanation is the fact that the calculated average QEMSCAN® Fe wt % is closest to that of the XRF which suggests that the preferential separation of minerals into the various size fractions is the most likely explanation for the discrepancies in correlation. Preferential segregation of magnetite into the coarser size fraction is clear on Figure 8.3.

Some of the back calculated values in Figure 8.4 show much greater deviation from the XRF values and have been labelled A to G. A to D represent anomalously higher values from the -250/+180 µm fraction whilst E to G are anomalously low values from the -63/+45 µm fraction. Those with much higher Fe wt % i.e. A to D have much higher magnetite content than other minerals

whilst those with much lower values are either due to quartz as in F and G or gibbsite and chamosite as in E being the most abundant minerals.

Theron et al. (2012), worked on a meta-BIF ore body which is capped by a highly enriched supergene cap and essentially consists of three main zones, namely 1. a weathered Fe cap (> 50 mass % Fe), 2. an enriched transitional zone (40 to 50 mass % Fe) and 3. a fresh to slightly weathered ore (35 to 40 mass % Fe). According to them, the + 1mm fraction is enriched in Fe, P and MnO and depleted in SiO_2, Al_2O_3, TiO_2 and S. SiO_2 and Al_2O_3 are enriched in the – 600 µm and – 45 µm fractions. Even though -250 /+180 µm is the largest size fraction analyzed in this research compared to the larger maximum size of + 1 mm for Theron et al., with the exception of MnO, the chemical trend versus size fraction is the same in both research projects. The low Fe content in the fine size fraction is true provided the samples have not been beneficiated as was done using low and high intensity magnetic separations in this research. This is so because we expect the deleterious minerals of quartz and the Al Ox(OH) to be concentrated in the fines reducing the Fe grades. However if the fines are beneficiated, the resulting concentrate will have a higher Fe grade than the larger size fractions due to the better liberation of the Fe minerals expected in the fines. As such it can be concluded that the low Fe content in the fines in not due to analytical bias.

8.5.3 Mineral association

“Mineral association” quantifies which mineral grain is adjacent to or touches another in a particle. It is reported in a tabular format which is read column down then to the left across the row to see what percentage of a mineral is associated with another. The main mineral associations amongst the material types are quite similar and illustrated in Figure 8.5. Tables 8.8 gives the average mineral association data for the -125/+90 µm fraction of the weathered magnetite itabirite which is representative of the main associations in the EM, WMI and TMI material types.

In the three weathered sample types, the Fe oxides are closely associated with each other (Figure 8.5, rows 1 and 2), for example hematite is greater than 59

% associated with magnetite and 33 % associated with goethite/limonite in Table 8.8. This close association of the Fe oxides applies to all size fractions. The various goethites are also closely associated with each other (Figure 8.5, row 2). Chamosite is mainly associated with goethite/limonite (29.28 %), goethite (Al) (15.19 %) and to a lesser extent, magnetite (6.37 %) (Figure 8.5, rows 3). Of the major gangue materials, Al Ox(OH) (gibbsite) is mainly associated with various goethites and chamosites (Figure. 10, row 4) whilst quartz has low association with other minerals; the highest being 4.18 % with chamosite (Figure 8.5, row 5). Other minor gangue minerals such as kaolinite and chlorite (clinochlore) are associated with chamosite i.e. 60.70 % and 84.46 % respectively (Figure 8.5, row 6).

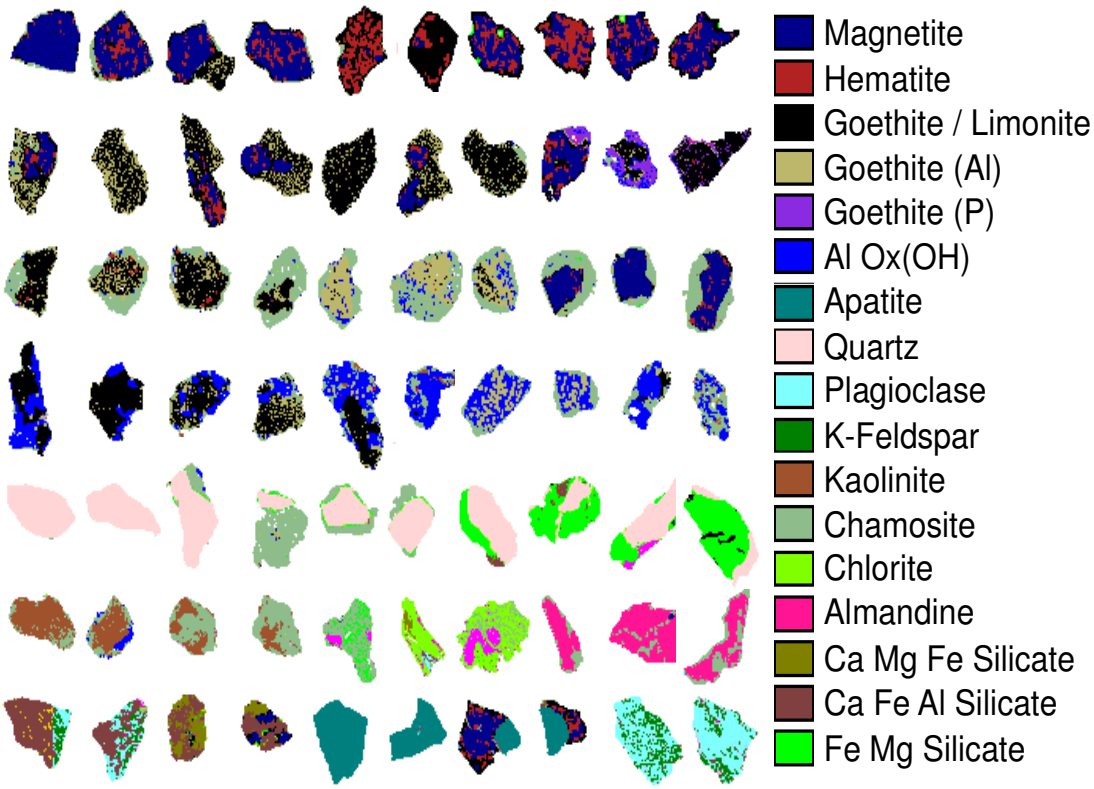

Figure 8.5 False colour QEMSCAN® image showing the main mineral associations present in the study area for the -180/+125 µm size fraction.

In the high and low grade magnetite itabirite, where magnetite is the dominant Fe oxide, the relatively small quantities of goethite/limonite and hematite are also closely associated with the magnetite (Table 8.9). Again the associations are similar in all three size fractions. Using the -125/+90 µm size fraction of the low grade magnetite itabirite for example (Table 8.9), it is noticeable that the aluminosilicates are less than 6 % associated with the Fe oxides.

Table 8.8 Average mineral association data for the -125/+90 µm fraction of the weathered magnetite itabirite which is representative of the main associations in the EM, WMI and TMI material types.

	Minerals	***Mag***	***Hem***	***Gt/Lm***	***Gt (Al)***	***Gt (P)***	***Al Ox/OH***	***Qtz***	***Chm***	***Kln***	***Mn phases***	***Chl***	***Ti-Mag***	***Fe Mg Sils***
WMI -125/+90	Mag	0.00	59.56	24.37	6.62	0.29	2.71	0.01	6.37	0.00	1.37	0.33	9.81	1.07
	Hem	40.44	0.00	10.96	1.82	0.46	1.39	0.00	1.44	0.02	2.32	0.24	5.09	0.16
	Gt/Lm	48.21	33.75	0.00	55.87	38.95	18.16	0.36	29.28	0.07	28.65	4.74	43.18	13.28
	Gt (Al)	3.31	2.44	25.20	0.00	41.71	24.89	0.00	15.19	0.05	15.55	1.79	26.28	0.64
	Gt (P)	0.02	0.05	0.36	0.41	0.00	1.07	0.00	0.00	0.00	0.00	0.00	0.59	0.00
	Al Ox/OH	0.46	0.29	1.20	2.17	7.78	0.00	0.01	3.94	0.01	0.05	0.00	0.44	0.00
	Qtz	0.00	0.00	0.02	0.00	0.00	0.00	0.00	0.22	0.68	0.03	2.16	0.00	35.43
	Chm	1.31	0.84	6.93	12.58	0.00	26.38	4.18	0.00	60.70	3.51	84.46	2.94	9.75
	Kln	0.00	0.00	0.00	0.00	0.00	0.01	0.22	3.94	0.00	0.03	0.17	0.00	0.40
	Mn phases	0.00	0.01	0.02	0.02	0.00	0.01	0.02	0.02	0.00	0.00	0.00	0.00	0.00
	Chl	0.00	0.00	0.02	0.03	0.00	0.00	1.14	0.69	0.17	0.00	0.00	0.02	0.00
	Ti-Mag	0.03	0.02	0.10	0.09	0.18	0.02	0.00	0.01	0.00	0.00	0.01	0.00	0.00
	Fe Mg Sil	0.00	0.00	0.03	0.01	0.00	0.00	0.38	0.11	0.03	0.00	0.00	0.00	0.00

Note: The table should be read down the columns and across the rows to the left to see the associations. Values may not be the same if read the other way i.e. row first then column.

Table 8.9 Average mineral association data for the -125/+90 µm fraction of the low-grade magnetite itabirite which is representative of the main associations in magnetite itabirite.

		Mag	***Hem***	***Gt/Lm***	***Chm***	***Qtz***	***Ap***	***Alm***	***Py***	***Chl***	***Bt***	***Pl Fsp***	***K-Fsp***	***Ca Fe Al Sil***	***Ca Mg Fe Sil***	***Fe Mg Sil***
LMI -125/+90	Mag	0.00	57.61	42.09	2.40	0.09	1.34	0.63	2.84	1.06	0.40	0.00	0.00	0.25	0.08	2.54
	Hem	24.12	0.00	11.29	1.66	0.04	0.25	0.03	0.53	0.52	0.23	0.00	0.00	0.22	0.06	0.24
	Gt/Lm	60.90	34.24	0.00	9.47	0.30	1.75	0.35	3.28	4.36	1.23	0.01	0.01	1.07	0.36	5.15
	Chm	1.65	0.97	3.05	0.00	0.73	1.33	48.40	3.93	17.60	18.41	4.25	1.34	6.73	7.13	17.34
	Qtz	0.03	0.01	0.14	0.43	0.00	2.04	1.98	5.11	9.42	1.22	3.13	0.28	2.13	0.69	15.73
	Ap	0.02	0.01	0.03	0.05	0.08	0.00	0.08	0.00	0.03	0.09	0.02	0.01	0.77	1.93	0.00
	Alm	0.33	0.08	0.13	15.63	0.38	3.12	0.00	0.44	1.16	0.06	0.12	0.02	2.01	11.79	5.76
	Py	0.04	0.06	0.03	0.05	0.04	0.00	0.02	0.00	0.06	0.03	0.01	0.01	0.21	0.12	0.16
	Chl	0.32	0.20	0.65	5.78	3.50	0.12	0.50	1.11	0.00	9.77	0.27	0.44	0.97	7.82	7.19
	Bt	0.29	0.15	0.52	19.29	1.34	0.51	0.10	1.82	24.34	0.00	0.41	10.54	2.69	3.38	15.02
	Pl Fsp	0.00	0.00	0.00	2.08	2.31	0.19	0.09	0.14	0.86	0.80	0.00	45.52	22.57	1.31	0.17
	K-Fsp	0.00	0.00	0.00	0.85	0.20	0.11	0.00	0.03	0.82	4.41	31.68	0.00	4.54	0.48	0.08
	Ca Fe Al Sil	0.11	0.11	0.28	2.48	1.52	5.56	0.35	1.44	1.77	3.79	8.60	2.53	0.00	44.71	3.82
	Ca Mg Fe Sil	0.00	0.01	0.01	0.47	0.15	1.18	1.64	0.51	1.60	0.51	0.08	0.08	25.85	0.00	1.43
	Fe Mg Sil	0.68	0.34	1.28	9.51	3.95	0.50	0.68	3.71	10.49	10.04	0.03	0.04	5.70	3.05	0.00

Note: The table should be read down the columns and across the rows to the left to see the associations. Values may not be the same if read the other way i.e. row first then column.

Almandine is 48.40 % associated with chamosite (Figure 8.5, row 6) whilst Ca Fe Al silicates are mainly associated with plagioclase (22.57 %) and Ca Mg Fe silicates (25.85 %) (Figure 8.5, row 7). Quartz, the main gangue mineral, has little association with any other mineral; the highest being 3.95 % with Fe Mg silicates (Figure 8.5, row 5). Apatite is 1.34 % associated with magnetite and 1.75 % associated with goethite/limonite (Figure 8.5, row 7). The alkali and plagioclase feldspars are closely associated (Figure 8.5, row 7).

8.5.4 Mineral liberation

A mineral is considered in this study as being liberated if > 90 % is free, high grade intergrown if it is > 60 % ≤ 90 %free, low grade inter-grown if it is > 30 % ≤ 60 % free and locked if it is ≤ 30 % free. In some beneficiation processes, only particles containing > 90 % Fe oxides are recovered when producing a high grade concentrate as in, for example, Petruk (2000). Table 8.10 is arranged in terms of increasingly liberated grains in the -125/+90 µm size fraction of the weathered magnetite itabirite. The mineral association values within the material types are reflected in the liberation values. The liberation values are similar for the various material types even though they in general increase with decreasing grain size.

Table 8.10 Average liberation for the -125/+90 µm fraction of the weathered magnetite itabirite material type.

	Minerals	***% Liberation***			
		≤ 30 %	***> 30 % ≤ 60 %***	***> 60 % ≤ 90 %***	***> 90 %***
WMI -125/+90 µm	Hem	83.15	16.06	0.79	0.00
	Gt (P)	99.97	0.03	0.00	0.00
	Gt (Al)	62.68	22.27	14.60	0.45
	Mag	9.53	44.59	45.36	0.52
	Gt/Lim	38.58	36.94	22.39	2.09
	Chm	47.57	19.65	25.12	7.66
	Al Ox(OH)	64.50	13.07	8.93	13.50
	Kao	23.82	13.05	23.90	39.23
	Fe-oxides	0.37	1.61	15.54	82.48
	Qtz	0.11	0.23	0.89	98.77

Gt – goethite, Chm – chamosite, Hem – hematite, Kao – kaolinite, Lim – limonite, Mag – magnetite, Qtz – quartz

The close association hematite has with magnetite results in 83.15 % of hematite being locked i.e. ≤ 30 % liberated, similarly the close association of goethite (P) with the other goethite and its trace to minor concentrations results in it being completely locked (99.97 %). Magnetite has the highest percentage i.e. 45.36 % in the high grade intergrown category (liberation > 60 % ≤ 90 %) and liberated grains make up just 0.52 %. The liberations of the individual Fe oxides minerals increase substantially when considered as a group (82.48 %) Of the main gangue minerals; Al Ox(OH) is mainly locked (64.50 %) whilst quartz and apatite in general within the magnetite itabirite are > 90 % liberated.

8.5.4.1 Effect of chamosite on liberation

The presence of chamosite in the samples has a marked effect on liberation. For example in Figure 8.6, the samples in the middle i.e. NCS04 and NES04 have higher chamosite concentration (31.85 wt % and 13.67 wt %, respectively) compared to < 0.01 wt % for the other 2 on the edges i.e. G02 and Out02. Chamosite like other chlorites occurs in the form of aggregates which may explain the low liberation.

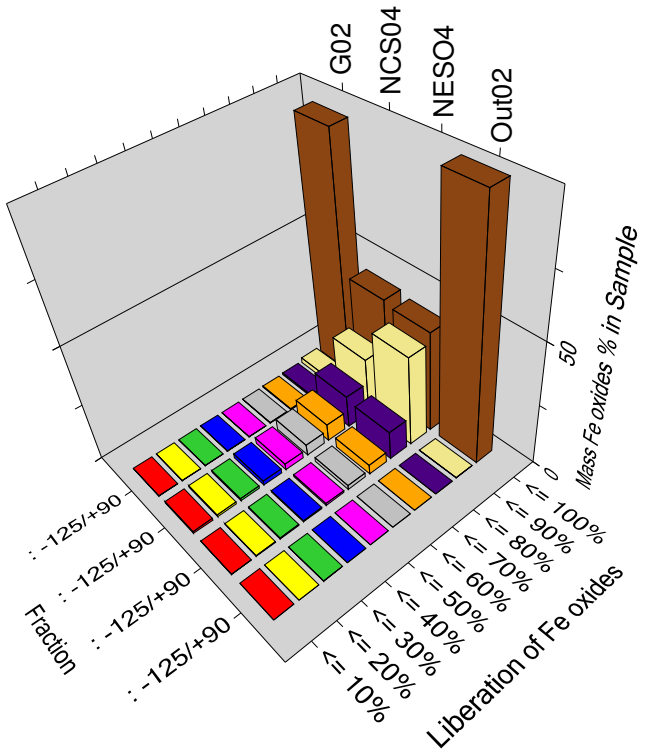

Figure 8.6 Liberation for 4 enriched samples. Note that the 2 samples in the middle (i.e. NCS04 and NES04) have higher chamosite concentrations (31.85 wt. % and 13.67 wt. %, respectively) compared to < 0.01 wt. % for the other 2 on the edges, i.e. G02 and Out02.

A plot of chamosite wt % against the percentage of liberated (> 90 % free) Fe oxides (Figure 8.7) shows that above 6 wt % chamosite, the liberation of the Fe oxides drops significantly. This effect is worse if Al Ox(OH) and to a lesser extent kaolinite are also present as major minerals. For example even though the sample at point A in Figure 8.7 contains 4.38 wt% of chamosite, it also contain 9.92 wt % of Al Ox(OH) and the liberation of the Fe oxides is just 49.94 wt %. The sample at point B contains 5.15 wt % of chamosite and 2.71 wt % of kaolinite with the Fe oxide liberation being 72.36 wt %.

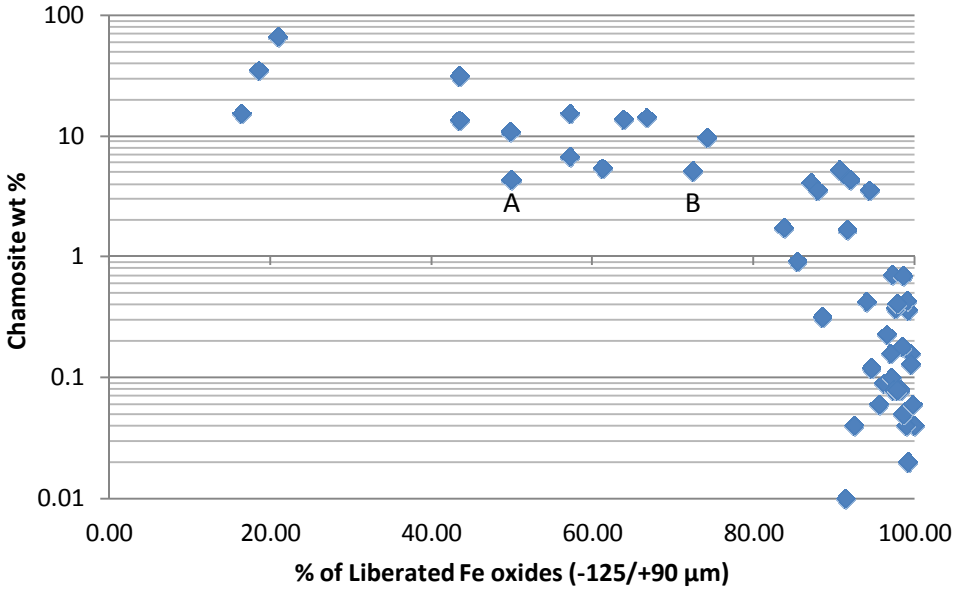

Figure 8.7 The effect of chamosite on the liberation of the Fe oxides. The effect is more pronounced for chamosite weight percentage greater than 6 wt % and is compounded if Al Ox(OH) is also present as a major mineral (see text).

8.5.5 Theoretical grade recovery

The QEMSCAN® theoretical grade recovery (TGR) reports are graphs in which the potential recovery of single or groups of minerals or elements is plotted against the grade for a given sample analysed. The grade of an ore is the concentration in percentage of the actual mineral or element that can be extracted from an ore. The recovery includes the ore mineral or element but might also include other minerals the ore mineral is associated with or have similar properties as those used to recover the valuable ore mineral or element. TGR takes into consideration factors such as the mineral associations, liberation and mineral chemistry to propose a relationship between the recovery and grade. In the mine environment, the TGR is used to analyse feed products

to predict the best possible grade that can be achieved for a given recovery of a mineral or element. If the particles in a sample were 100 % liberated and concentrated, then we expect the grade of the concentrate to be 100 % of the mineral being concentrated or the percentage of the element calculated for the mineral formula. This is not the case for the deposits studied and we expect factors such as mineral associations to affect the grades. The average theoretical grade recoveries for the various samples have been made but should only be considered as rough guides as the grade can vary considerably throughout a deposit. The theoretical grade recovery for three samples (-63/+45 µm), one each from the WMI, TMI and MI groups, are shown in Figure 8.8.

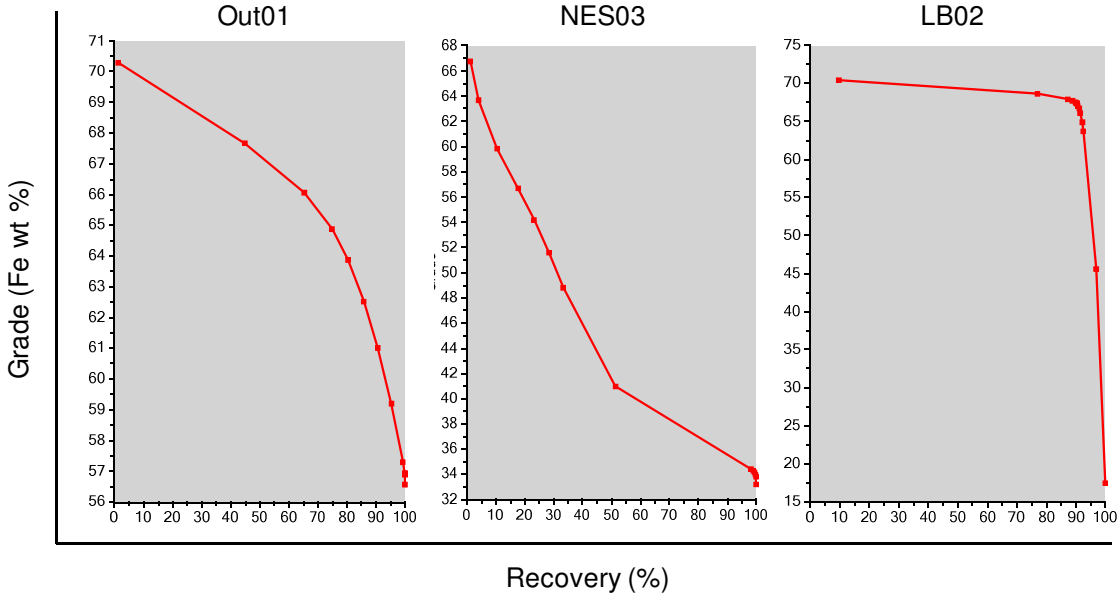

Figure 8.8 Theoretical grade recovery for 3 fractions of the transitional magnetite itabirite (TMI).

Figure 8.8 shows the QEMSCAN® generated TGR curves for three samples (-63/+45 µm), one each from the WMI, TMI and MI groups. The calculated grade information can only be considered accurate for the particular size fractions selected for the TGR analysis. It is seen that the fresh BIF sample, LB02, from the MI material type has the potential of producing high grades with good recoveries. The problems with the chamosite-rich sample (NES03) are also evident in its TGR curve, especially so when the smallest size fraction contains the highest chamosite concentration. It has the lowest grades for similar recoveries to the other two samples. TGR curves act as guides to monitor processing plant performances and to spot potential problems related to the ore

or plant efficiency. The grades for the weathered sample Out01 may not be as high as those of the MI sample for similar recoveries but it has the potential for obtaining grades of > 60 wt % Fe for recoveries of up to 90 %.

The theoretical grade recovery of 10 samples was compared to the actual grade recovery obtained from magnetic separation of the iron rich minerals and is reported in the next chapter (Chapter 9). This is a metallurgy chapter which includes the magnetic separation details and the results of the XRF conducted on the concentrates.

8.6 Conclusions on the Nkout deposit

The use of QEMSCAN® has enabled the following conclusions to be made regarding the process mineralogy at Nkout.

1. The deposit contains magnetite throughout (updating the conclusion by Suh et al. (2009) that the weathered material is predominantly hematite). The magnetite is being replaced by hematite and therefore the deposits can be described as a hematite-martite–goethite ore which is similar to hematite–martite–goethite ore of the BIF-hosted iron ore deposits in the Windarling Range, Yilgarn Craton, Western Australia (Angerer et al., 2013).
2. The presence of chamosite is important because even though it is a significant host of Fe (about 30 wt % Fe), it has deleterious effects on liberation characteristics of the ore when present at concentrations above 6 wt %. This effect is compounded if the samples are also rich in Al Ox(OH), which at Nkout is mainly gibbsite. Chamosite is mainly associated with goethite/limonite as far as the Fe oxides are concerned but also has a much higher association with gangue minerals such as kaolinite, Al Ox(OH) and the Mg, Fe and/or Ca aluminosilicates compared to the Fe oxides. The locations of chamosite within the deposit are important and should be noted. According to the samples studied so far, it the chamosite occurs mainly in the eastern part of the deposit.
3. The major gangue minerals in the weathered martite - goethite ore are

gibbsite and quartz. A major potential problem in upgrading this ore is removing Al and P which has been shown to be associated with the goethite. However since their quantities are relatively low they might not be the main targets for removal, compared to for example gibbsite and quartz in upgrading to a customer's specification.

4. The major gangue mineral in the magnetite itabirite ore is quartz, followed by the aluminosilicates. The quartz is in general liberated for the size fraction studied and when associated with other minerals, it is not associated with Fe oxides. Apatite is a potential problem in LMI ores but occurs mainly as well liberated grains (> 90 % free) and as such will not be problematic to remove when upgrading the magnetite itabirite.
5. The Al Ox(OH) could be removed by attrition scrubbing whilst quartz and other gangue can be removed by grinding and screening. Magnetite could then be recovered using less expensive low intensity magnetic separation (LIMS) whilst hematite and goethite can be removed using a combination of Wet High Intensity Magnetic Separation (WHIMS), SLon Magnetic Separation and Flotation. The LIMS should be employed initially and the rejects subjected to the WHIMS to remove the hematite and goethite. This will reduce energy consumption.

8.7 Comparison of the Nkout and Putu deposits

8.7.1 Modal Mineralogy

The major difference between the two study areas in terms of the Fe oxides is the higher concentration of magnetite at Nkout whereas hematite is higher at Putu in the enriched material to transitional magnetite itabirite. Goethite/limonite is the most abundant goethite at Putu and Nkout. However goethite (Al) and chamosite are limited to the enriched material whist goethite (P) occurs in trace quantities at Putu. Goethite (P) occurs in minor quantities at Nkout but goethite (Al) and chamosite occurs as major minerals in the enriched material to transition magnetite itabirite. The Al content of the enriched material to the transitional magnetite itabirite at Nkout is higher than that at Putu due to the presence of Al Ox(OH) which is present mainly in the enriched material at Putu. In the magnetite itabirites, the Al is present in the form of the aluminosilicates in both study areas. CaO is higher at Putu mainly due to the higher concentration

of Ca Mg Fe silicates. The same trend in which SiO_2 increases from the enriched material to the low-grade magnetite is present in both localities and is due to the quartz content. The loss on ignition in general decreases from the enriched material to the magnetite itabirites in both study areas but is higher at Nkout mainly due to its higher goethite concentration.

8.7.2 Mineral association and liberation

Both the mineral associations and liberation are considered with respect to the modal mineralogy; the –63/+45 µm size fraction which has been shown to be the optimum fraction for beneficiation and is therefore used as an example. The Fe oxides are closely associated at both localities with hematite being about 60 % associated with magnetite. The various goethites are closely associated in the enriched material group in both deposits. At Putu, the Fe oxides are also associated with the silicates even though their maximum association in the enriched material is with Fe Mg silicate which is 12.50 % associated with goethite / limonite. As far as the gangue minerals in the enriched material are concerned, quartz has very little association with any other minerals and is essentially liberated at Nkout whereas at Putu it is 13.89 % associated with Fe Mg silicates and 14.72 % associated with chlorite. These associations do not pose processing problems as both groups of minerals are also gangue. The association of Al Ox(OH) is similar in both localities with it being mainly associated with chamosite (54.66 % at Putu and 31.03 % at Nkout) and goethite (between 10 to 20 % in both deposits). Chamosite is mainly associated with the goethite in both localities.

As none of the Putu samples met the requirement of being classified as weathered magnetite itabirite, this material type is not discussed in this comparison of both deposits. The association of the Fe oxides in the transitional magnetite itabirite is quite similar to that in the enriched material. Chamosite is mainly associated with goethite/limonite and the silicates in both deposits. Quartz is not associated with the Fe oxides and is < 10 % associated with the silicates. A point of concern at Putu is the presence of andradite which is about 20 % associated with goethite/limonite. The associations of the Fe oxides and that of quartz within the magnetite itabirite are quite similar to that of the

transitional magnetite itabirite described above. Apatite is < 2 % associated with the Fe oxides (mainly goethite) in both deposits and the silicates are associated with themselves and not the Fe oxides.

The close association of magnetite and hematite has resulted in hematite being > 90 % locked in the enriched material of both deposits. The aluminium rich goethite at Nkout is > 65 % locked compared to 51 % locked at Putu. Magnetite in both deposits occurs as low grade intergrown crystals i.e. > 30 % ≤ 60 % locked. In general, the Fe oxides as a group at Nkout are > 90 liberated compared to 64.17 % at Putu. This relatively low liberation at Putu is due to the association of the Fe oxides with silicates as explained above. Chamosite is about twice as liberated at Putu as it is at Nkout i.e. 33.05 % to 16.74 % respectively. A major difference in the enriched material is in the gangue minerals quartz and Al Ox(OH). Whereas the quartz in the enriched material at Nkout is > 95 % liberated, at Putu it is 59 % liberated. This low liberation of quartz at Putu is due to its association with other gangue minerals such as the silicates and not the Fe oxides. Al Ox(OH) is 72.52 % locked at Putu compared to 38 % locked, 30 % liberated at Nkout. It should be noted that the Nkout samples contained about 3 times more Al Ox(OH) than those from Putu.

Unlike the case for the enriched material, the Fe oxides within the transitional magnetite itabirite at Putu is about 78 % liberated compared to just 57.15 % at Nkout. This relatively low liberation at Nkout is due to its higher chamosite content which has been shown to reduce the Fe oxide liberation. Quartz, the main gangue in this material group is > 75 % liberated in both deposits. Even though the silicates are essentially locked in the transitional magnetite itabirite in both deposits, they are associated with themselves and not the Fe oxides and so do not pose processing problems. The Fe oxides in the magnetite itabirite are > 88 % liberated in both deposits as is quartz, the main gangue. The silicates are usually greater than 55 % liberated and as is the case of the transitional magnetite itabirite, they are usually associated with themselves.

8.8 Comparison of analytical methods and relative merits of QEMSCAN®

The main methods of quantitative mineralogy are the SEM based methods (e.g. QEMSCAN® and mineral liberation analyser (MLA)) and quantitative XRD using Rietveld refinement (McCusker et al., 1999). The choice of the optimum method requires details of not only the ores in question but also the methods themselves. In the case of Nkout for example, mineralogical and mineral chemistry techniques such as optical microscopy, semi-quantitative XRD and EPMA have shown that goethite is an important mineral in the oxidised cap, which has potential of being a DSO or upgraded to DSO specifications. A major problem is determining the amount of goethite present. Finely powdered goethite is in most cases weakly crystalline to amorphous and produces broad XRD peaks which are not proportional to the actual goethite content (Petruk, 2000). As such QEMSCAN® is the preferred technique rather than quantitative XRD.

Although it is necessary to verify the QEMSCAN® results using other techniques such as the semi-quantitative XRD, EPMA and optical microscopy and the set up for new ore deposits is time consuming, the technique provides a vast amount of mineralogical information which can be used to solve potential processing problems related to upgrading or beneficiation of iron ore deposits. An example here is the recognition of the presence of phosphorus-bearing goethite i.e. goethite (P) which was not found by the other techniques. The importance of developing a suitable SIP based on knowledge of not only the study area but also knowledge obtained from other techniques cannot be over emphasised. The same may be said for good sample preparation and suitable experimental conditions. The advantage of the QEMSCAN® over the EPMA and SEM/EDS is the capability of much more rapid data acquisition and thus the ability to analyse many thousands of particles, one or two orders of magnitude more than with more traditional techniques. The importance of developing a suitable SIP based on knowledge of not only the study area but also knowledge obtained from other techniques cannot be over emphasised. The same may be said for good sample preparation and suitable experimental conditions.

Several workers including Tonžetić and Dippenaar (2011), Donskoi et al. (2011), Thella et al. (2012) and Lund et al. (2013) have presented the effectiveness of QEMSCAN® as a tool for iron ore characterisation. Tonžetić and Dippenaar (2011) mentioned that QEMSCAN® can be used as an alternative to the traditional quantification of iron ore sinter mineralogy which has been based on amongst others optical microscopy and XRD. Optical microscopy is based on grain morphology and XRD on crystal structure whereas classification of minerals by QEMSCAN® is based on chemical composition. However Donskoi et al. (2011) pointed out that it is still problematic for QEMSCAN® to distinguish between iron ore minerals very close in oxygen content, e.g. hematite and hydrohematite, or between different types of vitreous goethite. This is not a problem for optical image analysis software as it can easily recognise minerals with slight differences in their oxidation or hydration state by correlation with their reflectivity. They however concede that a combined approach using both techniques will provide the most detailed understanding of iron ore samples being characterised. Lund et al. (2013) used the QEMSCAN® to validate a technique using EPMA, XRF and SATMAGAN to quantify minerals from routine chemical assays. The samples considered in that study contained only magnetite as the Fe oxide and therefore were particularly well suited to QEMSCAN® analysis. The ability to tackle material that contains both magnetite and hematite is a major step forward in making process and geometallurgical studies more efficient by gaining maximum information with as few as possible analytical techniques.

The choice of optimum techniques varies according to the sample characteristics, as well as the more pragmatic considerations of available techniques and expertise. Table 8.11 gives a summary of the steps in process mineralogy of iron ore deposits to clarify the options and possible paths through assessment of a deposit. All potential iron ores will be subject to whole rock analysis, usually by X-ray fluorescence (XRF), and to tests of iron-bearing mineral extraction, e.g. by the Davis Tube test (Leevers et al., 2005) or SATMAGAN (Lund et al., 2013). For some deposits with simple mineralogy and high Fe contents few additional tests might be needed, although most will undergo reflected light optical microscopy.

Table 8.11 Summary of some techniques to carry out quantitative process mineralogy of iron ore deposits.

Function	***Optical image analysis***	***Electron beam automated mineralogy (e.g. QEMSCAN®)***	***Quantitative X-ray diffraction***
Distinguish and quantify proportions of the various Fe oxides	Yes, most sensitive technique	Yes, with careful set up and calibration	Yes, except for amorphous phases e.g. goethite
Identify other major minerals	Yes	Yes	Yes
Indentify minor minerals (< 5 modal %)	Yes	Yes	No
Distinguish chemical variants of minerals	No, unless reflected light characteristic can be calibrated against chemistry	Yes, measures chemistry directly via X-ray spectrum	No
Quantify mineral associations and liberation	Yes	Yes	No
Cost to purchase and run	Moderately expensive, needs dedicated expertise to set up image analysis	Expensive equipment and needs dedicated expertise	Expensive equipment and needs dedicated expertise for quantitative work

When it is necessary to remove gangue minerals, a more in depth study is required. Best practice is to use a variety of techniques in a preliminary study to augment the data gathered thus far, including an electron beam technique (which may be energy or wavelength dispersive but should be quantitative) and X-ray diffraction. The results of this preliminary study then determine the best technique to choose for full and statistically valid assessment of the deposit for geometallurgical modelling. Automated mineralogy techniques, either optical or electron beam have important advantages over quantitative X-ray diffraction in that they can determine mineral associations and liberation, and are also able to determine amorphous phases. The key differences between optical and electron beam methods are that optical microscopy is the most sensitive method for distinguishing the different varieties of Fe oxides whereas the

electron beam techniques can determine mineral chemistry directly and distinguish between varieties of iron ore minerals with varying levels of contaminants and between different chemical variations of gangue minerals.

Geological studies of iron ores also benefit from these techniques if there is a need to quantify mineral associations in order to study, for example, alteration patterns or determine modal mineral assemblages involved in reactions. Similar considerations apply to the choice of optimum technique. The technique that will potentially give the largest amount of information is QEMSCAN® or a similar electron beam method, if the technique is carefully set up and calibrated to distinguish the Fe oxide minerals.

Chapter 9

Metallurgical Analysis

9.1 Introduction

Magnetic separation is the main method of beneficiation for both the Nkout and Putu iron ore deposits. In order to test the results of the QEMSCAN® study, both low and high intensity magnetic separation has been conducted on twenty samples selected so that they are representative of the mineralogy of the study areas and contained all the iron oxide minerals and chamosite in various quantities. They consist of BIF and saprolite drill cores as well as grab and outcrop samples. The three size fractions studied using the QEMSCAN® i.e. -63/+45µm, -125/+90 µm and -250/+180 µm were selected for this study. Ideally, the low intensity separation should be able to concentrate the magnetite whilst the high intensity should be able to concentrate the hematite, goethite and chamosite. The Davis Tube Recovery (DTR) was used to concentrate the highly magnetic materials and the tailings were passed through a laboratory Wet High Intensity Magnetic separator (WHIMS) Type LHW.

XRF analyses were conducted on both the feed samples and the concentrates obtained from the magnetic separations, not only to compare the two but also to have an idea about the potential chemical specifications of the iron ore products. The recovery and grade obtained from the magnetic separations were compared to the modal mineralogy and theoretical grade recovery (TGR) report generated by the QEMSCAN® software (iDiscover). The magnetic separations were carried out at the mineral processing labs at Camborne School of Mines, University of Exeter, Penryn Campus, Cornwall UK.

9.2 Magnetic separation

Minerals could potentially behave differently when exposed to an induced magnetic field due to their different magnetic properties and this forms the basis of the magnetic separation technique. In the case of iron ores the technique is used to concentrate the iron minerals e.g. magnetite leaving behind the gangue minerals (e.g. quartz) which are essentially non-magnetic. Minerals and materials in general can fit into two broad groups based on their magnetic

properties; diamagnetic or paramagnetic. Diamagnetic minerals are repelled by a magnet whilst paramagnetic substances are attracted by a magnet and hence can be concentrated by a magnetic separator and are said to have low and high magnetic susceptibility respectively. Magnetic susceptibility is a measure of the magnetic response of a mineral to an external magnetic field (Hunt et al., 1995) and can be expressed either as volume susceptibility or as mass susceptibility. The volume/mass susceptibility is the ratio of the material magnetization per unit volume/mass to the external magnetic field. A third group of materials and minerals which is a special case of paramagnetic is ferromagnetic in which the magnetism acquired by such mineral/element/material is much stronger and hence can be attracted by lower magnetic intensity i.e. they have very high magnetic susceptibility. The recovery from a magnetic separation therefore depends on the magnetic susceptibility of the mineral in question, the applied magnetic field strength and the magnetic field gradient. The force on a particle in a magnetic field of field strength F is given by (Svoboda, 1987);

$$F = V\,(S_p - S_m)H\,\frac{dH}{dl} \qquad (9.1)$$

Where V is the volume of the particle, S_p and S_m are the magnetic susceptibility of the particle and the medium it is in respectively; H is the magnetic field intensity and $\frac{dH}{dl}$ is the magnetic field gradient. Equation 9.1 indicates that the magnetic force experienced by a particle decreases with decreasing grain size. The chemical formula and magnetic susceptibility of the iron oxides are given in Table 9.1 and we can see that magnetite has by far the highest magnetic susceptibility.

Table 9.1 Magnetic susceptibility of the main iron oxides (Modified from Hunt et al., 1995).

Mineral	***Chemical Formula***	***Volume Susceptibility (10^{-6} SI)***
Magnetite	Fe_3O_4	1,000,000-5,700,000
Hematite	α-Fe_2O_3	500-40,000
Goethite	α-FeOOH	1,100-12,000

9.2.1 Davis tube magnetic test

The Davis Tube Magnetic Test was mainly used to determine the magnetic content in the samples. It was invented by Edward W Davis in 1921 (US patent No. US1474624 A) (Schulz, 1964) to judge how effective magnetic separation of an ore would be. This information is useful in setting up magnetic separation plants in a mine environment. It consists of a glass tube oriented for this study at 45^{o} between the poles of electromagnets. When the current is switched on, an electric motor causes the glass tube to be agitated in a forward and backward motion along with some rotation. Varying magnetic field intensity can be produced by varying the current. For this research, the magnetic field intensity was set at 0.60 Tesla (6000 Gauss). This magnetic field is relatively low and as such is mainly suitable for magnetite recovery as magnetite is ferromagnetic and has a higher magnetic susceptibility than goethite and hematite which are mainly paramagnetic even though hematite may have both paramagnetic and ferromagnetic behaviour (Table 9.1).

The glass tube was filled with water so that the magnet poles are covered and the magnets switched on. Twenty grams of each sample, accurately weighed were mixed into slurry and poured into the glass tube. The tube was then sealed using a rubber bung. A steady flow of water at 8 cm^3/min was passed through the tube as it was being agitated until the non to weakly magnetic material (tailings) and slimes or cloudiness were washed out of the tube whilst the clean magnetic materials (concentrate) were attracted and held to the magnetic zone between the poles. Five minutes was allowed for the saprolite material and 3 minutes for the BIF due to the cloudiness of the saprolite material caused mainly by its Al oxide / hydroxide content. The magnetic materials were washed into an evaporation pan when the magnet field was turned off. The magnetic material was then dried and weighed and the percentage of magnetic materials (mass recovery) and concentrate characteristic determined. The glass tube was cleaned after each sample analysis. The experimental conditions are shown in Table 9.2

Table 9.2 Davis tube magnetic tester experimental conditions.

Sample weight	*Water flow rate*	*Magnetic intensity*	*Oscillation*	*Time*
20 g	8 cm^3/min	0.60 Tesla	80 strokes per minute	3 minutes for BIF 5 minutes for saprolite

9.2.2 Wet High Intensity Magnetic Separation

The tailings from the Davis tube analysis were passed through a laboratory Wet High Intensity Magnetic Separator (WHIMS) Type LHW in order to collect the weakly magnetic materials. Unlike the DTR which is a grid free, flow-through magnetic separator, the WHIMS consists of a grid in a holder which is slid into an aperture between electromagnetic poles. When the current is switched on, a magnetic field is created between the poles. For this research, the field strength was set at 1.2 Tesla which is twice the field strength used in the DTR experiment. The 1mm grid was used and the flow rate was set at 50 cm^3/min using a flow meter. As the water flows through the grid the non-magnetics were washed away and collected whilst the magnetics were attracted to the grid. After 2 minutes, the electric current was switched off and the magnetics washed from the grid and collected. These were dried and weighed so that the percentage recovery could be calculated. After each sample, the grid was thoroughly cleaned with water and compressed air to make sure no particle was trapped with the potential to contaminate other samples.

A review of magnetic separation including principle, devices and applications and recent developments can be obtained from Oberteuffer (1974) and Svoboda and Fujita (2003).

9.3 Results and Discussions

9.3.1 Analytical errors

Experimental errors could be classified as pre-analytical (before analysis), analytical (during analysis) and post analytical (after analysis). Pre-analytical errors include poor sample preparation and sample bias during the division of samples into subsamples. Analytical errors can be induced by things like wrong

labelling of samples to following wrong analytical procedures, not using the most appropriate instrument settings and changing the settings for re-runs. There could also be problems with the equipment due to lack of maintenance. Analytical errors could be divided into random and systematic errors. Random errors affect the reproducibility of the experimental results due to things like instability of the equipment. A significant proportion of analytical errors are introduced at the sampling stage – either because samples are of poor quality, too few or too small.

Analytical errors were checked by running 10 samples from the original twenty for a second time and comparing the results obtained in both experiments. Potential errors may be due to the sampling process as the same instrumental conditions were used. Even though the samples are essential the same, the experiments carried out are destructive meaning that exactly the same sample cannot be analyzed again. A second batch has to be used. Analytical errors in this work were calculated as the differences in percentage recovery between the separate runs of the tests. They were found to be < 9 % for the DTR and < 15 % for the WHIMS. The error bars are inserted on Figures 9.1 and Figures 9.3. Figures 9.2 and Figures 9.4 were plotted using the same data as Figures 9.1 and 9.3 respectively and as such error bars were not inserted on them. The analytical errors were in general found to decrease with increasing grain size, i.e. the errors in the -63/+45 µm are higher than those in the -250/+180 µm fraction. This may be due to the variability in the samples introduced due to larger number of particles (grains) in the smaller size fractions and their increased liberation.

9.3.2 Davis tube recovery (DTR)

Below are plots comparing the recovery from the Davis Tube test to the magnetite content (wt %) of the samples obtained by QEMSCAN®. In Figure 9.1, regression analysis was used to work out the correlation between the wt % of magnetite (QEMSCAN® in plot) and the recovery of magnetic material from the DTR (DTR in plot). The correlation is best for the -65/+45 µm and this is due to the fact that this fraction is the most liberated, being the smallest.

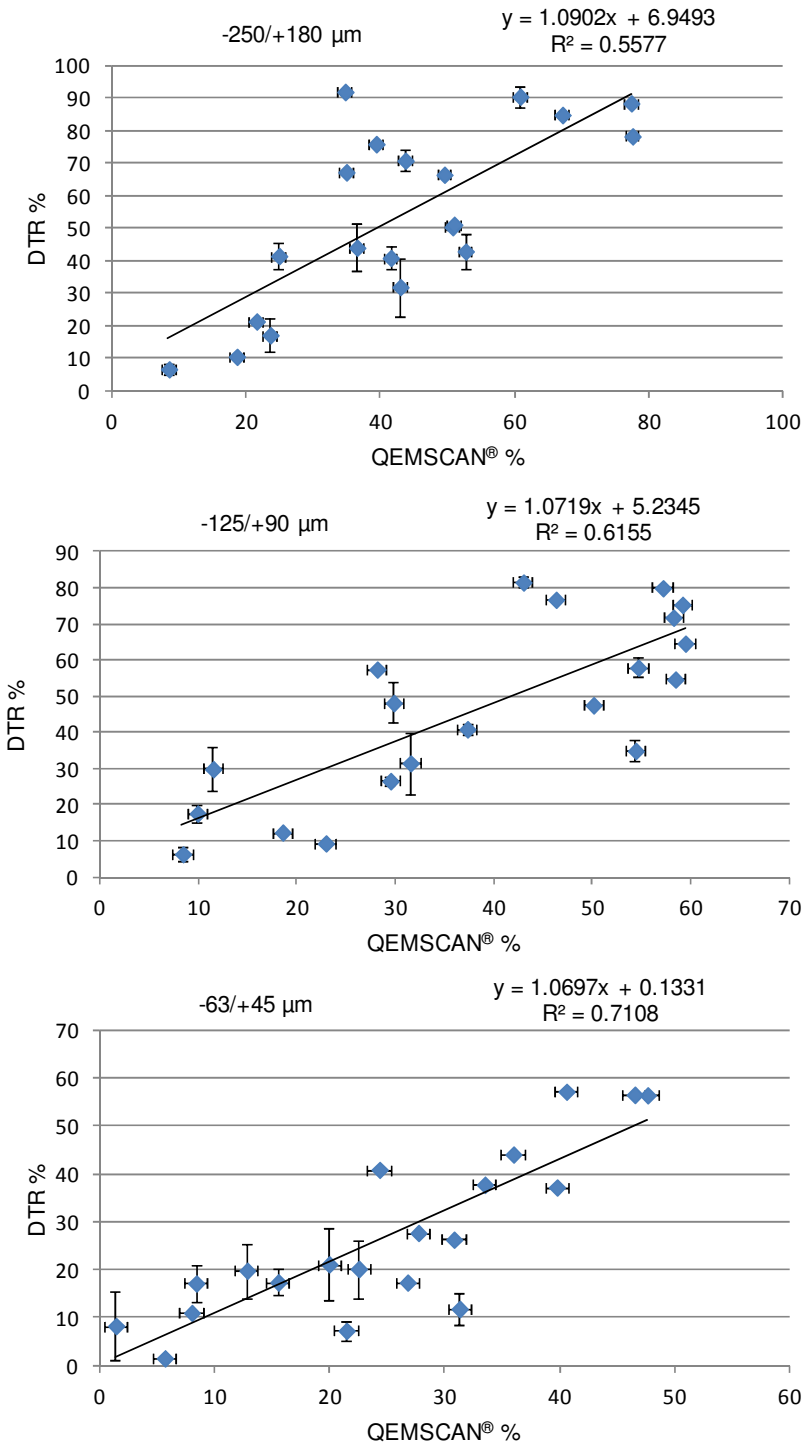

Figure 9.1 Relationship between magnetite wt % from QEMSCAN® to mass recovery of magnetic materials using DTR (%). Error bars show the difference in DTR recovery between the first and re-run of the analysis. The QEMSCAN® analysis was not repeated and as such error bars are not given for it.

On the contrary, the correlation of the recovery of the magnetics to that of the magnetite content obtained for the coarsest size fraction i.e. -250/+180 µm is the least with that for the -125/+90 µm lying in between the 2 extremes. The correlation is therefore related to the grain size. In most cases the recovery of

the highly magnetic material is higher than that of the QEMSCAN® magnetite but some discrepancies stand out and these are explained using Figure 9.2 which shows the samples and both the DTR recovery and magnetite content obtained from the QEMSCAN®. For the -63/+45 µm size fraction (Figure 9.2), samples NES01, LB01, LB03, LB04 gave much higher recoveries than the magnetite content obtained from the QEMSCAN® study whilst samples G03, LB06 and LB07 gave lower recoveries than the QEMSCAN®.

A combination of modal mineralogy, mineral association and mineral liberation can be used to explain these discrepancies. The modal mineralogy in this case is basically the percentage mass of a particular mineral in a sample and is density weighted. The mineral association is a measure of the adjacency of minerals in a sample i.e. which mineral is in contact with another in a particle and is displayed as a percentage. The data for mineral associations are not reciprocal because each mineral has its own unique associations and the data columns are independent from each other. For example, mineral X may be found mainly included in, and therefore associated with, mineral Y but mineral Y may be next to mineral Z, and several others, as well as having small inclusions of mineral X. The mineral liberation provides liberation data for particular size fractions of a sample and the liberation categories are set at 10 % intervals. The liberation data should be used with the modal mineralogy for it to be useful as the quantity of a particular mineral in a sample determines whether the liberation data is important.

From Table 9.3, the main minerals in the BIF samples LB01, LB03 and LB04 are magnetite, goethite, quartz and the Ca Mg Fe silicates whilst for the saprolite sample NES01, they are magnetite goethite and hematite. The BIF samples have a higher magnetite content but the saprolite sample have a higher goethite and hematite content. From Table 9.4, the main association of magnetite in the BIF samples is overwhelmingly with goethite i.e. 85.06 %, 84.79 % and 84.72 % for LB01, LB03 and LB04 respectively.

The association of magnetite and goethite is comparatively less for NES01. It is also seen from these data in Table 9.4 that magnetite does not have any

association with the main gangue minerals of quartz and the Ca Mg Fe silicates which occurs mainly as high grade intergrown and liberated grains (Table 9.5).

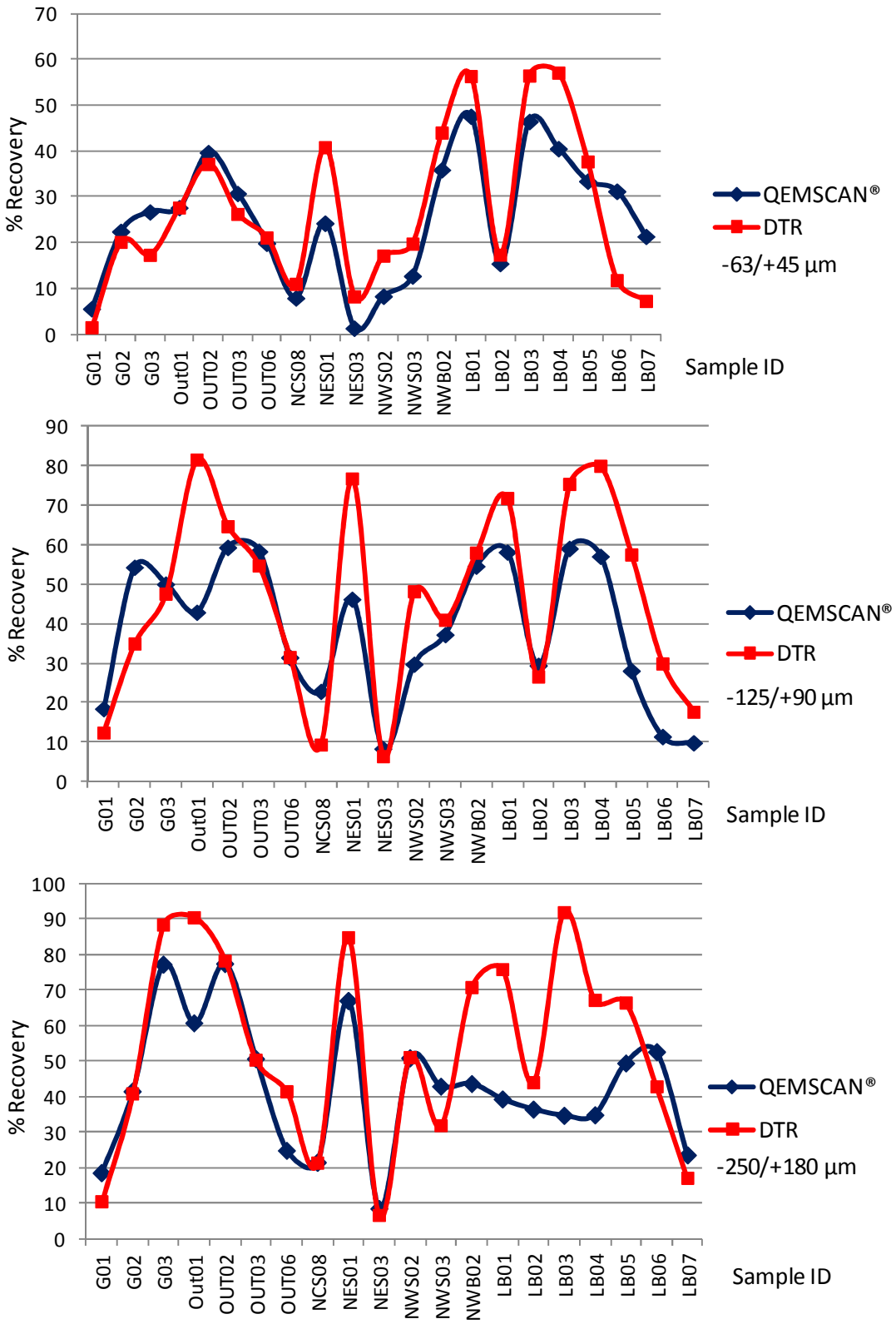

Figure 9.2 Correlation between the Davis tube recoveries and the magnetite content obtained from the QEMSCAN® analysis. a) -63/+45 µm, b) -125/+90 µm, c) 250/+180 µm.

Table 9.3 The major mineral composition of samples (-63/+45 µm) with higher recoveries than expected.

Sample	*Magnetite*	*Goethite*	*Hematite*	*Quartz*	*Ca Mg Fe Silicates*
LB01	47.61	18.40	0.80	21.57	8.07
LB03	46.48	20.46	1.32	21.30	7.29
LB04	40.55	25.70	1.46	1.61	13.98
NES01	24.28	38.50	10.66	0.31	0.01

Table 9.4 Mineral associations for four samples from the -63/+45 µm size fraction with higher recoveries than expected (read down column then across row (left) for each mineral).

		Magnetite	*Hematite*	*Goethite*	*Quartz*	*Ca Mg Fe Silicates*
LB01 -63/+45 µm	Magnetite	0.00	55.28	46.81	0.01	0.07
	Hematite	5.21	0.00	2.07	0.00	0.00
	Goethite	***85.06***	39.88	0.00	0.10	0.41
	Quartz	0.00	0.00	0.03	0.00	7.86
	Ca Mg Fe Silicates	0.01	0.00	0.05	2.62	0.00
LB03 -63/+45 µm	Magnetite	0.00	55.80	45.42	0.00	0.04
	Hematite	8.21	0.00	3.21	0.00	0.00
	Goethite	***84.79***	40.79	0.00	0.12	0.72
	Quartz	0.00	0.00	0.04	0.00	10.13
LB04 -63/+45 µm	Magnetite	0.00	53.05	38.40	0.00	0.06
	Hematite	8.31	0.00	3.05	0.00	0.01
	Goethite	***84.72***	42.95	0.00	0.23	1.86
	Quartz	0.00	0.00	0.01	0.00	0.44
NES01 -63/+45 µm	Magnetite	0.00	64.67	20.71	0.00	0.00
	Hematite	53.72	0.00	14.82	0.00	0.00
	Goethite	***44.10***	32.05	0.00	0.00	0.00
	Quartz	0.00	0.00	0.00	0.00	0.00

The magnetite and goethite on the contrary mainly occurs in the low grade intergrown category. The conclusion is that the goethites are responsible for the higher DTR recovery as they are attached to the magnetite being attracted to the magnetic force. The relatively low association between magnetite and goethite for sample NES01 is compensated by the relatively higher quantity of goethite present. The relatively high association of hematite with magnetite (Table 9.4) along with its very low liberation (locked) does not count for much in the BIF samples as its mass percentage in the modal mineralogy (Table 9.3) is small (< 2 %) and as such will make little contribution to the recovery.

Table 9.5 Mineral liberation data for 4 samples with higher than expected recoveries.

		≤ 30 %	> 30 % ≤ 60 %	> 60 % ≤ 90 %	> 90 %
LB03 -63/+45 µm	Magnetite	2.39	29.72	67.90	0.00
	Goethite	30.22	57.80	8.81	3.18
	Hematite	100.00	0.00	0.00	0.00
	Ca Mg Fe Silicate	5.86	4.81	13.29	76.04
	Quartz	2.43	2.77	11.91	82.88
LB03 -63/+45 µm	Magnetite	2.39	29.72	67.90	0.00
	Goethite	30.22	57.80	8.81	3.18
	Hematite	100.00	0.00	0.00	0.00
	Quartz	2.43	2.77	11.91	82.88
LB04 -63/+45 µm	Magnetite	5.58	47.40	47.03	0.00
	Goethite	19.35	57.58	18.67	4.40
	Hematite	99.98	0.02	0.00	0.00
	Quartz	7.05	8.43	37.53	47.00
NES01 -63/+45 µm	Goethite	15.97	40.53	39.93	3.57
	Magnetite	18.54	79.00	2.46	0.00
	Hematite	97.44	2.56	0.00	0.00

A closer look at the samples which gave lower recovery than the QEMSCAN® suggested shows that they have much less magnetite than those discussed above and magnetite is not the most abundant mineral (Table 9.6). In samples G03 and LB07, the most abundant minerals are not even iron oxides but quartz and andradite respectively whilst goethite is the most abundant in LB06. It is possible that these other minerals had a part in masking the fewer magnetites in the tube causing some to be washed away with them. This process could have been aided by the relatively small size of the grains and the resulting lower magnetic force felt by them (Equation 9.1) The Davis tube experiments were repeated and the difference noticed was within 9 % meaning that these high and low recoveries were not experimental errors.

Table 9.6 The major mineral composition of samples (-63/+45 µm) with lower recoveries than expected from the Davis tube.

ID	Mag	Gt	Hem	Chm	Qtz	Adr	Fe Mg Sils	Ca Mg Fe Sils	Ca Fe Al Sils
G03	26.72	21.59	4.91	1.11	43.83	0.00	1.19	0.02	0.01
LB06	31.24	31.90	6.50	18.52	8.15	0.01	0.77	0.16	0.02
LB07	21.40	21.19	5.77	0.04	16.46	23.93	1.73	3.00	2.92

Adr – andradite, Chm – chamosite, Gt – goethite, Hem – hematite, Mag – magnetite, Qtz – quartz, Sils - silicates

These criteria used to explain the discrepancies in the -63/+45 µm fraction as expected are more pronounced in the -250/+180 µm size fraction due to the increased grain size of the particles. The samples that gave higher recoveries than suggested by the QEMSCAN® are more or less the same ones as in the -63/+45 µm. The main difference between the two size fractions is that the recovery for those samples that gave lower than suggested by the QEMSCAN® in the -63/+45 µm fraction gave recoveries almost as suggested for the -250/+180 µm. This supports the arguments that these lower recoveries were due to the small particle size and lower magnetite concentration. In general, the magnetite concentration increases with grain size.

9.3.3 Wet high Intensity magnetic separation

As the tailings from the DTR were passed through the WHIMS and the recovery measured, it is expected that the recoveries from the DTR may affect that obtained from the WHIMS. The WHIMS recovery has been compared to the sum of the hematite, goethite and chamosite present in the samples as obtained from the QEMSCAN® analysis. These are the minerals expected not to have been concentrated by the Davis tube and were the main reason for the high intensity separation. In Figure 9.3, regression analysis is used to work out the correlation between the wt % of the sum of hematite, goethite and chamosite (QEMSCAN® in plot) and the recovery of magnetic material from the WHIMS (WHIMS in plot) The correlation is about the same obtained for the DTR for the -250/+180 µm fraction but lower for the other size fractions which shows about the same correlation.

In terms of the individual samples, the graphs of the -125/+90 and -250/+180 (Figure 9.4) µm are very similar in having lower WHIMS recovery for samples Out01, NES01, NES03 and higher WHIMS recovery for LB02. In the case of Out01 and NES01, they had already had a higher recovery using the DTR due to the high association of the goethite and magnetite and as such have lower WHIMS recovery than expected. The reason for the other discrepancies can be found in the modal mineralogy. In the case of NES03, the most abundant mineral in both these size fractions is chamosite which is known to have lower magnetic susceptibility than the Fe oxides and the low recovery suggests that

the applied magnetic force should be increased to attract all the chamosite if necessary.

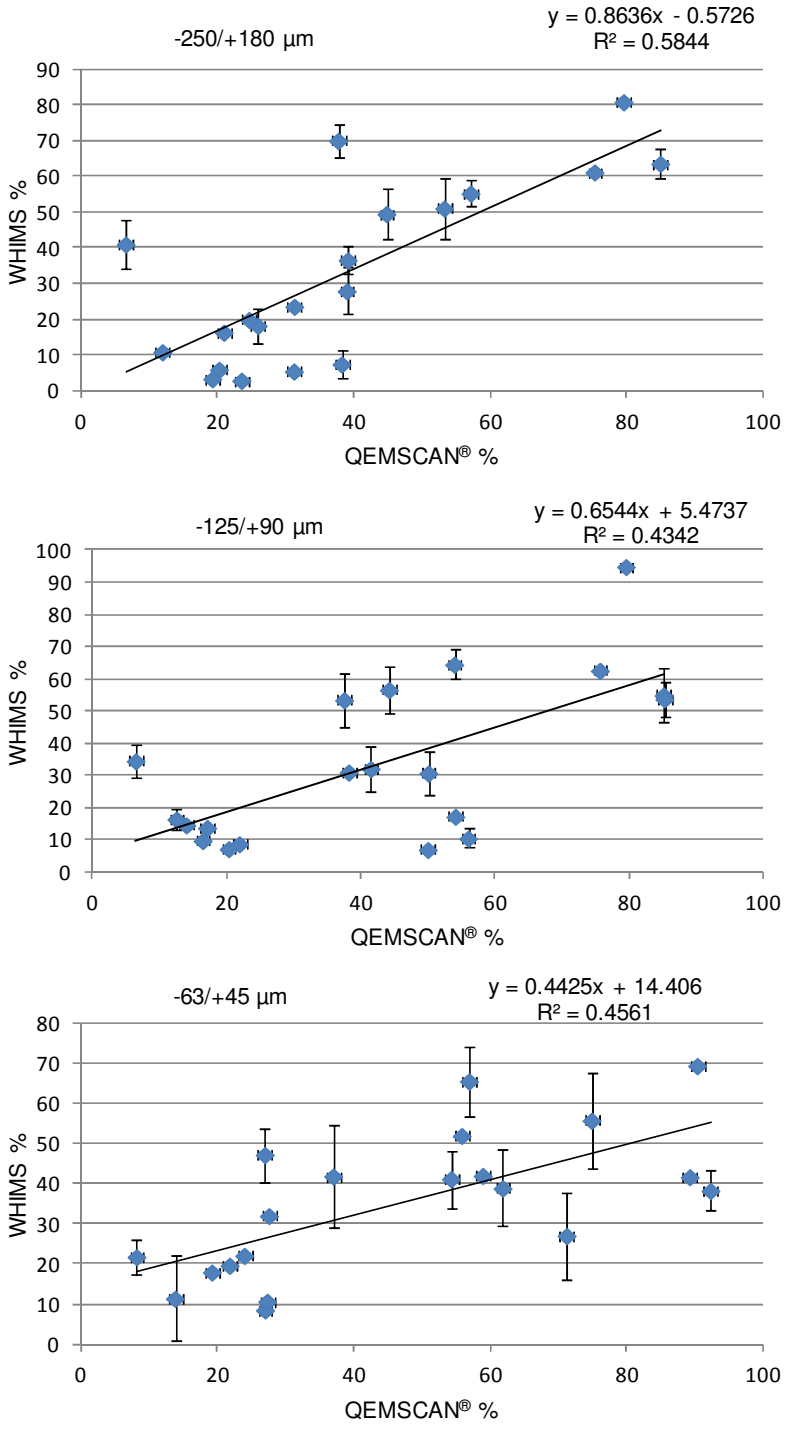

Figure 9.3 Relationship between the sum of hematite, goethite and chamosite wt % from QEMSCAN® to recovery of magnetic materials using WHIMS (%). Error bars show the difference in WHIMS recovery between the first and re-run of the analysis.

Achieving the right balance is by trial and error as for a higher magnetic intensity, the Fe silicates (in this case Ca Mg Fe silicates and biotite) could also be attracted and recovered as is the case for LB02 which gave higher recover

than expected. This is shown in Figure 9.4 and Table 9.7 which gives the modal mineralogy for samples NES03 and LB02 for the two size fractions.

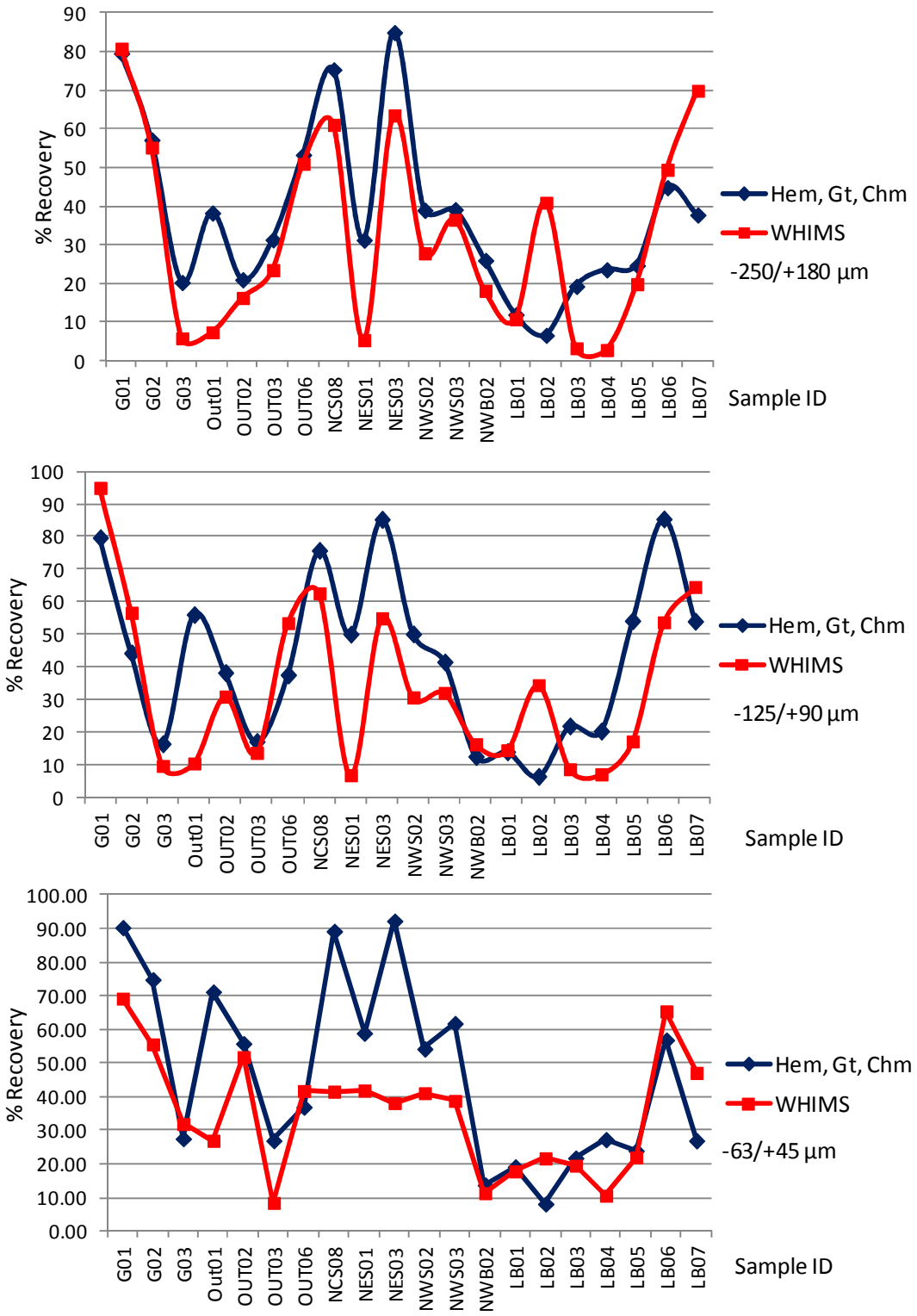

Figure 9.4 Correlation between the WHIMS and the sum of the hematite (Hem), goethite (Gt) and chamosite (Chm) content obtained from the QEMSCAN® analysis. a) -250/+180 µm, b) -125/+90 µm, c) -63/+45 µm.

The major difference between the two graphs is in the recovery of the samples LB06 and LB07. From Table 9.7 it is seen that the -125/+90 µm fraction of LB06, has hematite and goethite as its major minerals whist magnetite is the major mineral in the -250/+180 µm fraction. As we would see in the case of the -63/+45 µm, the magnetic intensity used was not enough to concentrate all the goethite present in the smaller size fractions. The andradite content (Table 9.7) is responsible for the higher recovery seen in sample LB07. Note that andradite is a Fe rich garnet with formula $Ca_3Fe^{2+}_2(SiO_4)_3$ and as such it is attracted by the high intensity magnetisation. Furthermore andradite is associated mainly with the goethite but also with magnetite and hematite (Table 9.8).

Table 9.7 Selected modal mineralogy showing reasons for similarity and differences between the recoveries for the -250/+180 µm and -125/+90 µm size fractions.

ID	Mag	Gt	Hem	Chm	Qtz	Bt	Ca Mg Fe Sils	Adr	Fe Mg Sils
LB02 (-250/+180 (µm)	36.42	5.57	0.32	0.71	29.28	5.34	***16.09***	0.04	0.47
LB02 (-125/+90 µm)	29.44	5.67	0.33	0.45	39.70	5.11	***14.23***	0.02	0.37
LB06 (-250/+180 µm)	52.59	24.24	11.21	9.38	1.17	bdl	0.03	bdl	0.46
LB06 (-125/+90 µm)	11.43	***36.58***	***38.80***	9.93	1.94	bdl	0.01	0.03	0.44
LB07 (-250/+180 µm)	23.53	19.09	18.62	0.03	9.64	0.05	1.84	***22.02***	1.40
LB07 (-125/+90 µm)	9.84	25.31	28.62	0.03	8.05	0.05	1.92	***21.54***	1.28
NES03 (-250/+180 µm)	8.36	14.98	1.15	***68.82***	3.42	0.01	bdl	bdl	0.22
NES03 (-125/+90 µm)	8.29	15.92	2.20	***67.06***	3.67	0.01	bdl	bdl	0.23

Adr – andradite, Bt - biotiteChm – chamosite, Gt – goethite, Hem – hematite, Mag – magnetite, Qtz – quartz, Sils - silicates

Table 9.8 The association of andradite and the Fe oxides in sample LB07 (-250/+180 µm).

	Magnetite	Hematite	Goethite	Andradite
Magnetite	0.00	52.51	22.18	6.17
Hematite	50.93	0.00	20.86	5.91
Goethite	37.79	36.65	0.00	***30.10***
Andradite	4.68	4.62	13.39	0.00

The -63/+45 µm fraction (Figure 9.4) displays a marked difference between the expected hematite, goethite + chamosite total and the WHIMS recovery compared to the other two size fractions. These marked difference can be seen for the following samples; G01, G02, Out01, NCS08, NES03, G01, NWS03.

A close look at the modal mineralogy of theses samples show that all have goethite as their most abundant mineral with the exception of NES03 which has chamosite as its most abundant mineral (Table 9.9). It is possible that the magnetic intensity used was not enough to attract all the smaller liberated goethite grains. On the contrary, the magnetic intensity was enough to attract the Ca Mg Fe silicates in the sample LB02 (Figure 9.4, Table 9.9) resulting in a higher than expected recovery.

Table 9.9 The major mineral composition of samples (-63/+45 µm) with lower recoveries than expected from the WHIMS.

ID	*Goethite*	*Magnetite*	*Hematite*	*Chamosite*	*Quartz*	*Ca Mg Fe Silicates*	*Biotite*
G01	***86.61***	5.59	3.68	0.08	0.01	bdl	bdl
G02	***62.95***	22.47	11.62	0.22	0.02	bdl	bdl
LB02	6.98	15.46	0.21	1.01	42.59	***15.53***	10.50
NCS08	***68.09***	7.94	11.30	9.88	0.19	bdl	bdl
NES03	13.76	1.34	0.90	***77.64***	2.48	0.01	0.01
NWS03	***39.43***	12.75	3.35	19.06	17.24	0.04	0.02
Out01	***37.42***	27.66	9.38	24.44	0.56	0.01	bdl

9.4 Concentrate grades

Three size fractions of the concentrates of 10 samples from the WMI, TMI, HMI, and LMI material types were sent for XRF analysis. The samples analysed can be broadly divided into saprolite and fresh BIF samples. The saprolite samples are G01, Out01, NES03, NWS02, NWS03, LB05 and LB07 whereas the fresh BIF samples are NWB02, LB01 and LB02. As the aim of the magnetic separation was to concentrate the Fe rich particles, the focus of the discussion will be on the Fe % of the concentrates and not the other deleterious elements. The XRF data for the size fractions that gave the highest Fe % in the concentrate are shown in Table 9.10. There is a general decrease in the SiO_2, Al_2O_3, P and LOI percentages for the concentrates compared to the head grade whilst Fe increases from the head grade to the concentrate as expected. Factors that can potentially affect the grade of the concentrates include the

modal mineralogy, mineral associations, liberation of the Fe rich grains and the head grade.

Table 9.10 X-ray florescence data for feed and concentrated products. Loss on ignition was conducted at 1000°C.

ID		SiO_2 %	Al_2O_3 %	Fe %	P %	S %	LOI %
G01	Head	4.36	5.89	*56.29*	0.86	0.02	11.17
	Conc (-125/+90)	0.28	3.96	*59.10*	0.61	0.02	5.65
Out01	Head	7.02	5.06	*58.33*	0.08	0.02	4.67
	Conc (-125/+90)	3.09	1.39	*66.58*	0.06	0.01	0.59
NES03	Head	17.10	16.15	*37.64*	0.06	0.04	11.51
	Conc (-63/+45)	12.80	12.10	*45.02*	0.07	0.03	7.77
NWS02	Head	8.00	15.85	*44.91*	0.04	0.03	11.23
	Conc (-125/+90)	3.66	3.31	*63.37*	0.04	0.01	3.68
NWS03	Head	17.15	2.50	*50.43*	0.18	0.05	7.51
	Conc (-63/+45)	5.51	1.41	*62.99*	0.08	0.02	2.82
NWB02	Head	44.90	0.09	*35.61*	0.02	<0.001	1.65
	Conc (-63/+45)	3.40	0.08	*67.71*	0.02	0.01	-0.31
LB02	Head	66.80	3.03	*15.83*	0.05	0.13	0.10
	Conc (-63/+45)	4.49	0.09	*68.64*	0.01	0.27	-2.49
LB05	Head	38.60	0.11	*41.99*	0.06	<0.001	1.11
	Conc (-63/+45)	15.05	0.16	*57.12*	0.05	0.00	0.14
LB07	Head	25.80	0.28	*45.27*	0.08	0.00	0.71
	Conc (-63/+45)	14.55	0.44	*53.42*	0.03	0.01	0.55

Conc - Concentrate

Table 9.11 gives the liberation of the Fe oxides (QEMSCAN®), the recovery of the Fe oxides as obtained from the DTR and WHIMS and the head and concentrate grades for the 3 size fractions of the 10 samples as obtained from XRF. From the table it is seen that the most favourable grind size for both the fresh BIF and saprolite material types is the -63/+45 µm size fraction even though 3 out of the 7 saprolite samples has the highest Fe wt % in the -125/+90 µm size fraction. The -250/+180 µm fraction has the least grade and liberation percentages of the 3 size fractions analysed. Three samples i.e. NES03, LB05 and LB07 were not upgraded to > 60 % Fe (DSO requirements). In addition samples G01 and NES03 gave the least increase between the Fe wt % from the head to the concentrate grades which is an indication of potential metallurgical challenges that could be faced when processing similar materials.

Graphs of head grade, liberation and recovery vs concentrate grades have shown that there is very little or no correlation between them. For example, samples G01 (-125/+90 µm) and LB05 (-63/+45 µm) have high Fe oxide liberations of 97.30 % and 93.13 % respectively. The head grade can not be the reason as the concentrates for sample LB02 has a grade of 68.64 % Fe from a head grade of 15.83 % compared to head grades of 56.29 % for G01, 41.99 % for LB05 and 45.27 % for LB07. The reasons for these discrepancies are found in the modal mineralogy (Table 9.12) of the samples and the type of magnetic separation done. For samples G01, NES03, LB05 and LB07, the concentrations from the WHIMS were added to that of the DTR as they are known to contain significant amounts of goethite, hematite and as is the case for NES03, chamosite. Concentrates from the DTR comprises mainly of magnetite and as such gave high Fe wt % whilst the WHIMS may have concentrated Fe silicates along with the hematite goethite and chamosite or may not have concentrated all the goethite and hematite with both scenarios resulting in lower Fe wt %. In the case of LB01 LB02 and NWB02, only the DTR concentrates were sent for XRF analysis as they were considered to be fresh BIF samples lacking or having only minor or trace amount of goethite and/or hematite.

From Table 9.12, it is seen that sample G01 consist of about 75 % goethite which has the lowest Fe % of the three Fe oxides and this is the reason why the Fe % of its concentrate is not as high as those of the fresh BIF samples. The Fe oxides liberation (97.30 %) and recovery (97.65 %) values for the -125/+90 size fraction for this sample are very high meaning that the modal mineralogy is the cause for its < 60 % Fe concentrate grade. For NES03, the highest ore grade achieved was for the -63/+45 µm fraction and was 45 % Fe. This is very low compared to the Fe % achieved for the other samples. The main reason for this is that from the modal mineralogy, we see that this sample consist of 68.82 % chm, 67.06 % chm and 77.64 % chm (Table 9.12) for the -250/+180 µm, -125/+90 µm and -63/+45 µm fractions respectively. The liberation of the Fe oxides in this sample ranges from 22 % to 44 % whilst that of the chamosite ranges from 83 % to 86 %. High percentage modal mineralogy combined with high liberation means that the ore is mainly chamosite and hence low grade. Further work is needed to find the optimum beneficiation route for the chamosite rich material.

Table 9.11 Head grade, liberation, recovery and ore grade for the three size fraction of the 10 samples analysed.

		-63/+45 µm			***-125/+90 µm***			***-250/+180 µm***		
Sample ID	***Head Grade (wt% Fe)***	***Liberation (Fe Oxide)***	***Recovery (%)***	***Ore Grade (wt% Fe)***	***Liberation (Fe Oxide)***	***Recovery (%)***	***Ore Grade (wt% Fe)***	***Liberation (Fe Oxide)***	***Recovery (%)***	***Ore Grade (wt% Fe)***
G01	***56.29***	92.76	70.83	***58.35***	***97.30***	97.65	***59.10***	96.98	91.24	***57.89***
Out01	58.33	75.84	54.69	***59.84***	80.72	92.04	***66.58***	76.04	97.85	***65.03***
NES03	***37.64***	22.56	46.50	***45.02***	42.91	61.33	***41.53***	44.11	70.13	***40.64***
NWS02	44.91	71.33	58.32	***54.83***	82.09	78.91	***63.37***	81.87	78.91	***60.14***
NWS03	50.43	86.41	58.67	***62.99***	96.80	73.02	***60.65***	96.36	68.40	***55.16***
NWB02	35.61	94.45	55.44	***67.71***	94.64	74.34	***61.99***	93.79	88.89	***45.44***
LB01	38.27	97.61	74.30	***68.99***	91.50	86.35	***55.75***	59.32	86.65	***30.89***
LB02	***15.83***	98.03	39.15	***68.64***	97.21	61.05	***53.64***	94.78	84.93	***37.37***
LB05	***41.99***	***93.13***	59.80	***57.12***	84.71	74.70	***53.41***	58.77	86.30	***45.18***
LB07	***45.27***	81.96	54.45	***53.42***	70.48	82.15	***51.42***	47.61	87.00	***47.75***

Table 9.12 Modal mineralogy for the optimum size fractions for the samples whose concentrates were analysed by XRF.

ID	***Size fraction***	***Gt (Al)***	***Gt/Lm***	***Hem***	***Mag***	***Chm***	***Adr***	***Al Ox/OH***	***Qtz***	***Ca Mg Fe Sils***	***Ca Fe Al Sils***	***Fe Mg Sils***
G01	-125/+90 µm	48.78	27.15	2.80	18.31	0.04	< 0.01	1.90	< 0.01	< 0.01	< 0.01	< 0.01
NES03	-63/+45 µm	8.70	5.06	0.90	1.27	77.64	< 0.01	2.39	2.48	< 0.01	< 0.01	0.38
NWS02	-125/+90 µm	5.45	23.36	6.89	29.73	14.38	< 0.01	14.59	1.53	< 0.01	< 0.01	< 0.01
NWS03	-63/+45 µm	7.26	32.14	3.35	12.75	19.06	< 0.01	0.85	17.24	< 0.01	< 0.01	0.21
Out01	-125/+90 µm	25.02	2.56	14.62	42.82	13.84	< 0.01	0.02	0.73	< 0.01	< 0.01	0.02
NWB02	-63/+45 µm	< 0.01	12.26	1.54	35.93	0.03	< 0.01	< 0.01	29.10	10.52	0.24	9.33
LB01	-63/+45 µm	< 0.01	18.40	0.80	47.56	< 0.01	< 0.01	< 0.01	21.57	8.07	0.12	0.43
LB02	-63/+45 µm	< 0.01	6.97	< 0.01	15.46	1.01	< 0.01	< 0.01	42.59	15.53	1.05	0.42
LB05	-63/+45 µm	0.14	21.15	2.21	33.43	0.41	< 0.01	< 0.01	34.05	4.40	0.08	2.67
LB07	-63/+45 µm	< 0.01	21.18	5.77	21.40	< 0.01	23.93	< 0.01	16.46	3.00	2.92	1.73

In the case of LB07 the highest ore grade was achieved for the -63/+45 µm at 53.42 % Fe from a feed grade of 45.27 % Fe. From the modal mineralogy, it is seen that andradite has a concentration ranging from 23.93 % which is significant. It is possible that some of this Fe rich garnet was concentrated using the WHIMS. Low intensity may have been used alone for this magnetic separation but this sample is known to consist of significant concentration of hematite and goethite which requires high intensity magnetic separation.

For the LB05, the -63/+45 µm has the highest Fe grade i.e. 57.12 % Fe. It is seen that even though quartz is the most abundant mineral in this size fraction, the Fe oxides has the highest liberation (93.13 %) compared to 84.71 % for the -125/+90 µm and 58.77 % for the -250/+180 µm. Notwithstanding this seemingly high liberation of the Fe oxides, goethite/limonite is 6.36 % associated with the Fe Mg silicates whilst they are 26.97 % associated with goethite/limonite, 17.59 % associated with quartz and 14.37% associated with clinochlore. As such it is most likely that the WHIMS concentrated some of the Fe Mg silicates along with their associated minerals. The relatively low liberation of the Fe oxides in Out01 is a reflection of their association with chamosite which has a concentration of 13.84 (Table 9.12). This clearly does not affect the grade as the Davis tube and WHIMS were able to concentrate the Fe oxides. Even though one of these samples has a grade of 61.99 % Fe for the -125/+90 µm fraction, the equivalent ore grade for the -63/+45 µm fraction is 67.71 % Fe.

Table 9.13 gives the average grade, recovery of magnetic material and chemistry for the optimum size fraction for the various material types. The most favourable size fraction for the WMI material type is the -125/+90 µm. It has the lowest Al_2O_3 (1.96 %), the highest Fe (62.11 %), lowest P (0.23 %) and TiO_2 (0.13 %). SiO_2 has its highest concentration for the -250/+180 µm fraction (7.35 %) and the least for the -63/+45 µm fraction (4.24 %). The SiO_2 content in these WMI samples is due mainly to the presence of quartz. Sulphur is lowest for the -125/+90 µm with 0.01 %. LOI is also lowest for this size fraction (2.63 %).

The XRF data for sample NES03 was not included in the calculation of the average composition of the TMI material type because of the various metallurgical challenges

this sample poses. The case of the TMI is similar to that of WMI in that the -125/+90 µm samples has the best properties with Fe % being the highest, Al_2O_3, SiO_2, TiO_2 and LOI all being the lowest (Table 9.13). Both the WMI and TMI has confirmed the suggestion that the optimum grind size for the saprolite material is to -125/+90 µm.

For the fresh BIF i.e. HMI and LMI, the optimum size fraction is the -63/+45 µm. This size fraction has the highest Fe %, lowest Al_2O_3, SiO_2 and P. TiO_2 for this fraction is 0.02 % compared to the 0.01 % for the other two size fractions (Table 9.13). Sulphur is 0.02 % for this fraction but less than 0.01 % for the other 2 size fractions.

Table 9.13 Average grade, recovery of magnetic material and chemistry for the optimum size fraction for the various material types.

Mat Type	Size Frac.	Recov. (%)	Grade (Fe %)	SiO_2	TiO_2	Al_2O_3	Fe_2O_3	P	S	LOI
WMI	-125/90	87.57	62.11	6.30	0.13	1.96	88.80	0.23	0.01	2.63
TMI	-125/90	78.59	56.07	13.82	0.04	1.23	80.16	0.04	0.01	1.51
HMI	-63/+45	64.87	68.35	4.39	0.02	0.08	97.72	0.01	0.02	-1.58
LMI	-63/+45	39.15	68.64	4.49	0.02	0.09	98.14	0.01	0.27	-2.49

Mat – Material, Recov. - Recovery

Recovery decreases from WMI to TMI to HMI to LMI mainly because the hematite and goethite content decreases in the same order to the magnetite itabirite which contains magnetite as by far the major or only Fe oxide. The higher concentration of magnetite in the HMI compared to the LMI is indicated by HMI having a higher recovery than LMI. The goethite content of WMI and TMI is also indicated by their LOI % which is highest for the WMI followed by TMI, HMI and then LMI. Phosphorus is highest for the WMI group which is cause for concern as the P in this material type is found within the goethite as opposed to in a phosphorus rich mineral like apatite as is the case of P in the MI.

9.5 Distribution of Fe

Table 9.14 shows the average Fe oxide and chamosite mineral composition for the various material types present at Nkout. Note that their total wt % decreases from the EM to the LMI. Less than 3 % of EM consists of gangue minerals compared to approximately 60 % in the LMI material class (Table 9.14).

Table 9.14 Average Fe oxide and chamosite composition of the various material types at Nkout.

Material Type	*Magnetite (wt %)*	*Goethite (wt %)*	*Hematite (wt %)*	*Chamosite (wt %)*	*Total (wt %)*
EM	49.29	33.47	9.08	6.13	97.97
WMI	33.07	40.70	8.80	6.80	89.37
TMI	32.13	21.45	6.63	17.27	77.49
HMI	36.15	18.41	6.78	8.20	69.54
LMI	26.06	8.93	3.01	2.84	40.84

These mineral compositions have been converted to Fe wt % based on the ideal Fe wt % present in the minerals as stated in Table 2.1. If the ideal Fe wt % is considered to be for the pure (100 %) mineral, then the % Fe present in the minerals based on their wt % in the material types (Table 9.14) can be estimated. The Fe wt % present in the minerals are given in Table 9.15. To check if identifying these minerals during drill core logging can assist in predicting the grade of the material types, the Fe wt % calculated using these Fe wt % based on the minerals is compared to that obtained from XRF analysis.

It is seen that the mineral composition can give a very good approximation of its XRF Fe grade especially in the weathered material types (EM, WMI and TMI). As the gangue mineral composition increases in the HMI and LMI, the difference between the XRF Fe wt % and that calculated based on the mineral composition increase mainly due to the reduction of the Fe wt % using XRF (bulk mineral technique) due to the gangue minerals.

Distribution models were created for Fe and the main gangue minerals (Figure 4.7). The procedures involved in creating them are explained in section 4.5.2 (stratigraphic reconstruction. In practice, it will be difficult to map the individual mineral composition as accurately as the QEMSCAN® but an approximate value can be obtained much faster using chemistry backed with a few metallurgical tests (e.g. Lund et al., 2013).

Table 9.15 Distribution of Fe wt % within the main Fe minerals in the material types present at Nkout. Note the similarity between the calculated Fe wt % based on the Fe content of the main Fe minerals and that obtained from XRF analysis.

	Magnetite (Fe wt %)	***Goethite (Fe wt %)***	***Hematite (Fe wt %)***	***Chamosite (Fe wt %)***	***Total Mineral (Fe wt %)***	***XRF (Fe wt %)***
EM	35.67	21.04	6.35	1.80	64.86	64.23
WMI	23.93	25.58	6.16	2.00	57.67	56.14
TMI	23.25	13.48	4.64	5.08	46.46	42.08
HMI	26.16	11.57	4.74	2.41	44.88	35.87
LMI	18.86	5.62	2.11	0.84	27.41	19.07

9.6 Multiple linear regression analysis.

Multiple regression is used to predict the value of a variable (dependent variable) based on the value of two or more other variables (independent variables). It also determines the overall fit (variance explained) of the model and the relative contribution of each of the predictors to the total variance explained. For this research, the ore grade is the dependent variable whist the liberation of the Fe oxides, the recovery, the head grade and the wt % composition of the main Fe minerals and gangues i.e. magnetite, hematite, goethite chamosite, quartz and AlOx(OH) in the unprocessed material are considered to be the independent variables. Field (2009) recommended that at least 10 to 15 points (samples) should be available per variable involved in a multiple regression analyses. Only 10 concentrates were analysed for their ore grade (i.e. Fe wt %) and this limited number of samples could limit the effectiveness of the technique and the reliability of the interpretations.

In order to test which of the variables should be included in the multiple regression, scatter plots were made with ore grade plotted against the individual variables. From these plots, it was seen that ore grade has the highest correlation with the liberation of the Fe oxides (%) followed by the wt % of chamosite, magnetite and quartz present in the samples respectively (Figure 9.5). All the other variables gave $R^2 < 0.115$ meaning they do not have any direct correlation with the ore grade.

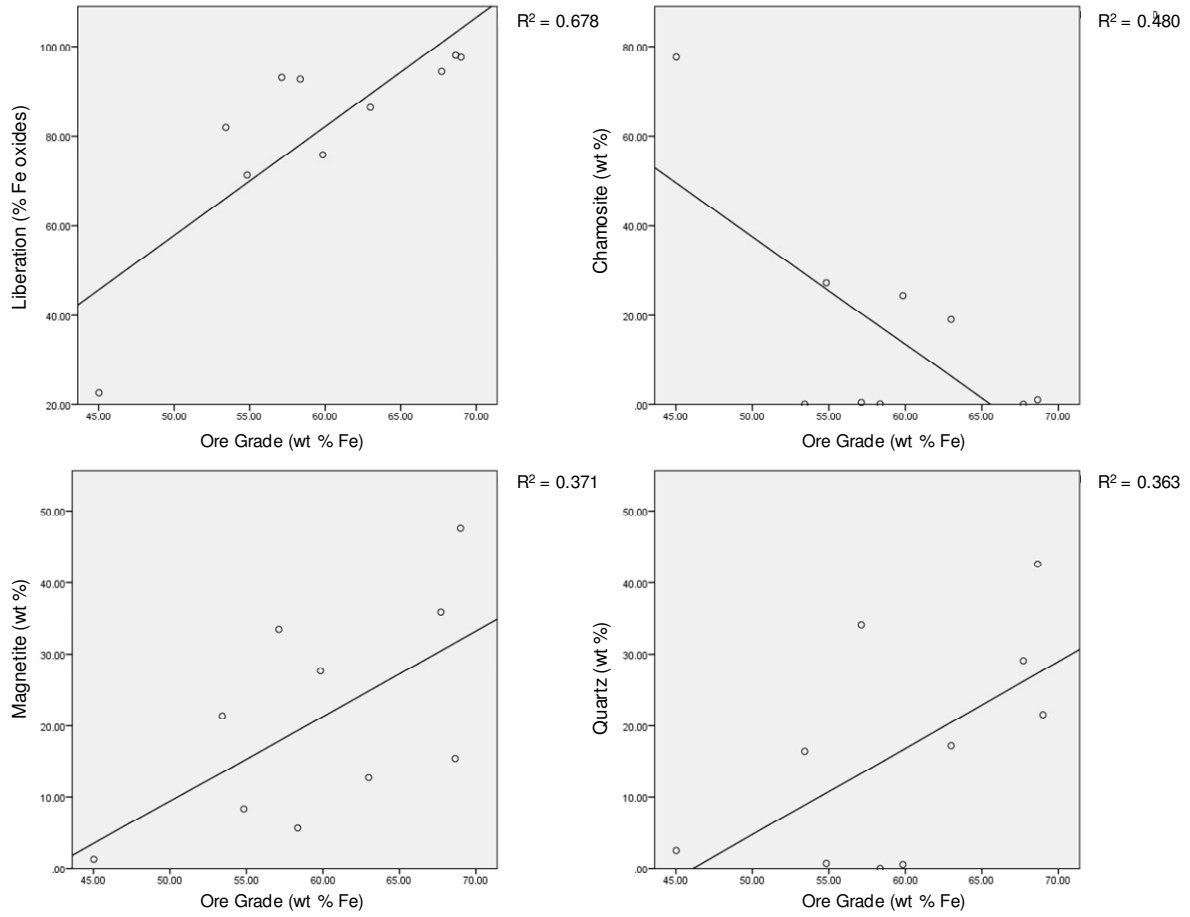

Figure 9.5 Scatter plots showing the correlation between ore grade (wt % Fe) and liberation (% Fe oxide), chamosite (wt %), magnetite (wt %) and quartz (wt %)

These scatter plots show a negative correlation between chamosite (wt %) and ore grade meaning that as chamosite content increases, the ore grade decreases. The correlation of magnetite (wt %) and quartz (wt %) with the ore grade is about half that between liberation and the ore grade implying that liberation of the Fe oxides is the main factor affecting ore grade.

Multiple regression was then carried out using the 4 variables but using the total Fe oxides instead of just magnetite. Even though the individual hematite and goethite wt % do not have a direct correlation with the ore grade, they are very important in its total Fe %. Multiple regression was carried out using the SPSS statistics software and the results are given below.

In Table 9.16, the R value is referred to as the multiple correlation coefficient and is a measure of the quality of the prediction of the dependent variable (Ore grade). A

value of 0.926 indicates a good level of prediction. The R^2 value known as the coefficient of determination is the proportion of variance in the ore grade that can be explained by the liberation and Fe oxide, chamosite, and quartz wt %. A value of 0.857 indicates that these variables explain 85.7 % of the variability of the ore grade. The adjusted R-squared is a modified version of R-squared that has been adjusted for the number of predictors in the model and at 0.713 still indicates a good level of prediction. The error of the estimates is just about 4 % which is good.

Table 9.16 Summary of the correlations from multiple regression model created.

Model	*R*	*R Square*	*Adjusted R Square*	*Std. Error of the Estimate*
1	0.926[a]	0.857	0.713	3.93719

a. Predictors: (Constant), Fe oxides (wt %), Quartz (wt %), Chamosite (wt %), Liberation (% Fe oxide)

To investigate the statistical significance of the prediction of the dependent variables by the independent variables the "sig" value which is 0.056 is used (Table 9.17). Values ≤ 0.05 means we have 95 % confidence in our analysis (Laerd statistics, 2014) and in this analysis, the "sig" value is just less than that for 95 % confidence required (0.056). We can conclude that our prediction is significant.

Table 9.17 Statistical significance of the prediction of the dependent variables by the independent variables.

Model		*Sum of Squares*	*df*	*Mean Square*	*F*	*Sig.*
1	Regression	370.282	4	92.570	5.972	0.056[b]
	Residual	62.006	4	15.501		
	Total	432.288	8			

a. Dependent Variable: Ore Grade (wt % Fe)

b. Predictors: (Constant), Fe oxides (wt %), Quartz (wt %), Chamosite (wt %), Liberation (% Fe oxide)

The general form of the equation to predict the ore grade is:

Ore grade = - 3.599 + (0.711 x Liberation) + (0.416 x chamosite) + (0.044 x quartz) – (0.040 x Fe oxides)

These values were obtained from the coefficient table Table 9.18, second column (Unstandardized Coefficients). To test for the statistical significance of each of the independent variable, the “t” and “sig” values are used. If sig < 0.05 for a particular variable, it is statistically significant (Laerd statistics, 2014). It is seen from Table 9.16 that only liberation meets this condition implying that the other variables are not statistically significant.

Table 9.18 Coefficent table for the multiple regression model.

Model	***Unstandardized Coefficients***		***Standardized Coefficients***	***t***	***Sig.***	***95.0% Confidence Interval for B***	
	B	***Std. Error***	***Beta***			***Lower Bound***	***Upper Bound***
(Constant)	-3.599	22.627		- 0.159	0.881	-66.421	59.222
Liberation (% Fe oxide)	0.711	0.253	2.242	2.807	0.048	0.008	1.413
Chamosite (wt %)	0.416	0.220	1.449	1.892	0.131	- 0.195	1.027
Quartz (wt %)	0.044	0.181	0.098	0.244	0.819	- 0.459	0.548
Fe oxides (wt %)	- 0.040	0.112	- 0.144	- 0.360	0.737	- 0.350	0.270

a. Dependent Variable: Ore Grade (wt % Fe)

Unfortunately, the number of samples studied was too small to make the statistical analysis reliable. Even in the case of the liberation, which the statistics have shown to be the most important variable, the interpretation is not quite true. For example, sample G01 has a head grade of 56.29 Fe wt % and an ore grade of 58.35 from a Fe oxide liberation of 93.76 %. Compare this to sample NWB02 which had a head grade of 35.61 wt % Fe and an ore grade of 67.71 wt % Fe from a similar liberation of 94.45 %. The significant differences in the ore grade could only be explained by their mineralogy with G01 rich in goethite (86.61 wt %) and sample NWB02 rich in magnetite (35.93 wt %). We can conclude that the interpretation of the metallurgical analysis described earlier supersedes the inferences from the multiple linear regression.

9.7 Theoretical grade recovery vs metallurgic grade recovery

In general, the QEMSCAN® Fe wt % is higher than the XRF Fe wt % for samples rich in Fe oxides and low for samples rich in gangue minerals and poor in Fe oxides. QEMSCAN® analysis produces more precise data on the particular sized fractions considered and this always risks a non-representative sample compared to XRF analyses which is carried out on whole rock samples ground to - 45 µm. The relationship between QEMSCAN® Fe wt % and XRF Fe wt % has been discussed in Chapter 8. As such when comparing the percentage recovery against grade from the QEMSCAN® and that from the magnetic separation, we also expect a similar relationship with the XRF.

The optimum size fraction were used for the graphs comparing the QEMSCAN® theoretical grade recovery for the samples to that obtained from the magnetic separation (Figure 9.6). The recovery and grade obtained from the magnetic separation has been plotted as points on the TGR curves obtained from the QEMSCAN® for effective comparison. Whereas the recovery and grade of seven out of the 10 samples concentrated by the magnetic separation are in good agreement with that predicted by the QEMSCAN® TGR, three gave grades significantly different from those predicted. These are samples G01, LB05 and LB07. A common feature in these 3 samples is that they have significant goethite concentrations or as is the case of LB07, significant amount of andradite which can have similar magnetic susceptibility as hematite and goethite (Figure 9.6 and Table 9.12). The reasons for their lower grades have already been explained in section 9.4 above i.e. under concentrate grades. Another source of potential difference in grades could be sample representivity and volume; 1g of sample was used for the QEMSCAN® analysis whist 20 grams were used for the magnetic separations.

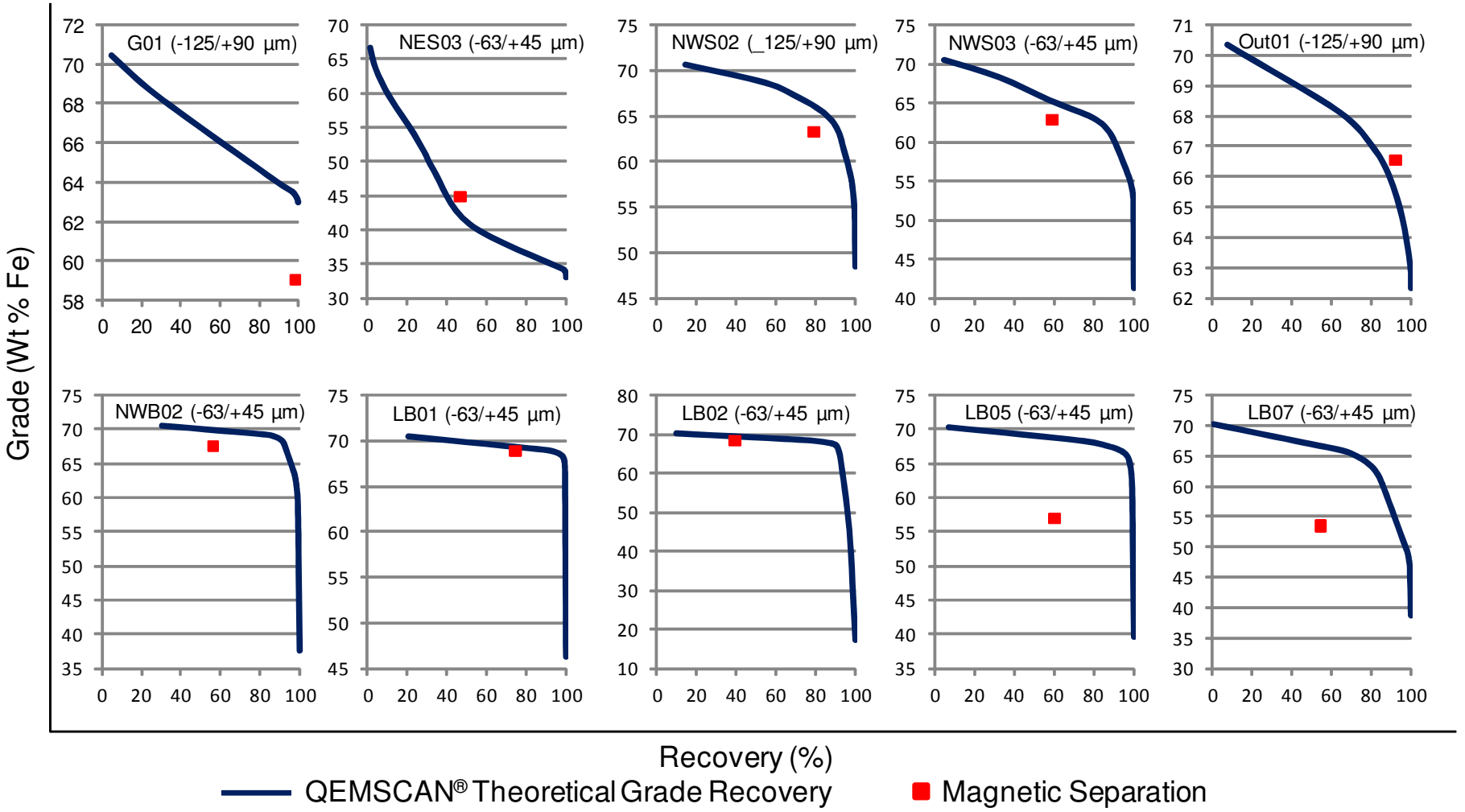

Figure 9.6 Plots of QEMSCAN® theoretical grade recovery and the grade and recovery obtained from magnetic separations.

9.8. Conclusions

Even though the mass percent of minerals from the QEMSCAN® modal mineralogy can give an indication of their possible recovery, the true recovery is affected by other mineralogical factors such as mineral associations, liberation and other ore characteristics. As such studying the mineralogy of an ore will help in explaining metallurgical problems such as lower than expected recoveries. A better comparison can be achieved between the grade and recovery from the QEMSCAN® theoretical recovery (which inherently takes into consideration the modal mineralogy, mineral associations and liberation) and the DTR / WHIMS recovery and XRF grade of the concentrates. The use of the theoretical grade recovery falls under the application of process mineralogy which is designed to model the grades and recoveries that can be expected as well as the metallurgical problems to be anticipated when mining begins (Lotter et al., 2003). The QEMSCAN® offers a powerful means of understanding the mineral characteristics of deposits which is invaluable in any process mineralogy programme. Theoretical grade recovery can be used at the beginning of a process mineralogy programme to assess the efficiency of latter separations (Lotter et al., 2011). The optimum magnetic intensity used can only be obtained by trial and error. BIF samples are suitable for low intensity magnetic separation and passing their tailings through a high intensity separation may result in concentration of Fe silicates, with which they are almost always associated with and some garnets if present.

Saprolite samples should be passed through low intensity magnetic separators to concentrate the magnetite as these will block the grids of the high intensity magnetic separators resulting in much higher recoveries and lower grades. The optimum intensity to be used for the tailings will vary from ore to ore but should be optimised to concentrate the weakly magnetic goethite and if necessary, chamosite.

It has been shown that the difference between the predicted grade and recovery and those obtained from metallurgical testing is due mainly to the modal mineralogy of the individual samples. Liberations are quite similar and therefore could not be the main factor responsible for the differences. As the magnetic

separations carried out where done in batches i.e. for the individual samples it is theoretically referred to as high gradient magnetic separation (HGMS) which is different from high intensity magnetic separation (HIMS) which is a continuous process.

Ideally for the fine grain sizes (< 100 µm), the SLon magnetic separation is the most effective means of separation due to its pulsation movement combined with high magnetic intensity resulting in much more effective separation of the Fe minerals. SLon magnetic separation was developed in China (Xiong, 1994, Svoboda and Fujita, 2003) to overcome multiple disadvantages with the WHIMS technology which has long been available for the separation of paramagnetic materials, but traditionally has encountered inefficiencies with finer feeds (< 100 µm).

Chapter 10

Discussions and Conclusions

10.1 Introduction

This chapter considers the significance of this research in terms of how the study of Nkout and Putu is relevant to other iron ore deposits, not only in the West and Central African subregion but also elsewhere in the world. The potential of this study to advance the general science of the QEMSCAN® technique and geometallurgy studies is also discussed. The main conclusions are summarised and recommendations made for future work.

10.2 Implications for geometallurgy of other iron ore deposits

This research has shown the effectiveness of the QEMSCAN® method in the characterisation of iron ore deposits. Especially for the quantification of the Al, Si, and P content within goethite. The significance of this is the fact that these elements within goethite might result in ores not meeting the chemical specification of a customer. For example in the Nkout deposit, the P content in the weathered magnetite itabirite is higher than that present within the low grade magnetite itabirite. Whereas the P content is due to apatite in the low grade magnetite itabirite, that in the weathered magnetite itabirite is due to P present within goethite. One key area of importance that has been found in this research is the effect of chamosite on the Fe oxides. Even though it contains enough Fe to be potentially mined for iron on its own, it can significantly reduce the liberation of the Fe oxides and could pose metallurgic problems during concentration as has been shown during the metallurgical aspect of the research. A major advantage of the research is the fact that it has looked at deposits that contain the full range of possible ores from banded iron formations. This means that it has looked at magnetite ores as well as ores containing hematite/martite-goethite. Both the Nkout and Putu deposits comprise both fresh magnetite banded iron formation (BIF) at depth and caps of enriched hematite/martite-goethite ores. They therefore provide an excellent example of multiple iron oxide minerals and complex mineral associations

The world's major iron ore deposits may be divided into 4 main types depending on the main ore minerals present. These are:

1. microplaty hematite
2. hematite,
3. martite-goethite
4. magnetite deposits.

Table 10.1 lists some of these major deposits and their main ore minerals including the Nkout and Putu deposits. The microplaty hematite (e.g. Tom Price, Nimba, Carajás, Guinea, Krivoy Rog, Noamundi, and Mount Whaleback) and hematite deposits (Sishen Mine and Quadrilatero Ferrifero) are usually DSO and so in most cases requires minor processing. The main problem in using SEM-based automated mineralogy for iron ore deposits has been the difficulty in distinguishing the iron oxides because of the similarity of hematite and magnetite on rapidly acquired energy-dispersive X-ray spectra. This problem was overcome by using backscattered electron signals instead of X-ray spectra and this study discusses the protocols required to identify not only these iron oxides but also variations in their compositions. The QEMSCAN® technique developed in this research to differentiate between the various iron oxides could be useful in quantifying the hematite/magnetite ratio in these microplaty hematite and hematite deposits which is important if any upgrading is necessary due to the different processing routes for hematite and magnetite.

I however agree with Donskoi et al. (2011) who suggested that optical image analysis (OIA) systems are faster and more cost-effective and more reliable for iron ores with high iron content and containing a variety of iron oxides and oxyhydroxides whereas QEMSCAN® can provide much more detailed information on gangue minerals especially for low iron content ores. Both methods have significant advantages over quantitative XRD as discussed in Chapter 8.

This research is more applicable to martite-goethite deposits (Koolyanobbing and Mining Area C) and magnetite deposits (Mount Gibson, Gongchangling, Empire and Malmberget). This is so, not only because of the characterisation of gangue elements within the goethite but more so for the gangue minerals

present. The limitation is that some of these major deposits contain silicate facies iron minerals such as stilpnomelane and carbonate facies iron minerals such as siderite which were not encountered in this research.

Table 10.1 Some of the world's major iron ore deposits and their main ore minerals**.**

Country	***Name of Deposit***	***Main Ore minerals***	***Processing***	***Reference***
Australia	Tom Price	Microplaty hematite	DSO	Morris, 2002
Australia	Mt Whaleback	Microplaty hematite	DSO	Everett and Howard, 2007
Liberia	Nimba	Microplaty hematite	DSO	Berge, 1974
Brazil	Carajás	Microplaty hematite	DSO	Rosière et al., 2006
Simandou Range	Guinea	Microplaty hematite	DSO	Cope et al., 2005
Ukraine	Krivoy Rog	Microplaty hematite	DSO	Roy et al., 2008
India	Noamundi	Microplaty hematite	DSO	Majumder et al., 2005
South Africa	Sishen Mine	Hematite	DSO	Carney and Mienie, 2003
Brazil	Quadrilatero Ferrifero	Hematite	DSO	Cabral and Rosière, 2013
Cameroon	Nkout	Magnetite, martite-goethite	Yes	Anderson et al., 2014
Liberia	Putu	Magnetite, martite-goethite	Yes	Anderson et al., 2013
Australia	Koolyanobbing	Martite goethite	Yes	Angerer et al., 2010
Australia	Mining Area C	Martite goethite	Yes	Bodycoat, 2010
Australia	Mount Gibson	Magnetite	Yes	Lascelles, 2006
China	Gongchangling	Magnetite	Yes	Wang et al, 2014
United states	Empire	Magnetite	Yes	Jorgenson, 2005
Sweden	Malmberget	Magnetite	Yes	Lund et al, 2013

In the microplaty hematite and martite-goethite deposits, a high proportion of the gangue occurs as bands of soft and porous kaolinite-rich shale (Clout and Simonson, 2005). The gangue present in magnetite iron ores are virtually the same all over the world (Clout and Simonson, 2005) and they are quartz, silicates (e.g. amphiboles and chlorite) and carbonates (e.g. dolomite and ankerite). The apatite iron ores of the world (e.g. the Malmberget) deposit have a different genesis to the sedimentary BIF deposits with a magmatic-hydrothermal process being the widely accepted model (Martinsson, 2004). However the mineralogy remains the same with Lund et al. (2009) reporting that in the case of the Malmberget apatite iron ore, the main gangue minerals are

apatite, amphiboles, pyroxenes, feldspars, quartz and biotite. The accessory minerals are pyrite, chalcopyrite, titanate and zircon with calcite being the most common. All these minerals are present in the SIP developed for the QEMSCAN® analysis (Table 8.4). The SIP also includes kaolinite which has been identified as the main gangue in the microplaty hematite and hematite deposits. As such if the SIP developed is modified to include the iron silicate and iron carbonate minerals, it will be to a large extent applicable to other world deposits. The approach for other deposits could be similar, with material types defined (e.g. here Fe wt % and degree of weathering were used as the main discriminants) so that they can be mapped through the deposit and readily identified in drill core and on the mine.

10.3 Contribution to QEMSCAN® and geometallurgy studies

Automated mineralogy systems are regarded as essential by companies involved in mineralogical and metallurgical research and their applications are wide and varied covering different commodities as well as disciplines (Schouwstra and Smit, 2011). Application of automated mineralogy to Fe ores has been limited by the difficulty in indentifying the constituent Fe oxides. This is now being overcome by a carefully controlled protocol using backscatted imaging as in this study. The use of QEMSCAN® for iron ores was discussed by Donskoi and Clout (2005) who compared the use of optical image analysis systems (OIAS) and QEMSCAN® in the study of the behaviour of fine iron ores in downstream processing operations. A large amount of information about the ore was obtained including particle mineralogy, porosity, mineral association, texture, hardness, size distribution, mineral association, texture, hardness, size distribution, mineral liberation, particle classification, class densities and mineral composition, and the molecular composition of each mineral. The main advantage of QEMSCAN® over OIAS is that in addition to all these properties, the chemistry of the minerals can be simultaneously provided. The deficiency of QEMSCAN® according to Donskoi and Clout (2005) is the inability to handle porosity in iron ore minerals effectively which can be done with OIAS even though OIAS does not report chemistry directly. Lane et al. (2008) demonstrated the power of OIAS for relatively straight forward or simple mineral assemblages mentioning its speed of gathering data, simplicity of functional

equipment and relatively low cost. They acknowledged the fact that the limiting factor of using OIAS is often the complexity of mineral content and non-opaque gangue mineral resolution.

Another different use of the QEMSCAN® is in the provision of high quality reference data for standards which were used in calibrating HyLogging spectral data to mineral abundances in weight percentage (Yang et al., 2011). They concluded that using their approach, "it is practical to acquire a large volume of mineral data for a single deposit to allow a detailed and objective study of occurrence and abundance variation of concerned gangue minerals for metallurgical design and mine planning, as well as for monitoring and analysing ore materials being mined from a production mine for mineral processing purpose".

Tonžetić and Dippenaar, (2011) used QEMSCAN® to develop an alternative means to the traditional quantification of iron ore sinter mineralogy. During the research, they were also able to differentiate magnetite from hematite using BSE as was done in this research. Dworzanowski (2012) studied the recovery of magnetite in the form of a pelletizing concentrate based on an evaluation of an iron ore by-product opportunity from an iron oxide copper-gold (IOCG) deposit. QEMSCAN® was used to determine the liberation and mineral associations of magnetite as was also in the case of Dowson et al. (2009). Makhija et al. (2013) worked on banded hematite jasper BIF testing whether gravity or magnetic separations will be the most suitable means of beneficiation. They used QEMSCAN® to study liberation and mineral associations. Thella et al. (2012) used QEMSCAN® to characterise hydrocyclone underflow to get inputs to process further using flotation. They were working on high alumina iron ore slimes. Lund et al. (2013) has worked extensively on the Malmberget iron ore deposit, Sweden, using QEMSCAN® to characterise the deposit and also to verify a method to quantify minerals using chemistry and metallurgical tests.

There are several differences between these uses of QEMSCAN® in the study of iron ore and this research. The first thing to notice is that most studies have been on just one of the following iron ores; magnetite iron ore, hematite iron ores and to a lesser extent martite-goethite iron ore. The deposits studied in this

research cover all these individual mineral types. Furthermore, none of their deposits were reported to contain chamosite which was investigated in details in this research. These other research projects have merely reported the results of their QEMSCAN® analysis without going into the detail of the development of the SIP/database and the checks that are made to ensure data integrity; crucial issues which were covered in detail in this research. The accuracy of the results of any QEMSCAN® is directly related to the accuracy of the SIP used in the analysis. As such its importance cannot be overestimated and knowledge on how to go about creating a suitable one is invaluable. It should also be noted that none of these deposits are from the West and Central Africa sub region, for which there are very few academic research publications. Furthermore the way in which the QEMSCAN® data was linked and discussed with the metallurgical analysis is innovative and not present in any known publication.

According to Lotter (2011), "Process diagnosis, flowsheet design and optimisation are most effectively and efficiently achieved through the use of metallurgical testwork combined with modern quantitative mineralogical techniques". This research has covered both these technique and the findings have added knowledge to the field of process mineralogy (an integral part of any geometallurgy programme) which is an integration of quantitative mineralogy and metallurgical test work. The full range of a geometallurgical program is quite extensive as was suggested by Williams (2010) who stated that "A strong geometallurgical approach to new project development or operational optimisation is to define variability of geology and mineralogy that exist within the proposed mine plan and then to develop a tailored process plant to the ore to be milled and an optimised mine plan given all other key project constraints (such as concentrate sales contracts, project macro economic considerations etc)". He also went on to say that the key first requirement in a geometallurgical program is to define and characterise the geological and mineralogical variability that exists in the deposit.

This research also supports the particle based approach to geometallurgy as proposed by Lamberg (2011). This approach to geometallurgy "uses minerals and particles as common parameters going through the geometallurgical program from the collecting of the geological data to the process simulations".

Three main quantitative models were proposed: (1) geological model, (2) particle breakage model and (3) unit process models. This study supports the first two models as the geological model gives the various geometallurgical domains present within the deposit and the particle breakage model "which forecasts which type of particles will be generated when different ore blocks and rocks break down" has been covered in our study of mineral associations and liberation. As far as the unit process model is concerned, even though this research has not looked into the comminution model due to the types and quantity of samples that were available, it has looked at the separation model which in this iron ore case was based on magnetic separation of the various Fe rich minerals from the gangue. The results have indicated that the most important parameter affecting the magnetic separation is the modal mineralogy. The third aspect of the Lamberg (2011) unit process model, i.e. leaching and precipitation models, were not considered in this research.

10.4 Summary of the main conclusions

In terms of the comparison of the deposits studied, the following conclusions can be drawn:

1. The Nkout and Putu deposits consist of iron oxide minerals with no evidence of iron carbonates. Iron sulphides are present mainly in the form of pyrite which is restricted to minor quantities in the magnetite itabirites. Both can be divided into a smaller hematite/martite–goethite ore and a much larger fresh magnetite BIF ore.

2. Hematite is the main Fe oxide in the enriched material to transitional magnetite itabirite at Putu whereas at Nkout it is magnetite. Magnetite content in the enriched material at Nkout is about 5 times than at Putu whilst for the hematite content the reverse is true with Putu having about 5 times more than Nkout.

3. Goethite (Al) and goethite/limonite occur in about equal quantities in the enriched material at Nkout and Putu. Problems with goethite (Al) at Nkout are more noticed in the transitional magnetite itabirite with Nkout having about 105

times more than in Putu. Goethite (P) occurs as a trace mineral in the enriched material at Putu but could be significant from a processing point of view at Nkout where it occurs as a minor mineral in the enriched material and weathered magnetite itabirite.

4. Chamosite which has been shown to affect liberation of the Fe-oxides is a major mineral at Nkout in all but one of the material types whereas at Putu, it is only a major mineral in the enriched material. Chamosite occurs in similar proportions in the enriched material but differs significantly in the transitional magnetite itabirite with Nkout having about 156 times more than Putu.

5. The main gangue minerals in the enriched material to transitional magnetite itabirite at Nkout are gibbsite and quartz. Quartz is the main gangue at Putu.

6. Apatite is the P-bearing mineral in the magnetite itabirite at both Nkout and Putu and occurs as a minor mineral associated with the silicates. Calcite occurs as a minor mineral in the magnetite itabirite at Putu and occurs in trace quantities at Nkout.

7. Minor differences have been observed between the two main areas at Putu; apatite and quartz seem to be the main gangue in the Jideh area whilst calcite and quartz are prominent in the Montroh range. In addition, micas are the main Al bearing phases at Putu. Apatite and calcite are the main bearing P and Ca bearing minerals respectively. The minerals are indicative of amphibolite to granulite facies metamorphism mineral assemblages.

8. Magnetite occurs in about equal proportion in the magnetite itabirite at Putu and Nkout. The magnetite itabirite is the main ore material at both Nkout and Putu. The liberation of the Fe oxides as a group for the -125/+90 µm size fraction of both deposits is about 90 % making them amenable to inexpensive processing such as crushing, grinding and magnetic separation. The liberation of the Fe oxides in the -63/+45 µm of the enriched material is lower at Putu mainly due to their association with silicates.

9. There is no evidence to show that there is any structural control on the BIF mineralisation at Nkout because metamorphism has significantly affected the lithological characteristics.

In terms of the development of the QEMSCAN® automated mineralogy technique and metallurgical testing carried out, the following conclusions could be made:

10. The QEMSCAN® offers a powerful means of understanding the mineral characteristics of deposits which is invaluable in any process mineralogy/geometallurgical programme.

11. A SIP was developed to enable the QEMSCAN® technique to be applied to iron ores. It is applicable to a wider range of iron ore deposits especially low grade iron ore. Addition of silicate and carbonate facies minerals would be a useful next step.

12. The iron oxides, magnetite, hematite and goethite were distinguished by QEMSCAN® using subtle variations in their backscattered electron coefficients (BSE). The exact BSE values may vary from one instrument to another and as such must be calibrated before separation is attempted.

13. Automated mineralogy techniques such as QEMSCAN® are most useful in geometallurgy studies of all types of iron ore but more so in the case of low grade ores with significant quantity of gangue minerals. In the case of direct shipping ores and other high grade iron ores, other techniques such as optical image analysis systems may be cheaper and as effective. QEMSCAN® is more suitable in the case of complex ores.

14. The mass percent of minerals from the QEMSCAN® modal mineralogy can give an indication of their possible recovery but the true recovery is affected by factors such as mineral associations, liberation and other ore characteristics. The grade and recovery from the QEMSCAN® theoretical grade recovery (which inherently takes into consideration the modal mineralogy, mineral associations

and liberation) correlates well with the DTR / WHIMS recovery and XRF grade of the concentrates.

15. BIF samples are suitable for low intensity magnetic separation. Passing their tailings through a high intensity separation may result in concentration of Fe silicates and some garnets if present.

16. The weathered magnetite itabirite, transitional magnetite itabirite and if necessary the enriched material, material types should be passed through low intensity magnetic separators to concentrate the highly magnetic material as these will block the grids of the high intensity magnetic separators resulting in much higher recoveries and lower grades. The optimum intensity to be used for the tailings will vary from ore to ore but should be optimised to concentrate the weakly magnetic goethite and if necessary, chamosite and can only be obtained by trial and error.

17. The difference between the predicted grade and recovery and those obtained from metallurgical testing is due mainly to the modal mineralogy of the individual samples with goethite and in some cases andradite being the minerals responsible for discrepancies (chapter 9).

10.5 Recommendations for further research

It is difficult to see what else can be done using the QEMSCAN® on these deposits and more importantly what new information can be obtained from further QEMSCAN® analysis. One thing that can however be done is to increase the count rate from the current 1000 used in this research to about 5000 which should aid in distinguishing minerals better. It should be noted that even though this approach might be the best way to compare the results of the QEMSCAN® to that of the optics and EPMA images, it could be time consuming and expensive to do and might only add new theoretical information rather than practical information. Optical image analysis systems could be used to further verify the magnetite / hematite concentrations but my main recommendations are for further work on the metallurgical issues.

The type of further work to be done could be dependent on the amount of samples that could be available. For example, breakage tests such as comminution were not considered in this research simply because the available drill core, grab and outcrop samples were restricted to weights of between 100 g to 150 g which were just enough to perform the bulk chemistry, mineral chemistry, mineralogy and magnetic separation tests. For example about 50 kg of sample are needed to conduct a drop weight test and much more for an effective bench scale comminution tests. If such sample weights are available, I recommend that some work be done on comminution which is one of the main areas of energy consumption in a mine. Tests could be carried out on crushing units for size reduction of coarse materials and grinding units for size reduction of finer material. Autogenous grinding (AG) and/or semi-autogenous grinding (SAG) could be carried out initially and the products pass through a ball mill to obtain the fine particles required for further beneficiation processes.

The magnetic separation conducted on chamosite rich samples gave the least recovery and much more important, least grades for all the samples analysed. Further work could be carried out on varying the parameters of the magnetic separation equipments to find the optimum experimental conditions and this could lead to better grade/recovery curves. The theoretical grade recovery curves for chamosite rich samples obtained from the QEMSCAN® have indicated that grades of > 60 % Fe are possible for recoveries between 30 % and 40 %. In general, more work could be carried out on chamosite in other iron ores to see if they have the same effect on the liberation of the Fe oxides as they have on the Putu and Nkout deposits.

The SLon magnetic separation is the most effective means of separation of Fe oxide minerals with a size fraction of < 100 µm due to its pulsation movement combined with high magnetic intensity resulting in much more effective separation of the Fe minerals. This method was not used in this research because it was not available but could be suitable for the beneficiation process of these deposits as it has been shown that the optimum size fraction for beneficiation is the -63/+45 µm fraction.

Other beneficiation routes such as gravity separation could be investigated. Gravity separation could work because of the differences between the densities of magnetite and hematite in particular (average of 5.15 and 5.30 respectively) compared to those of the gangues e.g. quartz and other alumino-silicates (2.50 – 2.80). Caution should be exercised when dealing with samples rich in goethite and chamosite as their average density is closer to that of the gangue minerals i.e. 3.8 and 3.2 respectively than those of magnetite and hematite.

References

Adekoya, J. A., 1998, The geology and geochemistry of the Maru Banded Iron-Formation, northwestern Nigeria: Journal of African Earth Sciences, v. 27, p. 241-257.

Adekoya, J. A., Okonkwo, C. T., and Adepoju, M. O., 2012, Geochemistry of Muro Banded Iron-Formation, Central Nigeria International Journal of Geosciences, 2, v. 3, p. 1074-1083.

Afferro-Mining, 2010, Selected iron ore projects in West and Central Africa (www.afferro-mining.com).

Alexandrov, E. A., 1973, The Precambrian Banded Iron-Formations of the Soviet Union: Economic Geology, v. 68 p. 1035-1062.

AMIRA, 2009, P843A - Geometallurgical Mapping and Mine Modelling: P843A Flyer.

Amlibgroup, 2013, http://www.amlibgroup.com/ Accessed 15 January 2013

Andersen, J. C. Ø., Rollinson, G. K., Snook, B., Herrington, R., and Fairhurst, R. J., 2009, Use of QEMSCAN® for the characterization of Ni-rich and Ni-poor goethite in laterite ores: Minerals Engineering, v. 22 p. 1119-1129.

Anderson, K. F. E., Rollinson, G. K., Wall, F., and Moon, C. J., 2013, A comparative automated mineralogical analysis of the Nkout (Cameroon) and Putu (Liberia) iron ore deposits, 12th SGA Biennal Meeting Uppsala, Sweden.

Anderson, K. F. E., Wall, F., Rollinson, G. K., and Moon, C. J., 2014, Quantitative mineralogical and chemical assessment of the Nkout iron ore deposit, Southern Cameroon: Ore Geology Reviews, v. 62, p. 25-39.

Angerer, T., and Hagemann, S. G., 2010, The BIF-Hosted High-Grade Iron Ore Deposits in the Archean Koolyanobbing Greenstone Belt, Western Australia: Structural Control on Synorogenic- and Weathering-Related Magnetite-, Hematite-, and Goethite-rich Iron Ore: Economic Geology, v. 105, p. 917–945.

Angerer, T., Hagemann, S. G., and Danyushevsky, L., 2013, High-grade iron ore at Windarling, Yilgarn Craton: a product of syn-orogenic deformation, hypogene hydrothermal alteration and supergene modification in an archean BIF-basalt lithostratigraphy: Mineralium Deposita, v. 48, p. 697-728.

Anike, O. L., Umeji, A. C., and Orajaka, I. P., 1993, Geology of Precambrian Banded Iron-Formation from Muro Hill, Nigeria: Economic Geology, v. 88, p. 1237-1241.

Ashley, K. J., and Callow, M. I., 2000, Ore Varaibility: Exercises in Geometallurgy: Engineering & Mining Journal v. 201, p. 24-28.

Ayling, B., Rose, P., Petty, S., Zemach, E., and Drakos, P., 2012, QEMSCAN® (Quantitative Evaluation of Minerals by Scanning Electron Microscopy): Capability and application to fracture characterization in geothermal systems:

Thirty-Seventh Workshop on Geothermal Reservoir Engineering, Stanford University, Stanford, California, January 30 - February 1, 2012.

Barley, M. E., Pickard, A. L., and Sylvester, P. J., 1997, Emplacement of a large igneous province as a possible cause of banded iron formation 2.45 billion years ago: Nature v. 385, p. 55-58.

Barratt, D., and Doll, A., 2008, Testwork Programs That Deliver Multiple Data Sets of Comminution Parameters For Use in Mine Planning and Project Engineering: International Mineral Processing Seminar - Procemin 2008 Santiago, Chile, 22–24 October, 2008.

Bell, A., 2011, Africa iron ore to hit Australia's trade, The Sydney Morning Herald: Sydney, Australia, 28 March 2011 (http://news.smh.com.au/breaking-news-business/africa-iron-ore-to-hit-australias-trade-20110328-1cd7r.html, Accessed 15 December 2011).

Benedictus, A., and Horsch, H., 2008, Enhanced measurement capabilities for iron ore deposits: 34th International Geological Congress, International Union of Geological Sciences, Brisbane, Australia, 2008.

Berge, J. W., 1971, Iron Formation and Supergene Iron Ores of the Goe Range Area, Liberia: Economic Geology, v. 66, p. 947-960.

Berge, J. W., 1974, Geology Geochemistry and Origin of the Nimba Itabirite and Associated rocks, Nimba County, Liberia: Economic Geology v. 69, p. 80-92.

Beukes, N. J., 1973, Precambrian Iron-Formations of Southern Africa: Economic Geology v. 68, p. 960-1004.

Beukes, N. J., Gutzmer, J., and Mukhopadhyay, J., 2003, The geology and genesis of high-grade hematite iron ore deposit: Applied Earth Science (Trans. Inst. Min. Metall. B) v. 112, p. 18-25.

Billa, M., Feybesse, J., Bronner, G., Lerouge, C., Milési, J., Traore, S., and Diaby, S., 1999, Banded ferruginous quartzite formations of the Nimba and Simandou ranges: tectonically stacjed units on an Archaean plutonic 'basement' (Kénéma-Man craton), during the Eburnean Orogeny: Académie des sciences / Earth and Planetary Sciences, v. 329, p. 287-294.

Bodycoat, F. M., 2010, Stratigraphic and structural setting of iron mineralisation at E Deposit (East), Area C, Hamersley Province, Western Australia: Applied Earth Science (Trans. Inst. Min. Metall. B), v. 119, p. 49-55.

Bontognalia, T. R. R., Fischerb, W. W., and Föllmic, K. B., 2013, Siliciclastic associated banded iron formation from the 3.2 Ga Moodies Group, Barberton Greenstone Belt, South Africa: Precambrian Research v. 226, p. 116–124.

Cabral, A., and Rosière, C., 2013, The chemical composition of specular hematite from Tilkerode, Harz, Germany: implications for the genesis of hydrothermal

hematite and comparison with the Quadrilátero Ferrífero of Minas Gerais, Brazil: Mineralium Deposita.

Carney, M. D., and Mienie, P. J., 2003, A geological comparison of the Sishen and Sishen South (Welgevonden) iron ore deposits, Northern Cape Province, South Africa: Applied Earth Science (Trans. Inst. Min. Metall. B), v. 112, p. 81-88.

Chapman, S. K., 1986, Working with a scanning electron microscope: Michigan, Lodgemark Press.

Clout, J. M. F., 2003, Upgrading processes in BIF-derived iron ore deposits: implications for ore genesis and downstream mineral processing: Applied Earth Science (Transactions of the Institutions of Mining and Metallurgy: Section B), v. 112, p. 89-95

Clout, J. M. F., and Simonson, B. M., 2005, Precambrian Iron Formations and Iron Formation-Hosted Iron Ore Deposits: Economic Geology, v. 100th Anniversary, p. 643-679.

Cope, I., 2008, Geology of the Pic de Fon iron ore deposit, Republic of Guinea, Imperial College London.

Cope, I. L., Wilkinson, J. J., Herrington, R. J., and Harris, C. J., 2005, Geology and Mineralogy of the Pic de Fon Iron Oxide Deposit, Simandou Range, Republic of Guinea, West Africa: Iron Ore Conference, Fremantle, Western Australia, 2005.

Coward, S., Vann, J., Dunham, S., and Stewart, M., 2009, The Primary-Response Framework for Geometallurgical Variables: Seventh International Mining Geology Conference, Perth, Western Australia, 17 - 19 August, 2009.

CSIRO, 2010, Securing the future for Australia's minerals industry.

Dalstra, H., and Guedes, S., 2004, Giant Hydrothermal Hematite Deposits with Mg-Fe Metasomatism: A Comparison of the Carajas, Hamersley, and other iron ores: Economic Geology, v. 55, p. 1793-1500.

Das, B., Prakash, S., Das, S. K., and Reddy, P. S. R., 2007, Effective Beneficiation of Low Grade Iron Ore Through Jigging Operation: Journal of Minerals & Materials Characterization and Engineering, v. 7, p. 27-37.

Deer, W. A., Howie, R. A., and Zussman, J., 1992, An introduction to the Rock Forming Minerals, Longman Group UK.

Donskoi, E., and Clout, J. M. F., 2005, Automated Textural Classification of Iron Ores Using 'Recognition' — A Specialised Software Package for Studying Iron Ores: Iron Ore Conference Fremantle, Western Australia, 19 - 21 September, 2005, p. 203-211.

Donskoi E, Manuel JR, Austin P, Poliakov A, and Peterson MJ, H. S., 2011, Comparative Study of Iron Ore Characterisation by Optical Image Analysis and QEMSCAN™, Iron ore conference Perth, Western Australia

Dowson, N., Connelly, D., and Yan, D., 2009, Trends in Magnetite Ore Processing and Test Work: Iron Ore Conference, Perth, Western Australia 231-241, 2009, p. 27 - 29.

Droop, G., 1987, A general equation for estimating Fe3+ concentrations in ferromagnesian silicates and oxides from microprobe analysis, using stoichiometric criteria, Mineralogical Magazine, p. 431-435.

Dukino, R. D., Loo, C. E., and Swain, M. V., 1997, Characterisation of strength of Australian iron ores by tumble drum and drop test: Transactions of The Institution of Mining and Metallurgy, v. 106, p. 80-88.

Dunbar, W. S., 2012, Basics of Mining and Mineral Processing, 2012 Americas School of Mines: British Columbia, University of British Columbia, p. 502.

Dunham, S., and Vann, J., 2007, Geometallurgy, Geostatistics and Project Value — Does Your Block Model Tell You What You Need to Know?: Project Evaluation Conference, Melbourne, Victoria, Australia 19 - 20 June 2007.

Dworzanowski, M., 2012, Maximizing the recovery of fine iron ore using magnetic separation: The Journal of The Southern African Institute of Mining and Metallurgy v. 112, p. 197-202.

Els, F., 2012, These 2 charts tell you everything you need to know about iron ore for the next 20 years, 2 December, 2012. (http://www.mining.com/these-2-charts-tell-you-everything-you-need-to-know-about-iron-ore-for-the-next-20-years-70401/)

European Country of Origin Information Network, 2013, http://www.ecoi.net/liberia/maps, Accessed 07 November 2010

Evans, A. M., 2009, Ore Geology and Industrial Minerals: An Introduction, John Wiley and Sons.

Everett, J. E., and Howard, T. J., 2007, Correcting for the Dilution of Rakes Processed Sequentially from Multiple Mines at the BHP Billiton Iron Ore Newman Joint Venture Operations: Iron Ore Conference, Perth, Western Australia 20 - 22 August 2007.

Fandrich, R., Gu, Y., Burrows, D., and Moeller, K., 2006, Modern SEM-based mineral liberation analysis: International Journal of Mineral Processing, v. 84, p. 310-320.

Ferenčić, A. J., 1969, Geology of the San Isidro Iron Ore Deposit, Venezuela: Mineral Deposita, v. 4, p. 283-297.

Feybesse, J. L., Johan, V., Triboulet, C., Guerrot, C., Mayaga-Mikolo, F., Bouchot, V., and N'dong, J. E., 1998, The West Central African belt: a model of 2.5–2.0 Ga accretion and two-phase orogenic evolution: Precambrian Research v. 87, p. 161-216.

Field, A. 2009. Discovering statistics using SPSS. Sage Publications Limited.

Firth, A. R., and Boucher, M.E., 2007, A Comparison of Mineralogy Development in Haematite and Magnetite Pellets, Iron Ore Conference Perth, Western Australia.

Fitzhugh, E. F., 1953, Iron Ore at Bomi Hill, Liberia: Economic Geology, v. 48, p. 431-436.

Forrest, M., 2009, Geometallurgy for mine data - explaining the advantages, Materials World, p. 48-50.

Foster, B., 2003, Côte d'Ivoire, in Mining annual review 2003: Mining Journal, p. CD-ROM.

Ghosh, G., and Mukhopadhyay, J., 2007, Reappraisal of the structure of the Western Iron Ore Group, Singhbhum craton, eastern India: Implications for the exploration of BIF-hosted iron ore deposits: Gondwana Research v. 12, p. 525-532.

Goldring, D. C., 2003, Iron ore categorisation for the iron and steel industry: Applied Earth Science (Trans. Inst. Min. Metall. B) v. 112, p. 5-17.

Goodall, W. R., Scales, P. J., and Butcher, A. R., 2005, The use of QEMSCAN® and diagnostic leaching in the characterisation of visible gold in complex ores: Minerals Engineering, v. 18, p. 877-886.

Goodwin, A. M., 1973, Archean Iron-Formations and Tectonic basins of the Canadian Shield: Economic Geology, v. 68, p. 915-933.

Gottlieb, P., Wilkie, G., Sutherland, D., Ho-Tun, E., Suthers, S., Perera, K., Jenkins, B., Spencer, S., and Butcher, A., 2000, Using Quantitative Electron Microscopy for Process Mineralogy Applications: JOM, v. 52 p. 24-25.

Gross, G. A., 1965, Geology of Iron Deposits in Canada, Economic geology report, 22 Department of Mines and Technical Surveys, Canada.

Gross, G. A., 1973, The depositional environment of the principal types of Precambrian iron formations: Proceedings Kiev Sym, Paris 1973, p. 15-21.

Gutzmer, J., Beukes, N. J., deKock, M. O., and Netshiozwi, S. T., 2005, Origin of High-Grade Iron Ores at the Thabazimbi Deposit, South Africa: Iron Ore Conference Fremantle, Western Australia, 19 - 21 September 2005.

Harmsworth, R. A., Kneeshaw, M., Morris, R. C., Robinson, C. J., and Shrivastava, P. K., 1990, BIF-derived iron ores of the Hamersley Province, in Hughes, F. E., ed., Geology of the mineral deposits of Australia and Papua New Guinea: Melbourne, Australasian Institute of Mining and Metallurgy, p. 617-642.

Hearn, S., and Dobbins, M., 2007, SLon® magnetic separator: A new approach for recovering and concentrating iron ore fines, Energy and Mines: Montreal, Canada.

Henderson, R., 1995, The potential and limitations of neutrons, electrons and X-rays for atomic resolution microscopy of unstained biological molecules: Quarterly Reviews of Biophysics, v. 28, p. 171-193.

Hindu newspaper, 2013, India may have to start importing iron ore soon: Steel Ministry, 24 November, 2013. (http://www.thehindu.com/business/Industry/india-may-have-to-start-importing-iron-ore-soon-steel-ministry/article5386470.ece) Accessed 20th December 2013

HIsmelt, 2008, The HIsmelt® Process: The Kwinana Plant Operation: 3rd International Meeting on Iron making - 2nd International Symposium on Iron Ore, São Luis do Maranhão, 2008.

Hitzman, M. W., Oreskes, N., and Oreskes, M. T., 1992, Geological characteristics and tectonic setting of Proterozoic iron oxide (Cu-U-Au-REE) deposits: Precambrian Research, v. 58, p. 241-287.

Hoal, K. O., Appleby, S. K., and Stammer, J. G., 2009, The Quantitative Mineralogy of Granular Materials, AIP Conference Proceedings: Golden (Colorado).

Howard, T. J., James, M. L., and Everett, J. E., 2005, Relating Iron Ore Lump and Fines Grade Split to Ore Type, Iron Ore Conference Fremantle, Western Australia.

http://www.mindat.org Accessed 2010 – 2014

http://webmineral.com Accessed 2010 – 2014

Hunt, C. P., Moskowitz, B. M., and Banerjee, S. K., 1995, Magnetic Properties of Rocks and Minerals, Rock Physics and Phase Relations, A Handbook of Physical Constant, American Geophysical Union., p. 189-204.

International Steel Statistics Bureau, 2013, Steel Products World Trade Reports - updated monthly, (http://www.issb.co.uk/global.html Accessed 16/12/2013).

Jacobson, C. E., and Sorensen, S. S., 1986, Amphibole compositions and metamorphic history of the Rand Schist and the greenschist unit of the Catalina Schist, Southern California: Contributions to Mineralogy and Petrology, v. 92, p. 308-315.

James, H. L., 1954, Sedimentary Facies of Iron-Formation: Economic Geology, v. 49, p. 235-293.

Johnson, R. C., Scott, G. W., and Lukey, H. M., 2007, Implications of Mineralogy, Grain Size and Texture on Liberation and Pellet Quality of Great Lakes Iron Ore, Iron Ore Conference: Perth, Western Australia

Jorgenson, J. D., 2005, Challenges Facing the North American Iron Ore Industry, Iron Ore Conference Fremantle, Western Australia.

King, I., 2009, The Latest Developments in Iron Ore Processing: Johannesburg, Council for Mineral Technology (MINTEK).

Klein, C., 2005, Some Precambrian banded iron-formations (BIFs) from around the world: Their age, geologic setting, mineralogy, metamorphism, geochemistry, and origin: American Mineralogist, v. 90, p. 1473-1499

Klein, C., and Beukes, N. J., 1993, Sedimentology and geochemistry of the glaciogenic late Proterozoic Rapitan Iron-Formation in Canada: Economic Geology, v. 88, p. 542-565.

Lamberg, P., 2011a, Particles – the bridge between geology and metallurgy: Conference in Mineral Engineering, Luleå, Sweden, 8–9 February, 2011, p. 1–16.

Laerd statistics, 2014, Multiple Regression Analysis using SPSS (https://statistics.laerd.com/spss-tutorials/multiple-regression-using-spss-statistics.php) Acessed 1 June 2014.

Lamberg, P., 2011b, Geometallurgy – what, why and how?: 8th Fennoscandian Exploration and Mining – FEM 2011, Levi, Finland, 1-3 November, 2011.

Lane, G. R., Martin, C., and Pirard, E., 2008, Techniques and applications for predictive metallurgy and ore characterization using optical image analysis: Minerals Engineering v. 21, p. 568-577.

Lascelles, D. F., 2006, Black smokers and density currents: A uniformitarian model for the genesis of banded iron-formations: Ore Geology Reviews v. 32, p. 381-411.

Lascelles, D. F., 2006, The Mount Gibson Banded Iron Formation-Hosted Magnetite Deposit: Two Distinct Processes for the Origin of High-Grade Iron Ore: Economic Geology, v. 101, p. 651-666.

Leevers, P., Gaughan, C., and Bubner, G., 2005, The Iron Magnet Deposit: Iron Ore Conference, Fremantle, WA, 2005, p. 19 - 21 September.

Lerouge, C., Cocherie, A., Toteu, S. F., Penaye, J., Milési, J.-P., Tchameni, R., Nsifa, E. N., Fanning, C. M., and Deloule, E., 2006, Shrimp U–Pb zircon age evidence for Paleoproterozoic sedimentation and 2.05 Ga syntectonic plutonism in the Nyong Group, South-Western Cameroon: consequences for the Eburnean–Transamazonian belt of NE Brazil and Central Africa: Journal of African Earth Sciences v. 44 p. 413-427.

Lersch, J., 1966, Geology of the Bong Range iron ore deposits: Bulletin of the Geological Society of Liberia, v. 1, p. 13-21.

Lotter, N. O., 2011 Modern Process Mineralogy: An integrated multi-disciplined approach to flow sheeting: Minerals Engineering, v. 24, p. 1229–1237.

Lotter, N. O., L.J. Kormos, Oliveira, J., Fragomeni, D., and Whiteman, E., 2011, Modern Process Mineralogy: Two case studies: Minerals Engineering, v. 24, p. 638-650.

Lotter, N. O., Kowal, D. L., Tuzun, M. A., Whittaker, P. J., and L., K., 2003, Sampling and flotation testing of Sudbury Basin drill core for process mineralogy modelling: Minerals Engineering, v. 16, p. 857-864.

Lund, C., 2009, Mineralogical, chemical and textural properties of the Malmberget iron deposit A process mineralogically characterisation, Luleå University of Technology.

Lund, C., Lamberg, P., and Lindberg, T., 2013, Practical way to quantify minerals from chemical assays at Malmberget iron ore operations – An important tool for the geometallurgical program: Minerals Engineering, v. 49, p. 7-16.

MARC Technologies, 2010, MARCET NEWS, (http://www.marctech.com.au) Acessed 9th December 2010.

Maddren, J., Ly, C. V., Suthers, S. P., Butcher, A. R., Trudu, A. G., and Botha, P. W. S. K., 2007, A New Approach to Ore Characterisation Using Automated Quantitative Mineral Analysis, Iron Ore Conference Perth, Western Australia.

Majumder, T., Chakraborty, K. L., and Bhattacharyya, A., 1982, Geochemistry of Banded Iron Formation of Orissa, India: Mineral. Deposita v. 17, p. 107-118.

Majumder, T., Venkatesh, A. S., Kumar, V., and Upadhyay, R. K., 2005, Mineralogical Characterisation of Iron Ores From Noamundi, India With Special Emphasis on Beneficiation of Iron Ore Fines, Iron Ore Conference Fremantle, Western Australia.

Makhija, D., Mukherjee, A. K., and Ghosh, T. K., 2013, Preconcentration Feasibility of Gravity and Magnetic Techniques for Banded Hematite Jasper International Journal of Mining Engineering and Mineral Processing, v. 2, p. 8-15.

Marmo, V., 1956, "Banded Ironstone" of the Kangari Hills, Sierra Leone: Economic Geology, v. 51, p. 798 - 810.

Martinsson, O., 2004, Geology and metallogeny of the northern Norrbotten Fe-Cu-Au province, Svecofennian Ore-Forming Environments: Volcanic-Associated Zn-Cu-Au-Ag, Intrusion-Associated Cu-Au, Sediment-Hosted Pb-Zn, and Magnetite-Apatite Deposits of Northern Sweden, Society of Economic Geologists Guidebook, p. 131-148.

Maurizot, P., and Abessolo, A., 1985, A Digest of BRGM "South West Cameroon Mining Inventory" Final Report

Maxton, D., Morley, C., and Bearman, R., 2003, A quantification of the benefits of high pressure rolls crushing in an operating environment: Minerals Engineering, v. 16, p. 827-838.

Mayhew, S., 2004, Oxford Dictionary of Geography, Oxford University Press, Inc. United States.

Mbarga, N., 2009, Cameroon Geological Setting: Investors Conference, Yaounde, 27 May, 2009.

McCusker, L. B., Von Dreele, R. B., Cox, D. E., Louër, D., and Scardi, P., 1999, Rietveld refinement guidelines: Journal of Applied Crystallography, v. 32, p. 36-50.

Mclanahan, 2014, Attrition Scrubbers/Cells. (http://www.mclanahan.com/Catalog/ViewItem?CatalogItemId=329&ParentId=327) Accessed 30 may 2014

Menzies, A., 2008, Automated mineralogy: Intellection QEMSCAN® User Group Meeting, Brisbane, Australia, 2008.

Milesi, J. P., Toteu, S. F., Deschamps, Y., Feybesse, J. L., Lerouge, C., Cocherie, A., Penaye, J., Tchameni, R., Moloto-A-Kenguemba, G., Kampunzu, H. A. B., Nicol, N., Duguey, E., Leistel, J. M., Saint-Martin, M., Ralay, F., Heinry, C., Bouchot, V., Doumnang Mbaigane, J. C., Kanda Kula, V., Chene, F., Monthel, J., Boutin, P., and Cailteux, J., 2006, An overview of the geology and major ore deposits of Central Africa: Explanatory note for the 1:4,000,000 map ‘‘Geology and major ore deposits of Central Africa’’: Journal of African Earth Sciences v. 44 p. 571-595.

Morris, R. C., 2002, Genesis of High-Grade Hematite Orebodies of the Hamersley Province, Western Australia - A Discussion: Economic Geology, v. 97, p. 177-181.

Mücke, A., 2005, The Nigerian manganese-rich iron-formations and their host rocks—from sedimentation to metamorphism: Journal of African Earth Sciences, v. 41, p. 407 - 436.

Nentwich, F. W., and Yole, R. W., 1991, Polished thin section preparation of fine-grained siliciclastic rocks: Journal of Sedimentary Research, v. 61, p. 624-626.

Nesse, W. D., 2000, Introduction to mineralogy, Oxford University Press.

Nforba, M. T., Kabeyene, V. K., and Suh, C. E., 2011, Regolith Geochemistry and Mineralogy of the Mbalam Itabirite-Hosted Iron Ore District, South Eastern Cameroon: Open Journal of Geology v. 1, p. 17-36.

Ngnotué, T., Nzenti, J. P., Barbey, P., and Tchoua, F. M., 2000, The Ntui-Betamba high-grade gneisses: a northward extension of the Pan-African Yaoundé gneisses in Cameroon: Journal of African Earth Sciences, v. 31, p. 369-381.

Ngnotue, T., Sylvestre, G., Paul, N., Bernhard S, Depesquidoux, T., and Emmanuel, S., 2012, Geochemistry and Geochronology of Peraluminous High-K Granitic Leucosomes of Yaoundé Series (Cameroon): Evidence for a Unique Pan-African Magmatism and Melting Event in North Equatorial Fold Belt: International Journal of Geosciences, v. 3, p. 525-548.

Norton, G. B., 2009, Update Report - Djoum Exploration Program: Yaoundé, African Aura Resources Sarl p. 1-8.

Nystrom, J. O., and Henriquez, F., 1994, Magmatic features of iron ores of the Kiruna type in Chile and Sweden; ore textures and magnetite geochemistry: Economic Geology, v. 89, p. 820 - 839.

Oberteuffer, J. A., 1974, Magnetic Separation: A Review of Principles, Devices, and Applications: IEEE Transactions of Magnetics, v. MAG-10N, p. 223-238.

Ortiz, J. M., and Emery, X., 2006, Geostatistical estimation of mineral resources with soft geological boundaries: a comparative study: Journal of the South African institute of mining and metallurgy, v. 106, p. 577-584.

Petruk, W., 2000, Applied Mineralogy in the Mining Industry, Elsevier Science.

Petruk, W., Farrell, D., Laufer, E. E., Tremblay, R. J., and Manning, P. G., 1977, Non-tronite and ferruginoud opal from Peace River iron deposit in Alberta, Canada: Canadian Mineralogist, v. 15, p. 14-21.

Pickard, A. L., 2003, SHRIMP U–Pb zircon ages for the Palaeoproterozoic Kuruman Iron Formation, Northern Cape Province, South Africa: evidence for simultaneous BIF deposition on Kaapvaal and Pilbara Cratons: Precambrian Research, v. 125, p. 275-315.

Pirrie, D., Butcher, A. R., Power, M. R., Gottlieb, P., and Miller, G. L., 2004, Rapid quantitative mineral and phase analysis using automated scanning electron microscopy (QemSCAN); potential applications in forensic geoscience: Geological Society, London, Special Publications, v. 232, p. 123-136.

Pirrie, D., Power, M. R., Rollinson, G. K., Wiltshire, P. E. J., Newberry, J., and Campbell, H. E., 2009, Automated SEM-EDS (QEMSCAN®) Mineral Analysis in Forensic Soil Investigations: Testing Instrumental Reproducibility, in Ritz, K., ed., Criminal and Environmental Soil Forensics, Springer Science + Business Media B.V.

Pirrie, D., and Rollinson, G., 2011, Unlocking the applications of automated mineral analysis: Geology Today, v. 27, p. 226–235.

Plessis, G. D., Jonck, G. J., and Kruger, R., 1997, Potential low-grade iron ore deposits in metamorphosed banded iron formations, Northern Province, South Africa: Mineralium Deposita (1997), v. 32, p. 362-370.

Ramanaidu, E., Wells, M., Belton, D., Verrall, M., and Ryan, C., 2008, Mineralogical and Microchemical Methods for the Characterization of High-Grade Banded Iron Formation-Derived Iron Ore: Society of Economic Geologists, SEG Reviews, v. 15, p. 129-156.

Rao, D. S., Kumar, T. V. V., Rao, S. S., Prabhakar, S., and Raju, G. B., 2009, Mineralogy and Geochemistry of A Low Grade Iron Ore Sample from Bellary-

Hospet Sector, India and their Implications on Beneficiation: Journal of Minerals & Materials Characterization & Engineering, v. 8, p. 115-132.

Rao, V. K., Rao, R. C., and Narayana, A. C., 2014, Assessing Grade Domain of Iron Ore Deposit using Geostatistical Modelling: A Case Study Journal Geological Society of India, v. 83, p. 549-554.

Rollinson, G., 2008ii, Polishing a Resin block, CSM laboratory technical sheet No. 13, Camborne School of Mines.

Rollinson, G., 2008i, Resin Block Preparation CSM laboratory technical sheet No. 13, Camborne School of Mines.

Rollinson, G. K., Andersen, J. C. Ø., Stickland, R. J., Boni, M., and Fairhurst, R., 2011, Characterisation of non-sulphide zinc deposits using QEMSCAN: Minerals Engineering, v. 24, p. 778-787.

Rosiére, C. A., Baars, F. J., Seoane, J. C. S., Lobato, L. M., Silva, L. L. d., Souza, S. R. C. d., and Mendes, G. E., 2006, Structure and iron mineralisation of the Carajás Province: Applied Earth Science (Trans. Inst. Min. Metall. B), v. 115, p. 126 - 133.

Roy, S., Das, A., and Venkatesh, A. S., 2007, Characterisation of Iron Ore from the Jilling Area of Eastern India with a View to Beneficiation, Iron Ore Conference: Perth, Western Australia.

Roy, S., Das, A., and Venkatesh, A. S., 2008, A comparative mineralogical and geochemical characterisation of iron ores from two Indian Precambrian deposits and Krivoy rog deposit, Ukraine: implications for the upgrading of lean grade ore: Applied Earth Science (Trans. Inst. Min. Metall. B), v. 117, p. 125-147.

Sahoo, R., 2007 Degradation characteristics of steel making materials during handling: Powder Technology, v. 176, p. 77–87.

Sarkar, S., and Subrahmanyam, V. V. V., 2009, Method for Estimation of Na_2O and K_2O in Ores, Fluxes, Coal and Coke Ash by Inductively Coupled Plasma-Atomic Emission Spectroscopy: Journal of Minerals & Materials Characterization & Engineering, v. Vol. 8, p. 57-71.

Schmidt, R. C., and Kennedy, B. E., 1983, Geology of the Mont Klahoyo Iron Ore Deposit, Ivory Coast: Society of Mining Engineers of AIME, v. 27, p. 1801-1810.

Schouwstra, R. P., and Smit, A. J., 2011, Developments in mineralogical techniques – What about mineralogists?: Minerals Engineering, v. 24, p. 1224-1228.

Schulz, N. F., 1964, Determination of the Magnetic Separation Characteristic with the Magnetic Separation Characteristic with the Davis Magnetic Tube: AIME Transactions, Society of Mining Engineers, v. 229, p. 211-216.

Schwartz, M. O., and Melcher, F., 2004, The Faleme Iron District, Senegal: Economic Geology, v. 99, p. 917-940

SGS, 2011, Geometallurgy (www.met.sgs.com/metallurgy_home_v2/commodities/met_iron_ore_expertise/met-geometallurgy). Accessed 25 April 2011

SGS minerals services, 2014, Metallurgical testing for Iron Ore, (http://www.sgs.co.uk/~/media/Global/Documents/Flyers%20and%20Leaflets/SGS-MIN-WA116-Metallurgical-Testing-for-Iron-Ore-EN-11.pdf) Accessed 02 June 2014.

Shang, C. K., Satir, M., Siebel, W., Nsifa, E. N., Taubald, H., Liégeois, J. P., and Tchoua, F. M., 2004, TTG magmatism in the Congo craton; a view from major and trace element geochemistry, Rb–Sr and Sm–Nd systematics: case of the Sangmelima region, Ntem complex, southern Cameroon: Journal of African Earth Sciences v. 40, p. 61–79.

Siehi, A., and Thein, J., 1989, Minette-type ironstones, in Young, T. P., and Taylor, W. E. G., eds., Phanerozoic Ironstones, 46, Geological Society Special Publication, p. 175-193.

Siivola, J., and Schmid, R., 2007, International Union of Geological Sciences. Subcommission on the Systematics of Metamorphic Rocks, Cambridge University Press.

Singh, R., Rath, R., Nayak, B., and Bhattacharyy, K., 2010, Development of process for beneficiation of low-grade iron ore samples from Orissa, India: 25 International Mineral Processing Congress Brisbane, Australia, 6 - 10 september, 2010.

Soto-Viruet, Y., 2010, The Mineral Industry of Gabon, US. Geological Survey Minerals Year book: USGS.

Stanley, C. J., and Laflamme, J. H. G., 1998, Preparation of specimens for advanced ore-mineral and environmental studies, in Cabri, L. J., and Vaughan, D. J., eds., Modern Approaches to Ore and Environmental Mineralogy, 27, Mineral Association of Canada p. 111-121.

Suh, C. E., Cabral, A. R., and Ndime, E., 2009, Geology and ore fabrics of the Nkout high-grade haematite deposit, southern Cameroon Smart Science for Exploration and Mining, Proceedings of the Tenth Biennial SGA Meeting, Townsville, Australia, 2009, The origin of enriched iron and manganese ore deposits, p. 558 - 560.

Suh, C. E., Cabraral, A. R., Shemaemaemang, E. M., Mbinkarar, L., and Mboudou, G. G. M., 2008, Two Contrasting Iron Deposits in the Precambrian Mineral Belt of Cameroon, West Africa: Exploration and Mining Geology, v. 17, p. 197-207.

Svoboda, J., 1987, Magnetic Methods for the Treatment of Minerals: Amsterdam, Elsevier.

Svoboda, J., and Fujita, T., 2003, Recent developments in magnetic methods of material separation: Minerals Engineering v. 16, p. 785-792.

Swindell, K., 1967, Iron Ore Mining in West Africa: Some Recent Developments in Guinea, Sierra Leone, and Liberia: Economic Geography, v. 43, p. 333-346.

Tagne-Kamga, G., 2003, Petrogenesis of the Neoproterozoic Ngondo Plutonic complex (Cameroon, west central Africa): a case of late-collisional ferro-potassic magmatism: Journal of African Earth Sciences v. 36, p. 149-171.

Tamen, J., Nkoumbou, C., Mouafo, L. Reusser, E. Tchoua, F. M. , 2007, Petrology and geochemistry of monogenetic volcanoes of the Barombi Koto volcanic field (Kumba graben, Cameroon volcanic line): Implications for mantle source characteristics: Comptes Rendus Geoscience v. 339, p. 799-809.

Taylor, C. D., Schulz, K. J., Doebrich, J. L., Orris, G. J., Denning, P. D., and Kirschbaum, M. J., 2009, Geology and nonfuel mineral deposits of Africa and the Middle East:, U.S. Geological Survey Open-File Report 2005-1294-E, p. 246.

Taylor, R., 1992, On-line grain size measuring system for electrical steels production: Journal of Magnetism and Magnetic Materials, v. 112, p. 95-98.

Teo, C. S., Waters, A. G., and Nicol, S. K., 1990, Quantification of the breakage of lump materials during handling operations: International Journal of Mineral Processing, v. 30, p. 159-184.

Thella, J. S., Mukherjee, A. K., and Srikakulapu, N. G., 2012, Processing of high alumina iron ore slimes using classification and flotation: Powder Technology, v. 217, p. 418–426.

Theron, S. J., Richards, J. M., Naudé, G., Seroto, F., Walliser, A., and Bergmann, C., 2012, Mineralogical and Metallurgical Characterization of Highly Weathered to Fresh Metamorphosed Banded Iron Formations: Process Mineralogy, Cape Town, South Africa, November 7-9, 2012.

Timbillah, S., Aabulleh, P. N., and Agorhom, E. A., 2007, Iron Ore Surge in the World — The Role of Ghana: Iron Ore Conference, Perth, Western Australia, 20 - 22 August, 2007, p. 197-202.

Tohver, E., D'Agrella-Filho, M., and Trindade, R., 2006, Paleomagnetic record of Africa and South America for the 1200–500 Ma interval, and evaluation of Rodinia and Gondwana assemblies: Precambrian Research, v. 147, p. 193-222.

Tonžetić, I., and Dippenaar, A., 2011, An alternative to traditional iron-ore sinter phase classification: Minerals Engineering, v. 24 p. 1258-1263.

Trendall, A. F., and Morris, R. C., 1983, Iron-Formation: Facts and Problems, Elsevier Science Publishers B. V.

Tysdal, R. G., 1978, Geology of the Juazohn Quadrangle, Liberia, USGS Bulletin. Report number: B 1448: Reston, VA, United States, U. S. Geological Survey

Upadhyay, R. K., and Venkatesh, A. S., 2006, Current strategies and future challenges on exploration, beneficiation and value addition of iron ore resources with special emphasis on iron ores from Eastern India: Applied Earth Science (Transactions of the Institute of Materials, Minerals and Mining and The AusIMM), v. 115, p. 187-195.

USGS, 2013, Iron Ore, (http://minerals.usgs.gov/minerals/pubs/commodity/iron ore/mcs-2013-feore.pdf), Accessed 12 February 2014)

University of Cape Town centre for minerals research, 2013, Process Mineralogy (http://www.cmr.uct.ac.za/Research_Areas/ProcessMineralogy/index.html) Accessed 20 June 2013

University of Tasmania, CODES – ARC Centre of Excellence in Ore Deposits, 2013 (www.utas.edu.au/codes/research/recovery/theme-1-p4a1-predictive-environmental-indices) Accessed 20 December 2013

Varajão, C. A. C., Bruand, A., Ramanaidou, E. R., and Gilkes, R. J., 2002, Microporosity of BIF hosted massive hematite ore, Iron Quadrangle, Brazil: Anais da Academia Brasileira de Ciências v. 74, p. 113-126.

Vatandoost, A., Fullagar, P., Walters, S., and Kojovic, T., 2009, Towards Petrophysical Characterization of Comminution Behavior: 41st Annual Meeting of the Canadian Mineral Processors, Ottawa, Ontario, Canada, January 20 to 22, 2009.

Vicat, J. P., Pouclet, A., Nkoumbou, C., and Seme Mouangue, A. C., 1997, Le volcanisme fissural néoprotérozoïque des séries du Dja inférieur, de Yokadouma (Cameroun) et de Nola (RCA) : signification géotectonique: Comptes Rendus de l'Académie des Sciences, v. 325, p. 671-677.

Wang, E.-D., Xia, J.-M., Fu, J.-F., Jia, S.-S., and Men, Y.-K., 2014, Formation mechanism of Gongchangling high-grade magnetite deposit hosted in Archean BIF, Anshan-Benxi area, Northeastern China: Ore Geology Reviews v. 57, p. 308-321.

Waters, A. G., and Mikka, R. A., 1989, Segregation of Fines in Lump Ore Due to Vibration on a Conveyor Belt, 3rd International Conference on Bulk Materials Storage, Handling and Transportation Newcastle, p. 89 - 93.

Williams, H. R., 1978, THE Archaean Geology of Sierra Leone: Precambrian Research, v. 6, p. 251-268.

Williams, S., 2010, Introduction, about geometallurgy (www.geomettech.com).

Williams, S. R., and Richardson, J. M., 2004, Geometallurgical Mapping: A New Approach That Reduces Technical Risk: Proceedings 36th Annual Meeting of

the Canadian Mineral Processors, Ottawa, Ontario, Canada, January 20 - 22, 2004.

Wills, B. A., 1977, Mineral Processing Technology 3rd Edition, Oxford, Butterworth, Heinemann,

Woodtli, R. A., 1961, Iron Ore Resources of the North-Eastern Congo: Economic Geology, v. 56, p. 1385-1391.

Wright, J. B., Hastings, D. A., Jones, W. B., and Wiliams, H. R., 1985, Geology and Mineral Resources of West Africa: London, George Allen and Unwin Ltd.

Xiong, D., 1994, New development of the SLon vertical ring and pulsating HGMS separator: Magna Electric, v. 211, p. 211-222.

Yang, K., Huntington, J., Ehrig, K., Whitbourn, L., Mason, P., and Munday, T., 2011, HyLogging for Quantifying Gangue Minerals for Geometallurgy: GEOMIN2011, Antofagasta, Chile, 8-10 June, 2011.

Young, T. P., 1989, Phanerozoic ironstones: an introduction and review: Geological Society Special Publication, v. 46, p. 9-25.

Zanaga iron ore, 2010, http://zanagairon.com/ Accessed 30 November 2010

Zhao, G. C., Sun, M., and Wilde, S. A., 2002, Did South America and West Africa marry and divorce or was it a long-lasting relationship?: Gondwana Research, v. 5, p. 591-596.

Zou, J., 2007, Advances of Iron Ore Beneficiation in China, Iron Ore Conference Perth, Western Australia.

Appendices

Appendix 1 - 3 are copied to a CD accompanying this thesis

Appendix 4 – The following extended abstract and paper are attached below:

“Anderson, K. F. E., Rollinson, G. K., Wall, F., and Moon, C. J., 2013, A comparative automated mineralogical analysis of the Nkout (Cameroon) and Putu (Liberia) iron ore deposits, 12th SGA Biennal Meeting Uppsala, Sweden.

Anderson, K. F. E., Wall, F., Rollinson, G. K., and Moon, C. J., 2014, Quantitative mineralogical and chemical assessment of the Nkout iron ore deposit, Southern Cameroon: Ore Geology Reviews, v. 62, p. 25-39.

.

A comparative automated mineralogical analysis of the Nkout (Cameroon) and Putu (Liberia) iron ore deposits

Anderson K. F. E.[1], Rollinson G. K.[1], Wall F.[1] and Moon C. J.[1]
1 Camborne School of Mines
College of Engineering, Mathematics and Physical Sciences
University of Exeter
Cornwall Campus
Penryn
TR10 9EZ
United Kingdom
Email: kelloandy@yahoo.com

Abstract. The Nkout and Putu iron ore deposits form part of an emerging iron ore region in Central and West Africa. This study aimed to improve the understanding of the mineral deposits in order to predict the metallurgical and environmental responses of the ores. Quantitative mineralogical and geochemical analysis was carried out using automated mineralogy (QEMSCAN®) and the results corroborated with other techniques. The QEMSCAN® species identification protocol developed during the project includes three goethite entries; goethite/limonite, goethite (Al) and goethite (P) and, importantly, a procedure was developed to separate the different Fe-oxides based on their backscattered electron coefficients, thus overcoming one of the main problems in using QEMSCAN® analysis for iron ores. Magnetite was found to be dominant in the weathered profile at Nkout whist hematite is dominant at Putu. Goethite (Al) and chamosite occur as minor minerals at Putu whist goethite (P) occurs in trace quantities. All but goethite (P) occur as major minerals at Nkout. Chamosite is shown to affect the liberation of the iron oxides. The main gangue minerals at Nkout are gibbsite (Al Ox/OH) and quartz whilst quartz is the main gangue at Putu. Apatite is a minor mineral in the magnetite itabirite of both deposits.

Keywords. Automated Mineralogy, Iron ores, Fe-oxides, Central / West Africa

1 Introduction

The Nkout and Putu iron ore deposits form part of a growing region for the development and production of iron ore deposits in Central and West Africa. The growth of these regions is the result of three main factors; a) they are strategically located to markets in China, Europe and North America compared to either or both of the major suppliers, Brazil and Australia, b) renewed interest in magnetite deposits that can be used for pellet production suitable for blast furnace and c) these regions have been stable for the past decade after years of rebel insurrections making them attractive for investment.

This study aims to improve the mineralogical understanding of these mineral deposits in order to predict the metallurgical and environmental responses of the ores. Quantitative mineralogical analysis of samples from both deposits has been done using automated mineralogy (QEMSCAN®) and the results corroborated with other techniques such as optical microscopy, X-ray diffraction (XRD), X-ray fluorescence (XRF) and electron probe microanalysis (EPMA). A particular aim of the study was to establish a protocol to overcome the difficulty of identifying hematite and magnetite by the QEMSCAN® technique.

2 Geology of the Study Areas

2.1 Regional Geology

Southern Cameroon is underlain by an Archean to Proterozoic cratonic basement which extends across parts of several West and Central African countries. This basement forms part of the northern extension of the Congo craton and the rocks include quartzites, schists, amphibolites, charnockites, greenstones, granulites and gneiss (Tagne-Kamga 2003). The banded iron formations (BIF) in the region are Archean, hosted by greenstones, and associated with granites and gneiss of similar age.

The Republic of Liberia rests on the Archean West African shield. In Liberia it has been intensely folded and faulted. The dominant rock types in the West African shield are granites, schist and gneiss. The rock types in the northern and western parts of Liberia are mainly gneiss units with siliceous BIFs and schist which are Liberian (2.7 Ga) in age (Tysdal, 1978).

2.2 Deposit Geology

According to ground magnetic survey (conducted by one of the authors), Nkout consists of a cap of laterite and saprolite material with a lateral extent of about 9 km E-W, enriched in iron oxide over magnetite rich BIF (itabirite). Itabirite is a term that originated from the province of Itabirito (Pico de itabirito), in the state of Minas Gerais in Brazil which hosts major banded quartz hematite magnetite metamorphosed oxide facies banded iron formations. The BIF at Nkout is hosted by greenstones and has been tilted towards the north. The magnetite itabirite forms the bulk of the deposit.

The Putu deposit is divided into two mountain ranges with different trends; Jideh has a NNW – SSE trend with a lateral extent of about 15 km and Montroh has an E – W trend and a lateral extent of about 4 km. The dominant rock type in the area is the granodiorite gneiss.

Iron minerals within the Putu deposit consist predominantly of magnetite-itabirite. A thick layer of hematite-itabirite lies over the magnetite-itabirite minerals in the Jide mountain range. The itabirites are mainly fine grained and composed or quartz, iron oxides and minor silicates. Magnetite is the main iron-oxide but Jideh in particular is known to have a hematite cap of up to 80m thick with potential to be used as a direct shipping ore (DSO).

3 Classification of Material Types

Thirty three drill cores representative of the Nkout deposit based on detailed core logs were selected and sampled. They include saprolites, laterites and fresh BIF. Outcrop and grab samples were also collected during mapping of the area and nine were selected for analysis. Nine coarse rejects samples representative of the Putu deposit were selected by the chief geologist at the time and sent along with eleven representative BIF drill cores for analysis.

Both sets of samples were divided into 4 main groups based on the whole rock Fe content determined by XRF analysis and their degree of weathering. The groups are enriched material (EM), weathered magnetite itabirite (WMI), transitional magnetite itabirite (TMI) and magnetite itabirite (MI). The magnetite itabirite group is divided into 2 groups; high-grade (HMI) and low-grade magnetite itabirite (LMI). The degree of weathering which is an expression of the physical characteristics of the ore grade materials is classified using an intensity of weathering (WI) on a scale of 1 to 6. 1 and 2 represents hard materials such as fresh itabirite or hard massive hematite and BIF outcrops, 3 and 4, medium hard materials and 5 and 6, friable biscuity or lateritic material. Table 1 gives the adopted classification.

Table 1. Classification scheme adopted for this research. It is based on the total Fe content and a weathering index of 1 to 6 in which 1 represents fresh itabirite and 6, completely weathered material.

Code	Material Types	Description
EM	Enriched material	$\geq$ 60 wt%, WI = 2 to 6
WMI	Weathered magnetite itabirite	50 wt% $\leq$ Fe < 60 wt%, WI $\geq$ 4
TMI	Transitional magnetite itabirite	15 wt% $\leq$ Fe < 50 wt%, WI = 3 or 4
MI	High-grade magnetite itabirite	Fresh itabirite, 30 wt% $\leq$ Fe < 60 wt%, WI = 1 or 2
	Low-grade magnetite itabirite	Fresh itabirite, 15 wt% $\leq$ Fe < 30 wt%, WI = 1 or 2

4 Methodology

XRF analysis was conducted at Omac Laboratory, Ireland. QEMSCAN® and all other analyses were conducted at Camborne School of Mines, University of Exeter. The original LCU5 SIP file that was provided with the QEMSCAN® was modified based on the geology of the study area and the results of analyses by EPMA, XRD, SEM/EDS and optical microscopy.

The modified SIP includes 3 goethite entries: goethite/limonite, phosphorus bearing and aluminium bearing goethite i.e., goethite (P) and goethite (Al) respectively. This is because EPMA confirmed the presence of Al and P within the goethite in the study areas; a result also confirmed previously for goethite in general (Ramainadu 2008). Goethite (P) contains > 3% P and < 3% Al, Goethite (Al) contains < 3% P and > 3% Al whilst goethite/limonite contains < 3% P and Al. Three percent is the detection limit of the QEMSCAN® settings used in this study. Chamosite, the Fe-rich chlorite was separated from the others i.e. clinochlore (Mg-rich) and pennantite (Mn-rich). Chamosite was found to be present and is intergrown with the Fe-oxides, mainly goethite and hence affected liberation of the Fe-oxides.

One of the main problems in using QEMSCAN® analysis on iron ores is that there is only a 3 wt% difference in the Fe-oxide content of magnetite and hematite and so the 1000 count x-ray spectra used in this technique do not contain enough counts to be able to distinguish the two minerals (e.g. Andersen et al 2009). In order to overcome this, a procedure was developed to separate hematite and magnetite based on their backscattered electron signal (BSE). The BSE range is calibrated to quartz at the lower end (42) and gold at the top end (232). For this research, magnetite is from 89 to 100 and hematite is from 80 to 88. Geothite is less than 80 and includes limonites at the lower range (about 50 or less).The BSE will vary between QEMSCAN® systems (Tonzetic & Dippenaar 2011) and so the signal needs to be carefully set up and calibrated.

The garnet group was divided into two, almandine and andradite because it was noted from EPMA and XRD analysis that almandine was present at Nkout whilst andradite was present at Putu. The issues such as edge effects and variation in BSE signals identified by Rollinson et al. (2011) and Benedictus and Horsch (2008) where considered during the data processing stages.

5 Results

5.1 Modal Mineralogy

The QEMSCAN® back calculated Fe% in general decreases with decreasing size fraction i.e. decreases from -250/+180 to -125/+90 to -63/+45. Of these three size fractions, the -63/+45 gave back calculated Fe % that is ± 3 % that obtained for the XRF but could be greater when quartz is one of the most abundant minerals in the sample. The other two size fractions gave QEMSCAN® back calculated Fe% higher than the error margin of the -63/+45 fraction. Differences between the XRF and QEMSCAN® are expected due to the differences in techniques and particle sizes. Figure 1 summarises the modal mineralogy, expressed in weight percentages, for the samples from Nkout and Putu. The major difference between the two study areas in terms of the Fe-oxides is the higher concentration of magnetite at

Nkout whereas hematite is higher at Putu in the enriched material to transitional magnetite itabirite. Goethite/limonite is the most abundant goethite at Putu and Nkout. However goethite (Al) and chamosite are limited to the enriched material whist goethite (P) occurs in trace quantities at Putu. Goethite (P) occurs in minor quantities at Nkout but goethite (Al) and chamosite occurs as major minerals in the enriched material to transition magnetite itabirite.

The Al content of the enriched material to the transitional magnetite itabirite at Nkout is higher than that at Putu due to the presence of Al Ox(OH) which is present mainly in the enriched material at Putu. In the magnetite itabirites, the Al is present in the form of the aluminosilicates in both study areas. CaO is higher at Putu mainly due to the higher concentration of Ca Mg Fe silicates (Figure 1). The same trend in which SiO_2 increases from the enriched material to the low-grade magnetite is present in both localities and is due to the quartz content. The loss on ignition in general decreases from EM to the magnetite itabirites in both study areas but is higher at Nkout mainly due to its higher goethite concentration.

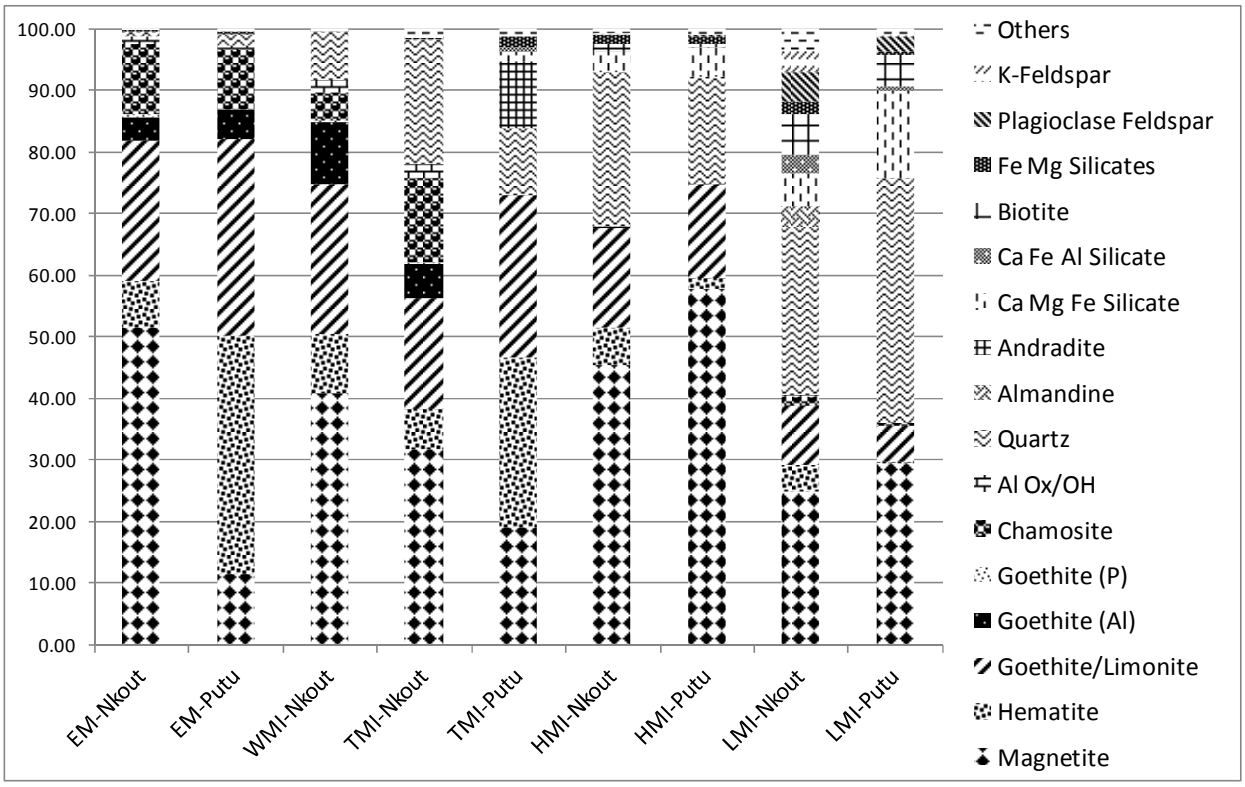

Figure1. Summary of the modal mineralogy (weight %) of the Nkout and Putu deposits. Similar material types are placed side by side for easy comparison. Note that WMI-Putu is absent as none of the samples from Putu fit into this category. See Table 1 for explanations of the material types.

5.2 Mineral Association and Liberation

The mineral association is calculated using the QEMSCAN® software to determine which minerals are adjacent for a given particle. The liberation data is classified into 10 % intervals and is based on the weight of a particular mineral in each particle. For this research, a mineral is considered as being liberated if > 90% is free, high grade inter-grown if it is 60-90%, low grade inter-grown if 30-60% and locked if it is < 30%. Both the mineral association and liberation are considered with respect to the modal mineralogy.

The Fe-oxides are closely associated at both localities with magnetite and hematite being about 60% associated. When chamosite is present in both localities, it is mainly associated with Fe-oxides (goethite/limonite in particular) and reduces liberation of the Fe-oxides as illustrated in Table 2 and Figure 2.

Table 2. Modal mineralogy weight % data for 4 enriched material samples. The samples with high chamosite have poorer liberation, see Figure 2.

ID	Mag	Gt/ Lim	Hem	Chm	Qtz
G02	54.34	35.07	4.68	0.09	0.03
NCS04	35.49	16.17	3.68	**31.85**	1.19
NES04	56.81	14.74	8.51	**13.67**	0.18
OUT02	59.37	24.58	13.47	0.04	2.35

In Table 2, the second and third samples have higher chamosite concentration than the first and fourth and this is reflected in the liberation of the Fe-oxides in Figure 2.

Whereas almandine is mainly associated with chamosite at Nkout, andradite at Putu is mainly associated with goethite/limonite. Quartz in both localities is mainly associated with the Fe Mg silicates such as the serpentine group (antigorite).

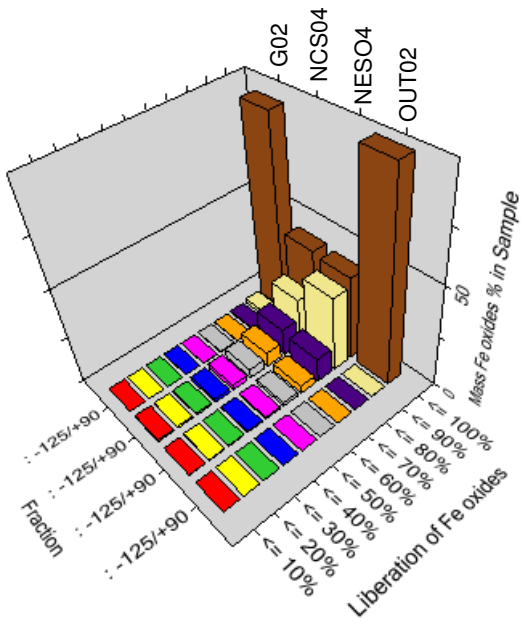

Figure 2. Liberation for 4 enriched samples. Note that the 2 samples in the middle have higher chamosite (Table 2) concentration compared to the other 2 on the edges.

For the -125/+90 fraction, as far as the Fe-oxides are concerned, about 36% of magnetite are > 90 % liberated and 57 % are high-grade inter-grown. When magnetite, hematite and the different goethite are combined as Fe-oxides, liberation is > 90 %.

6 Conclusions

- The Nkout and Putu deposits consist of iron oxide minerals with no evidence of iron carbonates. Iron sulphides are present mainly in the form of pyrite which is restricted to minor quantities in the magnetite itabirites.
- Hematite is the main Fe-oxide in the enriched material to transitional magnetite itabirite at Putu whereas at Nkout it is magnetite. Magnetite content in the enriched material at Nkout is about 5 times than at Putu whilst for the hematite content the reverse is true with Putu having about 5 times more than Nkout.
- Goethite (Al) and goethite/limonite occur in about equal quantites in the enriched material at Nkout and Putu. Problems with goethite (Al) at Nkout are more noticed in the transitional magnetite itabirite with Nkout having about 105 times than in Putu. Goethite (P) occurs as a trace mineral in the enriched material at Putu but could be significant from a processing point of view at Nkout where it occurs as a minor mineral in the enriched material and weathered magnetite itabirite.
- Chamosite which has been shown to affect liberation of the Fe-oxides is a major mineral at Nkout in all but one of the material types whereas at Putu,it is only a major mineral in the enriched material. Chamosite occurs in similar proportions in the enriched material but differs significantly in the transitional magnetite itabirite with Nkout having about 156 times more than Putu.
- The main gangue minerals in the enriched material to transitional magnetite itabirite at Nkout are gibbsite (Al Ox/OH) and quartz. Quartz is the main gangue at Putu.
- Apatite is the P-bearing mineral in the magnetite itabirite at both Nkout and Putu and occurs as a minor mineral associated with the silicates. Calcite occurs as a minor mineral in the magnetite itabirite at Putu and occurs in trace quantities at Nkout.
- Magnetite occurs in about equal propotion in the magnetite itabirite at Putu and Nkout. The magnetite itabirite is the main ore material at both Nkout and Putu. The liberation of the Fe-oxides as a group for the -125/+90 µm size fraction is about 90 % making them amenable to inexpensive processing such as crushing, grinding and magnetic separation. The Al Ox(OH) at Nkout could be removed by attrition scrubbing.

Acknowledgements

The authors are grateful for the support of the Association of Commonwealth Universities in sponsoring this PhD research. We would like to acknowledge Afferro Mining Ltd and the Putu Iron Ore Mining for their support during field work exercises and the provision of samples.

References

Andersen JCØ, Rollinson GK, Snook B, Herrington R, Fairhurst RJ (2009) Use of QEMSCAN for the characterization of Ni-rich and Ni-poor goethite in laterite ores. Minerals Engineering 22 1119-1129. doi:10.1016/j.mineng.2009.03.012

Benedictus A, Horsch H (2008) Enhanced measurement capabilities for iron ore deposits 34th Int. Geol Congr, International Union of Geol Sciences. Brisbane, Australia.

Ramanaidu E, Wells M, Belton D, Verrall M, Ryan C (2008) Mineralogical and Microchemical Methods for the Characterization of High-Grade Banded Iron Formation-Derived Iron Ore. Soc Econ Geol, SEG Reviews 15: 129-156

Rollinson GK, Andersen JCØ, Stickland RJ, Boni M, Fairhurst R (2011) Characterisation of non-sulphide zinc deposits using QEMSCAN. Minerals Engineering 24: 778-787. doi:10.1016/j.mineng.2011.02.004

Tagne-Kamga G (2003) Petrogenesis of the Neoproterozoic Ngondo Plutonic complex (Cameroon, west central Africa): a case of late-collisional ferro-potassic magmatism. Journal of African Earth Sciences 36:149-171. doi:10.1016/S0899-5362(03)00043-5

Tonžetić I, Dippenaar A (2011) An alternative to traditional iron-ore sinter phase classification. Minerals Engineering 24 1258-1263. doi:10.1016/j.mineng.2011.04.012

Tysdal RG (1974) Geology of the Juazohn Quadrangle, Liberia. United States Geological Survey.

Ore Geology Reviews 62 (2014) 25–39

Contents lists available at ScienceDirect

Ore Geology Reviews

journal homepage: www.elsevier.com/locate/oregeorev

Quantitative mineralogical and chemical assessment of the Nkout iron ore deposit, Southern Cameroon

Kelvin F.E. Anderson *, Frances Wall, Gavyn K. Rollinson, Charles J. Moon

Camborne School of Mines, College of Engineering, Mathematics and Physical Sciences, University of Exeter, Penryn Campus, Penryn TR10 9EZ, United Kingdom

ARTICLE INFO

Article history:
Received 10 December 2013
Received in revised form 18 February 2014
Accepted 28 February 2014
Available online 6 March 2014

Keywords:
Iron oxides
Iron ore
Material characterisation
Automated mineralogy
QEMSCAN®

ABSTRACT

The Nkout deposit is part of an emerging iron ore province in West and Central Africa. The deposit is an oxide facies iron formation comprising fresh magnetite banded iron formation (BIF) at depth, which weathers and oxidises towards the surface forming caps of high grade hematite/martite–goethite ores. The mineral species, compositions, mineral associations, and liberation have been studied using automated mineralogy (QEMSCAN®) combined with whole rock geochemistry, mineral chemistry and mineralogical techniques. Drill cores (saprolitic, lateritic, BIF), grab and outcrop samples were studied and divided into 4 main groups based on whole rock Fe content and a weathering index. The groups are; enriched material (EM), weathered magnetite itabirite (WMI), transitional magnetite itabirite (TMI) and magnetite itabirite (MI). The main iron minerals are the iron oxides (magnetite, hematite, and goethite) and chamosite. The iron oxides are closely associated in the high grade cap and liberation of them individually is poor. Liberation increases when they are grouped together as iron oxides. Chamosite significantly lowers the liberation of the iron oxides. Automated mineralogy by QEMSCAN® (or other similar techniques) can distinguish between Fe oxides if set up and calibrated carefully using the backscattered electron signal. Electron beam techniques have the advantage over other quantitative mineralogy techniques of being able to determine mineral chemical variants of ore and gangue minerals, although reflected light optical microscopy remains the most sensitive method of distinguishing closely related iron oxide minerals. Both optical and electron beam automated mineralogical methods have distinct advantages over quantitative XRD in that they can determine mineral associations, liberation, amorphous phases and trace phases.

1. Introduction

Iron oxide minerals occur in many geological materials and their characterisation is essential in determining the process mineralogy of potential iron ores. Understanding the process mineralogy is an essential step in the development of an iron ore mine because there are maximum acceptable levels for the common contaminants in iron ores and although in general contaminants should be kept as low as possible, requirements vary from customer to customer. Clout and Simonson (2005) summarise contaminant levels and their effect on the downstream process performance of iron ores.

The 'time honoured' practice for iron ores has been to use reflected light microscopy to manually achieve results similar to those of the Quantitative Evaluation of Minerals using a Scanning Electron Microscope (QEMSCAN®). However, ore bodies are often highly complex and cannot always be adequately quantified by manual quantitative microscopy (Gottlieb et al., 2000). Several workers (Donskoi et al., 2007, 2011; Fandrich et al., 2006; Ramanaidu et al., 2008) have sought to bring to the attention of the iron ore industry the value of applying techniques such as the use of reflectance spectroscopy, X-ray diffraction (XRD), scanning electron microscope (SEM) and electron probe microanalysis (EPMA). The main problem in using SEM-based automated mineralogy for iron ore deposits has been the difficulty in distinguishing the iron oxides because of the similarity of hematite and magnetite on rapidly acquired energy-dispersive X-ray spectra. This problem can be overcome by using backscattered electron signals instead of X-ray spectra (Tonžetić and Dippenaar, 2011) and this study discusses the protocol required to identify the mineral species, associations, liberation and also variations in mineral compositions. The analysis uses QEMSCAN®, a well established technique that generates high volumes of mineral data to aid mineral and metallurgical processing (e.g. Thella et al., 2012). In this work QEMSCAN® is shown to be an important tool for studies that require an understanding of the mineralogical relationships and compositional information on distribution of deleterious elements such as P, Al, and Si.

The work arose from a study of the Nkout deposit in southern Cameroon, which is part of an emerging new large iron ore province in West and Central Africa, about which very little has been published

* Corresponding author. Tel.: +44 7503667041.
E-mail address: kelloandy@yahoo.com (K.F.E. Anderson).

http://dx.doi.org/10.1016/j.oregeorev.2014.02.015
0169-1368/

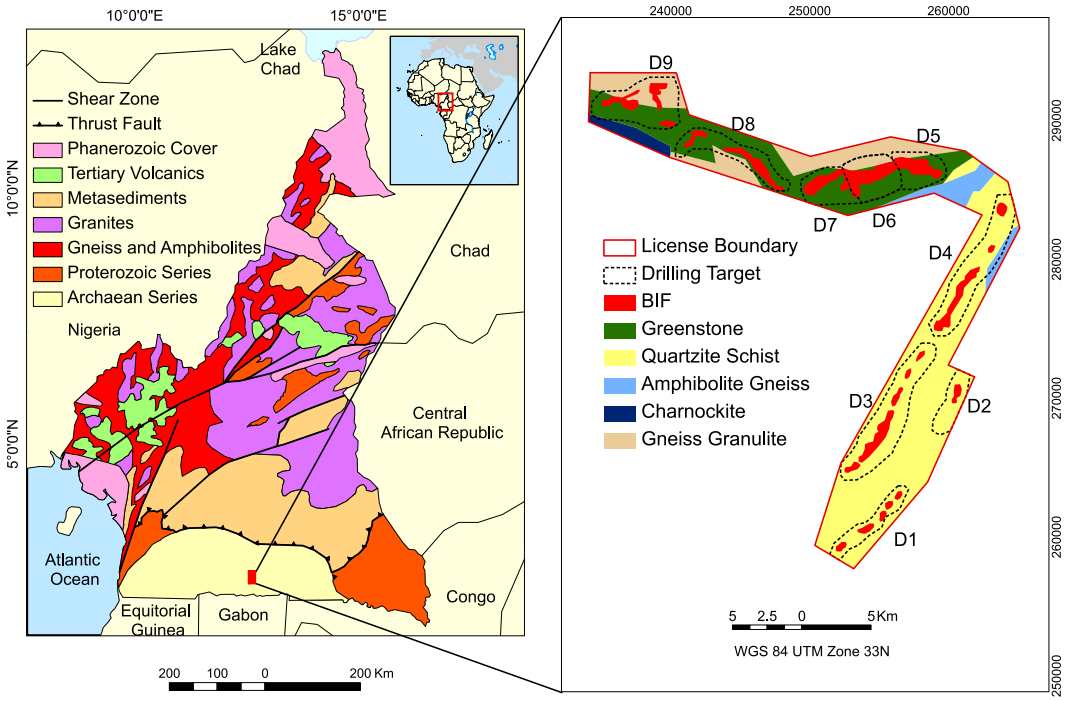

Fig. 1. Simplified geological map of Cameroon (modified from Ngnotué et al., 2000; Tagne-Kamga, 2003) and geological outline of the Djoum License (modified from various internal reports). Ntem Complex (NC); Dja Series (DS); Nyong series (NS); Adamaoua fault (AF), Kribi- Campo fault (KCF), Sanaga fault (SF); Tchollire-Banyo Fault (TBF). Nkout centre = D6, Nkout east = D5, Nkout south = D3, Nkout west = D7.

(Suh et al., 2009). Nkout is an oxide facies iron formation comprising fresh magnetite banded iron formation (BIF) at depth which weathers and oxidises towards the surface forming caps of enriched hematite/martite-goethite ores. It thus provides an excellent example of multiple iron oxide minerals and complex mineral associations.

This study concentrates on process mineralogy but the technique can be equally well applied to geological studies of iron oxide-rich materials where large data sets and statistically valid information are required.

2. Geological context

Southern Cameroon is underlain by an Archean to Proterozoic cratonic basement (2500 to 600 Ma) which forms part of the northern extension of the Congo craton and comprises the Ntem Formation composed of the Ntem Complex (NC), the Dja Series (DS) and the Nyong series (NS) (Tagne-Kamga, 2003) (Fig. 1). These rocks have been metamorphosed and include quartzites, schists, amphibolites, charnockites, greenstones, granulites and gneiss. The BIFs in the region are Archean in age, hosted by greenstones (Fig. 1) and associated with granites and gneiss of similar age.

The BIFs are a variety called itabirite, a term that originated from the province of Itabirito (Pico de itabira), Minas Gerais, Brazil to describe metamorphosed oxide facies BIF (Cabral and Rosière, 2013) in which quartz has been recrystalized into megascopic quartz and the iron is in the form of hematite, martite (hematite pseudomorphs after magnetite), goethite and magnetite. This region of Brazil hosts major deposits, encompassed by the Quadrilatero Ferrifero, and was once linked to the Congo Craton (Tohver et al., 2006).

The deposit at Nkout comprises a number of areas with elevated iron concentrations (Fig. 1), including greater than 50 m of iron-enriched cap (45% Fe cut off) at Nkout East (D5) and Nkout Centre (D6). The current resource estimate is 1.6 billion tonnes at 33.3% Fe indicated, 0.9 billion tonnes at 30.8% Fe inferred and this includes 64.3 million tonnes at 54.5% Fe indicated and 8.2 million tonnes at 50.1% Fe inferred. This resource estimate is from 12 km of 20 km total strike of a major magnetic geophysical anomaly. 54,500 m has been drilled to date (Affero Mining Inc., 2013).

3. Materials and methods

3.1. Analytical setup

With the exception of the XRF analysis which was outsourced to ALS Minerals, Loughrea, Ireland (formerly OMAC Laboratory), all other mineral chemistry and mineralogical analyses were conducted at the Camborne School of Mines (CSM) laboratory, University of Exeter, Penryn Campus, Cornwall. Approximately 30 g of each sample was sent to ALS Minerals Laboratory to be analysed using package

Table 1
Classification scheme adopted for this research.

Abbreviation	Material types	Fe content and degree of weathering
EM	Enriched material	≥60 wt.%, WI = 2 to 6
WMI	Weathered magnetite itabirite	50 wt.% ≤ Fe < 60 wt.%, WI ≥ 4
TMI	Transitional magnetite itabirite	15 wt.% ≤ Fe < 50 wt.%, WI = 3 or 4
HMI	High-grade magnetite itabirite	Fresh itabirite, 30 wt.% ≤ Fe < 60 wt.%, WI = 1 or 2
LMI	Low-grade magnetite itabirite	Fresh itabirite, 15 wt.% ≤ Fe < 30 wt.%, WI = 1 or 2

Fe contents determined by XRF.
Arbitrary weathering index of 1 to 6 in which 1 represents fresh itabirite and 6 is highly weathered material.

ME-XRF21u for iron in which the following elements and oxides were analysed: Al_2O_3, As, Ba, CaO, Cl, Co, Cr_2O_3, Cu, Fe, K_2O, MgO, Mn, Na_2O, Ni, P, Pb, S, SiO_2 Sn, Sr, TiO_2, V, Zn and Zr. Fe_2O_3 was calculated and reported as part of the result. Loss on ignition (LOI, code OA-GRAO5x) at 1000 °C was also done. The accuracy and precision of the analysis done at ALS Minerals Laboratory were tested using the results of a blind reference material i.e. European certified reference material Euronorm-crm No. 682-2 iron ore, 4 duplicate samples and 4 blanks were sent in addition to 51 samples. In addition to these, ALS Minerals created their own duplicate

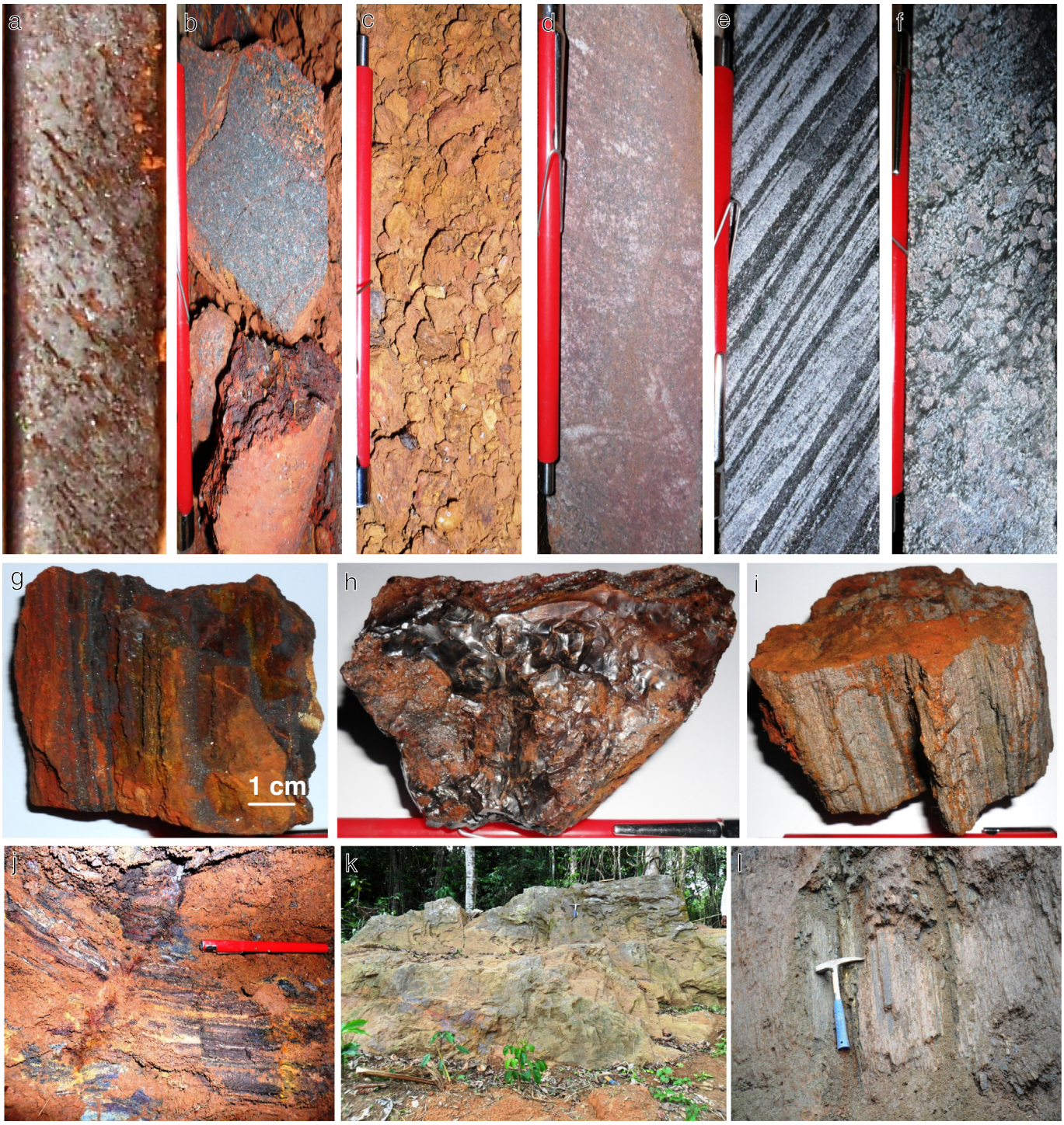

Fig. 2. Examples of material types a) Enriched material with silver-grey hematite crystals; drill hole NKHC040, 12.6 m WI = 4 (Sample NCS09), (b) Weathered magnetite itabirite with black magnetite and red hematite; drill hole NKEHC007, 6.3 m WI = 5 (Sample NES04), (c) Lateritic weathered magnetite itabirite containing yellowish limonite/goethite; drill hole NKHC020, 20 m WI = 6 (Sample NCS08), (d), Transitional magnetite itabirite showing initial stage of weathering of fresh itabirite; drill hole NKEHC008, 28.35 m WI = 3 (Sample NES05), (e) High-grade magnetite itabirite with alternating bands of magnetite, quartz and silicates; drill hole NKWHC002, 73.00 m, WI = 1 (Sample NWB02), (f) Low-grade magnetite itabirite with round pink garnet grains; drill hole NKWHC001, 85.60 m WI = 1 (Sample NWB01), (g) Grab sample with blue/black hematite/magnetite and yellow goethite minerals, WI = 3 (Sample G02), (h) Magnetite and goethite rich grab sample with glassy texture; WI = 3 (Sample G01), (i) Siliceous grab sample WI = 4 (Sample G03), (j) Saprolite outcrop WI = 6 (Sample Out02), (k) Hard massive outcrop WI = 2 (Sample Out01). (l) Silica rich saprolite outcrop WI = 6 (Sample Out03). (For interpretation of the references to colour in this figure legend, the reader is referred to the web version of this article.)

Table 2
Average major element geochemistry (XRF) for the various classified material types.

Mat. type	EM	WMI	TMI	HMI	LMI
SiO_2	2.57	8.65	28.13	45.48	58.1
TiO_2	0.06	0.12	0.35	0.17	0.24
Al_2O_3	2.29	4.12	6.79	0.84	7.96
Fe_2O_3	91.83	80.26	60.16	51.28	27.27
Mn	0.07	0.06	0.05	0.06	0.08
MgO	0.03	0.02	0.03	1.49	2.15
CaO	bdl	bdl	bdl	0.97	2.17
Na_2O	bdl	bdl	bdl	0.23	1.04
K_2O	bdl	bdl	0.04	0.17	1.35
P	0.09	0.23	0.05	0.03	0.13
S	0.01	0.03	0.02	0.39	0.1
LOI	2.93	6.91	5.03	bdl	0.17
Total	99.88	100.4	100.65	101.11	100.76

Analyses by XRF, see text., LOI = loss on ignition conducted at 1000 °C, bdl = below detection limit.

samples and analysed in-house reference materials and blanks. Comparison of the ALS Minerals results for the reference material and the average expected values are within ±5% for values >0.1% and ±10% for values <0.05% which are near the detection limits of the elements and oxides. Similar variability in values was also observed when the results for the duplicate samples were compared.

Scanning Electron Microscopy with Energy Dispersive X-ray Spectrometer (SEM–EDS) using a JEOL JSM-5400LV instrument provided high resolution imaging of the samples and their elemental compositions and was also used as a guide for the elements to be analysed by EPMA.

A JEOL JXA-8200 Super probe EPMA was used to map the distribution of the major, minor and trace elements in the samples. A 15 nA specimen current, acceleration voltage of 15 kV, spot size of 5 μm and a ZAF matrix correction routine were used. The results were quantified with reference to pure metal and oxide primary standards. Chemical formulae of the minerals were calculated using methods described by Droop (1987) and Deer et al. (1992). Twelve samples representative of the various material types were selected for EPMA studies and 318 point analyses were made in order to support the QEMSCAN® identifications.

The mineralogical characteristics of the samples were also studied using polished thin sections under reflected light microscopy and by photomicrographs taken using a Nikon Eclipse E600 Pol with instant image capture through a Nikon Digital Sight 5MP camera. In addition, qualitative powder XRD was done to provide the bulk mineral assemblages in the samples. The instrument used was a Siemens D5000 X-ray diffractometer using a voltage of 40 kV, current of 30 mA and samples run from 20 to 70°, 2θ. The detection limit is about 5% but it is also dependent amongst other factors, on the crystallinity of the minerals being identified e.g. less crystalline minerals such as goethite does not provide distinct peaks. The raw data was smoothed for some samples in order to aid the interpretation which used the JCPDS PDF-2 (2004) database and Bruker EVA software V.10.0.1.0.

Quantitative mineralogical analysis was carried out on a QEMSCAN® 4300, based on the Zeiss EVO 50 Scanning Electron Microscope (SEM) platform with four light element Bruker silicon drift droplet (SDD) X-ray detectors (Rollinson et al., 2011). Most of the analysis was done using particle mineral analysis (PMA) mode. Using PMA, the mineral grains in the sample are mapped by applying grids of pixels each with an analysis point (Pirrie and Rollinson, 2011). The result is a particle map showing the mineral composition of the individual grains measured. iMeasure v.4.2 software was used for data acquisition and iDiscover v. 4.2 was used for the spectral interpretation and data processing. Analysis was conducted on three size fractions i.e. -250/+180 μm, -125/+90 μm and -63/+45 μm. These size fractions were chosen as time and cost had to be considered for the project and they represent every other size fraction (after -45 μm) in order to cover the range of size fractions. For this research, major minerals refer to those that occur >1 wt.%, minor minerals, between 0.1 wt.% and 1 wt.% whilst trace minerals are those <0.1 wt.%. For details on the basic QEMSCAN® methodology and analytical modes see Gottlieb et al. (2000) and Pirrie et al. (2004). Further details and discussion of the development of the analytical protocol are given below.

3.2. Samples

A total of 51 samples comprising 42 drill core samples, 3 grab samples and 6 outcrop samples were analysed. The drill core samples were carefully selected so that they were representative of the deposit based on detailed core logging. They are from 31 drill holes and include saprolite, laterite and fresh BIF samples. Iron rich grab and outcrop samples were collected during detailed mapping of the area and 9 of these were selected for analysis. Other rock types were also collected in order to sample the variability of rock types present.

The outcrop, grab and core samples were crushed using a Retsch steel jaw crusher (to -3 mm), then milled using a tungsten-carbide mill so that various size fractions necessary for other techniques could be produced. They were then divided using a Jones Riffle into three parts. One part was milled into powder (< -45 μm) for XRF analysis, including loss-on-ignition (LOI) and powder XRD studies, another part was sieved with a Ro-Tap shaker into various size fractions for EPMA and QEMSCAN® and the third set reserved. Sand or glass beads were used to clean the tungsten-carbide mill in-between samples. The -250/+180 μm, -125/+90 μm, and -63/+45 μm size fractions were studied using the QEMSCAN®. Since the samples comprise different minerals with different densities and sizes, it was essential to have random samples to avoid bias and this was achieved using a rotary microriffler.

3.3. Sample classification

The samples were divided into 4 main groups based on the whole rock Fe content determined by XRF analysis and the degree of weathering determined by visual estimation. The groups are enriched material (EM), weathered magnetite itabirite (WMI), transitional magnetite itabirite (TMI) and magnetite itabirite (MI) (Table 1, Fig. 2). The magnetite itabirite group is divided into 2 sub-groups; high-grade (HMI) and low-grade magnetite itabirite (LMI). The physical characteristics of the ore grade materials have been classified using their intensity of weathering (WI) on a scale of 1 to 6. One and two represent hard materials such as fresh itabirite or hard massive hematite and BIF outcrops (Fig. 2, e, f), 3 and 4 medium hard materials (Fig. 2 a, d, g and h) and 5 and 6, friable biscuity or lateritic material (Fig. 2 b, c, j & l). EM and WMI materials at Nkout are dominated by friable biscuity, laterite and saprolite material although at least one hard hematite/goethite outcrop is present (Out01, Fig. 2k) and was studied. These groups were chosen to represent processing requirements and characteristics rather than geological origin.

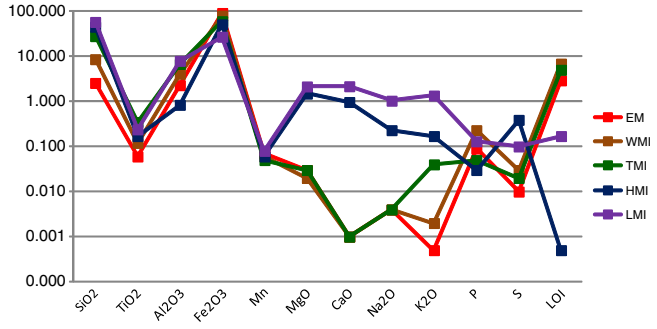

Fig. 3. Plot of average chemical compositions for the various material types as described in Table 1.

Table 3
Major element geochemistry (XRF) with depth through the enrichment profile of drill hole NKHC027. The material types are based on the classification scheme of Table 1.

Depth (m)	Material type	SiO_2	TiO_2	Al_2O_3	Fe_2O_3	Mn	MgO	CaO	Na_2O	K_2O	S	P	LOI	Total	Fe
3.60	WMI	2.12	0.18	5.59	83.37	0.04	0.03	0.01	0.06	0.01	0.02	0.18	7.50	99.12	58.31
8.10	EM	0.77	0.09	6.06	86.61	0.05	bdl	bdl	bdl	bdl	0.02	0.18	7.22	101.02	60.58
12.60	EM	0.44	0.06	3.20	91.68	0.09	bdl	bdl	bdl	bdl	bdl	0.11	4.76	100.36	64.13
17.10	EM	0.51	0.03	2.01	92.74	0.08	bdl	bdl	bdl	bdl	bdl	0.18	5.43	101.00	64.87
27.60	EM	0.78	0.02	1.27	94.80	0.09	bdl	bdl	bdl	bdl	bdl	0.14	3.32	100.44	66.31
30.60	EM	0.44	0.01	0.50	95.30	0.11	bdl	bdl	bdl	bdl	bdl	0.08	3.06	99.53	66.66
39.60	EM	1.27	0.02	0.82	97.51	0.12	bdl	bdl	bdl	bdl	bdl	0.05	1.46	101.29	68.20
41.60	EM	2.19	0.01	0.63	96.22	0.15	bdl	bdl	bdl	bdl	0.01	0.04	1.44	100.73	67.30
46.10	EM	3.46	0.01	0.87	93.26	0.10	bdl	bdl	bdl	bdl	bdl	0.04	1.72	99.49	65.23
48.10	EM	8.76	0.02	0.46	89.68	0.09	bdl	bdl	bdl	bdl	bdl	0.03	1.46	100.53	62.73
50.10	WMI	22.52	0.01	0.55	74.66	0.08	bdl	bdl	bdl	bdl	bdl	0.03	1.38	99.25	52.22
54.10	TMI	29.54	0.03	1.14	67.57	0.03	bdl	bdl	bdl	bdl	bdl	0.02	0.72	99.06	47.26
56.10	TMI	42.43	0.06	2.33	52.68	0.02	0.01	bdl	bdl	bdl	bdl	0.03	1.98	99.54	36.85
58.10	TMI	38.77	0.04	1.57	57.32	0.02	0.01	bdl	bdl	bdl	bdl	0.03	0.92	98.69	40.09
60.10	TMI	45.98	0.04	1.57	50.47	0.04	bdl	bdl	bdl	bdl	bdl	0.02	1.02	99.15	35.30
62.10	TMI	34.59	0.02	1.12	62.64	0.02	bdl	bdl	bdl	bdl	bdl	0.05	1.16	99.62	43.81
64.10	WMI	27.98	bdl	0.26	71.63	0.08	0.02	bdl	bdl	bdl	bdl	0.03	0.90	100.92	50.10
66.10	TMI	35.73	bdl	0.30	63.20	0.04	0.03	bdl	bdl	bdl	bdl	0.04	0.30	99.65	44.21
68.10	HMI	41.74	bdl	0.14	55.35	0.04	1.33	0.85	bdl	0.03	bdl	0.03	bdl	99.52	38.71
70.10	HMI	42.19	bdl	0.13	54.83	0.05	1.79	1.27	0.08	0.03	bdl	0.03	bdl	100.41	38.35
72.60	HMI	41.95	bdl	0.10	53.76	0.05	1.76	1.09	0.09	0.03	bdl	0.03	bdl	98.87	37.60

Analyses by XRF, see text., bdl = below detection limit, LOI conducted at 1000 °C. See Table 1 for explanation of material types. Analysis was conducted on composite samples at 2 m intervals. Some intervals were omitted to minimise the size of the table but the material type remains the same for the missing intervals. Fe_2O_3 includes FeO recalculated.

The enriched material (EM) group consists of all samples with high Fe contents ≥60 wt.%. Material types that meet this threshold are usually considered to be direct shipping ores (DSOs) provided that other deleterious elements are within the customer's specifications. The weathered magnetite itabirite by definition will require minimal processing to meet the DSO specifications. Materials containing lower concentrations of Fe and are at an earlier stage of weathering compared to EM and WMI are classified as transitional magnetite itabirite (TMI).

Table 4
Mineral categories, abbreviations and their descriptions as used in this paper.

Mineral category	Mineral description
Andradite (Adr)	Any phase with Fe, Ca, Al, Si.
Al oxy-hydroxide (Al Ox(OH))	Any phase with Al, O. May include gibbsite and any other mineral with Al, O, or Al OH
Almandine (Alm)	Any phase with Fe, Al, Si, possibly trace Mg, Mn (see SIP development for difference with chamosite)
Apatite (Ap)	Any phase with Ca P, O
Biotite (Bt)	Biotite and phlogopite mica, may include other mica
Ca Fe Al Silicate	Any Ca Fe Al silicates such as epidote and zoisite may include ferrohornblende and hedenbergite
Ca Mg Fe Silicate	Any phase with Ca, Mg, Fe, Si (with or without Fe & Al) such as hornblende, diopside, tremolite, augite, actinolite, maybe amphiboles and pyroxenes
Calcite (Cal)	Includes calcite (Ca, O, C), with minor dolomite (Ca, Mg, C, O) and ankerite (Fe, Ca, Mg, O)
Chalcopyrite (Ccp)	Includes any phase with Cu, Fe, S such as chalcopyrite. May include trace amounts of bornite and Cu sulphides (chalcocite/covellite)
Chamosite (Chm)	Any phase with Fe, Al, Si, possibly low Mg
Chlorite (Chl)	Any phase with Fe, Al, Si, and Fe, Al, Mg, Si, such as chlorite/clinochlore, nontronite
Fe Mg silicates	Any phase with Fe, Mg, Si such as the serpentine group (antigorite) and minnesotaite
Goethite (Al) (Gt(Al))	Any phase with Fe, O, and low Al (>3 wt.%). May contain trace Si, Al, P and Mn, and OH. Separated from hematite and magnetite by BSE - goethite BSE is lower due to hydration.
Goethite (P) (Gt(P))	Any phase with Fe,O, and low P(>3 wt.%). May contain trace Si, Al, Mn, and OH. Separated from hematite and magnetite by BSE - goethite BSE is lower due to hydration
Goethite/limonite (Gt/Lm)	Any phase with Fe, O. May contain trace Si, Al, P and Mn, and OH. Separated from hematite and magnetite by BSE - goethite BSE is lower due to hydration.
Hematite (Hem)	Any phase with Fe, O, adjusted to a hematite internal standard based on BSE and verified with XRD.
Ilmenite (Ilm)	Any phase with Fe, Ti, O (ilmenite). Also, includes Fe pyrophanite (Mn, Ti, Fe, O)
Kaolinite (Kln)	Includes kaolinite/halloysite/dickite and any other Al silicates such as kyanite/sillimanite/andalusite. Maybe trace topaz.
K-feldspar (K-Fsp)	K-feldspars: any phase with K, Al, Si, O
Magnetite (Mag)	Any phase with Fe, O, adjusted to a magnetite internal standard based on BSE & verified with XRD.
Mn phases	Includes Mn silicates (pyroxferroite), Mn oxides (pyrolusite), Mn Fe oxides and pyrophanite (Mn, Ti, O)
Muscovite/illite (Ms/ill)	muscovite (K, Al, Si, O)
Plagioclase feldspar (Pl Fsp)	Plagioclase feldspars: phases with Na, Al, Si, O to Ca, Al, Si, O
Pyrite (Py)	Includes pyrite/marcasite, boundary effects, minor pyrrhotite and trace jarosite
Quartz (Qtz)	Quartz and other silica minerals (Si, O)
REE phase	Includes mainly xenotime with trace monazite.
Rutile (Rt)	Any phase with Ti, O
Talc (Tlc)	Any phase with Mg, Si, O
Ti-magnetite (Ti-Mag)	Any phase Fe, O, low Ti (0.1–5 wt.%)
Titanite (Ttn)	Any phase with Ca, Ti, Si, O and minor Al, F, Fe.
Zircon (Zrn)	Any phase with Zr, Si, O
Others	Any other mineral not included above, edge effects. Includes trace sphalerite, galena, cassiterite, gypsum, cobaltite and contamination from grinding

Note: Abbreviations which are given in brackets next to the names of the mineral categories are from recommendations by Siivola and Schmid (2007) (International Union of Geological Sciences (IUGS) Sub-commission on the Systematics of Metamorphic Rocks).

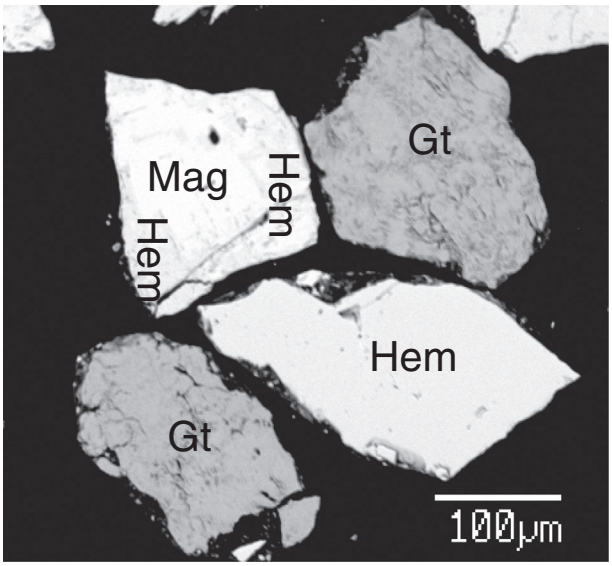

Fig. 4. Backscattered electron image (BSE) illustrating the variation in BSE of magnetite (Mag), hematite (Hem) and goethite (Gt). The magnetite is associated and partially surrounded by hematite. Although little difference between magnetite and hematite is observed by eye, there is sufficient contrast to be resolved in the digital signal (see text).

The low-grade magnetite itabirite in Fig. 2f is garnetiferous; the garnet being almandine. The EM constitutes a minor part of the deposit and is mainly found at Nkout East and Centre whilst the magnetite itabirite (MI) forms the bulk of the deposit.

4. Whole rock geochemistry and mineralogical composition determined by XRD

The average amount of iron varies in the sample types, decreasing in the order EM–WMI–TMI–HMI–LMI whilst SiO_2 increases as can be seen in Table 2 and Fig. 3 whereas Table 3 shows the major element geochemistry (XRF) with depth through the enrichment profile of drill hole NKHC0273. TiO_2 is in general low. The Al_2O_3 content decreases in the order LMI–WMI–TMI–EM–HMI and is mainly due to Al Ox(OH) i.e. Al oxy-hydroxides such as gibbsite in the EM, WMI and TMI whereas for HMI and LMI, it is hosted by aluminosilicates such as feldspar, pyroxene and amphibole. These aluminosilicates are also responsible for the relatively higher Mg, Ca, Na and K seen especially not only in the LMI but also in the HMI compared to the EM, WMI and TMI material types. The highest Al percentage is recorded for the surficial material which is classified as WMI (Table 3) and is due to the presence of clays, Al Ox(OH), and/or goethite. Note that its corresponding P_2O_5 and LOI percentages are higher than those of the other material types indicating the presence of goethite which can have phosphorus and Al in its lattice.

Phosphorus is highest in WMI followed by LMI, EM, TMI and HMI respectively. The P in the LMI, HMI and to a lesser extent TMI is due to apatite which occurs mainly as a minor mineral and that in the WMI and EM samples is mainly hosted in goethite. This result is not apparent from XRD and is made from the QEMSCAN® analyses presented below.

5. QEMSCAN® Mineral Species Identification Protocol (SIP) development

Three size fractions of each of the 51 samples were run by QEMSCAN®. The size fractions are -250/+180 µm, -125/+90 µm and -63/+45 µm. Optimum characterisation of a deposit using QEMSCAN® requires an appropriate mineral list, which must be calibrated and customised. The LCU5 SIP file provided with the QEMSCAN® contains common minerals and was used as a starting point and modified to suit the project. Initial mineralogical knowledge of the samples under investigation was obtained from knowledge of the study area and using analytical techniques such as XRD, SEM/EDS, EPMA and optical microscopy in order to produce the categories of minerals to be used (Table 4). The main issues faced when developing the SIP for this research were the separation of magnetite and hematite, distinguishing compositional variants in the goethite group and the separation of chamosite from other chlorites and almandine.

5.1. Separation of magnetite and hematite

Magnetite and hematite differ by about 3 wt.% in their Fe content, which is not enough to allow them to be distinguished using the 1000 count X-ray spectra acquired during the QEMSCAN® analysis (Andersen et al., 2009; Rollinson et al., 2011).

Minor element concentrations are in general higher in hematite than in magnetite. In particular Al_2O_3 occurs up to 1.57 wt.% in the WMI, up to 3.00 wt.% in the TMI, up to 0.36 wt.% in the HMI and up to 0.25 wt.% in the LMI. Even though the dominant composition is Fe_2O_3 (up to 100 wt.% in the TMI) , minor amounts of FeO occur up to 1.38 wt.% in the WMI, up to 0.78 wt.% in the TMI and up to 0.33 wt.% in the HMI. However, there is no consistent difference that permits differentiation of the two minerals at Nkout.

The most useful characteristic to enable separation of hematite and magnetite was found to be the small difference in the back scattered electron (BSE) signal (a measure of average atomic density) (Fig. 4). The BSE range is specific to the QEMSCAN® system used and will vary between different QEMSCAN® systems (Andersen et al., 2009; Tonžetić and Dippenaar, 2011), which are calibrated to quartz at the lower end (42) and gold at the higher end (232) of the grey scale. Grains of well-characterised magnetite and hematite were set into a resin block and polished to form a standard block that could be used to set

Table 5
EPMA average compositions including standard deviations (S.D.) for goethite analysed.

	Goethite (Al)				Goethite/limonite					
	WMI		TMI		WMI		TMI		HMI	
	Avg wt%	S.D.	Avg wt%	S.D.	Avg wt%	S.D.	Avg wt%	S.D.	Avg wt%	S.D.
SiO_2	1.13	1.27	3.16	2.22	2.29	1.24	1.24	1.98	2.30	4.14
TiO_2	0.41	1.11	0.33	0.33	0.22	0.72	0.10	0.13	bdl	bdl
Al_2O_3	7.88	3.60	6.76	2.57	1.98	0.85	0.67	0.99	0.40	0.63
FeO	70.54	4.31	71.53	6.56	75.42	5.50	80.42	4.23	75.02	3.49
MnO	0.02	0.06	0.01	0.02	0.06	0.08	0.08	0.05	0.01	0.02
P_2O_5	1.84	1.20	0.41	0.31	0.37	0.38	0.13	0.25	0.38	0.64
SO_3	0.17	0.21	0.16	0.11	0.21	0.23	0.03	0.06	0.08	0.05
Total	81.99		82.36		80.55		82.67		78.19	1.54

bdl = below EPMA detection limits of about 0.05 wt.%. Material types WMI, TMI and HMI are as defined in Table 1. Total Fe as FeO. Fe-oxides with totals between 70% and 90% when recalculated for magnetite were assigned as goethite. Goethite with Al concentration ≥3% is classified as goethite (Al). Total Fe as FeO.

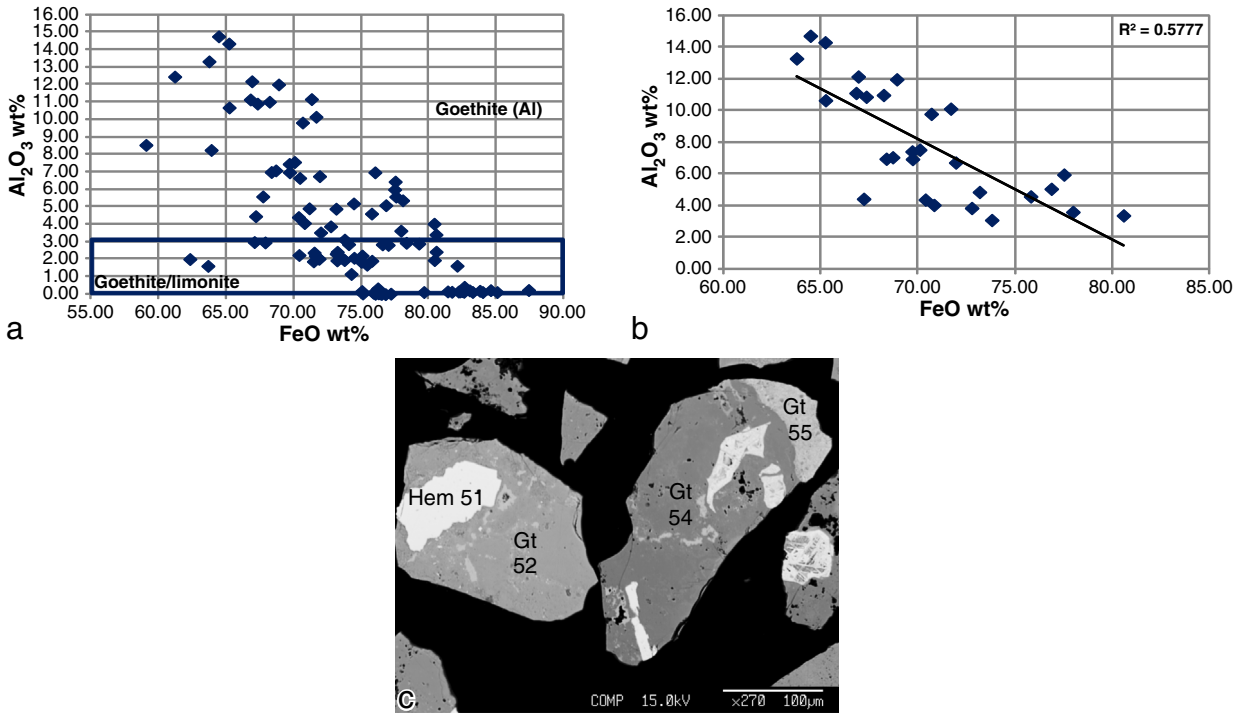

Fig. 5. (a) All goethites analysed (b) Goethite (Al) from the WMI category showing negative correlation between Al_2O_3 and FeO. (c) Sample G01 showing hematite (Hem) and goethite (Gt) showing variation in backscattered coefficient due to varying Al concentration. All the goethites belong to the goethite (Al) category.

up and test the BSE range for each mineral. This standard was used as a quality control before each QEMSCAN® run. The magnetite was found to range from 89 to 100 and hematite from 80 to 88 on the BSE scale; goethite was less than 80 and includes limonites at the lower range (about 50 or less). The limitations of this distinguishing technique include edge effects, which cause the BSE signal to vary, if for example it is a mixture of the mineral with resin or neighbouring minerals, and changes in BSE brightness during the measurement process caused by variations in the chamber vacuum or room temperature change (Benedictus and Horsch, 2008). Edge effects were reduced by high quality polishing of the samples and post-processing filters in the iDiscover software. Temperature effects were reduced by stable air conditioning in the laboratory and the vacuum effects reduced by allowing the chamber vacuum to settle for a few hours after loading the sample so that an absolutely stable level was achieved before the measurement began (typically $<5.0^{-06}$ Torr).

It should be noted that when working with spectra containing higher counts, as in the more usual SEM/EDS spot analysis, it is possible to separate Fe-oxides using the Fe counts or the Fe:O count ratio in the X-ray spectra. However, when mapping at higher count rates, the edge effect problems are still experienced and the mapping is too slow to have practical applications in acquiring the large amounts of data required for minerals processing applications.

5.2. Goethite group minerals

Goethite was separated from magnetite and hematite, using the BSE signal. It has a significantly lower BSE coefficient than either mineral because it is less dense. Goethite group minerals are known to vary in composition, thus a further aim of the research was to characterise this compositional variability by QEMSCAN®. In particular, goethite can contain Al, Si and P in its lattice (Ramanaidu et al., 2008).

The automated mineralogy detection limit for elements in goethite was approximately 3 wt.% for the QEMSCAN® settings used. EPMA results showed that some of the goethite contained >3% Al_2O_3 and that >95% of the Si content observed in the goethite was below the 3% threshold and hence not detectable (Table 5). Based on the EPMA results (Table 5), two categories of goethite were made, namely goethite/limonite and aluminium bearing goethite (goethite (Al)). The detection limit of 3% Al_2O_3 was set as an arbitrary cut off point with goethite (Al) containing >3% Al_2O_3 and goethite/limonite containing <3% Al_2O_3. A plot of FeO vs Al_2O_3 (Fig. 5a) for all the goethites analysed shows the division into goethite/limonite and goethite (Al).

Goethite/limonite occurs mainly in the TMI and HMI material types but is also present in the WMI. Goethite (Al) is confined to the WMI and TMI groups. Lack of goethite (Al) in the magnetite itabirites is consistent with them being fresh BIF. The Si content in both goethite (Al) and goethite/limonite increases from WMI to TMI to HMI and the Al_2O_3 content is highest in the WMI group.

There is a negative correlation between FeO and Al_2O_3 (Fig. 5b) for the goethite (Al) especially those in the WMI category where goethite (Al) is most abundant. The Al content in the goethite also affects their backscatter coefficients. In Fig. 5c which shows hematite and goethite (Al), those with lower Al are brighter than those with elevated Al; Gt-55 contains 4.61% Al_2O_3, Gt-52 contains 7.45 wt.% whilst Gt-54 contains 14.75 wt.%.

Owing to its automated nature, which permitted the analysis of many thousands of particles by QEMSCAN® compared to hundreds by EPMA, a third category called goethite (P) was discovered during the QEMSCAN® analysis. Al and P are important to the quality and processing of iron ore. The SIP therefore contains 3 goethite entries; goethite/limonite, phosphorus bearing (goethite (P)) and aluminium bearing (goethite (Al)) goethite. Goethite (P) contains >3% P and <3% Al, goethite (Al) contains <3% P and >3% Al whilst goethite/limonite contains <3% P and Al.

5.3. Fe-oxide textures

The Fe-oxides are highly intergrown. In most cases, hematite replaces magnetite and goethite replaces both magnetite and hematite. Alteration of hematite to goethite seems to start at the periphery of the grains and also through voids, cracks and other fissures within the hematite and may be due to hydration (Fig. 6a, b and c). The grains therefore display

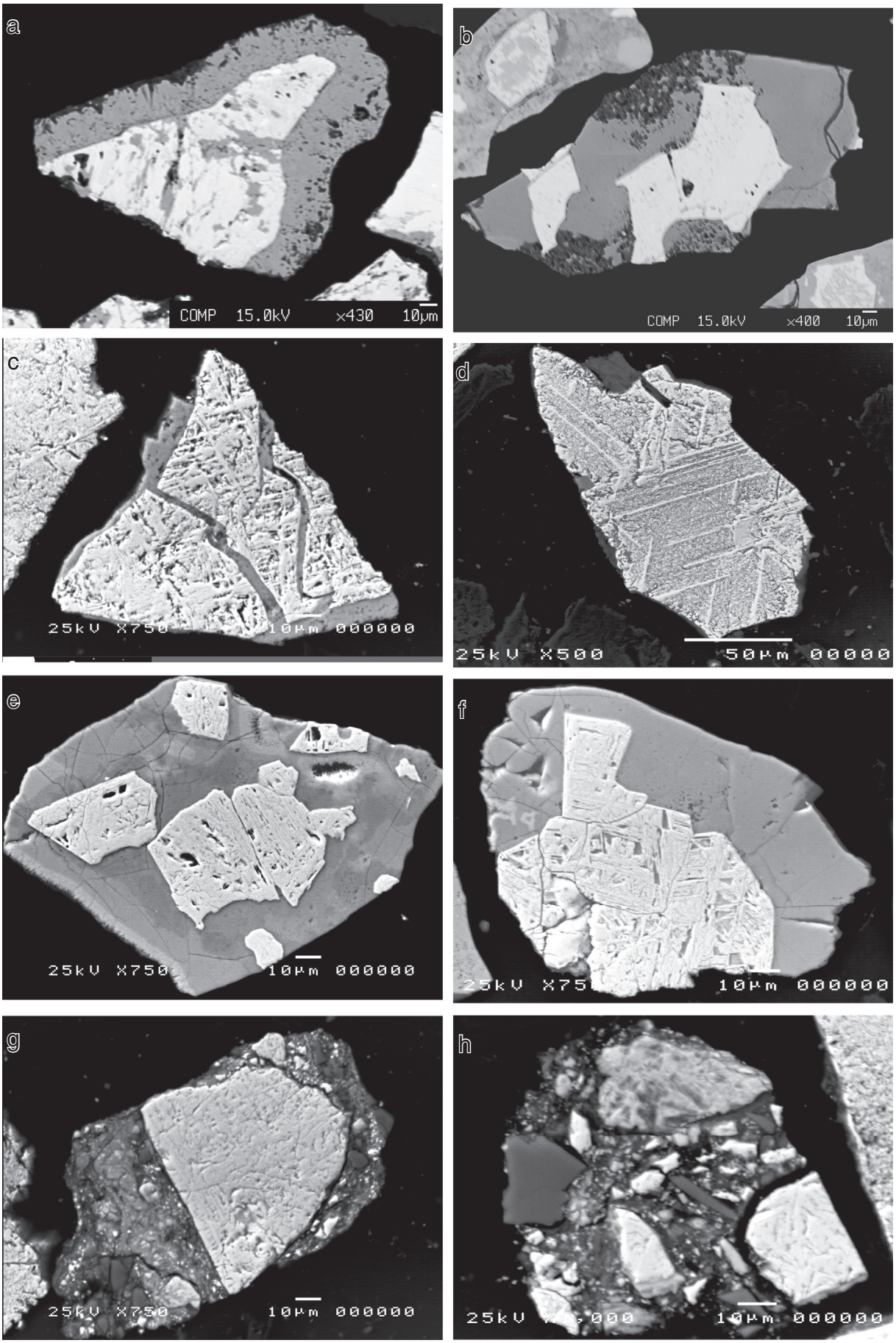

Fig. 6. Fe oxide textures present.

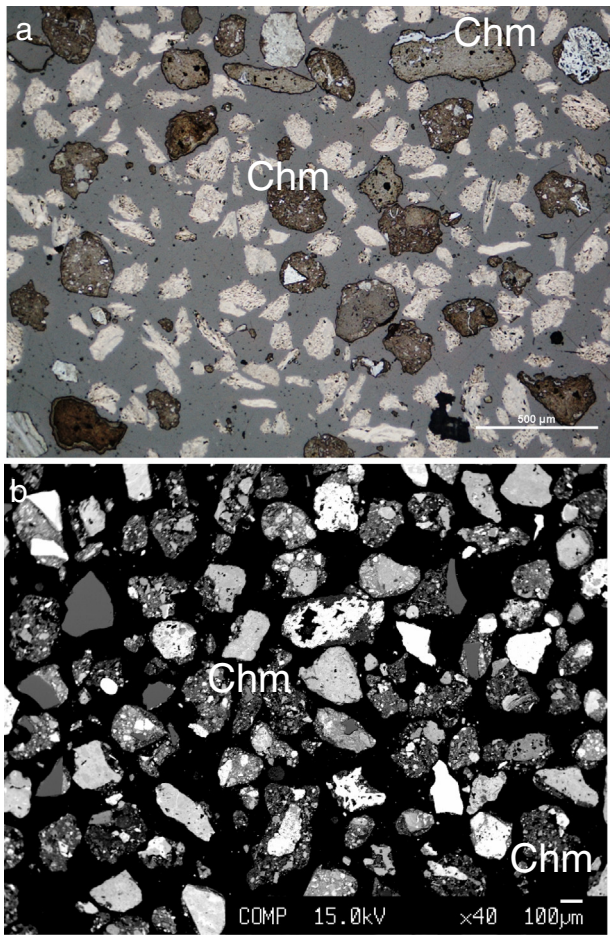

Fig. 7. Reflected light microscopy (a) and EPMA (b) images showing chamosite (Chm) present in the study area. The chamosite is mainly associated with the Fe-oxides.

both intragranular texture i.e. the voids are filled with goethite, and intergranular texture i.e. the goethite occupies the interstitial spaces between the hematite/magnetite grains. Goethite also has rims of Al rich minerals such as gibbsite and kaolinite. Hematite forms lamellae within the magnetite (Fig. 6c, d, e, f). The goethite has cracks looking like mud cracks which are an indication of the fine grained nature of the sample (Fig. 6e and f). Hematite replacing magnetite can appear porous, with its pores now filled by goethite. Chamosite is associated with clay minerals such as kaolinite, cements goethite/limonite, hematite and magnetite grains (Fig. 6g and h).

5.4. Chlorite minerals

Chlorites are renowned for their substantial, varied and often continuous cation substitution making it difficult to assign specific names (Deer et al., 1992). Simple nomenclatures for the Mg-rich, Fe-rich and Mn-rich chlorites are clinochlore, chamosite and pennantite respectively. Optical microscopy and EPMA analysis confirmed the presence of the iron chlorite, chamosite, in the study area, occurring as weathered aggregates closely associated with the Fe-oxides (Fig. 7, Table 6). Chamosite is known to be associated with metamorphosed iron deposits around the world (Rivas-Sanchez et al., 2006). Since it is regarded as a low grade iron mineral (about 29 wt.% Fe), it was considered worth separating from the other chlorites. This was achieved by modifying the chlorite entries in the SIP to only allow Fe, Al, Si, and O as chamosite.

Separation of chamosite from clinochore was achieved using the higher Mg content of clinochlore. Separating almandine from chamosite was more problematic, as both contain similar elements (Fe–Al–Si), and the fact that the possible low Mg content of chamosite was ignored in order to separate it from the other chlorites. To complicate the issue, almandine has a variable chemistry as it is an end member of the pyralspite garnets (solid solution mineral). Investigation revealed that in theory almandine has a higher average density implying it could be separated based on BSE signal, but, the actual density and Fe content of various grains of chamosite and almandine were very variable and had significant overlaps. They could therefore not be reliably separated based on chemistry or BSE signal. Further examination using a real example of almandine from a Namibian beach sand job was attempted and it was determined that a BSE of 60 was a reasonable threshold to separate them. That is, chlorite should be <60 and almandine should be >60, which also matches the relative density of the minerals. However, this still results in an overlap caused by edge effects, polishing issues and possible variation of these minerals, thus it may not be 100% accurate. However, only one sample was found to contain significant almandine according to the XRD and EPMA analyses.

5.5. Other minerals

The main gangue minerals in the WMI and TMI are the Al Ox(OH), mainly gibbsite, plus quartz and to a lesser extent kaolinite, whilst quartz and aluminium silicates are dominant in the magnetite itabirite (Table 7). The amphiboles in the HMI are mainly Ca Mg amphiboles in the tremolite–actinolite series. In LMI, Fe Mg amphiboles such as cummingtoninite–grunerite are dominant. The micas (mainly lath shaped) in the HMI and LMI have similar compositions with the FeO, Al_2O_3 and K content of the LHI being higher than those of other material types. Pyroxenes were encountered in the LMI and show varying Fe, Ca, Al and Mg concentrations. Both plagioclase and K-feldspars were identified in the magnetite itabirite. Fluorapatite is a minor to trace mineral in the magnetite itabirite.

After database (SIP) development further data processing involved checking all the entries, creating a secondary list that reflected the needs of the study, applying any post processors to resolve/minimise errors and then outputting the data for further analysis and interpretation. Data processing also considered the issues discussed in Rollinson et al. (2011).

6. Modal mineralogy determined by QEMSCAN®

Magnetite is a major mineral in all of the material types (Table 8, Fig. 8) The bulk of the weathered material comprising the EM, WMI and TMI material types, which was initially considered to be a hematite deposit (Suh et al., 2009) contains magnetite, hematite and goethite. Goethite/limonite and magnetite are the dominant minerals in EM and WMI whilst quartz and magnetite are dominant in the HMI and LMI material types. The transitional (TMI) ore contains magnetite and more or less equal proportions of goethite and quartz. Goethite (Al)

Table 6
Average compositions and standard deviations (S.D.) for chamosite.

	WMI		TMI	
	Avg wt%	S.D.	Avg wt%	S.D.
SiO_2	17.77	3.66	19.09	4.04
TiO_2	0.16	0.27	0.49	0.19
Al_2O_3	15.53	3.37	20.57	2.73
Fe_2O_3	17.02	9.81	5.62	6.24
FeO	41.39	4.65	38.75	3.92
CaO	0.08	0.02	0.05	0.01
Na_2O	0.06	0.02	0.05	0.02
P_2O_5	0.09	0.02	0.16	0.10
SO_3	0.06	0.08	0.07	0.07
Total	92.16		84.85	

Notes: Material types WMI and TMI as in Table 1. Chamosite was recalculated using 20 cations and 28 O; ignoring H_2O (Deer et al., 1992). FeO/Fe_2O_3 proportions were calculated using the method of Droop (1987).

Table 7
Representative EPMA for gangue minerals.

Mineral	SiO_2	TiO_2	Al_2O_3	Fe_2O_3	FeO	MnO	MgO	CaO	Na_2O	K_2O	P_2O_5	SO_3	F	Total
Ap	0.05	bdl	0.01	0.17	bdl	0.14	bdl	55.06	0.02	bdl	44.08	0.02	1.37	100.92
Ap	0.05	bdl	0.02	0.2	bdl	0.1	bdl	55.32	0.02	bdl	44.08	0.01	1.14	100.94
Ca Amp	54.19	bdl	2.72	4.1	8.55	0.32	15.56	11.64	0.52	0.19	0.08	bdl	0.16	98.03
Fe Amp	51.02	0.02	0.23	bdl	39.1	0.83	6.33	0.66	0.07	bdl	bdl	bdl	bdl	98.26
Gbs	0.04	bdl	81.81	bdl	0.14	bdl	bdl	0.01	bdl	bdl	0.01	bdl	0.06	82.07
Kao	46.21	0.05	38.36	bdl	0.99	0.02	0.02	0.06	0.09	0.12	0.00	0.04	0.00	85.96
Kao	42.69	0.00	33.82	bdl	0.96	0.02	0.02	0.07	0.11	0.01	0.04	0.12	0.01	77.91
K-Fsp	51.59	bdl	31.22	bdl	1.58	0.14	0.5	0.26	1.67	8.6	bdl	0.01	0.02	95.59
Pl Fsp	58.2	bdl	26.1	bdl	0.33	bdl	bdl	8.71	6.53	0.19	0.03	bdl	bdl	100.09
Mca	36.89	1.61	17.21	bdl	18.85	0.01	11.12	0.06	0.42	8.78	bdl	0.01	0.03	94.99
Mca	36.44	1.92	16.79	bdl	19.01	bdl	10.69	0.02	0.41	8.86	bdl	0.05	0.07	94.26
Pyx	42.92	0.05	7.53	10.45	20.36	0.23	3.68	10	1.52	1.38	0.05	0.01	bdl	98.19
Pyx	38.63	0.02	20.87	bdl	34.11	0.41	2.63	3.71	0.01	0.02	bdl	bdl	bdl	100.41
Qtz	101.57	bdl	0.02	bdl	0.12	bdl	bdl	0.01	0.01	bdl	bdl	bdl	bdl	101.73

Notes: bdl = below detection limit. X = no. of oxygen, T = no. of cations used in mineral formulae calculations. Amp = amphibole (X = 23, Ca; T = 13, Fe; T = 15), apatite (X = 26, T = 16), Gbs = gibbsite, Fsp = feldspar (X = 32, T = 12; K = alkali, plagioclase), kaolinite (X = 18, T = 16), mica (X = 22, T = 16), pyroxene (X = 6, T = 4), quartz. Analysis gave Fe in terms of FeO. Fe_2O_3 was calculated using the method of Droop (1987).

occurs mainly in the weathered sample types and is highest in WMI. Concentrations are low in the itabirite sample types (TMI and LMI, Table 8, Fig. 8). There is a rather low (up to 2 wt.%) but important concentration of phosphorus bearing goethite (Gt (P)) in the weathered EM and WMI material types in which this is the only P-bearing mineral. WMI in particular contains the highest P levels in the deposit due to its goethite (P) content. There is no evidence of iron carbonate minerals at Nkout. Iron sulphides are present mainly as pyrite, which occurs as a minor mineral within the magnetite itabirite. Chamosite occurs in quantities greater than 30 wt.% in occasional samples, as in the case of the TMI sample NES03 where it is the most abundant mineral. The TMI contains the highest average chamosite concentration of 17.27%.

The main gangue minerals in the weathered material types are quartz and the Al Ox/OH phases mainly gibbsite. There is a significant increase in the quartz concentration from EM to WMI to TMI with the highest (10.02 wt.%) in the -63/+45 μm fraction of the TMI. Al Ox(OH) is also highest in the -63/+45 μm fraction of this material type. Other gangue trace minerals in the EM group include kaolinite, Fe Mg silicates, Ti magnetite, chlorite and titanite. Minor gangue minerals present in the WMI that were not seen in the enriched material include Mn phases, plagioclase, biotite, pyrite and calcite. The other minor to trace gangue minerals present in the TMI that were not encountered in the previous two categories are muscovite/illite, K-feldspar and zircon.

Gangue minerals form between 55 and 63 wt.% of the LMI samples. Throughout the itabirite sample types, quartz is the main gangue with the highest concentration being in the -63/+45 μm fractions. Al Ox(OH) is only present in the -63/+45 μm fraction of the HMI which also has the highest concentration of kaolinite (4.82 wt.%). Almandine garnet can be present in the LMI up to 12.40 wt.% in the -250/+180 μm fraction. Plagioclase is dominant over K-feldspar within the magnetite itabirite. Other gangue minerals include aluminosilicates, especially in the LMI, including biotite, Ca Fe Al silicates and Ca Mg Fe silicates, clinochlore which occurs in minor and trace quantities.

There is significant variation in the modal mineralogy of the different grain size fractions. Magnetite content is in general highest in the coarsest -250/+180 μm fraction and decrease to the -63/+45 μm finest fraction analysed (Fig. 8). Hematite is more evenly distributed between 8 wt.% and 10 wt.% in all weathered size fractions and it is goethite in the weathered material that increases as the magnetite content decreases in the finer grained material.

The other most noticeable grain size effect is that chamosite is in general highest in the -63/+45 μm fractions and lowest in the coarse -250/+180 μm fraction, and this is especially marked in the transitional, TMI type, material (Fig. 8).

6.1. Comparison of Fe wt% by XRF and QEMSCAN®

If the QEMSCAN® analysis is a precise measure of modal mineralogy and includes some mineral compositional information, a calculated value for Fe wt % using the QEMSCAN® results should be similar to that of the whole rock (XRF). The back calculated QEMSCAN® Fe wt% in general decreases with decreasing grain size (Fig. 9) and is in general higher than that obtained using the whole rock XRF for the larger grain sizes (-250/+180 μm, -125/+90 μm) but lower for the -63/+45 μm fraction. An average composition of the three size fractions analysed using the QEMSCAN® is closest to the XRF Fe value (Fig. 9). Explanations for this can be based on the mineralogy and sample preparation of the blocks for the QEMSCAN®. The QEMSCAN® analysis was not done on whole rock samples but on screened size fractions, selected from the following six size fractions made; +250 μm, -250/+180 μm, -180/+125 μm, -125/+90 μm, -90/+63 μm, and -63/+45 μm. QEMSCAN® analysis thus produces more precise data on the particular sized fractions considered and this always risks a non-representative sample compared to XRF analysis which was carried out on whole rock samples ground to -45 μm.

Furthermore, the QEMSCAN® back calculations are done based on the mineral quantities exposed on the surface of the polished sections. These surface minerals may not be 100% representative of the mineral quantities in the original sample not only due to mineral segregation

Table 8
Average mineralogical composition for the various material types. These averages were calculated using data from all three size fractions analysed.

	Mag	Hem	Gt/Lm	Gt (Al)	Gt (P)	Chm	Qtz	Al Ox/OH	Fe Mg Sils	Ap	Ilm	Ti-Mag	Kln	Py	Bt	Pl Fsp	Ca Fe Al Sils	K-Fsp	Ms/ill	Ca Mg Fe Sils	Others
EM	49.29	9.08	29.17	4.27	0.03	6.13	0.96	0.92	0.03	bdl	0.01	0.01	0.03	0.01	bdl	bdl	bdl	bdl	bdl	bdl	0.02
WMI	33.07	8.80	27.21	13.33	0.16	6.80	7.90	1.69	0.06	bdl	0.01	0.06	0.63	0.01	bdl	0.01	bdl	bdl	bdl	bdl	0.22
TMI	32.13	6.63	18.04	3.40	0.01	17.27	16.85	2.37	0.35	bdl	0.10	0.08	2.23	0.01	0.02	0.03	bdl	bdl	0.03	bdl	0.41
HMI	41.40	6.10	16.28	0.17	bdl	0.28	27.44	bdl	1.49	0.12	0.01	0.03	0.03	0.28	1.19	0.75	0.27	0.36	0.08	3.11	0.56
LMI	26.06	3.01	8.66	0.28	bdl	2.84	21.53	0.04	3.81	1.23	0.27	0.16	0.20	0.26	7.43	6.00	4.54	2.25	1.17	0.66	9.60

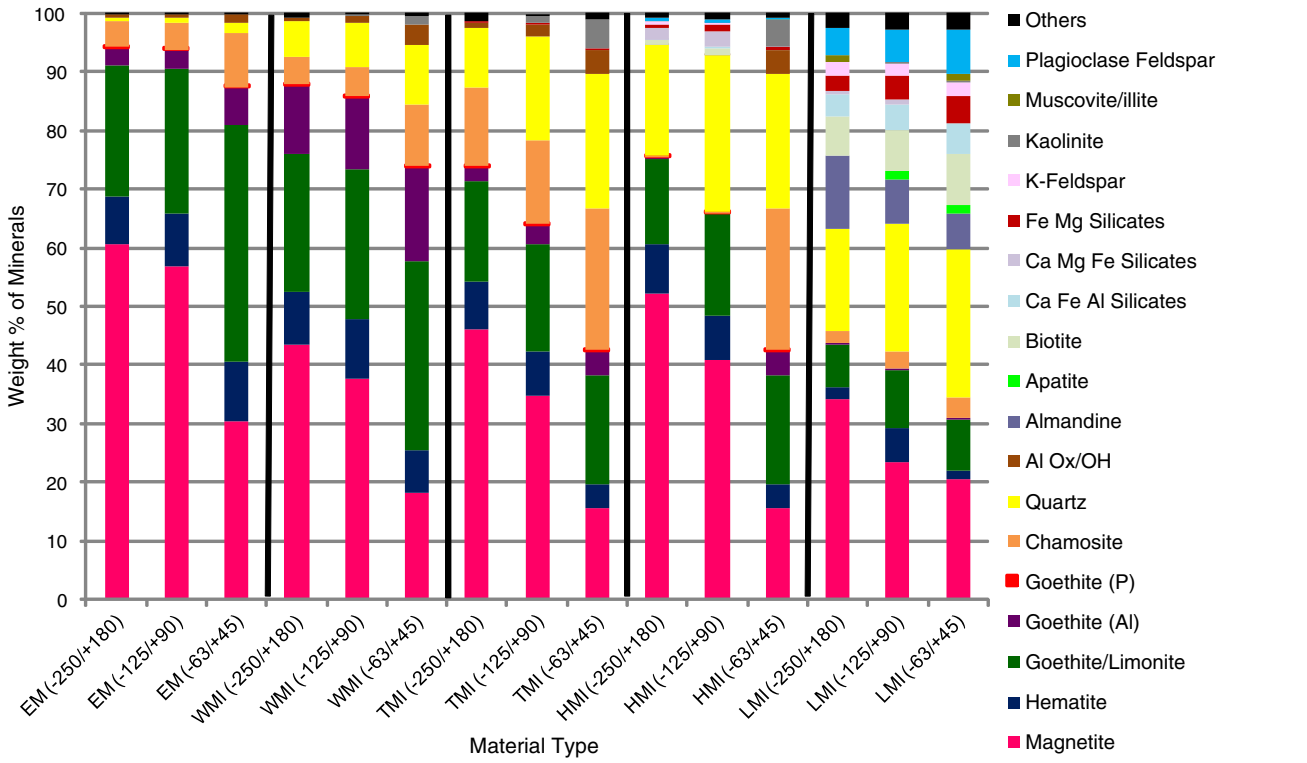

Fig. 8. Average modal mineralogy (weight %) for the various size fractions (μm) analysed. Similar material types are placed side by side for easy comparison. The others category is larger than that in Table 8 as with the exception of goethite (P) only major minerals are included in this plot whilst the table contains minor and trace minerals in addition to the majors. See Table 1 for explanations of the material types.

during sieving but also due to mineral segregation during preparation of the sample blocks (Petruk, 2000). Denser magnetite and hematite may settle to the bottom of the sample mount i.e. the polished surface faster than goethite, chamosite gibbsite and quartz resulting in more of them on the surface that is actually present in the sample. The result is that samples with high amounts of magnetite and hematite will give higher calculated Fe content whilst those with relatively low magnetite and hematite but higher chamosite, gibbsite and/or quartz will give lower calculated Fe. Even though this effect is minimised by using graphite to improve particle separation and minimise differential settling it cannot be completely eliminated.

An additional or alternative explanation comes from the fact that the calculated average QEMSCAN® Fe wt% is closest to that of the XRF which suggests that that preferential separation of minerals into the various size fractions is the most likely explanation for the discrepancies in correlation. Preferential segregation of magnetite into the coarser size fraction is clear in Fig. 8. Some of the back calculated values in Fig. 9 show

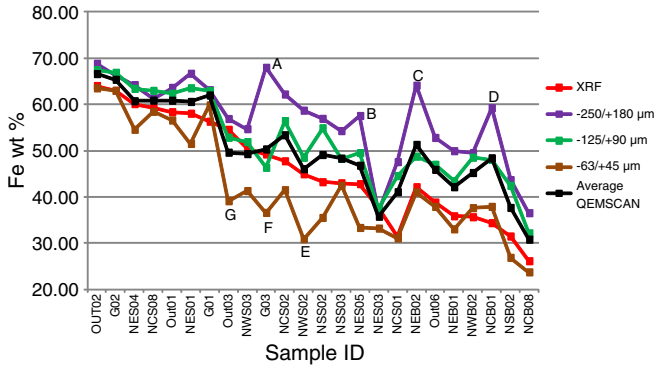

Fig. 9. Comparison of the Fe wt% determined by XRF and Fe wt% calculated from the QEMSCAN® results.

much greater deviation from the XRF values and have been labelled A to G. A to D represent anomalously higher values from the -250/+180 μm fraction whilst E to G are anomalously low values from the -63/+45 μm fraction. Those with much higher Fe wt % i.e. A to D have much higher magnetite content than other minerals whilst those with much lower values are either due to quartz as in F and G or gibbsite and chamosite as in E being the most abundant minerals.

7. Mineral association

Mineral association quantifies which mineral grain is adjacent to or touches another in a particle. It is reported in a tabular format which is read column down then to the left across the row to see what percentage of a mineral is associated with another (Table 9). The data for mineral pairs in Table 9 are not reciprocal because each mineral has its own unique associations and the data columns are independent from each other. For example, mineral X may be found mainly included in, and therefore associated with, mineral Y but mineral Y may be next to mineral Z, and several others, as well as having small inclusions of mineral X. The main mineral associations amongst the material types are quite similar and illustrated in Fig. 10.

In the three weathered sample types, the Fe-oxides are closely associated with each other (Fig. 10, rows 1 and 2), for example hematite is greater than 59% associated with magnetite and 33% associated with goethite/limonite in Table 9. This applies to all size fractions. The various goethites are also closely associated with each other (Fig. 10, row 2). Chamosite is mainly associated with goethite/limonite (29.28%), goethite (Al) (15.19%) and to a lesser extent, magnetite (6.37%) (Fig. 10, rows 3). Of the major gangue materials, Al Ox(OH) (gibbsite) is mainly associated with various goethites and chamosites (Fig. 10, row 4) whilst quartz has low association with other minerals; the highest being 4.18% with chamosite (Fig. 10, row 5). Other minor gangue minerals such as kaolinite and chlorite (clinochlore) are associated with chamosite i.e. 60.70% and 84.46% respectively (Fig. 10, row 6).

Table 9
Average mineral association data for the -125/+90 μm fraction of the weathered magnetite itabirite which is representative of the main associations in the EM, WMI and TMI material types.

	Minerals	Mag	Hem	Gt/Lm	Gt (Al)	Gt (P)	Al Ox/OH	Qtz	Chm	Kln	Mn phases	Chl	Ti–Mag	Fe Mg Sil
WMI -125/+90	Mag	0.00	59.56	24.37	6.62	0.29	2.71	0.01	6.37	0.00	1.37	0.33	9.81	1.07
	Hem	40.44	0.00	10.96	1.82	0.46	1.39	0.00	1.44	0.02	2.32	0.24	5.09	0.16
	Gt/Lm	48.21	33.75	0.00	55.87	38.95	18.16	0.36	29.28	0.07	28.65	4.74	43.18	13.28
	Gt (Al)	3.31	2.44	25.20	0.00	41.71	24.89	0.00	15.19	0.05	15.55	1.79	26.28	0.64
	Gt (P)	0.02	0.05	0.36	0.41	0.00	1.07	0.00	0.00	0.00	0.00	0.00	0.59	0.00
	Al Ox/OH	0.46	0.29	1.20	2.17	7.78	0.00	0.01	3.94	0.01	0.05	0.00	0.44	0.00
	Qtz	0.00	0.00	0.02	0.00	0.00	0.00	0.00	0.22	0.68	0.03	2.16	0.00	35.43
	Chm	1.31	0.84	6.93	12.58	0.00	26.38	4.18	0.00	60.70	3.51	84.46	2.94	9.75
	Kln	0.00	0.00	0.00	0.00	0.00	0.01	0.22	3.94	0.00	0.03	0.17	0.00	0.40
	Mn phases	0.00	0.01	0.02	0.02	0.00	0.01	0.02	0.02	0.00	0.00	0.00	0.00	0.00
	Chl	0.00	0.00	0.02	0.03	0.00	0.00	1.14	0.69	0.17	0.00	0.00	0.02	0.00
	Ti-Mag	0.03	0.02	0.10	0.09	0.18	0.02	0.00	0.01	0.00	0.00	0.01	0.00	0.00
	Fe Mg Sil	0.00	0.00	0.03	0.01	0.00	0.00	0.38	0.11	0.03	0.00	0.00	0.00	0.00

Note: The table should be read down the columns and across the rows to the left to see the associations. Values may not be the same if read the other way i.e. row first then column.

In the high and low grade magnetite itabirite, where magnetite is the dominant Fe-oxide, the relatively small quantities of goethite/limonite and hematite are also closely associated with the magnetite (Table 10). Again the associations are similar in all three size fractions. Using the -125/+90 μm size fraction of the low grade magnetite itabirite for example (Table 10), it is noticeable that the aluminosilicates are less than 6% associated with the Fe oxides. Almandine is 48.40% associated with chamosite (Fig. 10, row 6) whilst Ca Fe Al silicates are mainly associated with plagioclase (22.57%) and Ca Mg Fe silicates (25.85%) (Fig. 10, row 7). Quartz the main gangue has little association with any other mineral; the highest being 3.95% with Fe Mg silicates (Fig. 10, row 5). Apatite is 1.34% associated with magnetite and 1.75% associated with goethite/limonite (Fig. 10, row 7). The alkali and plagioclase feldspars are closely associated (Fig. 10, row 7).

8. Mineral liberation

A mineral is considered in this study as being liberated if >90% is free, high grade inter-grown if it is 60% - 90% free, low grade inter-grown if it is 30% - 60% free and locked if it is <30% free. In some beneficiation processes, only particles containing >90% Fe oxides are recovered when producing a high grade concentrate as in, for example, Petruk (2000). Table 11 is arranged in terms of increasingly liberated grains in the -125/+90 size fraction of the weathered magnetite itabirite. The mineral association values within the material types are reflected in the liberation values. The liberation values are similar for the various material types even though they in general increase with decreasing grain size. The close association that hematite has with magnetite results in 83.15% of hematite being locked i.e. ≤30% liberated, similarly the close association of goethite (P) with the other goethites and its trace to minor concentrations results in it being completely locked (99.97%). Magnetite has the highest percentage i.e. 45.36% in the high grade intergown category (liberation > 60% ≤ 90%) and liberated grains make up just 0.52%. The liberations of the individual Fe oxides minerals increase substantially when considered as a group (82.48%).

Of the main gangue minerals; Al Ox(OH) is mainly locked (64.50%) whilst quartz in general and apatite within the magnetite itabirite are >90% liberated.

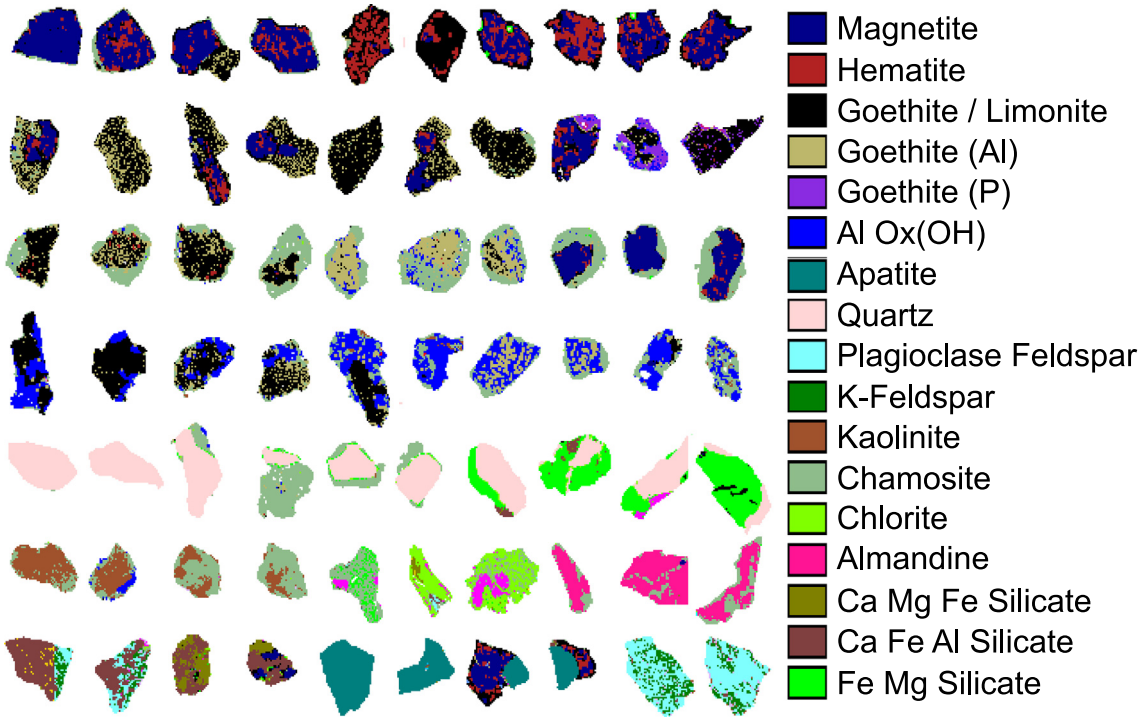

Fig. 10. False colour QEMSCAN® image showing the main mineral associations present in the study area for the -125/+90 μm size fraction. See text for locations of examples of the associations described.

Table 10
Average mineral association data for the -125/+90 μm fraction of the low-grade magnetite itabirite which is representative of the main associations in magnetite itabirite.

		Mag	Hem	Gt/Lm	Chm	Qtz	Ap	Alm	Py	Chl	Bt	Pl Fsp	K-Fsp	Ca Fe Al Sil	Ca Mg Fe Sil	Fe Mg Sil
LMI -125/+90	Mag	0.00	57.61	42.09	2.40	0.09	1.34	0.63	2.84	1.06	0.40	0.00	0.00	0.25	0.08	2.54
	Hem	24.12	0.00	11.29	1.66	0.04	0.25	0.03	0.53	0.52	0.23	0.00	0.00	0.22	0.06	0.24
	Gt/Lm	60.90	34.24	0.00	9.47	0.30	1.75	0.35	3.28	4.36	1.23	0.01	0.01	1.07	0.36	5.15
	Chm	1.65	0.97	3.05	0.00	0.73	1.33	48.40	3.93	17.60	18.41	4.25	1.34	6.73	7.13	17.34
	Qtz	0.03	0.01	0.14	0.43	0.00	2.04	1.98	5.11	9.42	1.22	3.13	0.28	2.13	0.69	15.73
	Ap	0.02	0.01	0.03	0.05	0.08	0.00	0.08	0.00	0.03	0.09	0.02	0.01	0.77	1.93	0.00
	Alm	0.33	0.08	0.13	15.63	0.38	3.12	0.00	0.44	1.16	0.06	0.12	0.02	2.01	11.79	5.76
	Py	0.04	0.06	0.03	0.05	0.04	0.00	0.02	0.00	0.06	0.03	0.01	0.01	0.21	0.12	0.16
	Chl	0.32	0.20	0.65	5.78	3.50	0.12	0.50	1.11	0.00	9.77	0.27	0.44	0.97	7.82	7.19
	Bt	0.29	0.15	0.52	19.29	1.34	0.51	0.10	1.82	24.34	0.00	0.41	10.54	2.69	3.38	15.02
	Pl Fsp	0.00	0.00	0.00	2.08	2.31	0.19	0.09	0.14	0.86	0.80	0.00	45.52	22.57	1.31	0.17
	K-Fsp	0.00	0.00	0.00	0.85	0.20	0.11	0.00	0.03	0.82	4.41	31.68	0.00	4.54	0.48	0.08
	Ca Fe Al Sil	0.11	0.11	0.28	2.48	1.52	5.56	0.35	1.44	1.77	3.79	8.60	2.53	0.00	44.71	3.82
	Ca Mg Fe Sil	0.00	0.01	0.01	0.47	0.15	1.18	1.64	0.51	1.60	0.51	0.08	0.08	25.85	0.00	1.43
	Fe Mg Sil	0.68	0.34	1.28	9.51	3.95	0.50	0.68	3.71	10.49	10.04	0.03	0.04	5.70	3.05	0.00

Note: The table should be read down the columns and across the rows to the left to see the associations. Values may not be the same if read the other way i.e. row first then column.

8.1. Effect of chamosite on liberation

The presence of chamosite in the samples has a marked effect on liberation. For example in Fig. 11, the samples in the middle i.e. NCS04 and NES04 have higher chamosite concentration (31.85 wt.% and 13.67 wt.% respectively) compared to <0.01 wt.% for the other 2 on the edges i.e. G02 and Out02. Chamosite like other chlorites occurs in the form of aggregates which may explain the low liberation. A plot of chamosite wt% against the percentage of liberated (>90% free) Fe oxides (Fig. 12) shows that above 6 wt.% chamosite, the liberation of the Fe oxides drops significantly. This effect is worse if Al Ox(OH) and to a lesser extent kaolinite are also present as major minerals. For example even though the sample at point A in Fig. 12 contains 4.38 wt.% of chamosite, it also contain 9.92 wt.% of Al Ox/OH and the liberation of the Fe oxides is just 49.94%. The sample at point B contains 5.15 wt.% of chamosite and 2.71 wt.% kaolinite with the Fe oxide liberation being 72.36%.

9. Comparison of analytical methods and relative merits of QEMSCAN®

The main methods of quantitative mineralogy are the SEM based methods (e.g. QEMSCAN® and mineral liberation analyser (MLA)) and quantitative XRD using Rietveld refinement (McCusker et al., 1999). The choice of the optimum method requires details of not only the ores in question but also the methods themselves. In the case of Nkout for example, mineralogical and mineral chemistry techniques such as optical microscopy, semi-quantitative XRD and EPMA have shown that goethite is an important mineral in the oxidised cap, which has potential of being a DSO or upgraded to DSO specifications. A major problem is determining the amount of goethite present. Finely powdered goethite is in most cases weakly crystalline to amorphous and produces broad XRD peaks which are not proportional to the actual goethite content (Petruk, 2000). As such QEMSCAN® is the preferred technique rather than quantitative XRD.

Although it is necessary to verify the QEMSCAN® results using other techniques such as the semi-quantitative XRD, EPMA and optical microscopy and the set up for new ore deposits is time consuming, the technique provides a vast amount of mineralogical information which can be used to solve potential processing problems related to upgrading or beneficiation of iron ore deposits. An example here is the recognition of the presence of phosphorus-bearing goethite i.e. goethite (P) which was not found by the other techniques. The importance of developing a suitable SIP based on knowledge of not only the study area but also knowledge obtained from other techniques cannot be over emphasised. The same may be said for good sample preparation and suitable experimental conditions.

Table 11
Average liberation for the -125/+90 μm fractions of the weathered magnetite itabirite material type.

	Minerals	% liberation			
		≤30%	>30% ≤ 60%	>60% ≤ 90%	>90%
WMI -125/+90 μm	Hem	83.15	16.06	0.79	0.00
	Gt (P)	99.97	0.03	0.00	0.00
	Gt (Al)	62.68	22.27	14.60	0.45
	Mag	9.53	44.59	45.36	0.52
	Gt/Lim	38.58	36.94	22.39	2.09
	Chm	47.57	19.65	25.12	7.66
	Al Ox(OH)	64.50	13.07	8.93	13.50
	Kao	23.82	13.05	23.90	39.23
	Fe-oxides	0.37	1.61	15.54	82.48
	Qtz	0.11	0.23	0.89	98.77

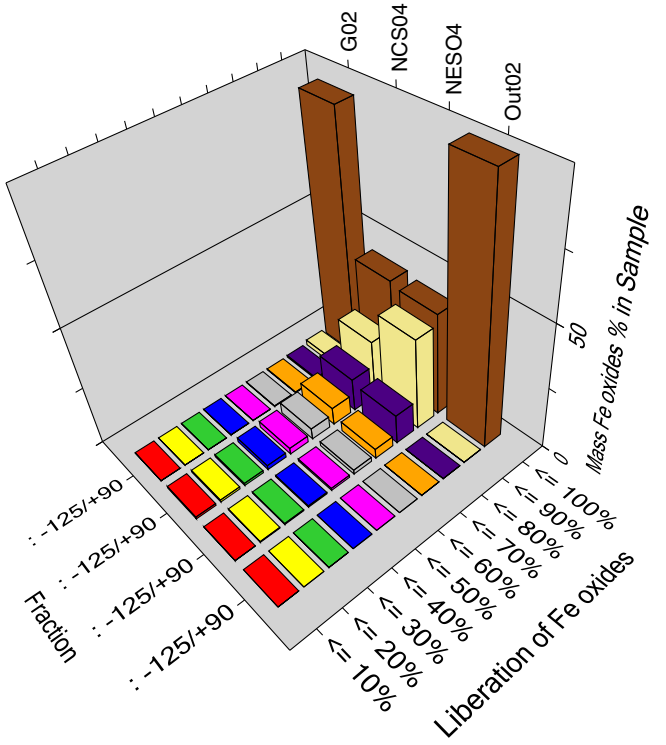

Fig. 11. Liberation for 4 enriched samples. Note that the 2 samples in the middle i.e. NCS04 and NES04 have higher chamosite concentration (31.85 wt.% and 13.67 wt.% respectively) compared to <0.01 wt.% for the other 2 on the edges i.e. G02 and Out02.

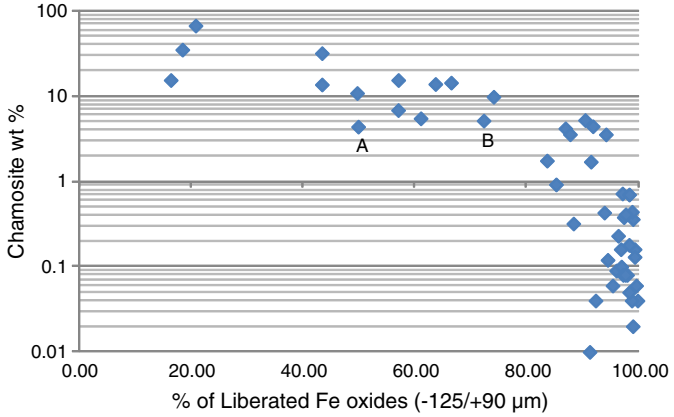

Fig. 12. The effect of chamosite on the liberation of the Fe oxides. The effect is more pronounced for chamosite greater than 6 wt.% and is compounded if Al Ox(OH) is also present as a major mineral (see text).

The advantage of the QEMSCAN® over the EPMA and SEM/EDS is the capability of much more rapid data acquisition and thus the ability to analysing many thousands of particles, one or two orders of magnitude more than on the more traditional techniques.

Several workers including Tonžetić and Dippenaar (2011), Donskoi et al. (2011), Thella et al. (2012) and Lund et al. (2013) have presented the effectiveness of QEMSCAN® as a tool for iron ore characterisation. Tonžetić and Dippenaar (2011) mentioned that QEMSCAN® can be used as an alternative to the traditional quantification of iron ore sinter mineralogy which has been based on amongst others optical microscopy and XRD. Optical microscopy is based on grain morphology and XRD on crystal structure whereas classification of minerals by QEMSCAN® is based on chemical composition. However Donskoi et al. (2011) pointed out that it is still problematic for QEMSCAN® to distinguish between iron ore minerals very close in oxygen content, e.g. hematite and hydrohematite, or between different types of vitreous goethite. This is not a problem for optical image analysis software as it can easily recognise minerals with slight differences in their oxidation or hydration state by correlation with their reflectivity. They however concede that a combined approach using both techniques will provide the most detailed understanding of iron ore samples being characterised. Lund et al. (2013) used the QEMSCAN® to validate a technique using EPMA, XRF and SATMAGAN to quantify minerals from routine chemical assays. The samples considered in that study contained only magnetite and therefore were particularly well suited to QEMSCAN® analysis. The ability to tackle material that contains both magnetite and hematite is a major step forward in making process and geometallurgical studies more efficient by gaining maximum information with as few as possible analytical techniques.

The choice of optimum techniques varies according to the sample characteristics, as well as the more pragmatic considerations of available techniques and expertise. We have summarised the steps in process mineralogy of iron ore deposits (Table 12) to clarify the options and possible paths through assessment of a deposit. All potential iron ores will be subject to whole rock analysis, usually by X-ray fluorescence (XRF), and to tests of iron-bearing mineral extraction, e.g. by the Davis Tube test (Leevers et al., 2005) or SATMAGAN (Lund et al., 2013). For some deposits with simple mineralogy and high Fe contents few additional tests might be needed, although most will undergo reflected light optical microscopy. When it is necessary to remove gangue minerals, a more in depth study is required and best practice uses a variety of techniques in a preliminary study to augment the data gathered thus far, including an electron beam technique (which may be energy- or wavelength dispersive but should be quantitative) and X-ray diffraction. The results of this preliminary study then determine the best technique to choose for full and statistically valid assessment of the deposit for geometallurgical modelling (Table 12). Automated mineralogy techniques either optical or electron beam have important advantages over quantitative X-ray diffraction in that they can determine mineral associations and liberation, and are also able to determine amorphous phases. The key differences between optical and electron beam methods are that optical microscopy is the most sensitive method for distinguishing the different varieties of Fe oxides whereas the electron beam techniques can determine mineral chemistry directly and distinguish between varieties of iron ore minerals with varying levels of contaminants and between different chemical variations of gangue minerals.

Geological studies of iron ores also benefit from these techniques if there is a need to quantify mineral associations in order to study, for example, alteration patterns or determine modal mineral assemblages involved in reactions. Similar considerations apply to the choice of optimum technique. The technique that will potentially give the largest amount of information is QEMSCAN® or a similar electron beam method, if the technique is carefully set up and calibrated to distinguish the Fe oxide minerals.

10. Implications and conclusions for the process mineralogy of the Nkout iron ore deposit

The use of QEMSCAN® has enabled the following conclusions to be made regarding the process mineralogy at Nkout.

1. The deposit contains magnetite throughout (updating the conclusion by Suh et al. (2009) that the weathered material is predominantly hematite). The magnetite is being replaced by hematite and therefore the deposits can be described as a hematite-martite–goethite ore which is similar to hematite–martite–goethite ore of the BIF-hosted iron ore deposits in the Windarling Range, Yilgarn Craton, Western Australia (Angerer et al., 2012).
2. The presence of chamosite is important because it is a significant host of Fe (about 30% Fe) and has a deleterious effect on liberation characteristics of the ore when present at concentrations above 6%. This effect is compounded if the samples are also rich in Al Ox(OH),

Table 12
Summary of some techniques to carry out quantitative process mineralogy of iron ore deposits.

Function	Optical image analysis	Electron beam automated mineralogy (e.g. QEMSCAN®)	Quantitative X-ray diffraction
Distinguish and quantify proportions of the various Fe oxides	Yes, most sensitive technique	Yes, with careful set up and calibration	Yes, except for amorphous phases e.g. goethite
Identify other major minerals	Yes	Yes	Yes
Identify minor minerals (<5 modal %)	Yes	Yes	No
Distinguish chemical variants of minerals	No, unless reflected light characteristic can be calibrated against chemistry	Yes, measures chemistry directly via X-ray spectrum	No
Quantify mineral associations and liberation	Yes	Yes	No
Cost to purchase and run	Moderately expensive, needs dedicated expertise to set up image analysis	Expensive equipment and needs dedicated expertise	Expensive equipment and needs dedicated expertise for quantitative work

which at Nkout is mainly gibbsite. Chamosite is not only mainly associated with goethite/limonite as far as the Fe oxides are concerned but also has a much higher association with gangue minerals such as kaolinite, Al Ox(OH) and the Mg, Fe and/or Ca aluminosilicates compared to the Fe oxides. The locations of chamosite within the deposit are important and should be noted. According to the samples studied so far, they occur mainly in the eastern part of the deposit.

3. The major gangue minerals in the weathered martite - goethite ore are gibbsite and quartz. A major potential problem in upgrading this ore is removing Al and P which has been shown to be associated with the goethite. However since their quantities are relatively low they might not be the main targets for removal, compared to for example gibbsite and quartz in upgrading to a customer's specification.
4. The major gangue mineral in the magnetite itabirite ore is quartz, followed by the aluminosilicates. The quartz is in general liberated and when associated with other minerals, it is not associated with Fe-oxides. Apatite is a potential problem in LMI ores but occurs mainly as well liberated grains (>90% free) and as such will not be problematic to remove when upgrading the magnetite itabirite.
5. The -250/+180 fraction is the most suitable grind size for beneficiation because of the following reasons;
   - ➢ Less energy is needed to grind to this size fraction compared to finer fractions.
   - ➢ It contains a higher percentage of Fe oxide minerals.
   - ➢ It contains less chamosite than the other fractions and as such chamosite will have less effect on the liberation of its Fe oxides.
   - ➢ It contains less Al Ox(OH) and quartz compared to the other size fractions.
6. The Al Ox(OH) could be removed by attrition scrubbing whilst quartz and other gangue can be removed by grinding and screening. Magnetite could then be recovered using less expensive low intensity magnetic separation (LIMS) whilst hematite and goethite can be removed using a combination of Wet High Intensity Magnetic Separation (WHIMS), SLon Magnetic Separation and Flotation. The LIMS should be employed initially and the rejects subjected to the WHIMS to remove the hematite and goethite. This will reduce energy consumption.

Acknowledgements

This work was done as part of a PhD research funded by the Association of Commonwealth Universities (SLCA-2010-93). The authors are grateful to Afferro Mining Inc. especially Peter Taylor, Chief Operating Officer, for providing logistic support for the field work to be conducted in their company's license area in Cameroon. Special thanks go to the field geologists for their enthusiasm and support rendered during the field work.

References

Afferro Mining, 2013. http://afferro-mining.com/ (Accessed 8 November 2013).
Andersen, J.C.Ø., Rollinson, G.K., Snook, B., Herrington, R., Fairhurst, R.J., 2009. Use of QEMSCAN® for the characterization of Ni-rich and Ni-poor goethite in laterite ores. Miner. Eng. 22, 1119–1129. http://dx.doi.org/10.1016/j.mineng.2009.03.012.
Angerer, T., Hagemann, S.G., Danyushevsky, L., 2012. High-grade iron ore at Windarling, Yilgarn Craton: a product of syn-orogenic deformation, hypogene hydrothermal alteration and supergene modification in an Archean BIF-basalt lithostratigraphy. Miner. Deposita. http://dx.doi.org/10.1007/s00126-012-0450-3.
Benedictus, A., Horsch, H., 2008. Enhanced measurement capabilities for iron ore deposits. 34th International Geological Congress. International Union of Geological Sciences, Brisbane, Australia.
Cabral, A., Rosière, C., 2013. The chemical composition of specular hematite from Tilkerode, Harz, Germany: implications for the genesis of hydrothermal hematite and comparison with the Quadrilátero Ferrífero of Minas Gerais, Brazil. Miner. Deposita. http://dx.doi.org/10.1007/s00126-013-0459-2.
Clout, J.M.F., Simonson, B.M., 2005. Precambrian iron formations and iron formation-hosted iron ore deposits. Econ Geol 100th Anniversary 643–679.
Deer, W.A., Howie, R.A., Zussman, J., 1992. An Introduction to the Rock Forming Minerals. Longman Group, UK.
Donskoi, E., Suthers, S.P., Fradd, S.B., Young, J.M., Campbell, J.J., Raynlyn, T.D., JMF, C., 2007. Utilization of optical image analysis and automatic texture classification for iron ore particle characterisation. Miner. Eng. 20, 461–471.
Donskoi, E., Manuel, J.R., Austin, P., Poliakov, A., Peterson, M.J., Hapugoda, S., 2011. Comparative study of iron ore characterisation by optical image analysis and QEMSCAN™. Iron Ore Conference Perth, Western Australia, AusIMM, 11–13 July 2011.
Droop, G.T.R., 1987. A general equation for estimating Fe^{3+} concentrations in ferromagnesian silicates and oxides from microprobe analysis, using stoichiometric criteria. Mineral. Mag. 51, 431–435.
Fandrich, R., Gu, Y., Burrows, D., Moeller, K., 2006. Modern SEM-based mineral liberation analysis. Int. J. Miner. Process. 84, 310–320. http://dx.doi.org/10.1016/j.minpro.2006.07.018.
Gottlieb, P., Wilkie, G., Sutherland, D., Ho-Tun, E., Suthers, S., Perera, K., Jenkins, B., Spencer, S., Butcher, A., 2000. Using quantitative electron microscopy for process mineralogy applications. JOM 52, 24–25. http://dx.doi.org/10.1007/s11837-000-0126-9.
Leevers, P., Gaughan, C., Bubner, G., 2005. The iron magnet deposit. Iron Ore Conference. Fremantle, WA, AusIMM 19–21 September.
Lund, C., Lamberg, P., Lindberg, T., 2013. Practical way to quantify minerals from chemical assays at Malmberget iron ore operations — an important tool for the geometallurgical program. Miner. Eng. 49, 7–16. http://dx.doi.org/10.1016/j.mineng.2013.04.005.
McCusker, L.B., Von Dreele, R.B., Cox, D.E., Louër, D., Scardi, P., 1999. Rietveld refinement guidelines. J. Appl. Crystallogr. 32 (1), 36–50. http://dx.doi.org/10.1107/S0021889898009856.
Ngnotué, T., Nzenti, J.P., Barbey, P., Tchoua, F.M., 2000. The Ntui-Betamba high-grade gneisses: a northward extension of the Pan-African Yaoundé gneisses in Cameroon. J. Afr. Earth Sci. 31, 369–381. http://dx.doi.org/10.1016/S0899-5362(00)00094-4.
Petruk, W., 2000. Applied Mineralogy in the Mining Industry. Elsevier Science.
Pirrie, D., Rollinson, G.K., 2011. Unlocking the applications of automated mineral analysis. Geol. Today 27, 226–235. http://dx.doi.org/10.1111/j.1365-2451.2011.00818.x.
Pirrie, D., Butcher, A.R., Power, M.R., Gottlieb, P., Miller, G.L., 2004. Rapid quantitative mineral and phase analysis using automated scanning electron microscopy (QemSCAN); potential applications in forensic geoscience. Geol. Soc. Lond., Spec. Publ. 232, 123–136.
Ramanaidu, E., Wells, M., Belton, D., Verrall, M., Ryan, C., 2008. Mineralogical and microchemical methods for the characterization of high-grade banded iron formation-derived iron ore. Econ Geol, SEG Reviews, 15 129–156.
Rivas-Sanchez, M.L., Alva-Valdivia, L.M., Arenas-Alatorre, J., Urrutia-Fucugauchi, J., Ruiz-Sandoval, M., Ramos-Molina, M.A., 2006. Berthierine and chamosite hydrothermal: genetic guides in the Peña Colorada magnetite-bearing ore deposit, Mexico. Earth Planets Space 58, 1389–1400.
Rollinson, G.K., Andersen, J.C.Ø., Stickland, R.J., Boni, M., Fairhurst, R., 2011. Characterisation of non-sulphide zinc deposits using QEMSCAN®. Miner. Eng. 24, 778–787. http://dx.doi.org/10.1016/j.mineng.2011.02.004.
Siivola, J., Schmid, R., 2007. International Union of Geological Sciences. Subcommission on the Systematics of Metamorphic RocksCambridge University Press.
Suh, C.E., Cabral, A.R., Ndime, E., 2009. Geology and ore fabrics of the Nkout high-grade haematite deposit, southern Cameroon. In: Angerer, T., Hagemann, S., Rosière, C.A. (Eds.), Smart Science for Exploration and Mining. Proceedings of the Tenth Biennial SGA Meeting. Society for Geology Applied to Mineral Deposit, Townsville, Australia, pp. 558–560.
Tagne-Kamga, G., 2003. Petrogenesis of the Neoproterozoic Ngondo Plutonic complex (Cameroon, west central Africa): a case of late-collisional ferro-potassic magmatism. J. Afr. Earth Sci. 36, 149–171. http://dx.doi.org/10.1016/S0899-5362(03)00043-5.
Thella, J.S., Mukherjee, A.K., Srikakulapu, N.G., 2012. Processing of high alumina iron ore slimes using classification and flotation. Powder Technol. 217, 418–426. http://dx.doi.org/10.1016/j.powtec.2011.10.058.
Tohver, E., D'Agrella-Filho, M.S., Trindade, R.I.F., 2006. Paleomagnetic record of Africa and South America for the 1200–500 Ma interval, and evaluation of Rodinia and Gondwana assemblies. Precambrian Res. 147, 193–222. http://dx.doi.org/10.1016/j.precamres.2006.01.015.
Tonžetić, I., Dippenaar, A., 2011. An alternative to traditional iron-ore sinter phase classification. Miner. Eng. 24, 1258–1263. http://dx.doi.org/10.1016/j.mineng.2011.04.012.